Diblock Copolymer Stabilized Nanoparticles for Drug Delivery via Flash Nanoprecipitation

A Dissertation

SUBMITTED TO THE FACULTY OF

UNIVERSITY OF MINNESOTA

BY

Jing Han

IN PARTIAL FULFILLMENT OF THE REQUIREMENTS

FOR THE DEGREE OF

DOCTOR OF PHILOSOPHY

Christopher W. Macosko

October 2014

October 2014

Acknowledgements

I have been very fortunate to attend University of Minnesota for graduate study at Department of Chemical Engineering and Materials Science, with enormous support of my advisors, colleagues, family and friends. Without all your help and encouragement, it would have been impossible for me to achieve my degree.

First of all, I would like to thank my advisor Prof. Macosko. Over the past six years, he has been a passionate, energetic and patient teacher and set a great example of being a world-class scientist. He has constantly taught me how to think scientifically, analyze results comprehensively, and benefit from interdisciplinary collaboration. Not only have I gained a lot of knowledge in polymer and colloidal science, but also other skills such as how to become resourceful through colleague discussion and social activities, how to clearly present research results by making a story-telling presentation and how to write precisely and concisely via academic publications. Chris, Thank you for all the time and energy you spent with me in my graduate study and job hunting process. You have my utmost gratitude and respect.

I would also like to thank Prof. Hoye and Prof. Panyam for all their expertise and help in the field of Chemistry and Pharmaceutics. With their guidance, I have been very grateful to work on this multi-disciplinary project across three fields, which is rare for a doctorate student. Prof. Hoye has been very supportive to my research, teaching me many chemical concepts, academic writing and results analysis. Prof. Panyam has been very generous allowing me to use his instruments and to provide critical pharmacological expertise to this project. His student Dr. Bharath Guru and Stephen Kalscheuer have taught me so much about pharmacokinetic studies. Without their diligent work on cell

and animal studies, this project would have never achieved so much depth and width. This research experience allowed me to learn from their expertise and to view things in different perspectives, both in scientific work and life. I would also like to thank Prof. McCormick and my colleague Hanseung Lee for their tremendous contribution sharing microscopy expertise for this project.

Thanks to this collaborative project, I have been able to work with many graduate, undergraduate students and post-docs in Chemistry and Pharmaceutics, and Macosko group. I would like to thank Dr. Zhengxi Zhu, Dr. Haitao Qian, Dr. Bharath Guru, Dr. Adam Wohl, Kevin Pustulka, Andrew Michel, Stephen Kalscheuer, Minjae Sun, Ge Qu, Dr. David Giles, Dr. Alex Grill, Dr. Lin Niu, Dr. Tanmoy Sadhukha, Ameya Kurtane, for their efforts on this project. I like to give my special thanks to Dr. Zhengxi Zhu who helped me start this project and taught me all the fundamental knowledge and experimental techniques. He also shared a lot of his job-hunting experience and tips to help me find a job. Dr. Adam Wohl and Andrew Michel are my most important partners from Chemistry. Without their dedication in polymer and drug synthesis work, this project can never progress this far. Dr. Bharath Guru and Stephen Kalscheuer have carried out the most time-consuming work in this project for in vitro and in vivo studies, and their commitment has always been my inspiration to work thoroughly and patiently and never give up despite failures and setbacks. Their technical guidance has helped me so much to revise experiment setting, modify research direction and incorporate research analysis.

My parents, Sixiao Han and Shuling Jin, have been very supportive all these years. I felt very guilty especially after I came to US for graduate study, because as the

only child, I have made their life more difficult than other Chinese families, because of being away from family thousands miles away and not having much opportunity to take care of them. However, they never complained. They have never stopped encouraging me to pursue my dream no matter what challenges I encountered. They constantly taught me to dedicate to what I do, to never lose faith and confidence, to respect everyone, and to be kind to friends in work and life.

I also feel very blessed to be friends with Victor Lai, Wei Xie, Ting Chen, Xi Chen, Yanfei Wu, Jie Lv, Xin Zhang since I came to US. They have been there with me every happy and sad moment, both in academic career and life. Moreover, I cannot forget all my friends back in China. I like to give my special thanks to my dearest friends since kindergarten You Xu, Miao Wang and Xi Luo, those from junior high school, Jian Tian, Lei Yang, Jing Gong, Yang Li, Wei Lei, and those from senior high school, Liyao Xue, Zhiyao Lv and Xin Zhang, and those from Zhejiang University, Yiwen Shou, Lanjie Liu, Shanshan Ying. They have helped me through all the tough time and frustrations just by talking and texting me. Their patience listening to me has always made me feel better and be stronger.

Thank you all for your support and love, I couldn't have come this far to achieve so much in my scientific career and personal life. I will always keep my appreciation and respect for you all.

I dedicate this thesis to

my parents and my friends.

Abstract

Cancer is one of the most challenge diseases to treat around the world. Drug delivery system, as one of the chemotherapeutic treatments has received enorrmous attention from researchers. This thesis is to develop amphiphilic diblock copolymer protected nanoparticles loaded with anti-cancer drug, with small size and high drug loading, to achieve selective drug delivery using EPR effect. Chapter 1 briefly describes the motivation and novelties of this research pursuit. Chapter 2 introduces a modified confined impingement jets mixer with dilution (CIJ-D mixer), using flash nanoprecipitation to produce nanoparticles made of hydrophobic drugs. The CIJ-D mixer was evaluated by the sizes of β-carotene nanoparticles at varied flow conditions compared to these made by multi-inlet vortex mixer. The CIJ-D mixer provides higher efficiency and easiness of handling for nanoparticle preparation. That is why CIJ-D mixer was used for all the work presented in the following chapters. In Chapter 3, we made the first attempt to produce PEG-*b*-PLGA protected paclitaxel loaded nanoparticles but failed, because paclitaxel is too hydrophilic to be captured in particles. Thus, a series of silicate ester derivatized paclitaxel were synthesized by Hoye research group and successfully encapsulated into nanoparticles. Several nanoparticle post-treatments, such as filtration, hollow fiber diafiltration, and ultracentrifugation were used and assessed, in order to purify nanoparticles. Lyophilization was found to induce nanoparticle aggregation due to the freezing process. The addition of sucrose as cryoprotectant was studied to prevent aggregation and recover nanoparticle. Chapter 4 focuses on developing *in vitro* drug release protocols, for more accurate quantification of highly hydrophobic paclitaxel prodrugs. Different dialysis devices were used such as dialysis tubes, dialysis

cassettes, and dialysis mini capsules. Infinite sink and limited sink conditions were compared as well to provide sufficient concentration gradient across dialysis semi-permeable membrane. At last, a reverse drug release experimental protocol was customized to determine the remaining drug left in dialysis mini capsules while the sink condition was maintained by frequently refreshing buffer solution during *in vitro* drug release study. Chapter 5 mainly presents the pharmacokinetics of paclitaxel prodrug nanoparticles loaded with different silicate ester derivatives, at different pH, both inside nanoparticles and in buffer solution. Chapter 6 includes a series of Cryo-TEM images of nanoparticles collected at different time, such as fresh nanoparticles immediately after being prepared by CIJ-D mixer, nanoparticles after ultracentrifugation, after lyophilization, 0hr, and 24 hr during drug release study. These images not only showed a reverse liner relation of average particle size and hydrophobicity of the loaded drug, but also displayed a core-shell internal structure of nanoparticles prepared via flash nanoprecipitation and potential particle disassembly after 24hr drug release. Finally, Chapter 7 summarizes the key results and conclusions obtained from previous chapters, lessons learned from mistakes and failures, and future directions for this project, in order to prepare nanoparticles with better controlled size and drug release kinetics and to understand deeply on nanoparticle formation and release mechanisms.

Table of Contents

List of Tables

List of Figures

Chapter 1 Overview and Motivation

1.1 Drug Delivery and EPR Effect

Cancer is the second deadly disease globally, causing about 13% of all human death[1]. Numerous researchers have endeavored for decades to find effective treatments for cancer. Currently, several methods have been developed, such as surgery, radiation and chemotherapy. However, chemotherapy, as the most effective and widely used treatment, has severe side effects on patients, mainly due to undesirable and non-specific anticancer drug delivery to normal tissues in human body. Accordingly, a goal of chemotherapeutic treatment is to achieve specific drug delivery allowing drug localized only in tumor tissues. Methods to achieve specific delivery can be categorized in two: active targeting and passive targeting[2]. Active targeting usually involves functionalizing drug delivery systems with particular functional groups which can be attracted to receptor on cancer cell surface. However, in this research work, we focus on drug delivery system via passive targeting. It means that specific drug delivery relies on nano-scale systems being uptaken via selective size and transport. It is called the enhanced permeation and retention effect, or EPR effect discovered in 1986[3-6].

Utilizing the EPR effect, macromolecular particles are first delivered by intravenous administration and circulated in blood as shown in Figure 1.1. When they reach normal tissue vasculature, normal endothelial cells are compactly aligned, and drug molecules or very small particles less than 50 nm in diameter can penetrate them. On the other hand, tumor tissues are poorly aligned with defective endothelial cells. Researchers have found open cell fenestrations range approximately between 50-400 nm depending

on different tumor types and their locations. Particles in this size range will penetrate through and localize in tumor tissues. Also vascular structure is poorly organized with dead ends. Moreover, tumor tissues typically lack effective lymphatic drainage system. Both factors mean particles lodging in tumors will have an elongated retention time.

There is a growing trend of tailoring particles smaller for the EPR effect. Several researchers have claimed that particle sizes below 30 nm are desirable in some cases[4-6]. It is also stated that sizes within 10-100 nm are able to deliver drug efficiently and to facilitate long circulation in blood and higher uptake of drug in tumor[7]. Meanwhile, there is a limit since particles smaller than 20 nm cannot be prevented from renal clearance[8-10]. It is pointed out that the reduction in size increases uptake by both dissolution and particulate pathways, but the increased self-agglomeration of small particles can, paradoxically, lead to reduced uptake[11]. Researchers have also shown that different tumors have different pore sizes and they also change as a function of time[12].

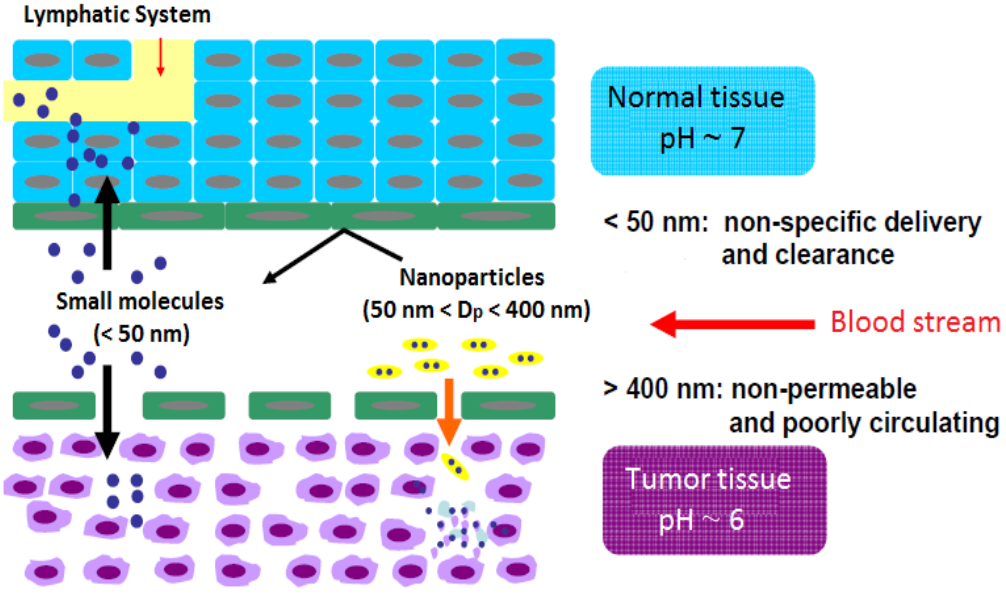

Figure 1.1 Specific drug delivery via the enhanced permeation and retention effect[103].

It is clear that there is no universally accepted standard, in regards to particle size for the EPR effect. Because pore sizes vary greatly, future development of nanoparticles for drug delivery must be customized in size depending on cancer type and position. Therefore, more specific particle size control is desired, we should be prepared to be able to produce nanoparticles with desirable sizes. There is a need for manufacturing processes, in which size of the resulting nanoparticles can be at least predicted and controlled. In order to utilize EPR effect, our goal was first to prepare nanoparticle in 50-400 nm and control their size by mixing condition, solvent systems, selection of drug and polymer.

1.2 Nanoparticles and Flash Nanoprecipitation

Nearly 40% of active pharmaceutical ingredients are hydrophobic, thus it is very challenging to deliver them in aqueous solution for clinical evaluation[13]. That is why nano-scale systems such as emulsion[14], micelle[15-20], liposomes[21], and polymersomes[22], draw enormous attention as drug delivery tools. Nevertheless, their loading capacities are typically low (less than 20%[23-25], and frequently less than 5% for paclitaxel) and limited by the solubility of drug in hydrophobic moiety of surfactant or polymer excipient[26]. Pure drug particles can overcome these limitations and have been widely used in industrial production and laboratory experiment. Industrial processes are usually in the top down category include media milling, grinding and high pressure homogenization. The disadvantages are large particle size, broad distribution, long processing time, contamination and high power source required. In laboratory studies, nanoparticles are often prepared from molecular level via bottom up processes, such as traditional drop-wise precipitation etc. But, these methods also have trouble producing nanoparticles

below 200 nm and need long processing time from a few hours to weeks[27-31] in order to reach thermodynamic equilibrium[32, 33]. To overcome this limitation, a kinetic process, flash nanoprecipitation, is introduced in this work.

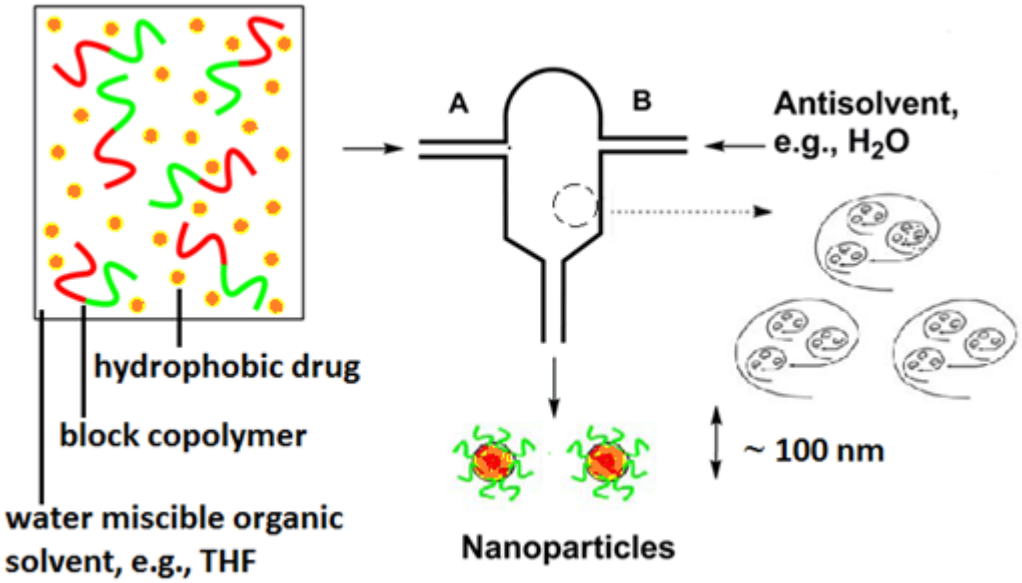

Figure 1.2 Schematic of flash nanoprecipitation to form hydrophobic drug loaded block copolymer protected nanoparticles[67].

Flash nanoprecipitation was developed by Prud'homme et al via vortex mixer and confined impingement jets (CIJ) mixer[34-39] and further improved in our laboratory via CIJ with a dilution (CIJ-D) mixer[40]. In this process as shown in Figure 1.2, amphiphilic block copolymer and hydrophobic drug are first dissolved in a water miscible organic solvent, which is impinged rapidly with antisolvent, typically water. The supersaturation condition drives organic solutes to precipitate out of the solvent mixture, nucleate and grow into particles. A diblock copolymer is added to provide steric stability to these particles. The hydrophobic block of copolymer co-precipitates with drug to form particle cores, while the hydrophilic block of copolymer arrests particle growth via steric stabilization. The solvent mixing can be achieved in a few seconds, which is obviously

more efficient that overnight drop-wise precipitation. Nanoparticles are kinetically formed which makes it possible to control particle size in a range of 50-400 nm by micromixing condition. The drug loading is extremely high which is beyond the capability of all thermodynamic equilibrium systems such as micelle, emulsion, or liposome. Therefore, flash nanoprecipitation has already been applied to anti-cancer drug formulation[41] and bioimaging[42-45] nanoparticles.

1.3 Paclitaxel Formulation and Controlled Drug Release

In this work, paclitaxel was chosen as the anti-cancer drug for nanoparticle chemotherapeutic formulation development. It was first discovered by Monroe E. Wall and Mansukh C. Wani in 1967, by isolating from the bark of the Pacific Yew tree[46]. It promotes polymerization of tubulin, stabilizes microtubules and interferes with the normal breakdown of microtubules in cell division, resulting in cell cycle arrest and eventually cell death. It is a mitotic inhibitor in chemotherapy, widely used for patients with ovarian, breast, non-small cell lung cancers and AIDS-related Kaposi's sarcoma[46, 47].

Current paclitaxel-based formulations have several limitations. For instance, in Taxol®, paclitaxel is dissolved in Cremophor EL®, a 1:1 mixture of polyethoxylated castor oil and ethanol, whereas Cremophor EL® is toxic with a large amount needed to enhance the low solubility of paclitaxel[48-51]. It causes non-specific delivery of paclitaxel during blood circulation with severe side effects[52]. Another formulation, Abraxane® is a nanoparticle formulation with albumin[53]. Although it eliminates the use of Cremophor and its toxicity, FDA approved its use only for certain types of patients at certain stages[54,55]. Also Taxol® is now generic, Abraxane® is more expensive[56] than Taxol® due to engineering challenges in formulation production. Genexol® uses block copolymer to

solubilize paclitaxel with much less toxicity related to delivery agents, but it is now facing neurotoxicity safety issues in phase II trials[57]. Briefly, those paclitaxel formulations have common problems, such as non-specific drug delivery, toxicity of delivery agent and low drug loading in 1-10 wt%[53, 58].

In order to improve paclitaxel delivery, the goal of this work was to use biodegradable amphiphilic block copolymer as delivery agent to prepare paclitaxel containing nanoparticles with high drug loading made via flash nanoprecipitation. More importantly, this thesis focused on characterizing drug delivery and controlling drug release by several strategies, such as controlling particle size, and prodrug modification of pacltiaxel, with customized hydrophobicity and hydrolytic lability etc.

1.4 Thesis Outline and Novelty

In Ch.2 we describe a simple and efficient mixer to prepare nanoparticles via flash nanoprecipitation. A modified version of Prud'homme's confined impingement jets (CIJ) mixer[34, 37] is introduced here with the addition of a dilution stage. The new design of CIJ-D mixer was manufacturing in our laboratory. β-carotene was used as a model drug. It is inexpensive and highly hydrophobic. The amphiphilic block copolymer (PEG-*b*-PLA) was used to stabilize nanoparticles in size and stability. To understand the importance of dilution stage, β-carotene nanoparticles were first prepared without dilution, or with an immediate or delayed dilution. Also, the dilution volume was varied. Particle sizes at different conditions clearly demonstrated that dilution is very necessary to quench particle growth and high supersaturation level is substantial to create multiple nuclei resulting smaller particle size. We have also compared sizes of nanoparticles prepared by

CIJ-D mixer and multi-inlet vortex mixer (MIVM). At varied flow rates, particle size decreased as flow became more turbulent, characterized by Reynolds number (*Re*). At the same *Re*, nanoparticles from CIJ-D mixer were slightly smaller, which indicated that head-on impingement in CIJ-D mixing provided better micromixing condition.

The novelties of this chapter are that 1) the confined impingement jets mixer was first modified with a dilution stage, to overcome the limitation on supersaturation level by equal volume impingement of solvent and antisolvent. 2) The effect of dilution was investigated in terms of particles nucleation and growth. The dilution needs to occur < 5s after mixing and > 5 fold in volume in order to create sufficient supersaturation. 3) The relation of particle size vs. flow conditions was established, and the threshold of sufficient turbulent condition was identified and estimated with *Re*>1000, to produce small and stable particles. Briefly, as an alternative to vortex mixer, CIJ-D mixer is simpler, cheaper, and more efficient to produce nanoparticles via flash nanoprecipitation. It is a smaller lab scale unit, especially convenient for rapid screening of small quantity of new materials. The research results shown in the following chapters are all based on CIJ-D prepared nanoparticles. Most of the content of this chapter has been published in the *Journal of Pharm. Science*[40].

In Ch.3, nanoparticles were successfully prepared with 2'-triethyl silicate (Si) paclitaxel (PTX) and 2',7-triethyl silicate (Si) paclitaxel (PTX). They are silicate derivatized paclitaxel prodrugs with a higher hydrophobicity which was synthesized by Wohl et al[59, 60]. Paclitaxel was introduced as a hydrophobic pharmaceutical ingredient for chemotherapy, and silicate paclitaxel prodrugs as prodrug of paclitaxel, return to be active anti-cancer ingredient. They were characterized by dynamic light scattering (DLS),

nanoparticle tracking analysis (NTA), scanning electron microscopy (SEM), Cryogenic-transmission electron microscopy (Cryo-TEM) and high performance liquid chromatography (HPLC) in terms of size, distribution, morphology and drug loading. In order to determine drug loading more accurately, nanoparticles were purified using several techniques, such as membrane filter, hollow fiber diafiltration and ultracentrifugation. Ultracentrifugation was found to be the best method to remove un-encapsulated drug molecules and empty polymer nanoparticles. Another advantage of using ultracentrifugation was that drug loading levels of the ultracentrifuged nanoparticles were higher than the initial formula due to the removal of empty polymer particles. For long-term storage, nanoparticles were then lyophilized to remove solvent content from nanosuspension. The resulting product was particles in dry powder. However, we encountered a problem to recover particle size when redispersing particles in aqueous solution. Thus, sonication was studied in the relation of particle size reduction. Also, cryoprotectant, sucrose was used to protect particles from aggregation during freezing process. Based on the shelf life concern of our prodrugs and nanoparticles, aging studies were conducted for 32 weeks to monitor composition change of prodrug affected by hydrolysis in dry state and in aqueous state for the entire nanoparticle preparation process, from the very beginning of prodrug synthesis, to CIJ-D mixing, ultracentrifugation, lyophilization and redispersing in aqueous solution for 24 hr.

The novelties of this chapter are that 1) paclitaxel containing nanoparticles were successfully formulated and characterized with an average size of 120 nm and high drug loading above 50%. 2) The performance of filtration techniques were compared in terms of purifying particles and concentrating particle suspension. 3) Hollow fiber diafiltration

was first introduced, but it was not able to separate prodrug loaded and polymer particles. It is very efficient to concentrate nanoparticle solution and can be used for dispersion containing other micro- and nano-scale systems such as carbon nanotubes and graphene. Compared with simple filter filtration and hollow fiber filtration, ultracentrifugation was found to be the best method to separate prodrug loaded nanoparticles from prodrug molecules, polymer nanoparticles, and prodrug loaded small nanoparticles. 4) The size and composition of nanoparticles and the distribution of drug/prodrug were first analyzed among supernatant and final pellet after each time of ultracentrifugation. It clearly demonstrated that a great amount of free molecules were removed along with empty polymer nanoparticles. The loading of prodrug loaded nanoparticles collected from pellet increased to over 70% in particle mass. One downside was particle mass loss during ultracentrifugation. 5) Aging studies were first carried out to monitor hydrolysis rate of paclitaxel prodrug in solid compound state for months and in the entire process of nanoparticle preparation and post-treatments. Prodrugs hydrolyzed quickly after nanoparticles were in aqueous solution within 24 hr, and even hydrolyzed significantly after 5 week in dry state. Meanwhile, we have found that empty polymer nanoparticles degraded at pH 5.0 only after several days, which ruled out the possibility that polymer degradation leaves particles less protected and induces prodrug hydrolysis more quickly. In summary, paclitaxel with more hydrophobic silicate esters were encapsulated in PEG-*b*-PLGA nanoparticles and they have an extraordinary high loading compared to current PTX-based formulations in the market. In the following chapters, a standard procedure was established to prepare nanoparticles using CIJ-D mixer, followed with

ultracentrifugation and lyophilization. They were lyophilized and kept in dry state until nanoparticles were needed for *in vitro* and *in vivo* studies.

In Ch.4, *in vitro* drug release studies were carried out with a series of silicate (Si) paclitaxel (PTX) prodrugs. They were 2'-triethyl Si PTX (1a), 2',7-triethyl Si PTX (2a), 2'-trioctyl Si PTX (1b), 2',7-trioctyl Si PTX (2b), 2'-triisopropyl Si PTX (1c) and 2',7-triisopropyl Si PTX, synthesized with different silicate esters either at 2'carbon or both 2'carbon and 7 carbon position by Wohl et al[59, 60]. To establish a standard drug release protocol, several experimental conditions were used including infinite sink, limited buffer, pH at 7.4 and 6.4 to mimic acid environment of healthy tissues and tumor tissues. Several dialysis devices were used and evaluated. Among dialysis tube, cassette and capsules, dialysis mini capsules were chosen for *in vitro* drug release study. The drug release rates were determined reversely by quantifying the remaining drug left in nanoparticles. The effect of silicate ester type and position were studied in terms of controlling particle size, morphology and more importantly, drug release rates.

The novelties of this chapter are that 1) a limited sink condition achieved consistent release profiles when compared with infinite sink condition, by frequently refreshing buffer. 2) Several dialysis devices were compared to deliver better performance of release characterization, and dialysis mini capsules (MWCO: 10kDa) were chosen as the best for accurate results and ease of handling. 3) A reverse release protocol was established to determine the remaining drug in nanoparticles instead of released ones in buffer, to overcome the difficulty of quantifying extremely low concentration of drug in buffer due to the limited water solubility. Nanoparticles studied in this chapter were unfortunately not ultracentrifuged after CIJ-D mixing, thus the

diffusion of un-encapsulated drug mixed with nanoparticles caused a significant burst-release pattern. However, the release study protocol was established by using mini dialysis capsules, with frequently refreshed buffer and by determining the remaining drug in nanoparticles by HPLC.

In Ch.5, seven types of silicate ester were introduced to silicate paclitaxel prodrug synthesis. They were 2'-triethyl Si PTX (1a), 2',7-triethyl Si PTX (2a), 7-triethyl Si PTX (3a), 2'-trioctyl Si PTX (1b), 2',7-trioctyl Si PTX (2b), 2'-triisopropyl Si PTX (1c), 2',7-triisopropyl Si PTX (2c), 2'-ditert butyl/ethyl Si PTX (1d), and 2'-trimenthyl Si PTX (1e). Nanoparticles formulated with these prodrugs were ultracentrifuged between CIJ-D mixing and lyophilization. The release profiles were more sustained without any drastic burst pattern. With a broad range of customized hydrophobicity and hydrolytic lability, nanoparticles displayed a trend of smaller nanoparticle size with more hydrophobic compounds, and they released slower with more hydrolytic stable prodrugs. To determine the accuracy of the reverse release protocol, a series of mass balance studies were conducted to determine whether the remaining and the released drug were complementary. Meanwhile, the composition of prodrugs, partially hydrolyzed prodrugs and PTX obtained from hydrolysis were determined, this helped us understand the release mechanism for particles encapsulating with different Si PTX prodrugs and their regeneration of PTX. The general delivery of PTX could be contributed by diffusion, hydrolysis, and a combination of the two. More hydrolytic labile prodrugs hydrolyzed relatively fast, more PTX regenerated from hydrolysis was found, while hydrolytically stable prodrugs hydrolyzed very slowly, so the diffusion of the prodrug was dominant.

These phenomena are potentially beneficial for our future work in order to control release rate by tuning the hydrolytic lability and hydrophobicity.

The novelties of this chapter are that 1) mass balance studies demonstrated that the reverse release protocol was able to provide release profiles as accurate as the traditional release protocol directly determining the released drug in buffer. 2) Composition change of drug and prodrug were different in nanoparticles and in buffer, which indicated prodrug hydrolysis was affected by the microenvironment of nanoparticles. 3) Nanoparticles with all prodrugs displayed a higher release rate when *in vitro* drug release studies were carried at pH =5.0. It implied that pH-responsive hydrolysis contributed to general release in varied levels, and potentially can be a strategy to control drug release and regeneration of PTX.

In Ch.6, nanoparticle size and morphology were mainly characterized by DLS, NTA and Cryo-TEM. Hundreds of Cryo-TEM images which obtained by Lee[61] were used to determine particle size and distribution as well. They clearly showed morphology change of nanoparticles from fresh state, to lyophilized and redispersed for release studies. The novelties of this chapter are that 1) DLS, NTA and Cryo-TEM gave consistent particle size. 2) The visualization of core-shell structure was obtained for the first time and it confirmed nanoparticles were kinetically formed via nucleation and growth. 3) Particle shrinking and disassembly was observed after 24 hr release, which lead to a speculation that polymer might degrade or particle collapsed and caused irregular shape of nanoparticles over time.

In Ch.7, key results in previous chapters are summarized. Recommendations for future research are discussed including loading two or more prodrug and other functional

ingredients in nanoparticles, using other block copolymer, drug release study in cell culture or serum (*in vitro* or *in vivo*) which is closer to biological condition, and polymer degradation study.

Chapter 2

Flash Nanoprecipitation: Multi-Inlet Vortex Mixer vs. Confined-Impingement Jets Mixer

Abstract: Johnson and Prud'homme[34] introduced the confined impingement jets (CIJ) mixer to prepare nanoparticles loaded with hydrophobic compounds (e.g., drugs, inks, fragrances, or pheromones) via flash nanoprecipitation (FNP). We have modified the original CIJ design to allow hand operation, eliminating the need for a syringe pump, and we added a second antisolvent dilution stage. Importantly, the dilution stage overcomes the need to operate the original CIJ mixer at equal flow rates of solvent and antisolvent. This new CIJ-D mixer (confined impingement jets with dilution) is simple, cheap and efficient to produce nanoparticles. We have made 55 nm diameter β-carotene nanoparticles using the CIJ-D mixer. They are stable and reproducible in terms of particle size and distribution. We have also compared the performance of our CIJ-D mixer with the vortex mixer, which can operate at unequal flow rates[39], to make β-carotene-containing particles over a series of turbulent conditions. Based upon dynamic light scattering (DLS) measurements, the new CIJ-D mixer produces stable particles of a size similar to the vortex mixer. Our CIJ-D design provides an easily operated and inexpensive tool to produce nanoparticles via FNP and to evaluate new nanoparticle formulation.

Key words: CIJ mixer, nanoparticles, flash nanoprecipitation, drug delivery, β-carotene

2.1 Introduction

Nanoparticles have recently received enormous attention as a drug delivery tool[2, 62-65]. Flash nanoprecipitation (FNP) is a simple technique that is used to prepare polymeric nanoparticles with a high loading of hydrophobic compounds, including drugs[34, 37, 66]. As shown in Figure 2.1[67], a hydrophobic drug and an amphiphilic block copolymer (e.g. PEG-*b*-PLA, polyethylene glycol-*b*-polylactic acid) are co-dissolved in a water miscible organic solvent (e.g. THF), which is then impinged at high velocity against an antisolvent (water) to create turbulent mixing and high supersaturation. The supersaturation promotes co-precipitation of the hydrophobic drug and the hydrophobic block of the copolymer to form nanoparticles[38, 39, 68, 69]. Mixing and precipitation occur within milliseconds inside the small internal mixing chamber.

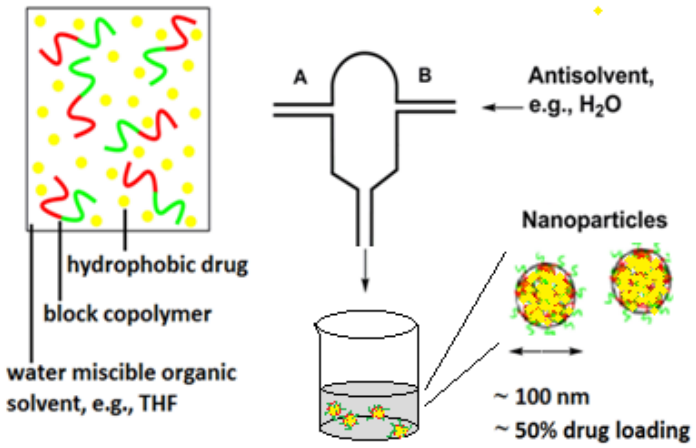

Figure 2.1 Schematic of flash nanoprecipitation process.

Johnson and Prud'homme[34] first described FNP using a confined impingement jets mixer (CIJ). In this design, a syringe pump was used to drive two opposing liquid streams (A and B in Figure 2.1) at high velocity into the mixing chamber. Prud'homme

and others[34-36, 59, 70-72] used this device to successfully make a variety of nanoparticles. The CIJ design was inspired by the simple T mixer that is commonly used to mix liquids or act as a chemical reactor[73, 74]. T mixers have also been used to mix monomers and oligomers for reaction injection molding[75-77].

To avoid reducing the mixing efficiency (via one stream backing up the other), the two streams in the CIJ mixer must operate at near equal momentum. In practice, this requires approximately a 1:1 volume flow rate, limiting the highest achievable supersaturation level. To operate at unequal flow ratios, Prud'homme and coworkers developed a multi-inlet vortex mixer[78, 79]. In this design, the mixing chamber is connected to four inlets and the liquid streams meet at an angle as opposed to the head-on impingement that is characteristic of the CIJ mixer. The vortex mixer can be applied to a wide range of solvent ratios and materials. However, the device is time consuming to clean and digitally programmed syringe pumps are usually required to control the inlet flow rates[80]. In terms of operation, cleaning and cost, the CIJ mixer is preferred. Nevertheless, the vortex mixer is able to achieve higher levels of supersaturation.

In this chapter, we report a modified CIJ design, the CIJ-D mixer, that is simpler than the original Johnson and Prud'homme design, yet overcomes the limitation of 1:1 solvent ratio. To emphasize its simpler design and easier handling with equivalent function, we have compared the average size of β-carotene nanoparticles made using our CIJ-D mixer vs. the vortex mixer at varied flow conditions.

2.2 Design

2.2.1 Interior Dimensions of CIJ-D Mixer

Figure 2.2 shows the confined impingement jets with dilution (CIJ-D) design. Two features distinguish it from the original CIJ mixer: hand operation and an antisolvent dilution stage. By using relatively small, low friction syringes, turbulent flow can be achieved with simple, rapid hand motion, eliminating the need for syringe pumps. A metal plate connects the two syringes to insure simultaneous actuation. To increase the supersaturation, the outlet stream from the CIJ-D chamber immediately flows directly into a large volume of water.

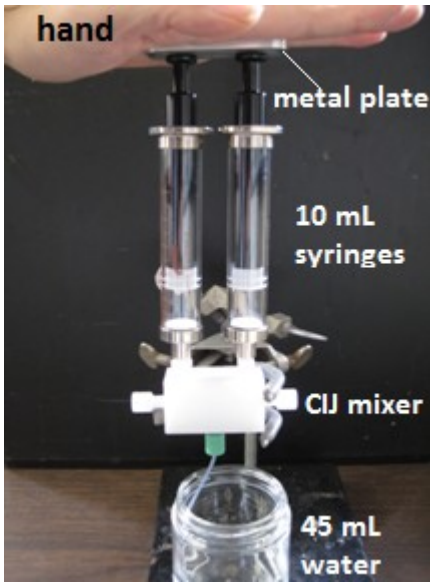

Figure 2.2 The CIJ-D mixer, hand operated with subsequent dilution.

The design dimensions for the CIJ mixing chamber was first recommended by Johnson and Prud'homme[34]. It has been redesigned in our laboratory and manufactured here in the physics machine shop (University of Minnesota). The innovation at UMN is to make an intact unit with the complete chamber and flow paths there, as composed to Prud'homme's CIJ mixer composed of three pieces merged together that were initially intended to get

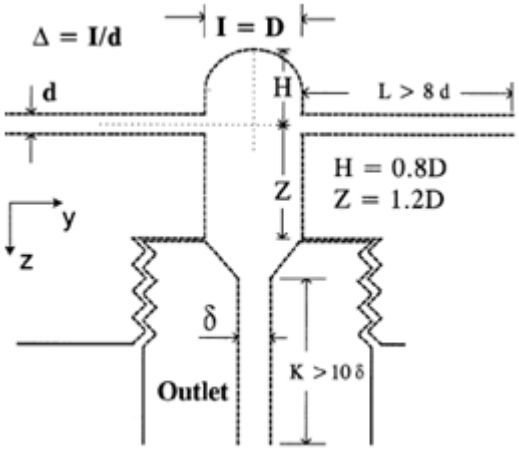

Figure 2.3 The original design of the CIJ mixer chamber by B.K. Johnson and R.K. Prud'homme.

interior chamber and paths exposed for manufacturing easiness. The original CIJ mixer was described with dimensions shown below[37]. In Figure 2.3, d=0.5 mm, L/d > 8 to insure the jets are stable, the chamber height to diameter H=0.8D, and length to diameter ratio H+Z=2.0D are held constant to maintain geometric similarity upon scale-up. The outlet tube runner is at least ten times the outlet diameter K/δ >10, in order to create a pressure drop and ensure that the chamber is filled with liquid during impingement.

Figure 2.4 shows the dimensions of our CIJ-D chamber. In order to build a standard for manufacturing our CIJ-D mixer, a complete specification list was presented here for dimensions and raw materials. d=0.5 mm, H=2 mm, Z=3 mm, D=2.5 mm (D/d=4.76, H=0.8D, Z=1.2D). A ratio of entrance channel length to diameter L/d=6.1 is used to insure stable jets. The chamber volume is 25 μL.

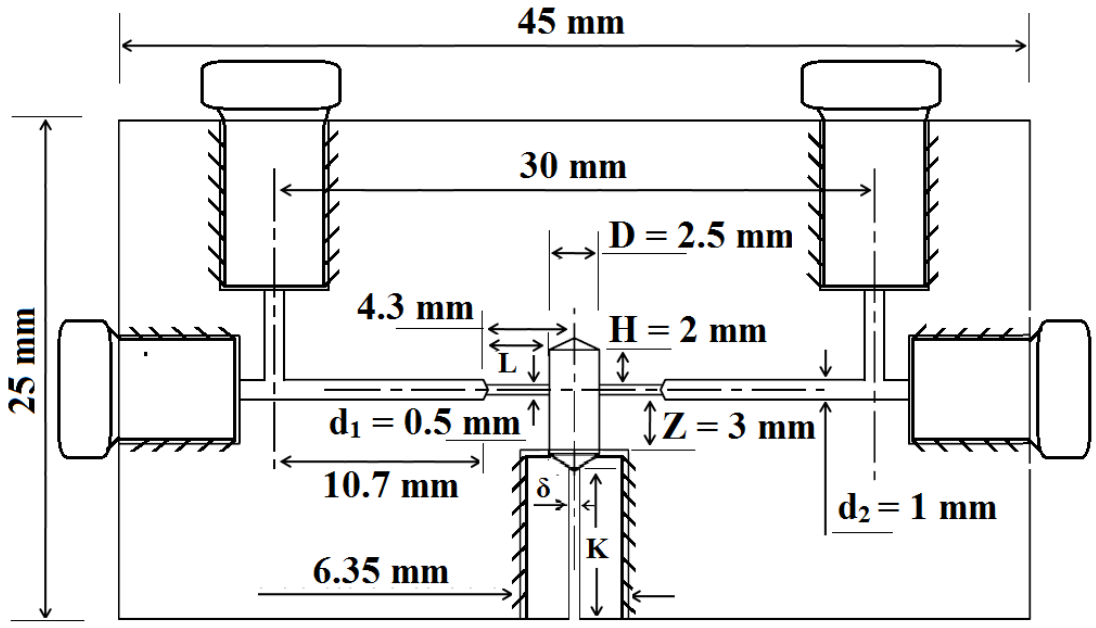

Figure 2.4 Dimensions of the CIJ-D mixer made of HDPE.

2.2.2 Raw Materials and Parts

The main body of the CIJ mixer is made of high density polyethylene (HDPE). All five openings are tapped with 1/4"-28 threads. The two inlets on the top in Figure 2.2 are threaded with white adapters (IDEX Health & Science, P604) fitted with glass or plastic syringes, and one outlet is threaded with green adapter (IDEX Health & Science, P205-X), and a blue cap (P-200X) inside threaded with a Teflon tube. Two additional side openings resulted when horizontal jet pathways were drilled during manufacturing. They are sealed with white plugs (IDEX Health & Science, P203-X) during FNP, but can be opened for thorough cleaning. An aluminum metal bar is placed on top of syringes to assure stable injection and simultaneous actuation.

2.3 Methods and Experiments

2.3.1 Materials

β-carotene was purchased from Sigma-Aldrich and used as received. PEG-*b*-PLA (MW: 5k-10kDa[81]) was synthesized in Hoye's lab. Water (H_2O, HPLC grade) and tetrahydrofuran (THF, HPLC grade) were purchased from Aldrich and used as received. Multiple 3 mL plastic syringes (Tyco Healthcare, MA) were used for solvent injection. A programmable pump (Harvard Apparatus, PHD 2000)[82] and a mechanical pump (Harvard Apparatus, model 945) were used for solvent injection with vortex mixer.

2.3.2 β-carotene (only) Nanoparticle Preparation

A typical procedure for making nanoparticles is as follows. β-carotene was used as the generic hydrophobic molecule. PEG-*b*-PLA was used as the amphiphilic block

copolymer. 25 mg β-carotene and 25 mg PEG-*b*-PLA were dissolved in 2.5 mL of THF and transferred to a 3 mL plastic syringe. 2.5 mL of water was loaded in a second 3 mL plastic syringe. The mixing occurred for 5 seconds and the co-mixed streams was immediately drained into a bottom reservoir pre-loaded with 45 mL of water. The final composition of the 50 mL dispersion was THF:H_2O = 5:95, containing 0.1 wt% of nanoparticles.

To prepare nanoparticles only composed of β-carotene via vortex mixer, which has same dimensions of Prud'homme's multi-inlet vortex mixer[39], 25 mg β-carotene was dissolved in 2.5 mL THF. The other three syringes contained 2.5 mL, 22.5 mL and 22.5 mL water, respectively. The four streams were all injected into vortex mixer at varied flow rates in order to complete mixing simultaneously. The resulting mixture was collected at the volume ratio of H_2O:THF= 95:5. The desired flow rates were programmed by digital and mechanical pumps.

To prepare nanoparticles only composed of β-carotene via CIJ-D mixer, 25 mg β-carotene was dissolved in 2.5 mL THF and impinged with 2.5 mL water. The mixture was diluted in 45 mL water resulting a same volume ratio as that made by vortex mixer. When they were prepared at different conditions, the desired flow rates were determined by the mixing time for the given volume of solvent when syringes were propelled by hand.

To investigate the effect of dilution stage in CIJ-D mixing, β-carotene nanoparticles were prepared without dilution, a delayed dilution or a smaller volume dilution. Their particle sizes and stability were compared with particles made by the standard procedure above.

To test performance of CIJ-D mixer, β-carotene nanoparticles made by the CIJ-D mixer were compared to those made by vortex mixer. The flow conditions were varied simply by changing hand velocity during CIJ-D mixing and adjusting flow rates on digital pumps during vortex mixing. Particle sizes were characterized at each flow rate.

2.3.3. Particle Size and Distribution

Mass average particle size and distribution was determined by dynamic light scattering (DLS) (ZetaPALS, Brookhaven) with a diode laser BI-DPSS wavelength of 659 nm, using REPES method[67, 83, 84]. The light intensity correlation function was collected at 25 ˚C and a scattering angle of 90˚.

DLS is based on the technique-photon correlation spectroscopy (PCS) of quasi-elastically scattered light (QELS), which is dependent on correlating the fluctuations about the average, the scattered and the laser light intensity. Light can be treated as an electromagnetic wave. The oscillating electro-magnetic field induces oscillations of the electrons in a particle. These oscillations change from the source of scattered light. The average intensity of the scattered light has been used to determine particle size, in DLS measurement. Generally speaking, DLS measurement is based on Stokes-Einstein relation, correlating diffusion coefficient with particle size.

$$D = \frac{K_B T}{6\pi\eta R} \qquad \text{Eq. 2.1}$$

D is the diffusion coefficient, k_B is Boltzmann's constant, T is the absolute temperature, η is viscosity, R is the hydrodynamic radius of spherical particles.

When we discuss particle size, the mass average size is mainly used

$$\overline{d_{\mathrm{m}}} = \sum n_i m_i d_i / \sum n_i m_i = \sum n_i d_i^{\,4} / \sum n_i d_i^{\,3} \qquad \text{Eq. 2.2}$$

n_i is the number of particles with a diameter of d_i, m_i is the mass of a particle with a diameter d_i.

Intensity Average Size:

$$\overline{d_I} = \sum n_i d_i^6 \Big/ \sum n_i d_i^5 \qquad \text{Eq. 2.3}$$

n_i is the number of particles with a diameter of d_i.

2.3.4 Reynolds Number

Mixer efficiency is typically correlated with Reynolds number, the ratio of inertial force to viscous force. The Reynolds number was calculated in

$$Re = \frac{inertial\ force (= \rho V^2)}{viscous\ force\ (= \frac{\mu V}{d})} = \frac{\rho V d}{\mu} = \frac{\rho Q d}{\mu A} \qquad \text{Eq. 2.4}$$

In our case, Reynolds number was calculated by accumulating multiple streams when using the CIJ-D or vortex mixer in Eq. 2.5.

$$Re = \sum_{i=1}^{n} Re_i = \frac{d}{A} \sum_{i=1}^{n} \frac{\rho_i Q_i}{\mu_i} = \frac{4}{\pi d} \sum_{i=1}^{n} \frac{\rho_i Q_i}{\mu_i} \qquad \text{Eq. 2.5}$$

where ρ is the density of the fluid (kg/m^3), V is the mean fluid velocity (s), d is the stream inlet diameter, μ is the viscosity of the fluid (kg/m·s), A is the pipe cross-sectional area (m^2) which in our case was the same for all inlets of a given mixer, and Q_i is the volumetric flow rate (m^3/s) of the ith inlet stream.

For example, in CIJ mixing, n=2 for two streams, ρ is 1.0×10^3 kg·m^{-3} for H_2O, or 8.89×10^2 kg·m^{-3} for THF at room temperature, μ is 1.0×10^{-3} Pa·s at room temperature for

H_2O, or 4.8×10^{-4} Pa·s for THF, and d is 5×10^{-4}m for the CIJ-D mixer. In vortex mixing, it has four inlets, each with diameter d=1.45×10^{-3} m. We assumed μ=1.0×10^{-3} Pa·s and ρ = 1.0×10^{-3} kg·m^{-3} at room temperature, since 95%H_2O/5%THF has a similar kinematic viscosity to that of water. More Reynolds number calculation are in Appendix B.

2.4 Results and Discussion

2.4.1 Design Comparison between MIV Mixer and CIJ-D Mixer

Currently, we have two apparatuses to make nanoparticles based on FNP process, the multi-inlet vortex (MIV) mixer and the CIJ-D mixer. The vortex mixer was manufactured by Prud'homme at Princetion University. The CIJ-D mixer was manufactured in our laboratory at University of Minnesota. The two mixers are shown in Figure 2.5(a) and (b). Though the CIJ mixer and the vortex mixer are two embodiments of flash nanoprecipitation, they are different in several aspects in terms of design.

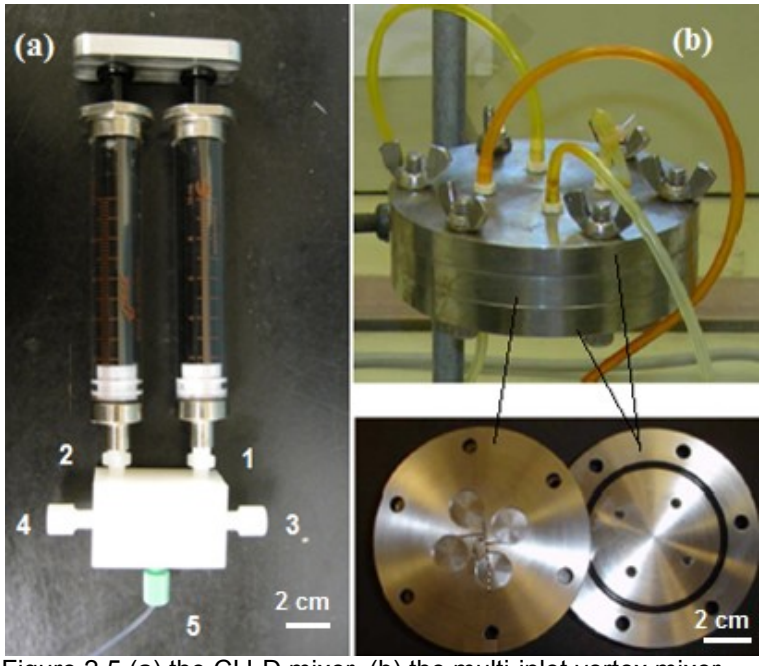

Figure 2.5 (a) the CIJ-D mixer. (b) the multi-inlet vortex mixer.

Streams Quantity: The CIJ-D mixer has only two stream pathways, as shown in Figure 2.5(a). Two syringes are inserted in the two inlets. The drug and BCP are both dissolved in the organic solvent in syringe 1, and water is contained in syringe 2. In the vortex mixer, four syringes are connected to four inlets as shown in Figure 2.5(b). One inlet delivers the drug and BCP dissolved in organic solvent. The other three deliver large amount of antisolvent water to achieve high supersaturation.

Injection operation: Using vortex mixer, two syringes containing smaller volume organic solvent and antisovlent are propelled by a programmable pump. The other two syringes containing water in larger volume are propelled by a mechanical pump. Both pumps can be digitally set with a wide range of flow rates, up to 120 mL/min, matching the solvent with the antisolvent streams to achieve simultaneous mixing. For the CIJ mixer, two syringe injections are operated by hand. The metal bar on top of them will keep syringes driven simultaneously and steady if a more accurate flow rate is needed, the two syringes can also be propelled by a programmable pump.

The incident angles of incoming streams: in Figure 2.6, the vortex mixer has four steams directed into a mixing chamber with the incident angle of 90°. They are forced to the walls of the mixing chamber by centripetal forces, instead of impinging with each other. In the CIJ-D mixer, two streams are directed towards each other with the incident angle of 180°. This essentially increases the mixing velocity in micromixing condition. Johnson and Prud'homme speculated that the angling

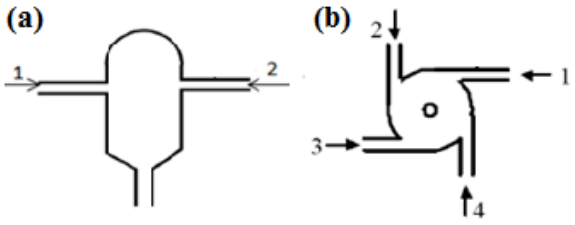

Figure 2.6 The mixing chamber of (a) the CIJ-D mixer and (b) the vortex mixer.

of inlet streams can affect the micromixing performance[37], but we have not gained any solid evidence to demonstrate this point.

Mixing processes: In the vortex mixing, unequal volumes of solvents can be used. In our case, syringe 1 contains 2.5 mL THF, and the other three streams contain 2.5 mL, 22.5 mL, and 22.5 mL of water respectively. This combined mixture has a composition of H_2O:THF=95:5. This is very high supersaturation level for hydrophobic drug and amphiphilic BCP, which can be reached directly in one-step vortex mixing. In the CIJ mixing, two identical volumes of solvent and antisovlent impinge with each other and collide at equal momentum. For instance, 2.5 mL of H_2O and 2.5 mL of THF (50:50 vol:vol) are impinged. This is far below the supersaturation level in vortex mixing, therefore the outlet of the mixer is connected to a beaker containing a large volume (45 mL) of H_2O to further dilute nanosuspension, with a final combined ratio of H_2O:THF=95:5. The dilution is expected to diminish Ostwald ripening and recrystallization of solutes.

2.4.2 The Necessity of Dilution in CIJ-D Mixing

When formulating nanoparticles by a “one-step” vortex mixing, the supersaturation level is determined by a volume ratio of H_2O:THF=95:5. In comparison, nanoparticles made by CIJ-D mixer follows a “two-step" process, during which a volumetric ratio of H_2O:THF reaches 50:50 in the first step of impingement in the mixing chamber. Then in the second step, the final ratio of H_2O:THF reaches 95:5 by dilution. As Prud’homme[85] and also Pustulka[85, 86] showed, there are two critical time scales involved in FNP process, mixing time (τ_{mix}) and nucleation and growth time (τ_{ng}). In order to understand their relation, especially to find out where particle nucleation and

growth occurs during CIJ-D mixing, β-carotene nanoparticles were prepared by CIJ-D mixing either with a complete two-step process, or only impingement or only dilution.

In Group 1, β-carotene particles were prepared by CIJ mixing followed with an immediate dilution. A volume of 2.5 mL THF containing 25 mg β-carotene was impinged with 2.5 mL H_2O in the CIJ mixer chamber and further diluted in 45 mL H_2O. It took 10-12 seconds to empty the syringes of 2.5 mL THF and H_2O simultaneously, thus the flow rate (Q) is 12.5~15 mL/min and Reynolds number (Re) = 1500~1800. In Group 2, β-carotene particles were only prepared by the first-step of impingement. A volume of 2.5 mL THF containing 25 mg β-carotene was impinged with 2.5 mL H_2O in the CIJ mixer chamber and collected directly without further dilution. The flow rate was controlled as the same as Group 1. In Group 3: β-carotene particles were prepared only by the second step of dilution. A volume of 2.5 mL THF containing 25 mg β-carotene and 2.5 mL H_2O were directly injected to 45 mL H_2O without using the CIJ mixer. The flow rate was controlled as the same as Group 1. This method is often the case for the traditional drop-wise precipitation or simple stirring in a tank, but drop-wise addition of solvents often takes place for hours. Two batches of β-carotene particles were formulated in each group. Their particle size and distribution was measured by DLS and averaged among two batches and three measurements in each batch. The mean mass average size in Group 1 was 60.0±4.0 nm, 412.2±7.2 nm in Group 2, and 69.5±3.3 nm in Group 3.

β-carotene nanoparticles had very similar size in Group 1 and 3, both of which were prepared with dilution. It implied that high supersaturation level is very important to make particles with small sizes, even the CIJ mixer is not employed. While CIJ impingement was not used in Group 3, the mixing time was longer than that in Group 1,

and particle size was slightly bigger in Group 3. Particles prepared in Group 2 were much larger than the other groups, because the supersaturation level was a lot less, indicated by the volume ratio of H_2O:THF=50:50. The nucleation and growth time was relatively fast as opposed to the mixing time, so particles had more chance to grow to a larger size. Without the quench effect of dilution, particles probably aggregated as well during the time interval about five minutes between mixing and DLS measurement.

Figure 2.7(a) shows schematically how supersaturation increases as THF (solvent) and H_2O (anti-solvent) mix during flash precipitation. Supersaturation is defined as

$$S = \frac{C}{C_\infty} \qquad \text{Eq. 2.6}$$

C is total mass of solute divided by the final volume of solvent mixture. C_∞ is the bulk solubility of drug in solvent mixture.

Initially, drug and polymer are dissolved in 100% THF where they are soluble. As more water is introduced in THF/H_2O mixture, the solubility of drug C_∞ gradually decreases indicated by the red line, while C remains constant indicated by the black line. Thus, supersaturation S increases as the distance between black and red lines get longer. When 50/50 THF/H_2O is mixed in the mixer chamber approximately within 10 ms shown by (2) CIJ in Figure 2.7(a), the blue arrow shows the difference of the initial concentration and solubility of drug, which is an indicator of supersaturation using CIJ mixer. As mixture is diluted in water, the supersaturation continues to increase shown by (1) CIJ-D in Figure 2.7(a). In comparison, vortex mixer allows THF and H_2O mixing in varied volume and achieve the desire solvent mixture ratio shown by (4) vortex.

Prud'homme[35, 39, 78] believed that the nucleation of particles occurs very quickly in 10-20 milliseconds, which is in the same timescale of mixing shown in Figure 2.7(a).

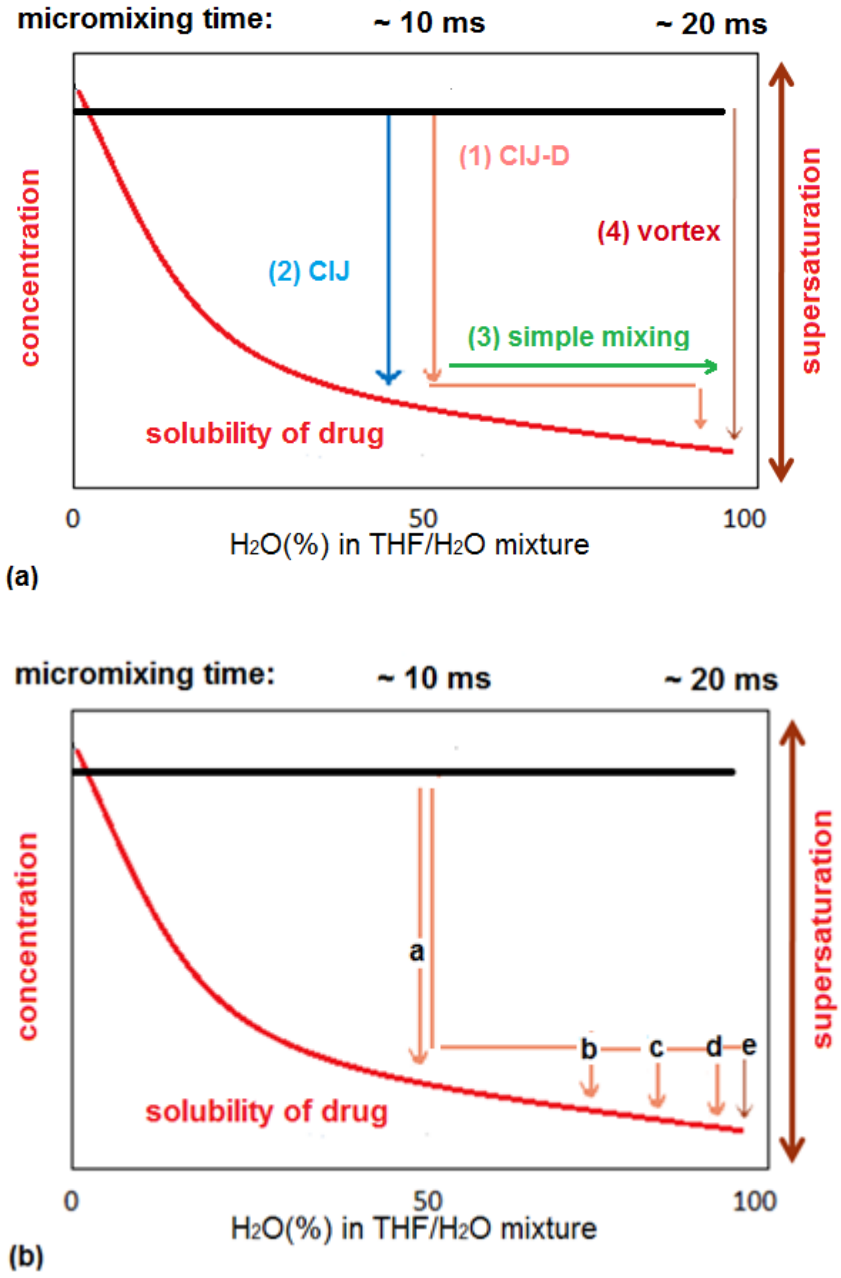

Figure 2.7 (a) Supersaturation condition when solubility of drug decreases as H_2O% increases in THF/H_2O mixture during micromixing of flash nanoprecipitation. (b) Supersaturation condition via CIJ-D mixing with dilution of (a) 0 mL, (b) 5 mL, (c) 10 mL, (d) 25 mL and (e) 45 mL.

The CIJ-D mixer provides more turbulent mixing in micromixing environment than the regular precipitation (simulated in Group 3), the kinetic energy of particles via the CIJ mixing is higher to prevent aggregation. Therefore, particle size in Group 1 was slightly smaller than that in Group 3. When supersaturation level is relatively low, nuclei continue to grow driven by diffusion (Group 2). When the supersaturation level is high, particle growth will be quenched by the limited diffusion (Group 1&2) shown in Figure 2.7.

2.4.3 The Effect of Varied Dilution

As mentioned above, the dilution stage allows high supersaturation while maintaining the 1:1 flow ratio of the impingement streams in CIJ-D mixer. In order to demonstrate the effect of dilution stage, four groups of β-carotene particles were made following the standard procedure described previously but with differing dilution. These particles showed good short-term (~4 hr) stability due to slightly negative surface charge[87] as judged by zeta potential (ζ) measurements[33].

In group same as 1 above, nanoparticles were made following the standard procedure, immediate dilution into 45 mL water as shown by (e) in Figure 2.7(b). The resulting mass average size was 55 nm. In group same as 2 above, nanoparticles were made without dilution as shown by (a) in Figure 2.7(b). They were unstable, and aggregated to micron size in seconds. In group same as 3 above, dilution was delayed from ~10 ms (residence time in the mixer and outlet tube) to 5 s. This also resulted in unstable microparticles (> 1 μm). In group 4, nanoparticles were made with immediate (10 ms) water dilution but less than 45 mL (e.g., (b) 5 mL, (c) 10 mL, and (d) 25 mL in Figure 2.7(b) or H_2O% in mixture=75.0%, 83.3% and 91.6% or THF/ H_2O=0.33, 0.20

and 0.091 shown in Figure 2.8). As shown in Figure 2.8, none of them produced 55 nm nanoparticles. Instead, all were much bigger, approximately 1400 nm, 200 nm and 167 nm, respectively and eventually unstable. These experiments show that immediate dilution with a significant amount of water is indispensable to produce small and stable nanoparticles.

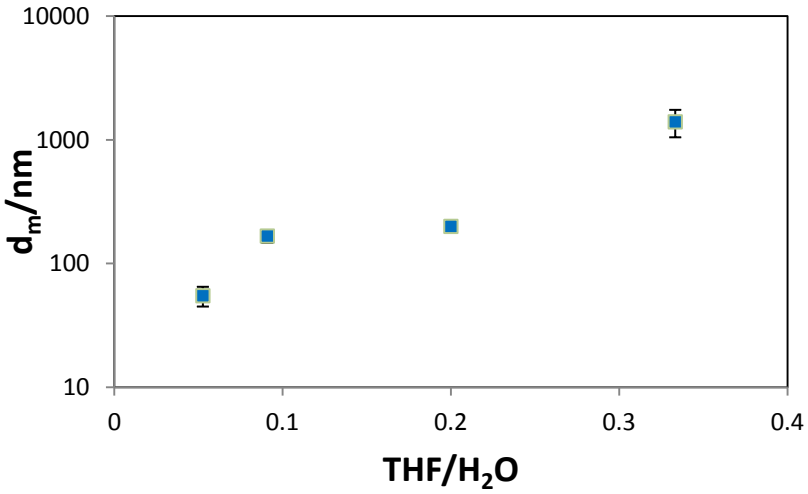

Figure 2.8 Mass average diameter of β-carotene particles vs. THF/water ratio in group 4.

2.4.4 Performance Comparison

To test the CIJ-D mixer, β-carotene loaded PEG-*b*-PLA stabilized nanoparticles were prepared following the typical procedure given above. DLS gave mass average diameter of 38 nm with polydispersity of 1.6 and standard deviation of 6 nm for three measurements on three separately mixed samples. The particles were stable for several weeks. In other block copolymer and model drug studies, we have also used PEG-*b*-PLA and PEG-*b*-PLGA (polyethylene glycol-*b*-poly (lactic-co-glycolic acid)) with a series of molecular weight (5k-*b*-10kDa, 5k-*b*-15kDa etc.) to make nanoparticles loaded with β-carotene. Zhu[67] used hydrocortisone, paclitaxel, betulin and their derivatives to test the

capability of the CIJ-D mixer for preparing polymeric nanoparticles. They were successfully produced, reproducible in terms of size.

We also compared the sizes of these pure β-carotene nanoparticles made by the CIJ-D mixer to those made by the vortex mixer. Particle size was varied by varying the flow rate, Q. This was accomplished simply by changing hand velocity during CIJ-D mixing and adjusting flow rate on programmable pumps during vortex mixing. The micromixing were characterized by Reynolds number.

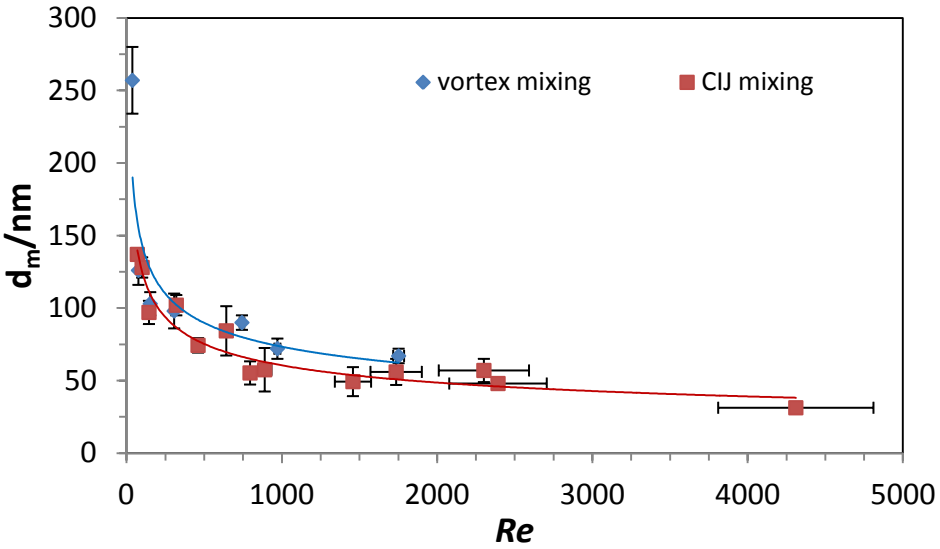

Figure 2.9 Mass average size of β-carotene particles (d_m) vs. Reynolds number (*Re*). Particles were made using both the vortex mixer and CIJ mixer.

The mass average diameters shown in Figure 2.9 are averages of three measurements on three separately samples prepared under the same conditions. The vortex mixing data were obtained from Zhu[67]. The error in the calculated Reynolds number came from variation of injection time. In vortex mixing, errors were minor since the injection time was mechanically controlled by syringe pumps, but it was relatively large in CIJ-D mixing due to uncertainty in timing the hand motion. At the highest

Reynolds number, the injection time of the CIJ-D mixer was 4.2±0.3s. 2.5 mL of solvents in two 3 mL syringes were used thus the flow rate was $1.2\times10^{-6}m^3/s$. Considering this flow rate and the tubing dimensions (1 mm inside diameter and 15 mm long), the residence time in the chamber and outlet tube before dilution was approximately 10 ms. For $Re<1000$, a syringe pump was used with the CIJ-D mixer because hand operation cannot be controlled well enough to create steady mixing over minutes.

The results in Figure 2.9 showed good agreement between the new CIJ-D design and the vortex mixer. Because of the rapid injection, the CIJ-D can reach $Re>4000$, twice the limit for the vortex mixer, and particle size of 30 nm, half the smallest size from the vortex mixer. At the same *Re*, particle size for the CIJ-D mixer was slightly smaller.

A potential problem with hand operation of the CIJ-D mixer is the start-up of flow. The *Re* at the beginning of impingement will be lower due to the time required to accelerate the syringes. The same problem occurs with syringe pumps, but because the impingement time is longer, it is possible to discard the first part of the product. This start-up transient could lead to broader particle size distribution, but we observed broad size distribution in both the CIJ-D mixer and the vortex mixer. For example, at $Re=1750$, DLS gave size polydispersity indices[67] of 0.5−0.8 for both samples.

2.5 Conclusion

A simple modification of Johnson and Prud'homme's confined impingement jets (CIJ) mixer has been used to make stable and reproducible nanoparticles. The addition of a dilution stage after mixing results in higher levels of supersaturation, and overcomes the limitation of equal volume ratios required in the original CIJ design. For our β-carotene

particles we found that the dilution needed to be rapid, < 5s after mixing, and extensive, >5 fold. Hand-operated impingement with small syringes creates sufficient turbulent mixing, ideal for flash nanoprecipitation of hydrophobic compounds with diblock copolymers to form kinetically trapped, sterically stabilized nanoparticles. With these modifications, the new mixer, called CIJ-D to emphasize the addition of a dilution stage, is easy to operate and inexpensive, making it more effective for rapid screening of small quantities of new materials, via FNP, compared to alternative mixers and other methods. It is especially attractive for evaluation of new drug formulations for their stability to produce nanoparticles[88-91].

Chapter 3

Silicate Paclitaxel loaded Block Copolymer Protected Nanoparticles: Preparation and Post-Treatment

3.1 Introduction

It is well known that cancer is a leading deadly disease, causing about 13% of all human death in the world (2008)[1]. Numerous researchers have dedicated their lives in an attempt to find effective methods to treat cancer. Several attractive methods have been developed, such as chemotherapy, radiation and surgery. Chemotherapy, is the most widely used and effective treatment for cancer. However, its undesirable toxicity causes adverse side effects on patients, due to non-specific delivery of anticancer drugs to normal tissues. Accordingly, the goal in my work is to develop nanoparticle formulations that can act as specific-delivery chemotherapeutic treatment, effective for targeting tumor tissues with minimal side effects.

Paclitaxel (PTX)[47, 92] is an anti-cancer drug approved by U.S. Food and Drug Administration (FDA). It was first discovered by Monroe E. Wall and Mansukh C. Wani in 1967, by isolating from the bark of the Pacific Yew tree[93]. It promotes polymerization of tubulin, stabilizes microtubules and interferes with the normal breakdown of microtubules in cell division, resulting in cell cycle arrest and eventually cell death. It is a

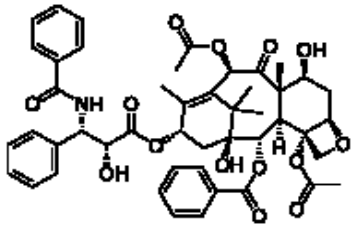

Figure 3.1 Chemical Structure of Paclitaxel[47].

mitotic inhibitor in chemotherapy, widely used for patients with ovarian, breast, non-small cell lung cancers and AIDS-related Kaposi's sarcoma[47, 93].

Currently, there are three major commercial formulations of PTX. One is under the trademark of "Taxol®", developed by Bristol-Myers Squibb (BMS). PTX is dissolved and delivered in Cremophor EL®, a 1:1 mixture of polyethoxylated castor oil and ethanol. Cremophor EL® is necessary to overcome the low solubility of PTX in aqueous medium[48-51]. Taxol® was completely approved by FDA, but only ca. 1 wt% of PTX in Taxol® (6 mg PTX/527 mg Cremophor EL®/1 mL solution) is possible for intravenous administration[58]. A series of adverse side effects, including hypersensitivity, nephrotoxicity and neurotoxicity[52], occurred with a large amount of Cremophor EL® accompanying high drug dosage.

A newer formulation, under the trademark of "Abraxane®" is manufactured by Abraxis BioScience. PTX is complexed with albumin to form 130 nm stable particles in water solution[53]. Abraxane® avoids all Cremophor-related toxicities, with a notably higher loading of PTX, 5mg PTX/ 45mg albumin in 1 mL water solution[54] (ca. 10 wt% PTX in Abraxane®). The FDA has approved Abraxane® for treatment of breast cancer but only after failure of combination chemotherapy or cancer relapse within 6 months of adjuvant chemotherapy[54], because Abraxane® failed to increase median survival time for "first-line" (those have never been treated previously) patients[55] and it is more expensive than Taxol®[56].

In Phase I trial, Abraxane® and Taxol® were administered in doses up to 260 mg/m^2 and 175 mg/m^2 (unit: drug amount/body surface area[94], respectively). It was found in Phase II and III trials that Abraxane® and Taxol® presented different pharmacokinetic

parameters, tumor response rates and toxicity profiles. Abraxane® presented no difference in overall survival as compared to Taxol®. Also, it had a higher incidence of peripheral neuropathy, nausea, vomiting, and asthenia, while Taxol® had a higher incidence of neutropenia and hypersensitivity reaction[54]. For both of them, the toxicity of PTX on normal tissues is serious and worse if higher dosage is used, due to inevitably non-specific delivery. It strengthens the importance of selective delivery of PTX to tumor.

Another formulation, Genexol®-PM is a paclitaxel-containing polymeric micellar system, developed by Samyang Genex Co[95, 96]. Previously, PTX in Taxol® was obtained by a semisynthetic process from Taxus baccata, but in Genexol® it was obtained by a plant tissue culture technology. This technology enables the production of Genexol® with high purity, low purification cost, constant yield and without environmental problems[57]. Another advantage of Genexol® is using non-toxic, biodegradable, low molecular weight diblock copolymer PEG-*b*-PLA to solubilize PTX instead of Cremophor EL® in Taxol®. This potentially will reduce toxicity caused by delivery agent. However, in phase II trials of non-small cell lung cancer (NSCLC), along with other anti-cancer agents, it has indicated that, though effective for advanced NSCLS patients, neurotoxicity is a safety issue for use of Genexol®[57]. Samyang Co. has accepted the investigation of U.S. FDA to begin Genexol®-PM phase I clinical trials in patients with refractory cancers since 2002. Genexol®-PM was FDA approved for use in patients with breast cancer[97].

Besides formulations mentioned above, there are also liposomal encapsulated paclitaxel (by NeoPharm), prodrug paclitaxel polyglumex (Xyotax® by Cell Therapeutics), polymeric-micellar paclitaxel (Nanoxel® by Dabur Pharma), paclitaxel vitamin E emulsion (Tocosol® by Sonus Pharmaceuticals), and a polymer microsphere

paclitaxel (Paclimer® by Gullford Pharmaceuticals). However, none of these has been approved by FDA[98]. Despite intense research in drug delivery, it is very challenging to develop non-toxic but effective delivery system for hydrophobic compounds like PTX. In those cases, researchers have attempted to create Cremophor-free formulation for PTX in order to eliminate the increased toxicity associated with solubilization agents. To sum up, the encapsulation of PTX into nano-sized non-toxic drug carriers has several advantages. First, they can be passively targeted to tumors by enhanced permeation and retention (EPR) effect[3] to improve specific delivery efficiency. Secondly, PTX solubilized in non-toxic carriers such as polymeric particles reduces side effect by avoiding solubilization agents like Cremophor EL®, which is associated with increased toxicity when administered intravenously. Meanwhile, nanoparticles provide high drug loading which is desirable, to achieve more drug localization with higher dosage.

In order to utilize these advantages, the delivery agent studied in this chapter is an amphiphilic block copolymer (BCP), poly(ethylene glycol)-*b*-poly(lactic-co-glycolic acid) (PEG-*b*-PLGA) shown in Figure 3.2. As for safety of PEG and PLGA, they were both approved by FDA as surgical sutures, implantable devices and drug delivery systems[99, 100], widely used in food, cosmetics and therapeutic devices, owing to their biocompatibility and biodegradability.

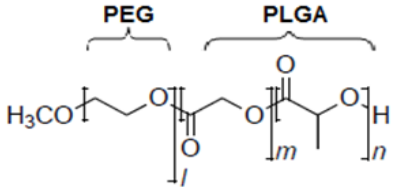

Figure 3.2 Chemical Structure of PEG-*b*-PLGA.

We believe that flash nanoprecipitation (FNP), pioneered by Prud'homme et al.[34,35], is a very valuable technique potentially to formulate nanoparticles composed of PEG-*b*-PLGA and paclitaxel in the range of 100-200 nm with high drug loading[70]. FNP

shown in Figure 3.3 involves rapid turbulent mixing of organic solutes dissolved in a water-miscible solvent (e.g., tetrahydrofuran, acetone, acetonitrile) with the antisolvent water in a confined space [67]. When the solvent and antisolvent streams collide with each other, the solutes rapidly precipitate due to the high supersaturation condition[101].

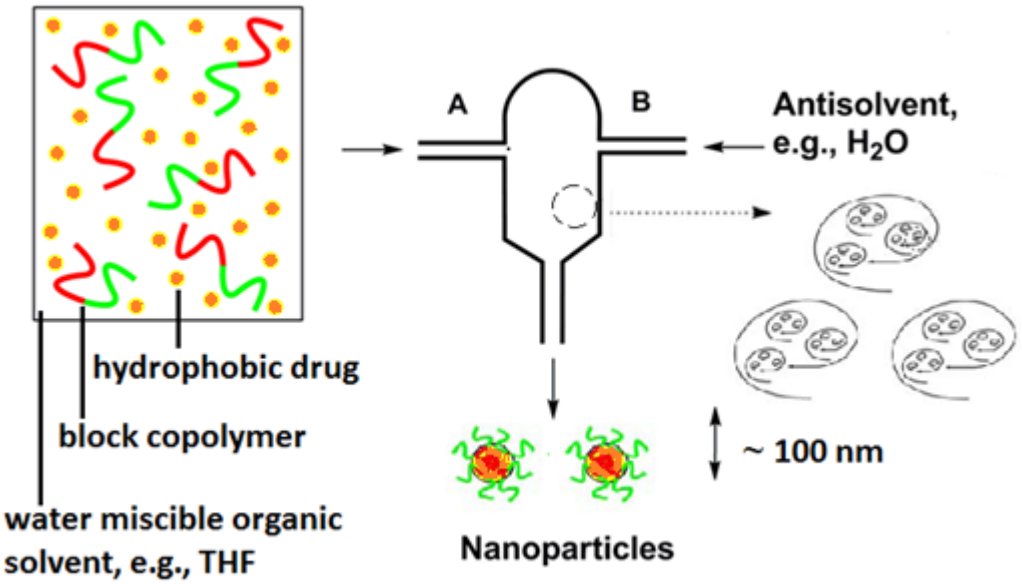

Figure 3.3 Schematic of flash nanoprecipitation to form hydrophobic drug loaded block copolymer protected nanoparticles[67].

When PEG-*b*-PLGA and PTX are dissolved as the organic solutes and co-precipitate via FNP, the mixing process kinetically controls the aggregation of PTX, with the BCP directing self-assembly described in Figure 3.4[35]. The following three time scales are important: (1) mixing time (τ_{mix}), (2) nucleation and growth time (τ_{ng}) of the solute, and (3) self assembly time of the BCP (τ_{sa}). To achieve homogeneous mixing, τ_{mix} must be much smaller than τ_{ng} and τ_{sa}. If τ_{ng} and τ_{sa} are closely matched, hydrophobic block PLGA will deposit on the surface of PTX nuclei, quench growth and aggregation of PTX to create small and stable particles. The hydrophilic block PEG will constitute a hydrated shell and provide steric stabilization to prevent nanoparticle aggregation and

protect nanoparticles against macrophage attack during circulation[102]. PEG-*b*-PLGA protected nanoparticles are expected to yield high loading of PTX and to eliminate Cremophor-related side effects simultaneously.

One advantage of using FNP is to make small particles in the range of 100 nm, because the controlled and relatively small particle size is very attractive to the application of drug delivery in chemotherapy. As mentioned before, the motivation for tailoring particle size is the EPR effect[3]. In order to explain it, the nature of tumor tissues and the drug delivery process is shown schematically in Figure 3.5[103].

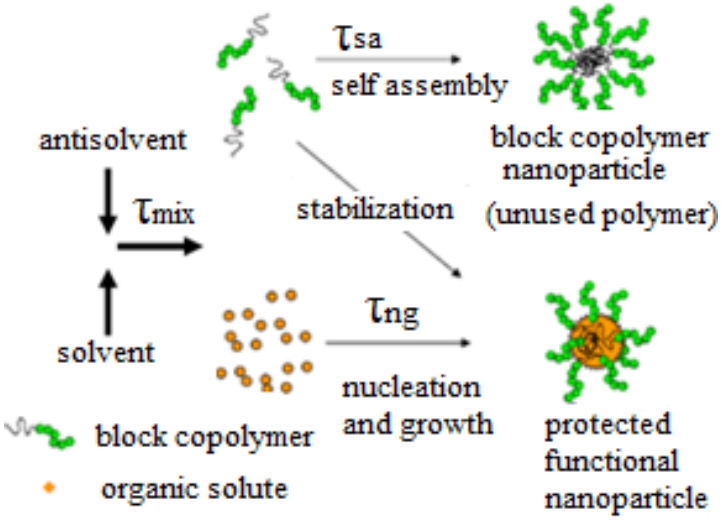

Figure 3.4 Flash nanoprecipitation with details of mixing, nucleation and growth of solutes, and self assembly of polymer[8].

Endothelial cells in normal tissues are regularly aligned, while newly formed tumor vessels in cancer are poorly-aligned, defective endothelial cells with wide fenestrations[3], so the vasculature is leaky[104, 105]. During blood circulation, particles loaded with drugs below the leakage size can pass through the tumor microvasculature without blockage[106, 107]. Also, tumor tissues typically lack effective lymphatic drainage, thus particles lodging there are cleared more slowly. The leaky vasculature and the lack of lymphatic recovery system will lead to drug-loaded nanoparticles accumulate in tumor tissues much more than in normal tissues[8]. This is the EPR effect. In order to exploit it,

the size of our particles needs to be controlled above the leakage size of normal tissues (<50 nm) and below large fenetration of tumor tissues (~400 nm), respectively. This goal plays a significant role in delivering the drug selectively to tumors, thereby reducing side effects caused by non-specific delivery to normal tissues.

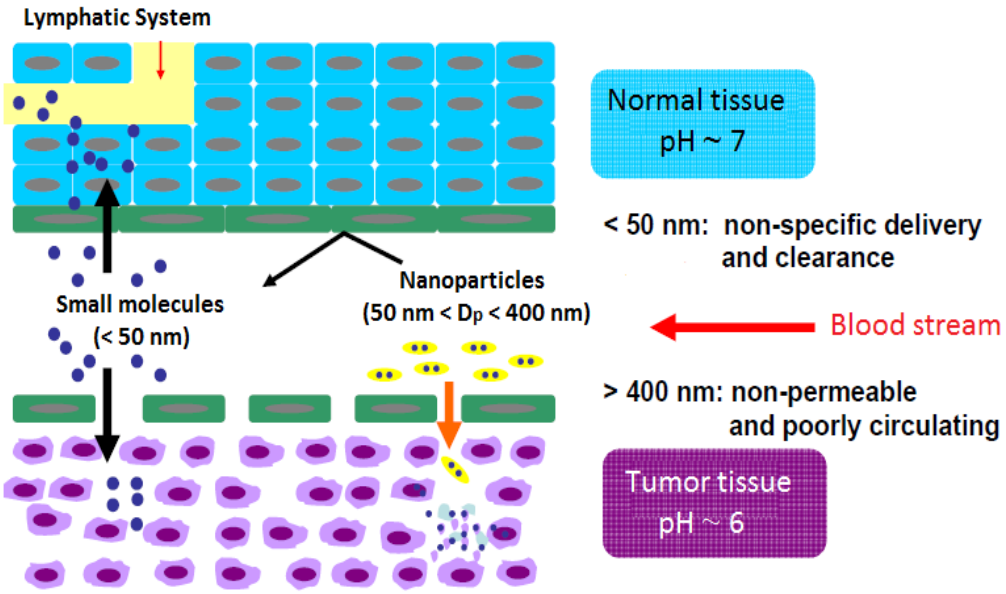

Figure 3.5 Specific drug delivery via the enhanced permeation and retention effect[103].

PTX-encapsulated polymeric nanoparticles made by FNP have been attempted but failed, ending with rapid aggregation and recrystallization of PTX[67, 92] shown in Figure 3.6. This is due to a sufficiently high water solubility of PTX to promote Ostwald ripening[108]. It indicated that PTX is too hydrophobic as a drug to be dissolved in aqueous medium, albeit too hydrophilic to be efficiently encapsulated and stabilized in particle cores. Thus, strategies must be developed to increase hydrophobicity of PTX in solvent mixture. One approach is to increase the ratio of antisolvent over organic solvent. However, the ratio used in FNP is 95:5 of H_2O vs. THF, which is already very high. Second, to choose a poor organic solvent, but options are very limited to water soluble

organic solvent, i.e, THF, acetone, DMF, and acetonitrile. Moreover, sufficient capability of dissolving BCP and drug before FNP needs to be considered as well. Therefore, it leads to the strategy of chemically modify PTX with a more hydrophobic moiety.

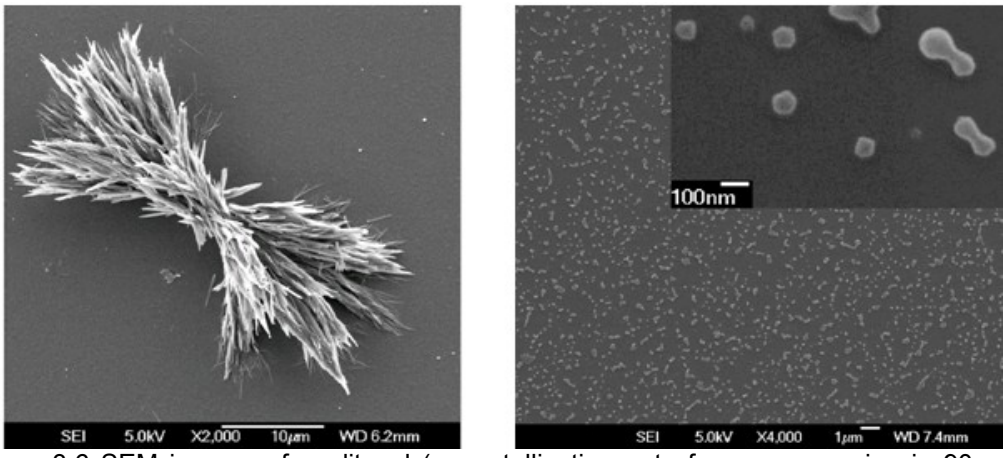

Figure 3.6 SEM images of paclitaxel (recrystallization out of nanosuspension in 90 min) (left) and stable 2',7-triethyl silicate paclitaxel nanoparticles[67,92].

A novel strategy, the conjugation of paclitaxel with a series of silicate esters (with varied –R) was proposed by Hoye et. al[59, 109]. PTX-$OSi(OR)_3$, is regarded as prodrug of PTX. A prodrug[59, 109, 110] is a pharmacological substance administered in an inactive form. Once administered, it is metabolized in vivo into an active drug[110]. Silicate Paclitaxel (Si-PTX) prodrug is rendered more hydrophobic, remaining stable as freeze dried powder for long-term storage. It will eventually convert to active PTX via hydrolysis[109, 111, 112] during administration (Figure 3.7)[111]. And, the more acidic medium in tumor tissues[4], is potentially beneficial to pH-responsive hydrolysis as well.

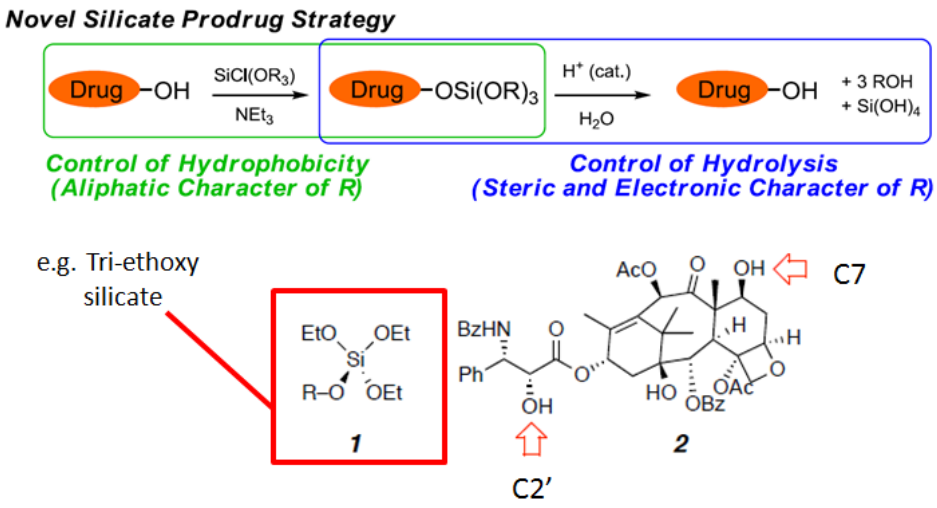

Figure 3.7 Silicate prodrug synthesis and hydrolysis (top); Conjugation of paclitaxel to paclitaxel silicate prodrug, example: 2',7-(triethyl orthosilyl)paclitaxel. Bz: benzoyl group; Ac: acetate group; Ph: phenyl group; $Si(OEt)_3$: triethoxy silicate ester (bottom).

Therefore, nanoparticles discussed in this chapter were prepared by CIJ-D mixer via FNP, encapsulating Si PTX prodrugs into PEG-*b*-PLGA. Dynamic light scattering (DLS) and scanning electron microscopy (SEM) were used to determine particle size, distribution, morphology and stability. They also demonstrated the success of silicate paclitaxel strategy in terms of increasing hydrophobicity of PTX and producing stable nanoparticles without recrystallization of PTX and aggregation of particles[67].

In order to purify nanoparticles and determine their properties with pharmaceutical industrial standards, several post-treatments were used, such as purification (meaning removing un-encapsulated drug from drug loaded nanoparticle dispersion) and lyophilization. Filter filtration, hollow fiber diafiltration and ultracentrifugation were employed to purify particles. DLS and HPLC measurements were utilized to detect the presence of drug and particles, their sizes in filtrates and waste and drug loading levels. The purpose was to find an efficient approach for removing un-

encapsulated drug and empty polymer particles from drug loaded nanoparticles. Ultracentrifugation proved to be most successful to achieve this goal. Afterwards, nanoparticles were lyophilized for storage and future use[113, 114]. We encountered a difficulty recovering particle size after lyophilization due to severe aggregation caused by the freezing process[85, 115]. Cryoprotectants[113, 116, 117] like sucrose, trehalose and glucose are often used to alleviate aggregation, particles sizes were reduced greatly, but it was still very challenging to recover initial size of fresh nanoparticles.

Since lyophilization was used to store particles in dry state with long term stability, we were very interested to find out the stability of Si PTX prodrugs either as pure compound or being encapsulated in nanoparticles, because both physical instability (e.g., aggregation) and chemical instability (drug leakage of particles, hydrolysis of drug and polymer, chemical reactivity of drug) severely limit use of hydrophobic compound loaded in nanoparticles. While these instabilities are potentially advantageous for drug delivery, they are not ideal for drug formulation storage. Therefore, aging studies were conducted by HPLC measurements to determine hydrolysis rate of 2',7-triethyl Si PTX as dry powder for several months. We found insignificant hydrolysis of the dry powder over two months. In contrast, after 2',7-triethyl Si PTX prodrug was encapsulated in nanoparticles, ultracentrifuged, lyophilized, and redispersed in aqueous solution, hydrolysis occurred fast within 24 hrs. Supporting information for this chapter is presented in Appendix C.

3.2 Methods and Experiments

3.2.1 Materials

Paclitaxel was obtained from Phytogen Life Sciences. PEG-*b*-PLA (MW: 5k-10kDa & 5k-15kDa) and PEG-*b*-PLGA (MW: 5k-10kDa) were synthesized in Hoye's lab as previously reported[81], β-carotene was purchased from Sigma-Aldrich and used as received. Silicate paclitaxel prodrugs were synthesized in Hoye's lab[59] as well. Water (H_2O, HPLC grade), tetrahydrofuran (THF, HPLC grade) and acetonitrile (ACN, HPLC grade) were purchased from Aldrich and used as received. 0.45 μm and 0.2 μm filters were purchased from Millipore. Hollow fiber diafiltration column (MWCO: 50 kDa) was purchased from Spectrum Lab, Inc.

3.2.2 Silicate Paclitaxel Strategy

2'-(triethyl orthosilyl) paclitaxel or 2'-triethyl Si PTX (1a), and 2',7-(triethyl orthosilyl) paclitaxel or 2',7-triethyl Si PTX (2a) shown in Figure 3.8 were synthesized in Hoye's lab as reported[59, 109]. The addition of silicate ester derivatives was meant to increase the hydrophobicity of PTX in order to be successfully encapsulated into polymeric nanoparticles. It also determines the diffusion rate of these Si PTX prodrugs when they release from nanoparticles due to tuned hydrophobicity. The cleavage of silicate ester via hydrolysis was designed for the conversion of prodrugs back to the parent drug, PTX, as the active anti-cancer form. The varied hydrolysis rate plays an important role in regeneration of PTX. Overall, the silicate ester derivatives can tune the hydrophobicity and the hydrolysis rate of Si PTX prodrugs[109, 112]. The hydrophobicity was calculated by empirical predictor of calculated logP using ALOPS2.1 program[118].

LogP, is a partition coefficient, as the ratio of the concentrations of a compound between octanol and water. The relative hydrolysis rates were determined by a ^{1}H NMR spectroscopy-based method[109, 112, 119].

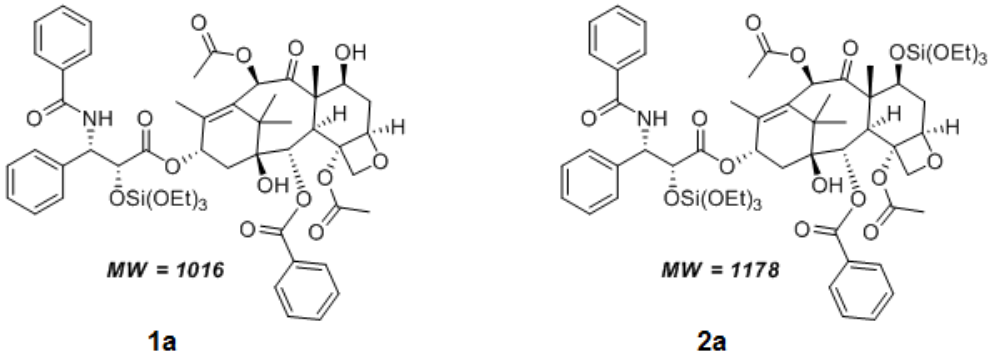

Figure 3.8 Chemical Structure of 2'-triethyl Si PTX (1a) and 2',7-triethyl Si PTX (2a).

3.2.3 Silicate Paclitaxel Nanoparticle Preparation

The following is a standard procedure for one batch of nanoparticles prepared using CIJ-D mixer. 2,7-triethyl Si PTX (MW: 1178 Da) was weighed 34.5 mg, equivalent of 25 mg paclitaxel (MW: 854 Da). It was dissolved in 2.5 mL THF with PEG-*b*-PLGA (MW: 5k-10kDa) and transferred to a 3mL syringe. The other syringe contained 2.5 mL water. Both syringes were connected with two top inlets on the CIJ-D mixer. The two solvent phases were impinged rapidly by pushing syringes simultaneously within 5 seconds. The mixture flowed immediately into 45 mL water also described in Ch. 2[40], in order to further quench particle growth. The resulting suspension had total volume of 50 mL with a ratio of 5:95 THF: H_2O and total mass of approximately 60 mg nanoparticles.

3.2.4 Nanoparticle Characterization

3.2.4.1 Nanoparticle Size and Distribution

The DLS apparatus (Brookhaven, CA) was used to measure size of 2',7-triethyl Si PTX nanoparticles shown in Figure 3.10. As nanoparticles were made, 2 mL of nanosuspension was transferred to glass cuvette. Three identical samples were prepared for measurements. The DLS apparatus (Brookhaven, CA) has a diode laser BI-DPSS wavelength of 659 nm. The intensity correlation function was collected at 25 ˚C and a scattering angle of 90˚. Correlation functions were fit using the REPES model to determine average particle sizes and distribution. GENDIST was used for the REPES algorithm[67, 83, 84].

Another DLS apparatus (Beckman Coulter, CA) was used to measure sizes of β-carotene loaded PEG-*b*-PLA nanoparticles filtered by hollow fiber filtration shown in Table 3.2 and 2',7-triethyl Si PTX loaded PEG-*b*-PLGA nanoparticles and supernatant after ultracentrifugation shown in Table 3.3. The apparatus was equipped with a laser operating at a scattering angle of 90˚. The refractive index was 1.33, the viscosity of solvent mixture was 0.89 mPa•S. The intensity correlation functions were collected at 25˚C. To prepare samples for DLS (Beckman Coulter, CA) measurements, 100 μL fresh nanoparticle suspension was removed by micro pipette, and diluted with 1 mL DI water in DLS square tube. The supernatant collected after ultracentrifugation was directly measured without dilution. Three identical samples were sealed with a plastic cap for measurements. Nanoparticle intensity size was averaged across 150 individual detections. The final size and standard deviation were determined by averaging three measurements. Size polydispersities were recorded automatically by instrument software.

Besides two DLS apparatus, nanoparticle tracking analysis (NTA, Nanosight, Malvern Instrument, UK) was also used to determine mass average of particle sizes. 100 μL fresh nanosuspension was diluted with 2 mL DI water, in order to reach the required concentration range: 10^{-7}~10^{-9} particles/mL. It was injected via the inlet port into chamber. When the instrument was stabilized at room temperature, a 60 second video of particle Brownian motion was recorded. The video was replayed with individual particles being tracked. The diffusion coefficient of individual particles was calculated and converted to particle size based on Stoke-Einstein relation shown in Eq. 2.1.

All particle sizes were accumulated to create size distribution. The mass average size is defined as

$$\overline{d_{\mathrm{m}}} = \sum n_i m_i d_i / \sum n_i m_i = \sum n_i d_i^{\,4} / \sum n_i d_i^{\,3} \qquad \text{Eq. 3.1}$$

where n_i is the number of particles with a diameter d_i, m_i is the mass of particles. The intensity average size is defined as

$$\overline{d_{\mathrm{I}}} = \sum n_i d_i^{\,6} / \sum n_i d_i^{\,5} \qquad \text{Eq. 3.2}$$

Polydispersity index (PDI) is defined as

$$PDI = \sum d_i^2 m_i / \sum d_i^2 \qquad \text{Eq. 3.3}$$

m_i is the mass of particles with a diameter of d_i.

3.2.4.2 Nanoparticle Morphology

To prepare samples for scanning electron microscopy (SEM), a glass Pasteur pipette was first filled with a small amount of the nanosuspension, and then emptied, leaving minute amounts of liquid on the inner wall. This was then aspirated onto a silica wafer that had been washed with HPLC grade THF and water. After evaporation at room temperature, the sample was sputter coated with a 30 Å layer of platinum and imaged with a Hitachi S-900 SEM. A small piece of double-side tape was used to place the silicon wafer on SEM sample stage.

The Cryo-TEM imaging was conducted by my colleague, Hanseung Lee[85]. To prepare samples for Cryo-TEM, both fresh nanoparticle suspension and re-dispersed freeze dried nanopaticles were used. A drop of the suspension was dropped onto the grid and frozen under vacuum condition. A lacey carbon Cu grid (01881, 200-mesh, Ted Pella, Ltd., Redding, CA) was glow discharged in a vacuum evaporator at 70 mTorr (DV-502A, Denton Vacuum Moorestown, NJ) for 30 seconds to create a hydrophilic surface on the carbon coated side of the grid. A 2 −3 μL of fresh sample was pipetted onto the carbon side at 22 °C in a Mark III Vitrobot chamber (FEI Company, Hillsboro, OR) with a relative humidity of ~100 %. The excess sample was blotted with 595 filter papers (Ted Pella, Ltd., Redding, CA) 1 − 2 times with a ~1.5 mm offset parameter for 5 seconds to form a thin liquid film. After the blotting, the sample was relaxed for ~3 seconds and immediately plunged into liquid ethane cooled by liquid nitrogen.

The vitrified sample was transferred to a Gatan 626 Cryo-transfer unit (Gatan, Pleasanton, CA) at -194 °C and characterized at -178 °C in the microscope. A 120 kV FEI Tecnai Spirit BioTWIN was used and images were taken digitally with Eagle™ 2k

CCD camera (FEI Company, Hillsboro, OR) in a low-dose mode. The images were processed with TEM Imaging and Analysis software package. (Version 4.2 SP1 build 816, FEI Company, Hillsboro, OR). To enhance phase contrast, the images were observed with objective lens in an under-focused mode (2 – 4 μm).

3.2.4.3 Nanoparticle Drug Loading

To prepare standards for high performance liquid chromatography (HPLC), 1 mg of PTX and 2',7-triethyl Si PTX were weighed and dissolved in 1 mL acetonitrile, respectively. These solutions were diluted to 100 μg/mL and further diluted in gradient to 50, 25, 12.5, 6.25, 3.125, 1.56 μg/mL. To analyze nanosuspension samples, 1 mg of lyophilized nanoparticles was weighed and dissolved in 1 mL acetonitrile. Three identical samples were prepared, to obtain reproducibility. 2',7-triethyl Si PTX in nanoparticles were extracted in acetonitrile for 24 hr before HPLC measurements. To prepare acetonitrile and water mixture injected at a volume ratio of 75:25, distilled water was filtered and degassed. Acetonitrile was degassed. The drug loading of nanoparticles was determined by comparing against the standards samples with known concentration.

AC-18 column (14.6×25 cm) with 5 μm packing (Beckmann Coulter, CA) was used to analyze acetonitrile extract by HPLC. The mobile phase consisted of a mixture of acetonitrile and water in a ratio of 75:25, and was delivered at a flow rate of 1 mL/min. A 30 μL volume of the acetonitrile extract was injected using an autoinjector (Model 508, Beckmann Coulter, CA). PTX and 2',7-triethyl Si PTX were quantified by UV detection (System Gold 168 detector) at 228 nm, against a series of PTX and 2',7-triethyl Si PTX standards, with premade concentrations of 1.56-100 μg/mL. The loading level (LL%)was calculated using the equation below:

$$LL = \frac{the\ actual\ amount\ of\ prodrug\ in\ NPs}{the\ mass\ of\ NPs} \times 100\% \qquad \text{Eq. 3.4}$$

3.2.5 Nanoparticle Post-Treatment

3.2.5.1 Filtration and Ultracentrifugation

Simple filtration: 0.45 μm and 0.2 μm Millipore filters were used to filter nanoparticles. Freshly made nanosuspension was injected through the filter for at least three times. The filtered nanosuspension was collected and measured by DLS and compared with non-filtered nanoparticles.

Hollow fiber filtration (Spectrum Labs, CA[120]): this method is an efficient and rapid alternative to traditional methods of nanoparticle purification (ultracentrifugation, stirred cell filtration, dialysis or chromatography). It is used to purify liposomes, colloids, magnetic particles and nanotubes. The flow process of hollow fiber is shown in Figure 3.9. When the sample is injected between two syringes back and forth, it is gently circulated through a tubular membrane with controlled pore size, which determines the retention or transmission of solution components. The tubular geometry of the hollow fiber is beneficial to particle applications due to the phenomenon known as tubular pinch effect[121]. Particles migrate to the center of the hollow fiber where flow velocity is the highest, while un-encapsulated solutes, in our case drug and empty polymer micelles will penetrate out of the membrane and be collected by the third syringe (blue in Figure 3.9).

To test the purification performance of hollow fiber diafiltration, two groups of nanoparticles were prepared and filtered. Nanoparticles were composed of β-carotene as a drug model and PEG-*b*-PLA as carrier. In experiment 1, 25 mg of β-carotene and 25 mg of PEG-*b*-PLA (MW: 5k-15k Da) were used to prepare nanoparticles by CIJ-D mixer, in 50 mL solvent mixture of H_2O:THF= 95:5. Nanoparticle size was determined by DLS. Then, nanosuspension was injected into hollow fiber diafiltration column and filtered for 10 min, in order to separate β-carotene loaded particles and blank PEG-*b*-PLA nanoparticles. The solution collected from the waster port was transparent and clear. The remaining β-carotene particle suspension was concentrated and collected from the other outlet. They were both measured by DLS again. In experiment 2, two batches of nanoparticles were prepared and characterized by DLS. One was blank PEG-*b*-PLA (MW: 5k-10k Da) nanoparticles and the other was β-carotene loaded PEG-*b*-PLA (MW: 5k-10k Da) nanoparticles. They were mixed at an equal volume and purified by hollow fiber diafiltration for 10 min. The filtered mixture and waste solution were collected and measured by DLS again.

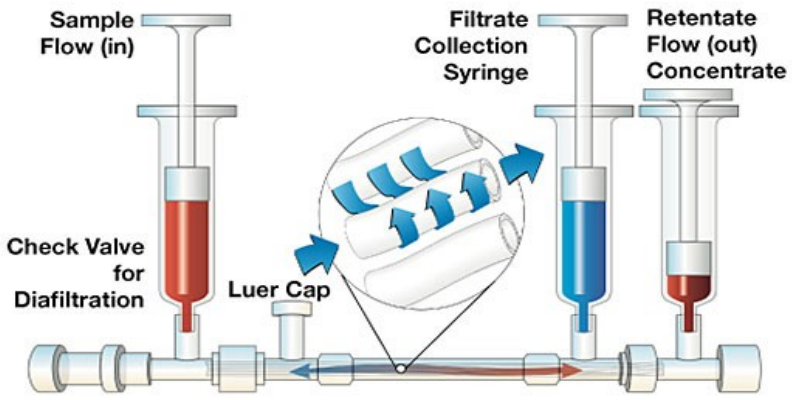

Figure 3.9 Schematic of hollow fiber diafiltration[120].

Ultracentrifugation: 2'7-triethyl Si PTX loaded PEG-*b*-PLGA nanoparticles were prepared and transferred into two 25 mL centrifugation tubes. They were

ultracentrifuged (Optima XPN-80 Ultracentrifuge, Beckman Coulter, CA) at 50,000 rpm, 4˚C for 30 min. The supernatant was removed. The pellet was resuspended in another 25 mL DI water. Tip sonication was used to redisperse particles using pulse model for five minutes, with 15 seconds pause in every minute. The power gradually increased from 3-9V. Pellet collection, redispersion and ultracentrifugation were repeated for three times, to remove free drug and empty polymer nanoparticles. After each ultracentrifugation, 1 mL nanosuspesion was removed from both redispersed pellet and supernatant. It is used to determine particle size and drug loading.

3.2.5.2 Lyophilization and Sonication

After 2',7-triethyl Si PTX nanoparticles were ultracentrifuged, the resulting pellet was resuspended in 5 mL water and transferred to 15 mL plastic tubes. They were lyophilized using lyophilizer (Freeze dryer system/Freezone 4.5, Labconco, MO) at-45ºC under vacuum for 24 hr. The resulting white powder was stored at 4˚C fridge for future use. Also, sucrose as cryoprotectant[122] was added in nanoparticles with a mass ratio of sucrose:NPs=1:10[86], claimed as necessary to achieve size recovery. After lyophilization, particles in dry powder were redispersed in DI water at a concentration of 1 mg/mL using micro-tip sonication (Misonix Sonicator 3000, NY) and sonication probe (1/8″) in pulse mode, 3-9 volt for 5 min. Sonication in each cycle took 1 minute, and the tube containing nanoparticles were immersed into ice water for 30s, to remove the heat generated by the sonicator. The sonication procedure above was repeated with five cycles. Then, DLS measurements were conducted to determine their sizes, SEM and Cryo-TEM to see particle aggregation and size distribution.

3.2.6 Aging

2',7-triethyl Si PTX prodrug(not in NPs) was kept in separate vials right after synthesis and purification, sealed with caps and double-layered parafilms (BEMIS, WI) and stored at 4 ˚C. At designated weeks and months, 1 mg was weighed out and dissolved in 1 mL acetonitrile. Samples were prepared in triplicate and measured by HPLC. The amount of 2',7-triethyl Si PTX, 2' or 7-triethyl Si PTX prodrugs and PTX obtained from hydrolysis were measured. To measure the hydrolysis rate of 2',7-triethyl Si PTX in aqueous solution, 10 mg of the lyophilized 2',7-triethyl Si PTX nanoparticles were redispersed in 10 mL water. At predetermined times (2, 4, 6, 8, 12, 24 hr), an aliquot of sample was removed and quantified by HPLC.

3.3 Results and Discussion

3.3.1 Silicate Paclitaxel Properties

The physical properties of two Si PTX prodrugs are listed in Table 3.1[59]. The hydrophobicity has been significantly increased from PTX to Si PTX (1a&2a) with greasier alkyl groups. The water solubility of PTX was experimentally measured by HPLC using supernatant of supersaturated PTX solution. We also attempted to determine the solubility of Si PTX prodrugs but failed because their concentration is so low, below the detection limit of HPLC (1.5 μg/mL). Due to the great challenge of solubility quantification, the relative hydrophobicity of Si PTX prodrugs was assessed in other ways. One is octanol/water partition coefficients (aLogP values calculated by ALOPS 2.1 software), as an empirical indicator of hydrophobicity. It well predicted that, Si PTX prodrugs have more tendency of being captured in nanoparticles, where hydrophobic

block PLGA creates hydrophobic microenvironment. Although Wohl et al determined the hydrolysis rates in acidic solvent mixture with a measured pH=1.2[59] in order to monitor hydrolysis in a reasonably short time, it indeed demonstrated that Si PTX prodrugs are capable of becoming active PTX with varied hydrolytic lability.

Table 3.1 Properties of PTX and triethyl Si PTX prodrugs

Substrate	MW(Da)	Water solubility (μg/mL)	aLogP[a]	ca. K_{rel}[b]	$t_{1/2}$(min)[c]
PTX	854	12	3.20	--	--
1a	1016	<1	4.96	18,000	3.7
2a	1178	--	6.31	15,000 (C2'), 2100 (C7)	4.6 (C2'), 33 (C7)

a:aLogP is calculated by using ALOPS 2.1. http://www.vcclab.org/lab/alogps/
b: ca. K_{rel} is calculated relative hydrolysis rate detailed in Wohl's NMR method[59,60].
c: $t_{1/2}$ is half time of hydrolysis defined in Wohl's NMR method[59,60].

3.3.2 Nanoparticle Characterization

3.3.2.1 Nanoparticle Size and Distribution

In Figure 3.10, DLS measurements of 2',7-triethyl Si PTX loaded PEG-*b*-PLGA nanoparticles exhibited an averaged mass average size of 70±3 nm and intensity average size of 132±20 nm. Nanoparticles showed a bimodal distribution, where the small size is possibly empty polymer micelles (~20-30 nm[67]) and kinetically formed polymer particles (~40-50) nm, Si PTX loaded particles were in the range of 100-200 nm. Because of the contribution of polymer micelles and particles, mass average size was far less than intensity average size, which was more skewed to larger nanoparticles and aggregates. In this case, intensity average size was a better representative of prodrug loaded nanoparticles.

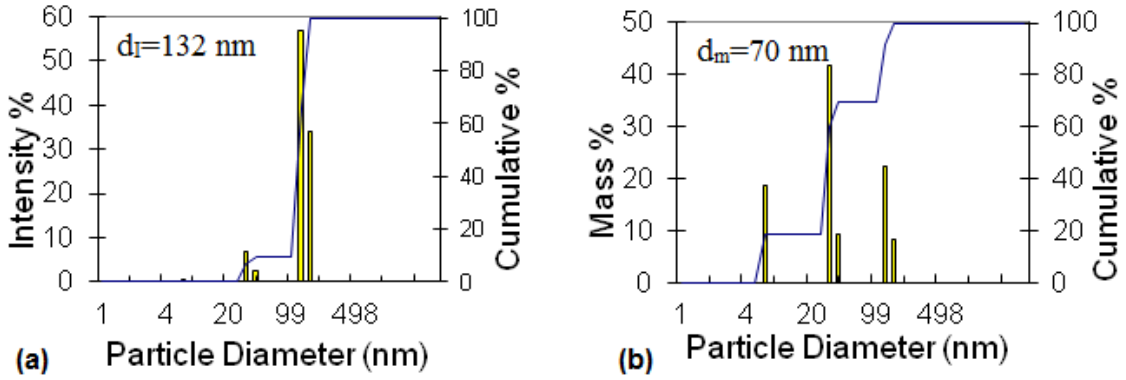

Figure 3.10 Intensity average size (a) and mass average size distribution (b) of 2',7-triethyl Si PTX nanoparticles calculated from DLS data using GENDIST software.

3.3.2.2 Nanoparticle Morphology

SEM images in Figure 3.11 were obtained from fresh 2',7-triethyl Si PTX nanoparticles and those obtained after lyophilization and resuspending in water at the same concentration. First of all, fresh nanoparticles Figure 3.11 (a) were spherical with size about 75 nm, which was very close to mass average size determined by DLS. Secondly, prodrug loaded nanoparticles had more contrast, while nanoparticles with less contrast were speculated to be blank polymer micelles and particles, because they were easily damaged by electron beam and very difficult to visualize in short time.

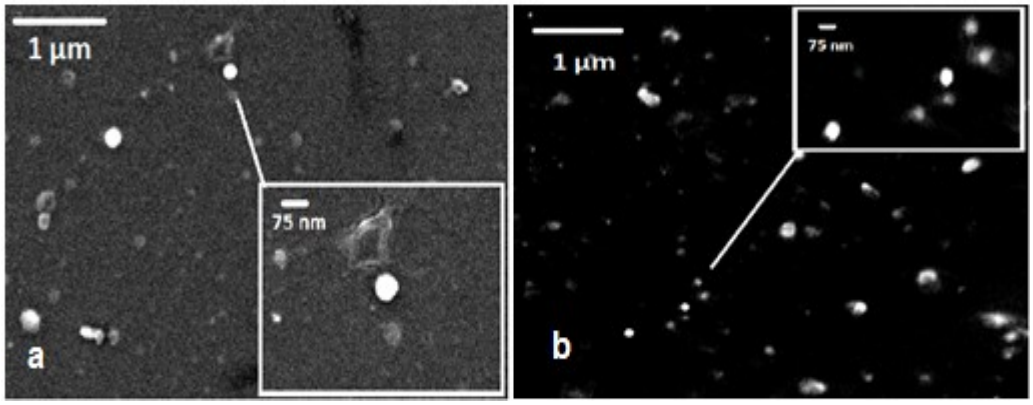

Figure 3.11 SEM images of 2',7-triethyl Si PTX NPs before (a) and after lyophilization (b).

It is known that lyophilization can cause nanoparticle aggregation and original particle size cannot be recovered[85, 86].

Figure 3.11 (b) showed nanoparticles after lyophilization had similar sizes with fresh ones but this image was taken from one of few areas. However, aggregates were observed in most of other imaging area. Also, Cryo-TEM images shown in Figure 3.12, the averaged size from lyophilized particles greatly increased due to aggregation of multiple particles.

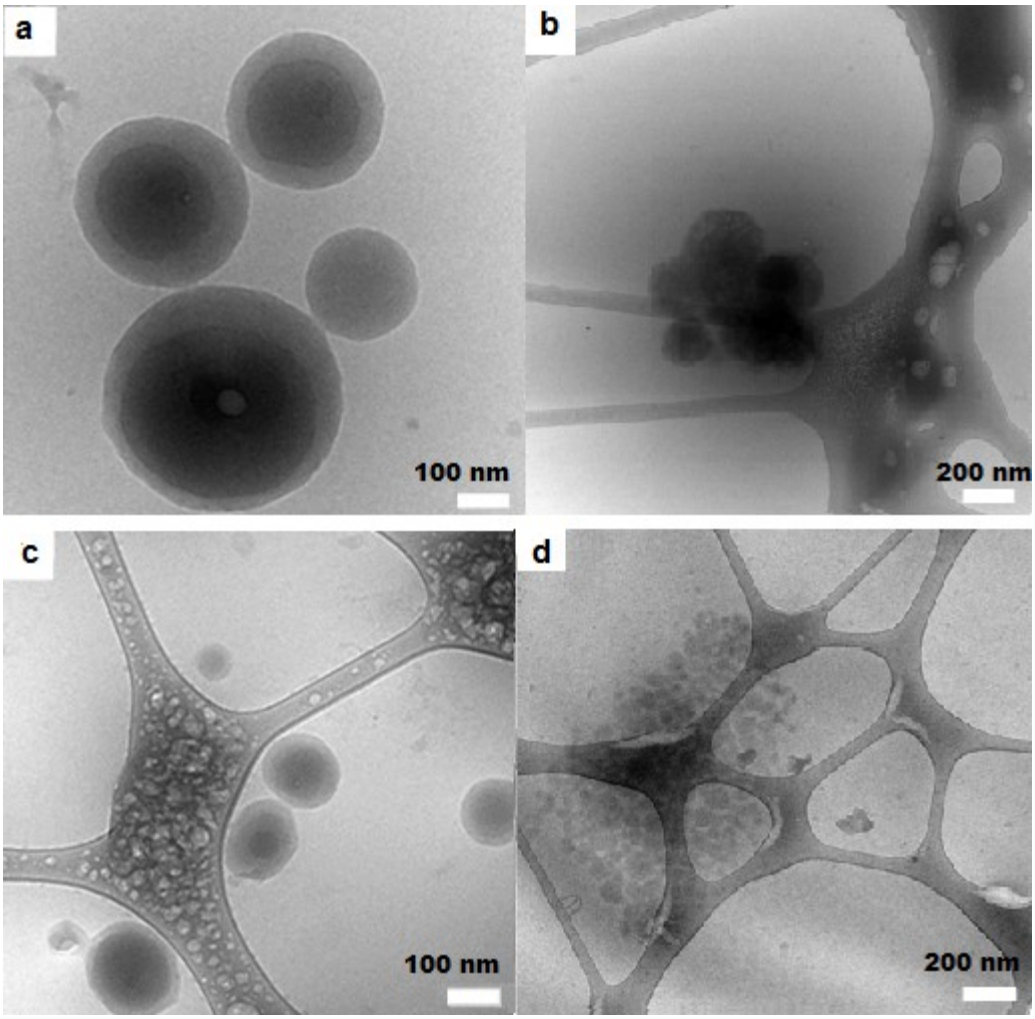

Figure 3.12 Cryo-TEM images of fresh (a) and lyophilized 2'-triethyl Si PTX NPs (b), fresh (c) and lyophilized (d) 2',7-triethyl Si PTX NPs.

3.3.2.3 Nanoparticle Drug Loading

Figure 3.13 is a representative of HPLC standard curve for 2;,7-triethyl Si PTX nanoparticles. PTX was characterized by the 1st peak with a retention time of approximately 2.5 min. The peak area was extremely small, which meant the amount of PTX in newly synthesized 2',7-triethyl Si PTX was negligible. The 2nd and 3rd peak with retention time of 4.25 min and 5.60 min indicated the presence of 7- and 2'-triethyl Si PTX, hydrolyzed from 2',7-triethyl Si PTX prodrug with one silicate ester cleavage. 2',7-triethyl Si PTX was characterized by the largest peak (the 4th peak) with a retention time of approximately 12 min. When Si PTX prodrug was calculated in loading level, both mono- (2' or 7-) and bis (2',7)-triethyl Si PTX were taken into account because they were considered as prodrugs, presumably an inactive form of PTX. The mass of 2' or 7-triethyl Si PTX was converted to 2',7-triethyl Si PTX, in loading calculation. The standard curves of concentration vs. signal of PTX and 2',7-triethyl Si PTX are show in Figure 3.14.

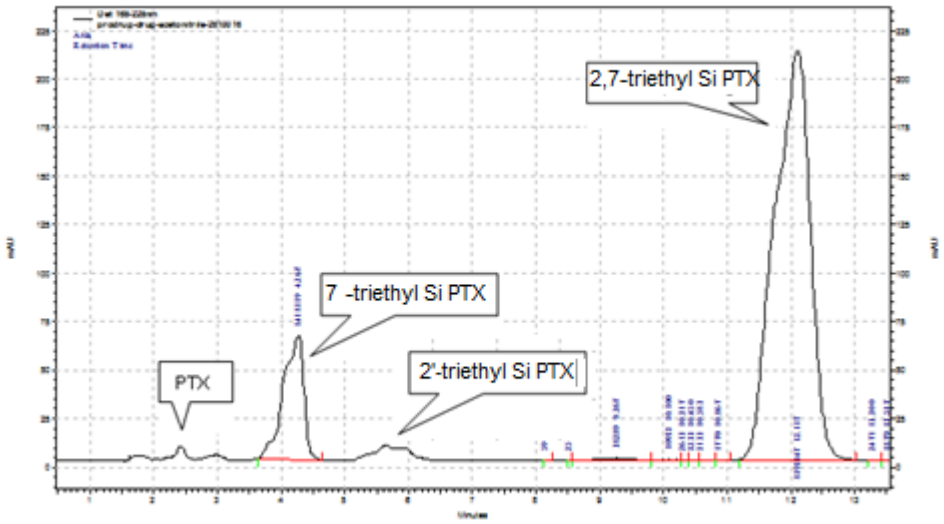

Figure 3.13 A representative HPLC analysis for 2',7-triethyl Si PTX NPs.

According to Eq. 3.4 and 3.5, the loading level of 2',7-triethyl Si PTX nanoparticles was 52.3±.6.5%. This was averaged over three batches of nanoparticles with three identical samples prepared in each batch. The averaged encapsulation efficiency was 90.2%. There was about 5% of nanoparticle loss during weighing samples and transferring suspension. With measurement error considered, nanoparticles prepared via flash nanoprecipitation had very high encapsulation efficiency.

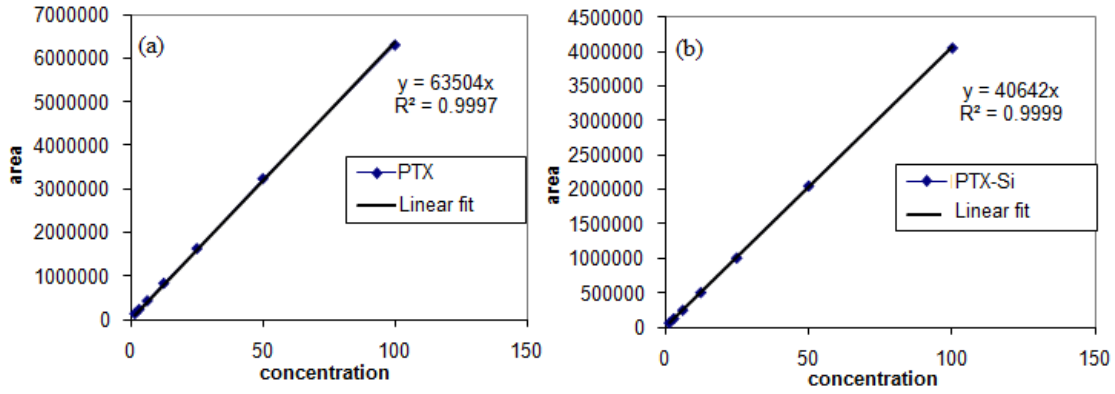

Figure 3.14 HPLC standard calculation of intensity peak area vs. concentration of (a) PTX and (b) 2',7-triethyl Si PTX in acetonitrile.

3.3.3 Nanoparticle Post-treatment

3.3.3.1 Filtration and Ultracentrifugation

Initially, I did not use dialysis method for purification and concentrating particle suspensions because it is very time consuming while the encapsulated Si PTX prodrugs are likely to hydrolyze in that period of time. Therefore, we were looking for fast approaches to filter particles, so membrane filter, hollow fiber filtration and ultracentrifugation were studied.

Simple filtration: most of particles smoothly passed through the 0.45 μm filter. Particles in the filtrate had almost equal size to the un-filtered ones. It implied that 0.45

μm filter was too large to separate particles. Through 0.20 μm filter, a few large particle aggregates were filtered out of suspension, and eventually clogged the filter. However, particle size was still same as the un-filtered ones, with standard deviation of mass average size of 75±3 nm and intensity average size of 127±10 nm. Though nanoparticles were polydisperse, they were mostly below 200 nm. Filter filtration was helpful to remove aggregates demonstrated by the observation that filter was clogged after filtration. Nevertheless, it was not able to purify prodrug loaded nanoparticles from un-encapsulated prodrug.

Hollow fiber filtration: in experiment 1, β-carotene loaded PEG-*b*-PLA nanoparticles were freshly made and injected in hollow fiber diafiltration column. The filtrated nanoparticle size increased from initially 104 nm to 160 nm shown in Table 3.2. Meanwhile, the waste solution showed a size of 91 nm. This indicated that, the waste collected smaller particles while the other outlet extracted the population of larger particles.

In experiment 2, β-carotene loaded nanoparticles and blank polymer nanopaticles (d_I=50 nm) were mixed at equal volume and then filtered by this hollow fiber column. The filtrated nanoparticles had insignificant size increase from 104 to 110 nm. The waste solution showed almost equal size of what we obtained from the waste in first experiment (90 vs. 91 nm). Though hollow fiber column showed consistent filtration performance in terms of separating particles into two ranges below and above 100 nm, yet the waste not only included blank polymer nanoparticles, but also relatively large β-carotene nanoparticles. Therefore, hollow fiber filtration did well in concentrating samples, the volume of nanoparticle suspension was reduced to 1/3 of initial volume, and the

concentration of nanoparticles increased roughly from 1 mg/mL to 3 mg/mL. But it still failed to purify nanoparticles from free molecules and empty polymer NPs.

Table 3.2 β-carotene PEG-*b*-PLA nanoparticle size comparison via hollow fiber diafiltration.

	Experiment 1		**Experiment 2**	
NP type	β-carotene PEG-*b*-PLA		β-carotene PEG-*b*-PLA	Blank PEG-*b*-PLA NPs
d_I&PDI	104 nm/0.15		104 nm/0.15	50 nm/0.18
concentration	1 mg/mL		1 mg/mL	
Action	Filtration		Mix & Filtration	
NP type	filtrate	waste	filtrate	waste
d_I&PDI	160 nm/0.18	91 nm/0.27	110 nm/0.17	90 nm/0.27
concentration	~3 mg/mL	n/a	~3 mg/mL	n/a

dI: intensity average size of nanoparticles
PDI: polydispersity index of particle size.

Ultracentrifugation: this method was able to separate particles from free prodrug left in supernatant, while loaded nanoparticles settled as pellet. However, DLS was able to detect strong scattering signals from supernatant, which indicated that there were still nanoparticles remaining in supernatant though very dilute.

$$D = \frac{k_B T}{f} \qquad \text{Eq. 3.5}$$

$$m\left(1 - \frac{\rho_1}{\rho_2}\right) w^2 = f \frac{\ln\left(\frac{r_2}{r_1}\right)}{(t_2 - t_1)} \qquad \text{Eq. 3.6}$$

m is particle mass, ρ_1 and ρ_2 is densities of medium and particle, w is angular velocity, r is the radius of centrifugation, f is the friction factor, t is time, D is diffusion coefficient, k_B is Boltzman constant, T is temperature.

Using Eq. 3.5, with diffusion coefficient D characterized from DLS measurement, the friction factor f can be obtained via Stokes-Einstein relation in Eq. 2.1. With known r_1, r_2, t_1, t_2, w and ρ_1, the calculated density of these small particles in supernatant (<80 nm) had less than 5% difference from that of water, which explained why the particles failed to settle after ultracentrifugation.

For example, nanoparticles obtained from supernatant 1 in Table 3.3 had an average size of 72 nm, w is 5000 rad/min, r_1 is 5 cm, r_2 is 10 cm, $\Delta t=t_2-t_1=30$ min. Using Eq. 3.6, $\Delta\rho=0.043$g/mL, the density difference against to water is 4.3%. In contrast, nanoparticles which were able to sediment into pellet had a density difference of 6.9%.

HPLC measurements showed that a fair amount of prodrug existed in supernatant. Though certain amount of prodrug loaded nanoparticles along with free prodrug were removed via ultracentrifugation, yet the resulting pellet was nanoparticles heavily loaded with 2',7-triethyl Si PTX loaded nanoparticles. Here is an example of 2',7-triethyl Si PTX NPs particle size and composition in fresh nanosuspension, supernatants and the resulting pellets in Table 3.3. Although more prodrug was found in pellet, the average particle size of the pellet also increased significantly. As a result, the density of particles from pellet calculated via Eq. 3.6 only showed 0.3% density difference from water. The same characterization of ultracentrifugation for other Si PTX prodrug loaded nanoparticles was also conducted and presented in Appendix C. It was very consistent in several aspects: 1) significant mass was lost by the removal of supernatant, 2) smaller particles lightly loaded with prodrug were present in supernatant, along with unencapsulated prodrugs dissolved in solvent, and 3) the pellet had a higher loading due to the removal of empty polymer particles in supernatant. In contrast, supernatant

contained very little amount of lightly loaded nanoparticles and free prodrug, the solubility of which is so low, far below the detection limit of HPLC. Another related phenomenon was that, the ultracentrifuged nanoparticles tended to release in a more sustained pattern compared to the non-centrifuged ones, which will be discussed in Ch.5.

Table 3.3 Physical properties of 2',7-triethyl Si PTX NPs during ultracentrifugation.

	d_i(nm)	PDI	NTA(nm)	NP:drug mass(mg)	Loading%
Fresh	132	0.13	109	48.3/27.5	52.3 (0/0/52.3)
Supernatant 1	72	0.24	91	17.7/7.9	44.5 (33.1/11.4/0)
Supernatant 2	111	0.18	103	10.9/3.7	34.3 (17.3/14.4/2.6)
Supernatant 3	150	0.15	105	2.1/0.2	6.6 (1.7/4.1/0.8)
Pellet	209	0.28	130	15.5/9.4	60.4 (1.6/16.3/42.5)

d_i: intensity average size of nanoparticles measured by DLS.
PDI: polydispersity index of particle size.
NTA: mass average size of nanoparticles measured by nanotracking analysis, Nanosight.
NP:drug is the mass of total nanoparticles vs. drug including Si PTX and PTX.
Loading is presented as the loading of PTX, 2'-triethyl Si PTX and 2',7-triethyl Si PTX.

3.3.3.2 Lyophilization

As discussed in section 3.3.2.3, after nanoparticles were freshly made, they were immediately freeze dried over 24 hr. Less than 1% of PTX and around 4% of partially hydrolyzed Si PTX was detected from 2',7-triethyl Si PTX nanoparticles. In comparison, there was still less than 1% of PTX, but about 10% of partially hydrolyzed Si PTX found in nanoparticles when they remained in water solution for 24 hr (Figure 3.15). This demonstrated that lyophilization effectively removed water via sublimation and prevented occurrence of hydrolysis. This indicated that nanoparticles can be stored in long term as lyophilized dry powder.

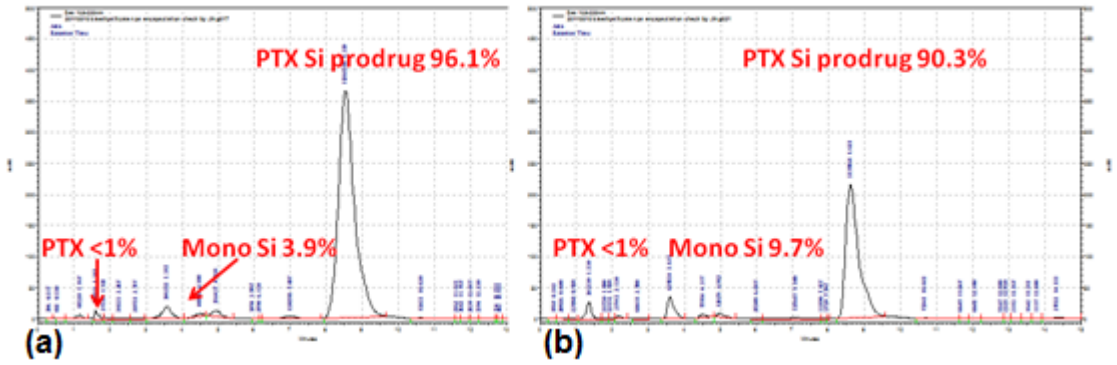

Figure 3.15 Composition comparison of 2',7-triethyl Si PTX nanoparticles freeze dried (a) and in aqueous solution (b) for 24 hr.

DLS measurements exhibited that particle mass average sizes increased drastically from 125 nm to 400 nm and above after lyophilization due to nanoparticle aggregation. To redisperse lyophilized particles, sonication was utilized to break aggregates apart. Micro-tip sonication was more effective than simply putting the entire tube of nanosuspension in water bath for sonication. But nanoparicle size was only reduced to 250-300 nm. Though the particle sizes in Figure 3.11 were small, aggregates above 200 nm were greatly observed from SEM and Cryo-TEM images in Figure 3.12. By the naked eye, the freeze dried particles appeared to be cloudy after redispersing in water shown in Figure 3.16. Thus, lyophilizaiton brought a great challenge to recover initial size.

Figure 3.16 The appearance of nanosuspension before and after freeze drying.

To recover particle size, the cryoprotectant, sucrose was added in fresh nanosuspesnion right after mixing with a mass ratio of 10:1 sucrose:NPs. Sonication beyond 7 min for particles without sucrose and 13 min with sucrose did not reduce particle size further as shown in Figure 3.17. With addition of sucrose, lyophilized nanoparticles had a reduced size of approximately 180 nm with broad distribution when sonicated longer as shown in Figure 3.17. Usually, it was extremely difficult to reduce size below 200 nm. Prud'homme et al.[122] have claimed that the ratio of sucrose:NP=60:1 was necessary to retain particle size.

One issue related to cryoprotectant was that, such large amount of sucrose was undesirable from a drug delivery point of view. High concentration of sucrose will lead to a higher osmotic strength than cells and cause cell shrink when nanoparticles along with sucrose was intravenously administered into blood. Therefore, nanoparticles with sucrose are not practically applicable for injection. Thus, we are still striving to find other cryoprotectants with lower concentration and better particle size recovery, or other strategies to maintain particle size during lyophilization.

It will be ideal to use a much lower concentration of sucrose or other effective cryoprotectants to achieve a high level of protection during freezing. Pulstulka et. al[86, 123, 124] have found that pluronic F68 was a better cryoprotectant, especially for PTX-based particles. Further investigation needs to continue in search of good cryoprotectant or developing other strategies to protect particles during lyophilization, but for the following work in this thesis, nanoparticles used in vitro and in vivo studies were not prepared with any cryoprotectant. Fresh particles d_I is 155 nm, after freeze drying without sucrose, sonicated for 10 min, 400 nm.

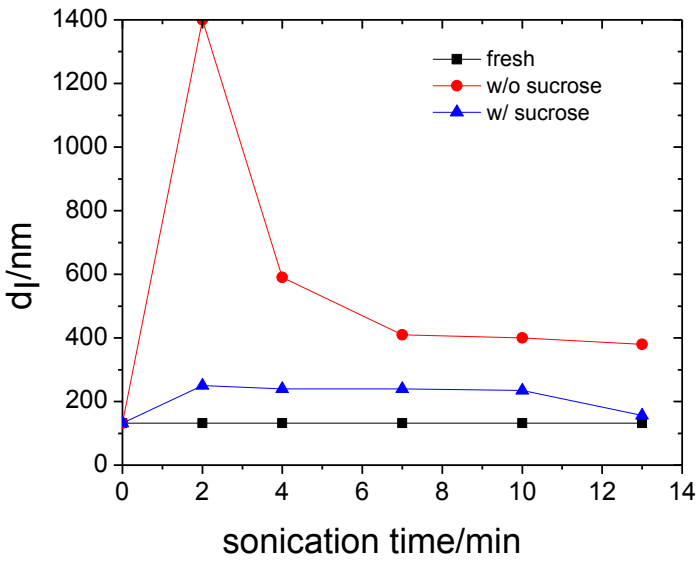

Figure 3.17 The intensity average diameter of 2',7-triethyl Si PTX NPs after lyophilization vs. sonication time.

3.3.4 Aging

Figure 3.18 showed that 2',7-triethyl Si PTX gradually hydrolyzed back to PTX over weeks when the hydrolyzed prodrug was stored at 4˚C. In short term, the hydrolysis was not very significant until one month later. In long term up to eight months, there were only less than 20% of PTX, while the rest was composed of 70% of partially hydrolyzed 2'and 7-triethyl Si PTX and 10% of 2',7-triethyl Si PTX. The hydrolysis from 2',7- to 7-triethyl Si PTX occurred relatively fast, but quite slow from 7-triethyl Si

PTX to PTX. There was a significant increase of 2' and 7-triethyl Si PTX between 5-10 weeks which indicated the hydrolysis time of 2',7- to 7-triethyl Si PTX lies in this period of time. Once Si PTX prodrugs became PTX, the redispersed nanoparticles loaded with PTX will not be stable due to Ostwald ripening of PTX. Therefore, 2',7-triethyl Si PTX loaded nanoparticles were relatively stable with a shelf life of approximately two month and nanoparticles are suggested to be used as received and stored within one month.

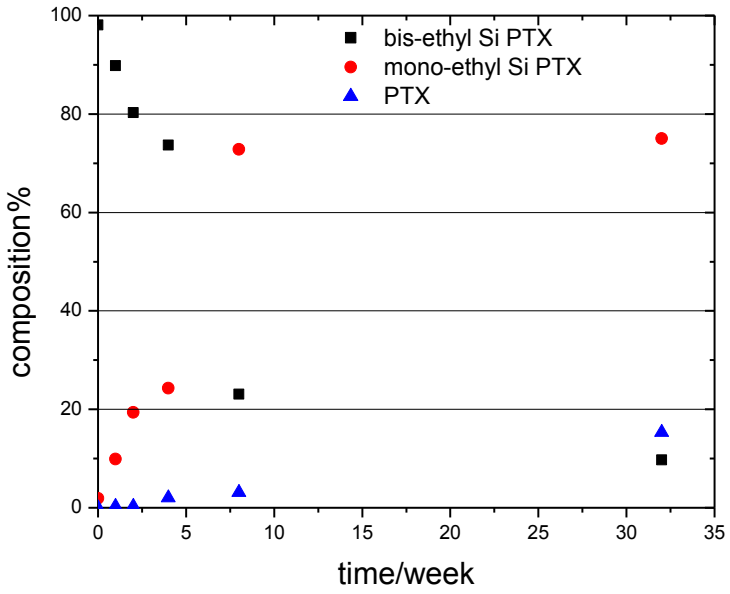

Figure 3.18 The aging process of 2',7-triethyl Si PTX in 32 weeks.

In contrast, Figure 3.19 showed hydrolysis occurred very fast in short term (within 24 hr) when 2',7-triethyl Si PTX were encapsulated in nanoparticles and dispersed in PBS at pH 7.4 and 37˚C. Similarly to prodrug in dry state, prodrug in nanoparticles quickly hydrolyzed to 2'or 7-triethyl Si PTX, but the hydrolysis rate was much faster in water. At the end of 24 hr, 40% of 2' and 7-triethyl Si PTX was obtained while PTX remained negligible. In comparison, nanoparticles before freeze drying

contained less than 5% of 2' and 7-triethyl Si PTX. Thus, the presence of water significantly expedited the hydrolysis. The key to store nanoparticles is to remove the moisture. Lyophilization is very necessary to maintain the stability of encapsulated prodrug, while how to recover nanopartcle size is still under investigation.

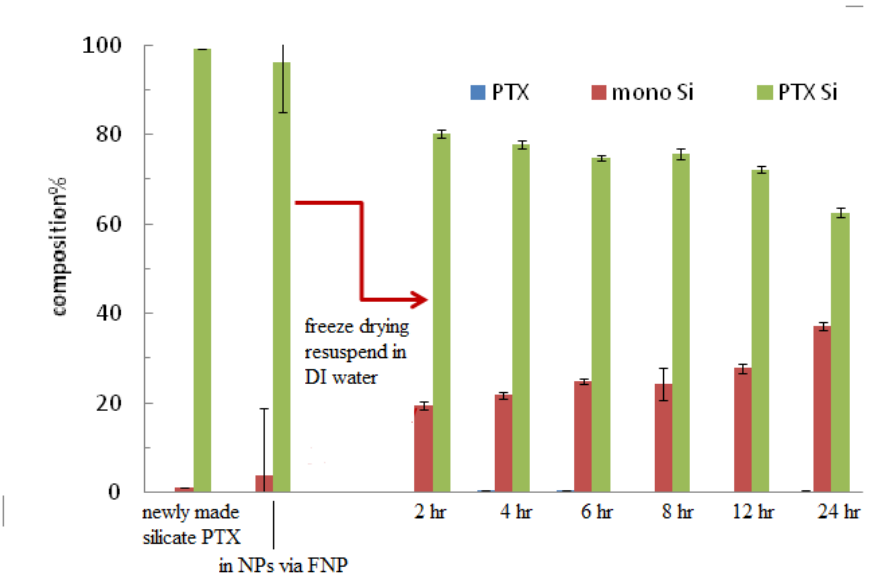

Figure 3.19 Composition change of 2',7-triethyl Si PTX during synthesis, flash nanoprecipitation, lyophilization, and resuspension.

3.4 Conclusion

It is not possible to make stable PTX encapsulated nanoparticles due to fast Ostwald ripening of PTX, thus silicate esterification of PTX was introduced to increase its hydrophobicity by Wohl and Hoye[59, 60]. 2',7-triethyl Si PTX loaded PEG-*b*-PLGA nanoparticles were successfully made to avoid the crystallization of PTX. The nanoparticles were stable with an averaged intensity size around 120 nm. They tended to have a bimodal distribution where polymer micelles, particles and drug loaded

nanoparticles coexisted. In order to remove free molecules un-encapsulated and empty polymer micelles/particles, ultracentrifugation was found to be the best method, compared to traditional filtration and hollow fiber filtration. The silicate paclitaxel prodrug loading levels are above 50% and up to 75% after ultracentrifugation, higher than current PTX-based formulations, such as Taxol®(~1wt%) and Abraxane®(~10 wt%). The high drug loading potentially leads more efficient dosing and reduced dosing cycles, in order to ease cancer patients' pain. By lyophilization, nanoparticles were stored in dry state, where hydrolysis rate was efficiently reduced but particle size increased dramatically since freezing process induced particle aggregation. We attempted to use cryoprotectant sucrose to recover particle size after lyophilization but more efforts should be made to discover more effective cryoprotectant to maintain initial size with small concentration. The aging study indicated 2',7-triethyl Si PTX prodrug in nanosuspension hydrolyzed relatively fast in 24 hr but can be stored as dry powder at 4˚C for a month. Beyond one month, hydrolysis will occur even in dry state.

Chapter 4

In Vitro Drug Release Study of Silicate Paclitaxel Diblock Copolymer Protected Nanoparticles (un-ultracentrifuged): Experimental Setting and Release Profile

4.1 Introduction

To be an effective drug delivery system, evaluation of release is essential during development and quality control of the formulations, via *in vivo* animals or *in vitro* using buffers at 37 ˚C (physical temperature). Due to the labor and expense involved with *in vivo* studies, *in vitro* drug release study has gained more attention in several aspects: first, it provides indirect measurement of drug release and predicts the timeframe of release, as preliminary stages for *in vivo* study. Secondly, it assesses manufacturing methods and formulation variables[125]. Thirdly, it screens one or more candidates among several formulations.

In our drug delivery system, the silicate paclitaxel (Si PTX) prodrug loaded PEG-*b*-PLGA nanoparticles are designed to be injected via intravenous (IV) administration. Once injected, nanoparticles release PTX-containing compounds over a period of time, depending on several factors, such as particle size and morphology, drug loading level of Si PTX prodrugs, their hydrolytic stability, diffusion of water into nanoparticles, polymer degradation etc. This chapter mainly focuses on the development of *in vitro* drug release

protocol, experiment methods and release kinetics characterization. We subjected six Si PTX nanopaticle formulations to different pHs and time and measure the release of prodrugs with one or two silicate derivatives.

There are various methods used to measure drug release. They fall into four broad categories[126, 127], in situ methods, continuous flow methods, sample and separate techniques and membrane diffusion techniques.

In situ method: It is intended only for drug with chromophores. When the drug system is dispersed in sink, the released drug can be assayed by UV/Vis spectroscopy, without separating the dispersion from sink. Unfortunately, it is not suitable for our particle system.

Continuous flow: the drug system is dispersed in a small sink which contained a filtration cell. The sink phase is removed for continuous analysis (by UV/Vis and fluorescence spectroscopy). Fresh sink is added to the suspension. However, flow rates might be varied when filter is clogged during the injection of sample. Though the method is not ideal, for Si PTX prodrugs might clog the filter and there is no compound observed by spectroscopy. But, the removal and replacement of sink condition is a good alternative to perfect sink condition if it can be done sufficiently rapidly.

Sample and separate: the drug system is dispersed in a medium. Periodically, the sample is separated by filtration or centrifugation. The medium is assayed. This technique is applicable only if the dispersion and the medium can be completely separated and rapidly[128]. However, as we showed in Ch.3, our nanoparticle system with small size around 100 nm proved to be extremely difficult to filter off and the time to sediment in ultracentrifugation takes hours, which will intervene in the time course of release.

Membrane diffusion: One method of *in vitro* release is to test the formulation in a diffusion cell. In this apparatus, the formulation is put in contact with a membrane that is immersed in receiving medium. The medium is sampled as a function of time. However, this technique is only applicable to the tested drug compound with relatively high solubility in the medium. In our case, PTX is poorly water soluble, not to mention Si PTX with increased hydrophobicity. The same problems apply to dialysis bag technique. The receiving medium, in our case, phosphate buffer solution (PBS) must have a sufficient volume to solubilize all possibly released drugs, while the saturated concentration is near the lower limit of HPLC, the analysis accuracy cannot be guaranteed. If PTX releasing into PBS is first lyophilized and re-dissolved in a small volume to a detectable concentration, it can take several days to lyophilize such larger volume of buffer. It is inefficient and impractical for *in vitro* release study in our case, which will be performed on several different nanoparticle formulations. And each of the formulations needs several days to complete, involving hundreds of samples to be processed.

There are technical problems to use most of the methods described above for *in vitro* release study, because the solubility of these Si PTX prodrugs predicted previously [112] were far less than pure paclitaxel (~12 μg/mL). Therefore, in this chapter, I adopted membrane diffusion method using dialysis mini capsules to conduct *in vitro* drug release studies with six Si PTX nanoparticles The dialysis mini capsules have a low-binding membrane with molecular weight cutoff size of 10kDa. They were tested beforehand to see whether the dialysis membrane limits drug diffusion. Pure PTX and 2',7-triethyl Si PTX were first dissolved in water and contained in dialysis capsules, which were

immersed in phosphate buffer solution. They completely diffused through membrane in 1-3 hr quantified by HPLC method shown in Figure 4.7, we do not think dialysis membrane limits drug diffusion.

The drug release mechanism is widely believed to be diffusion from carrier matrix, thus using membrane method and sink condition have been proposed a lot for *in vitro* drug release. When drug system is immersed in a continuous phase, drug partitions between the carrier phase and the continuous phase, due to the concentration gradient. Theoretically, the drug will leave the carrier and partition completely when infinite dilution is provided in continuous phase. This is considered as perfect sink condition[127], where true release profile can be measured. However, it is never attainable in practice. A finite sink condition is required to obtain valid experimental data. It is recommended that drug concentration in sink phase be kept below 10% of saturation[127]. For example, Langer's group has used 20 or 40L PBS to create sink condition for PTX release[129, 130]. However, this poses a problem that as the volume increases, the concentration of drug being measured in buffer decreases to an extent that it is too dilute to detect. Eventually, the released drug cannot be assayed in buffer.

It is the very reason that we developed a relatively new method specifically to study *in vitro* Si PTX prodrug and pure PTX release using frequent replacement of sink condition of phosphate buffer solution. This improvement has been demonstrated to achieve the same release profile obtained using the perfect sink condition. Meanwhile, dialysis tubes, dialysis cassettes[131] and dialysis mini capsules were utilized to verify if the geometry design of dialysis devices has any influence on experiment accuracy and use convenience.

After *in vitro* release protocol and experimental setup were determined, *in vitro* release studies were first conducted on 2',7-triethyl Si PTX nanoparticles at pH 7.4 and 6.4 to study the effect of buffer pH on release rate. The reason for that is, normal tissues usually have a neutral environment, while tumor tissues are usually more acidic with a pH at 6.4 or lower[4-6]. Thus, it is worth studying whether drug release varies at these two conditions, especially when the hydrolysis of Si PTX prodrug captured in nanoprticles potentially can be pH-responsive.

Also, the release profiles were plotted for both 2',7 and 2'-triethyl Si PTX nanoparticles to study the effect of silicate derivatives amount. Lastly, prodrugs with four other different silicate derivatives from Wohl et al[59, 60] were prepared in PEG-*b*-PLGA nanoparticles. With tuned hydrophobicity and hydrolytic lability, their physical and pharmacokinetic properties were customized to different levels, specifically in particle sizes and release rates.

4.2 Methods and Experiments

4.2.1 Materials

Paclitaxel was obtained from Phytogen Life Sciences. PEG-*b*-PLGA (MW: 5k-10kDa) was synthesized in Dr. Hoye's lab as previously reported [81]. Water (H_2O, HPLC grade), tetrahydrofuran (THF, HPLC grade) and acetonitrile (ACN, HPLC grade) were purchased from Aldrich and used as received. Phosphate buffer solution (PBS) was prepared by dissolving 3.12 g monosodium phosphate and 20.74 g diasodium phosphate in 1 L DI water to achieve pH 7.4, and 10.28 g monosodium phosphate and 6.84 g diasodium phosphate in 1 L DI water for pH 6.4. Monosodium phosphate and diasodium

phosphate were purchased from Fisher Scientific. Slide-A-lyzer dialysis cassette (MWCO: 10k Da, 0.5-3 mL, 6-12 mL) and dialysis mini capsule (MWCO: 10k Da, 0.5-1 mL) were purchased from Thermo Scientific. Six Si PTX prodrugs were synthesized in Dr. Hoye's lab as previously reported[109, 112]. Their chemical structures are shown in Figure 4.1. The physical properties and hydrolytic lability are shown in Table 4.1. The partitioning coefficient was calculated using several softwares, such as ALOPS 2.1, molinspiration and ACD/Labs. They all showed similar trend of values, but those obtained by ALOPS 2.1 were most consistent with other hydrophobicity indicators such as retention time in LC/MS method and calculated aqueous solubility, discussed,by Adam et al[59, 60]. Thus, only LogP values calculated by ALOPS 2.1 are provided in Table 4.1.

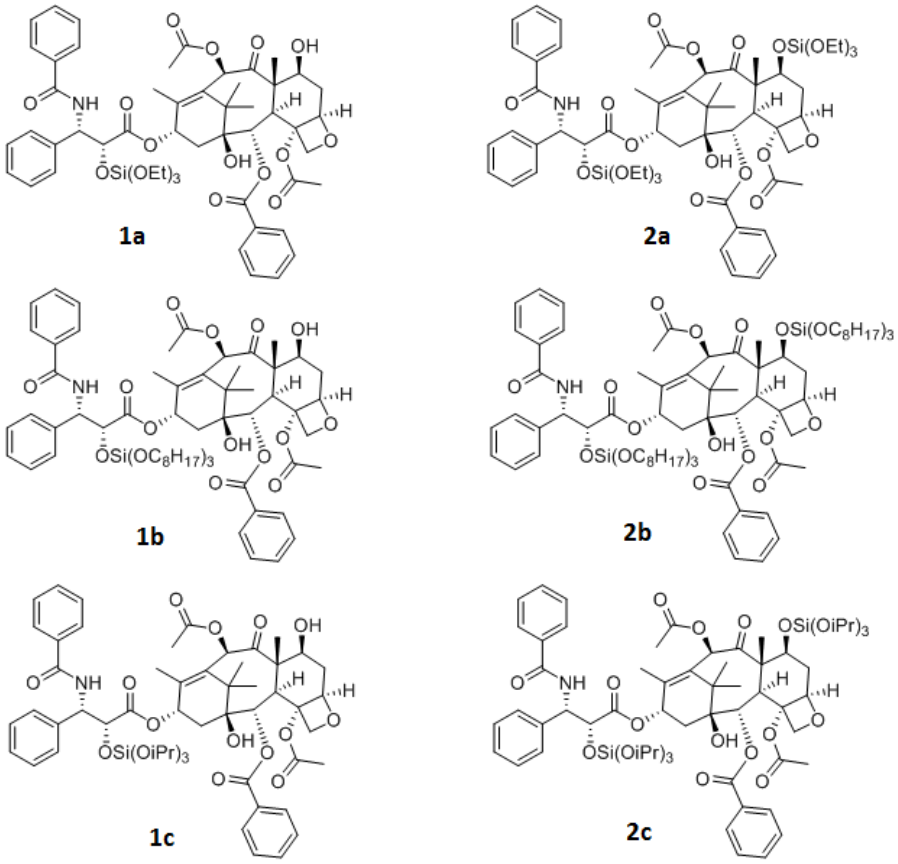

Figure 4.1 Chemical structures of 2'-triethyl Si PTX (1a), 2',7-triethyl Si PTX (2a), 2'-trioctyl Si PTX (1b), 2',7-trioctyl Si PTX (2b), 2'-triisopropyl Si PTX (1c) and 2',7-triisopropyl Si PTX (2c).

Table 4.1 Properties of PTX and Si PTX prodrugs

Drug	MW/Da	aLogP[a]	ca. Krel[b]	$t_{1/2}$/min[c]
PTX	854	3.20	--	--
1a	1016	4.96	18,000	3.7
2a	1178	6.31	15,000 (C2'), 2100 (C7)	4.6 (C2'), 33 (C7)
1b	1269	7.74	5,600	12
2b	1683	8.59	3,800	18
1c	1058	5.60	570	120
2c	1263	6.84	520	130

a: aLogP is calculated by using ALOPS 2.1.
b: ca. Krel is calculated relative hydrolysis rate by Wohl's NMR method[59,60]..
c: $t^{1/2}$ is half time of hydrolysis by Wohl's NMR method[59,60].

4.2.2 Nanoparticle Preparation

Nanoparticles made with each of six Si PTX prodrugs were prepared using CIJ-D mixer via flash nanoprecipitaiton. For single batch of nanoparticles, 35-40 mg of Si PTX prodrugs (with an equivalent of 25 mg PTX) and 25 mg of PEG-*b*-PLGA were dissolved in 2.5 mL THF, contained in a 3mL syringe. It was impinged rapidly with the other syringe containing 2.5 mL water within 5 seconds. The mixture was drained into 45 mL water, in order to further quench nanoparticle growth. The resulting nanoparticle suspension had total volume of 50 mL with a ratio of 5:95 THF: H_2O and total mass of approximately 60-65 mg nanoparticles.

4.2.3 Nanoparticle Characterization

4.2.3.1 Nanoparticle Size and Distribution

Nanoparticle size was characterized via dynamic light scattering (Beckman Coulter, CA). 100 μL suspension was removed by micro pipette, and diluted with 1 mL DI water in DLS square tube. The apparatus was equipped with a laser operating at a scattering angle of 90˚. The refractive index was 1.33, the viscosity of solvent mixture was 0.89 mPa•S. The intensity correlation functions were collected at 25˚C. Three identical samples were sealed with a plastic cap and prepared for measurements. Nanoparticle size was averaged across 150 individual detections. The final size and standard deviation were determined by averaging three measurements. Size polydispersity index (PDI) was calculated by instrument software. The mass average particle size, intensity average size and size polydispersity index defined as:

$$\overline{d_{\mathrm{m}}} = \sum n_i m_i d_i / \sum n_i m_i = \sum n_i d_i^{\,4} / \sum n_i d_i^{\,3} \qquad \text{Eq.4.1}$$

$$\overline{d_{\mathrm{I}}} = \sum n_i d_i^{\,6} / \sum n_i d_i^{\,5} \qquad \text{Eq.4.2}$$

$$PDI = \sum d_i^2 m_i \% / \sum d_i^2 \qquad \text{Eq.4.3}$$

where n_i is the number of particles with a diameter d_i, m_i is the mass of particles.

4.2.3.2 Nanoparticle Drug Loading

Samples preparation methods for HPLC was described in Ch.3 Section 3.2.3.4. Different from Ch.3, the mobile phase consisted of a mixture of acetonitrile and water, which was delivered at a flow rate of 1 mL/min in gradient from 100:0 to 50:50 acetonitrile:H_2O in first 4 min, and back to 100:0 in the following 4 min, and decreased to 50:50 acetonitrile: H_2O for another 4 min and remained at that ratio for 5 min in each sample analysis .

Every time new measurements started, new standard samples with known concentrations were prepared and calibration was repeated. The Si PTX prodrug loading levels in lyophilized nanoparticles were determined by analyzing the acetonitrile extract by HPLC. AC-18 column (14.6×25 cm) with 5 μm packing (Beckmann Instruments, CA) was used. The loading levels were calculated using the equation below:

$$LL = \frac{the\ actual\ amount\ of\ prodrug\ in\ NPs}{the\ mass\ of\ NPs} \times 100\% \qquad \text{Eq. 4.4}$$

4.2.4 In Vitro Drug Release

4.2.4.1 Sink Condition

The infinite sink condition is used for extremely hydrophobic drug release. Langer et al[130] used 40 L phosphate buffer solution (PBS) to create sink condition, where the extensively large volume of PBS avoided PTX to saturate. The huge volume of PBS created sufficient concentration gradient as the driving force for PTX to diffuse out of nanoparticles and through dialysis membrane as well.

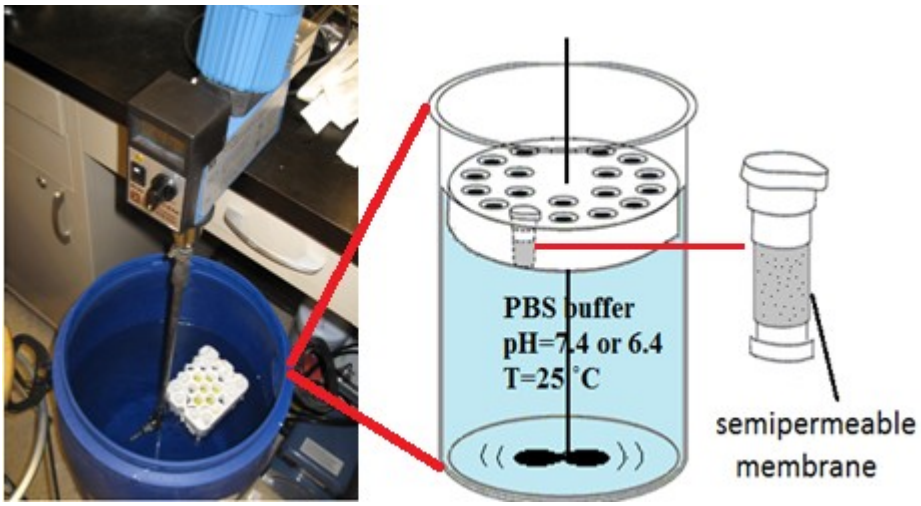

Figure 4.2 Infinite sink condition (40L) for drug release.

In order to investigate the effect of sink condition, lyophilized 2'7-triethyl Si PTX nanoparticles were redispersed in PBS (pH 7.4) at a concentration of 1 mg/mL. In group 1, they were put into 500 μL dialysis tubes and multiple tubes were immersed into 40 L PBS, at pH 7.4, at room temperature and stirred with an overhead, which is shown in

Figure 4.2. In group 2, dialysis tubes containing same nanoparticle suspension were immersed into 1 L PBS magnetically stirred, the buffer of which was periodically refreshed at designated time intervals (1, 2, 4, 6, 8, 12, 24 hr) to avoid saturation. At these predetermined time, three dialysis tubes were removed from both groups and lyophilized. Noted that, at 0hr, the lyophilized nanoparticles were first dispersed and dialyzed against buffer. They were removed immediately after being immersed in buffer less than 1 min.The dry powder of nanoparticles were dissolved in 1 mL acetonitrile and extracted overnight. HPLC was used to determine the concentration of PTX and Si PTX prodrugs from these lyophilized samples as the remaining/un-released drug from nanoparticles.

4.2.4.2 Dialysis Devices

Dialysis tubes, dialysis cassette and dialysis mini capsules were all used to contain nanoparticle suspension in drug release study shown in Figure 4.3 (a), (b) and (c). (a) Dialysis tube (500 μL) has a cylinder-like membrane compartment with two caps on the ends. (b) Dialysis cassette has a tape cassette compartment with two square-shape membranes clamped in the middle. (c) Dialysis mini capsule is a 500 μL cup with semi-permeable membrane on the bottom and sealed with a cap. In order to fully use the diffusion area of the membrane, dialysis tube and cassette were completely immersed in buffer, while dialysis mini capsule were floating with the bottom membrane immersed in buffer. Nanoparticles were injected via inlet port at the corner of dialysis cassette shown in Figure 4.3 (d) and placed into dialysis tubes and mini capsules by a pipette shown in Figure 4.3 (e).

To compare the performance of dialysis devices, 2’7-triethyl Si PTX nanoparticles were resuspended and put into dialysis tubes, cassettes and mini capsules.

In each group, multiple samples were prepared and immersed in PBS pH 7.4 at 37ºC to mimic body condition. The release study was conducted using the same protocol explained previously. We compared the release profiles obtained from three groups, to see if they showed consistent release rates. Or in the other case, different design of dialysis devices and varied surface areas immersed in buffer may play a diffusion-limiting factor.

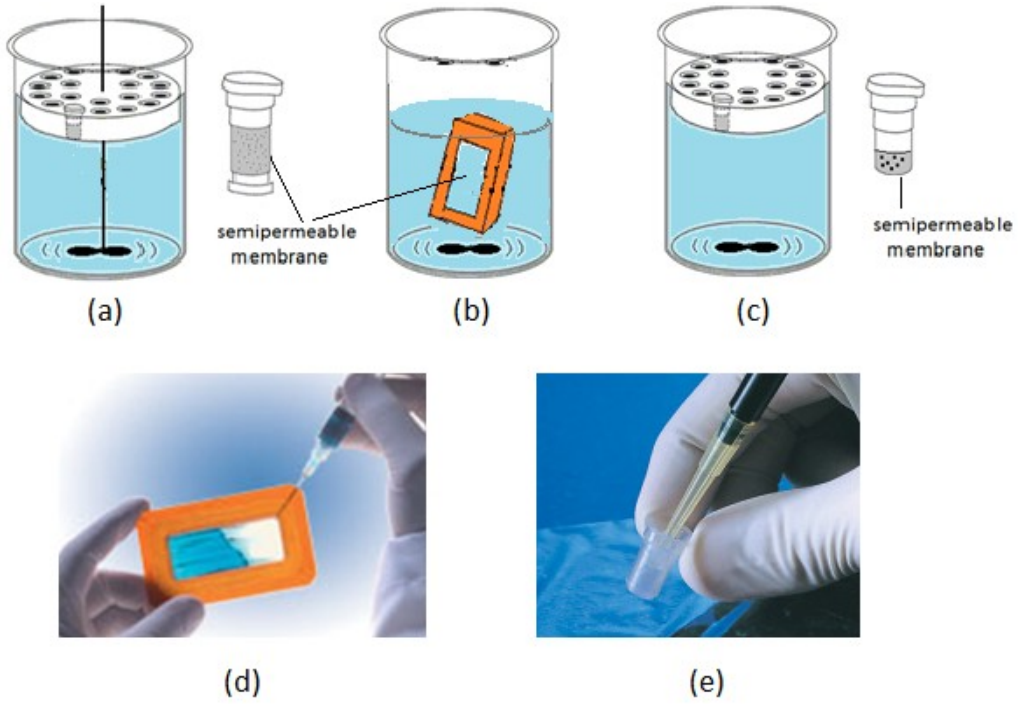

Figure 4.3 (a) dialysis tube, (b) dialysis cassette, (c) dialysis mini capsule immersed in PBS at 37ºC, pH=7.4 or 6.4; (d) sample injection and removal into dialysis cassette, and (e) into mini capsule.

4.2.4.3 pH 7.4 vs. pH 6.4

Release studies were conducted in PBS both at pH 7.4 and 6.4 to mimic normal tissue and tumor tissue conditions. The same release study protocols applied to the two buffer conditions. Release profiles of 2',7-triethyl Si PTX nanoparticles were plotted over

time in the hope of studying pH-responsive effect on release rates. The protocol of nanoparticle preparation, post-treatments and release study protocol are shown in Figure 4.4.

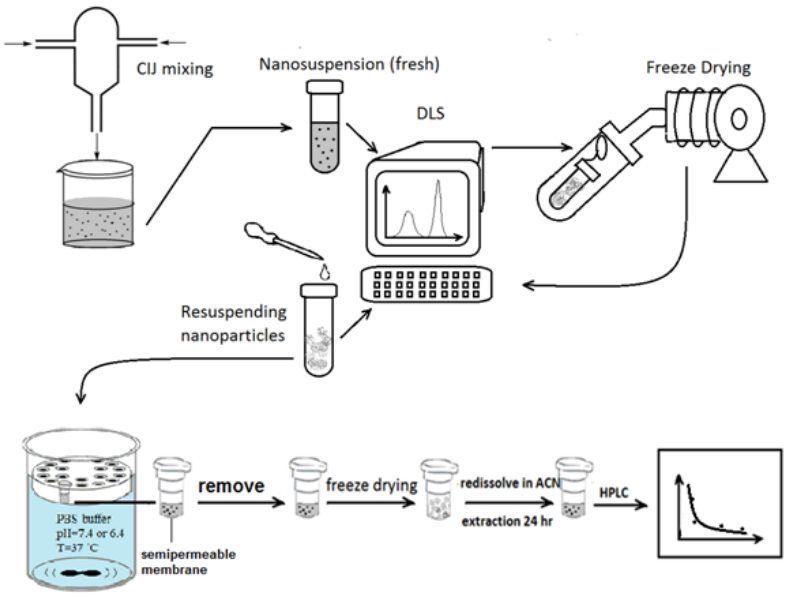

Figure 4.4 Nanoparticle preparation, size measurement, post-treatment and release kinetic characterization processes.

4.2.4.4 Silicate Derivatives of Paclitaxel Prodrugs

In this study, 2',7-triethyl Si PTX and 2'-triethyl Si PTX nanoparticles were used to conduct *in vitro* drug release studies. 15 mg of each were weighed and resuspended in 15 mL PBS separately, using microtip probe sonication for 5 min. They were put into multiple dialysis mini capsules (500 μL) and immersed into 2 L PBS. At predetermined time points, triplicate capsules were removed and lyophilized. The dry product remaining in capsules was dissolved in acetonitrile and extracted overnight. The extracts were

analyzed by HPLC to determine the amount of Si PTX/PTX as un-released drug. Release profiles were plotted as a function of time.

The comparison between two derivatives (bis-Si PTX) and one derivative (mono Si PTX) were first carried out on prodrugs with triethyl Si derivates. The similar comparisons were carried out on triisopropyl and trioctyl Si PTX nanoparticles as well. Meanwhile, the comparisons among different derivatives were also observed when the prodrugs were chosen with either one (mono-) or two (bis-) Si derivatives.

4.3 Results and Discussion

4.3.1 Nanopaticle Physical Properties

Nanoparticle sizes were measured by DLS apparatus (Beckman Coulter, CA) immediately after CIJ-D mixing and before ultracentrifugation. The results were recorded using mass average size and intensity average size shown in Table 4.2. Nanoparticles usually had a bimodal distribution which showed not only empty polymer nanoparticles in a range of 20-50 nm and drug loaded nanoparticles larger than 50 nm. The mass average sizes for all the nanoparticles were controlled in the range of 50-90 nm, while the intensity average sizes were more skewed towards larger particles, up to 150 nm. The size polydispersity index (PDI) values showed that the nanoparticles had a relatively broad distribution, which might be due to FNP process and further aggregation. The SEM and TEM images in Ch.3 also showed that nanoparticles were spherical with a size range of 50-150 nm. There was no obvious trend on nanoparticle size as a function of silicate derivatives or molecular weight.

Table 4.2 Properties of six Si PTX loaded nanoparticles

Prodrug	aLogP	d_m(nm)	d_I(nm)	PDI	Prodrug loading%
1a	4.96	78±13	145±9	0.10	49.1±5.4
2a	6.31	70±3	132±20	0.13	52.3±6.5
1b	7.74	77±15	83±6	0.16	55.3±3.5
2b	8.59	83±29	123±36	0.66	57.8±3.8
1c	5.60	52±17	136±1	0.17	50.8±2.3
2c	6.84	46±8	128±4	0.53	53.4±1.8

Note: aLogP is calculated by using ALOPS 2.1.
d_m & d_I: particle mass average diameter+standard deviation, and particle intensity average diameter+standard deviation of three batches of particles and three measurement in each.
PDI: size polydispersity index of particle intensity average size
Loading%: total of encapsulated prodrug in nanoparticles (without ultracentrifugation).

Note that nanoparticles prepared in this chapter were not ultracentrifuged, instead they were directly lyophilized after preparation. Thus, it is very likely that prodrug loaded nanoparticles were mixed with empty polymer particles and un-encapsulated prodrug. The loading was determined by the total amount of prodrug possibly including both encapsulated and un-encapsulated ones in dry nanoparticles. Therefore, Table 4.2 showed that the determined loadings were very close to the initial formulation used in FNP. This has been corrected in next chapter when ultracentrifugation was introduced before lyophilization, in order to remove all the empty polymer nanoparticles, lightly loaded nanoparticles and un-loaded free drug.

4.3.2 In Vitro Drug Release Setup/Protocol

Infinite sink condition has been claimed necessary to conduct *in vitro* release study for highly hydrophobic drug. Using Langer's method[130], we prepared 40 L PBS to dialyze 15 mg 2',7-triethyl Si PTX loaded nanoparticles in group 1. Meanwhile, the same

amount of nanoparticle suspension was dialyzed in 1 L PBS but refreshed at predetermined time. Figure 4.5 showed that nanparticles released in a similar rate, but uncertainty was huge in both groups. Generally, there was a burst release pattern in the first 10 hrs, followed with a more extended and slower release in next 3 days. This burst release and large error bars make this study of limited use. But, it indicated that frequent buffer refresh provided sufficient sink condition for 2',7-triethyl Si PTX/PTX, as good as the infinite sink condition provided by 40 L PBS. It can be an alternative to infinite sink condition, more economical, practical and easier to prepare.

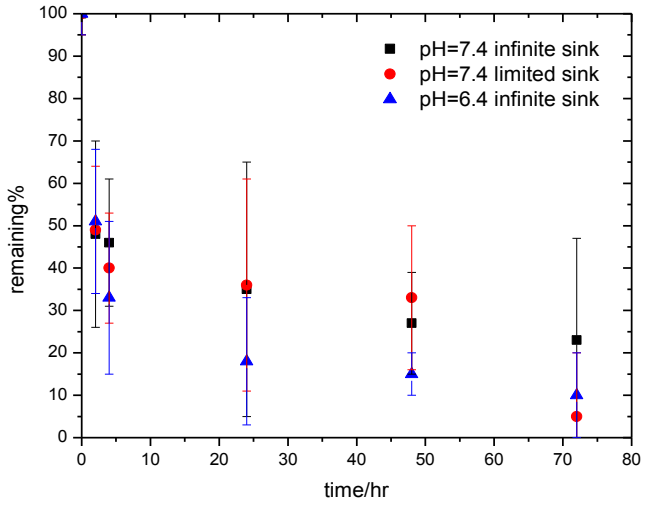

Figure 4.5 Reverse release profiles of 2',7-triethyl Si PTX NPs in different release conditions.

In comparison of dialysis devices, nanoparticles contained in dialysis tubes (black in Figure 4.5) and mini capsules (Red in Figure 4.5) had almost overlapped release rates using the same drug release protocol. However, when nanoparticles were contained in dialysis cassette, the release profiles showed a burst release pattern in short term as usual, but no significant release in long term up to 3 days. The possible reasons are, dialysis cassettes had a larger volume (6-12 mL) containing nanoparticles, and they were

immersed in beaker and placed on a plate shaker with a speed of 100 rpm and in the 37˚C incubator, instead of using magnetic stir bar. The rotation of the plate in incubator might not be sufficient to achieve flow exchange through dialysis membrane, despite that the membrane materials on dialysis cassette and capsules are same, provided by the same manufacturer. As a result, the aqueous solution in dialysis cassette was saturated with drug/prodrug released from nanoparticles and they crystallized to the bottom of the cassette. The release of drug through membrane was greatly inhibited. To investigate it, nanoparticle sedimentation with possible PTX crystallization was actually observed in dialysis cassette after 36 hrs pointed by the red arrow in Figure 4.6 (b). The nanosuspenion in cassette had a fraction of supernatant clear on the top and white precipitation accumulated on the bottom. It implied that the aggregation and the crystalline bulk of PTX limited the dissolution rate of prodrug/PTX, leading to no significant release in long term.

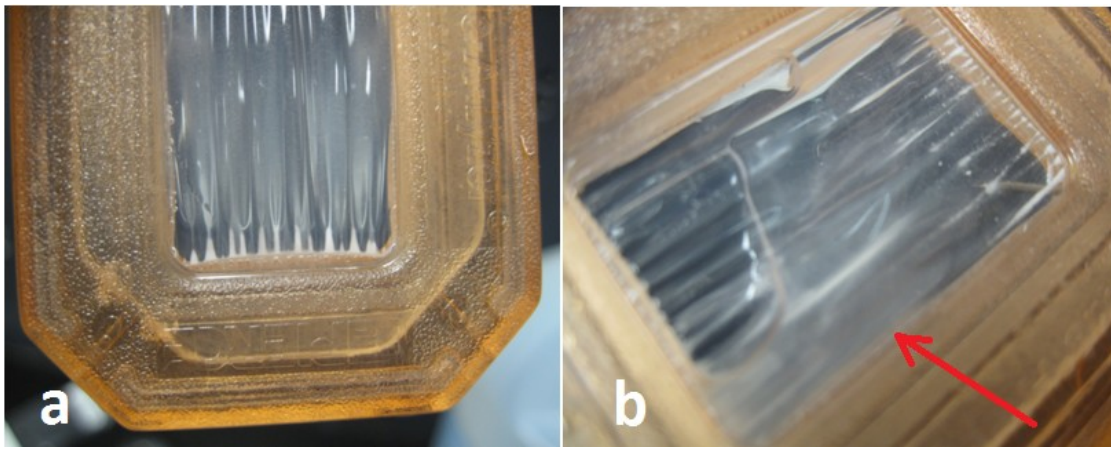

Figure 4.6 Redispersed 2',7-triethyl Si PTX NPs in dialysis cassette (a) right after redispersion and (b) 36hr during release study.

Finally, dialysis mini capsules were chosen for *in vitro* drug release study in future, since they are cheap, disposable, and easy to use. To point out, dialysis mini

capsules containing nanoparticles were removed and directly lyophilized, and no materials were transferred out of the capsule. This helped us to avoid mass loss during sample transfer, which is critical when the following HPLC analysis were usually conducted on samples in microliters.

To sum up, for all further *in vitro* drug release studies, I chose to use dialysis mini capsules and to refresh buffer solution frequently to avoid drug saturation. The drug remaining in capsules were mainly analyzed to show a reverse release profile, where the encapsulated/un-released drug decreased as a function of time. Temperature was controlled at 37 ^{o}C by the incubator rotating at a speed of 100 rpm, and PBS was controlled at pH 7.4 and 6.4, to mimic conditions in blood circulation/healthy tissues and tumor tissues. PBS was only used to mimic ion, pH and temperature conditions in healthy and normal tissues. It is simpler condition than in vivo conditions where clearance of the drug during circulation, possible protein binding, and macrophages uptake must be considered.

4.3.3 In Vitro Drug Release Profiles

4.3.3.1 Diffusion of Drug and Prodrug Only

To test whether PTX and 2',7-triethyl Si PTX can diffuse freely through semi-permeable membrane on dialysis mini capsules, 10 mg of PTX and 2',7-triethyl Si PTX were dissolved in 10 mL DI water, respectively. Based on their aqueous solubility estimated by Wohl et al[59], the solution of PTX and 2',7-triethyl Si PTX were oversaturated. The supernatant as saturated solution was removed and placed in dialysis mini capsules, which were immersed in 15 mL PBS at pH 7.4 and 37˚C. Each mini capsule contained 500 μL solution. PBS was refreshed every 30 min. At predetermined

time (0, 1, 3, 6, 8, 10, 24 hr), two dialysis mini capsules and 15 mL PBS were collected and lyophilized. The dry product was dissolved in 1 mL acetonitrile and extracted. The extracts were analyzed by HPLC to determine the amount of PTX and 2',7-triethyl Si PTX remaining in capsules and diffused in PBS.

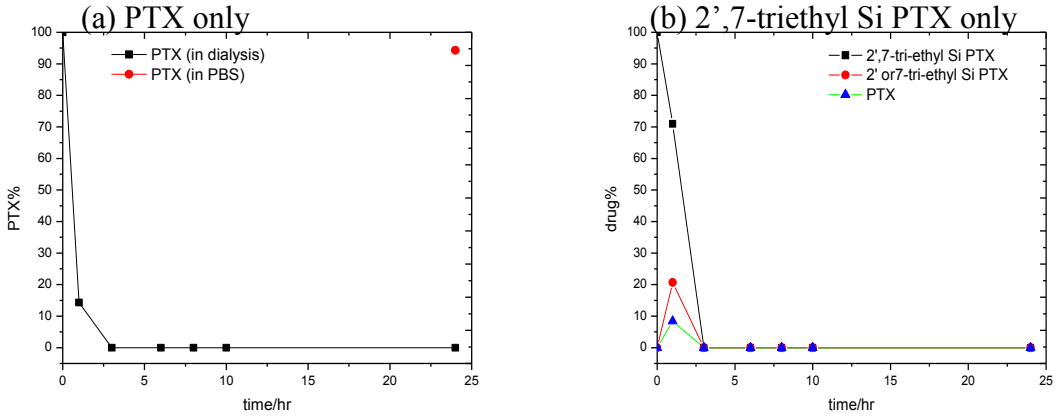

Figure 4.7 Percentage of (a) PTX in dialysis capsule and diffusing through membrane into PBS and (b) 2,7-triethyl Si PTX, intermediate 2' or 7-triethyl Si PTX and PTX obtained from hydrolysis remaining in dialysis capsule.

As shown in Figure 4.7 (a), about 15% of PTX remained in dialysis mini capsules after 1 hr. The retention of this 15% of PTX might be caused by the saturation of PTX in PBS outside dialysis capsules before buffer was refreshed. If the experiment was conducted in perfect sink condition, the diffusion of PTX should be rapid enough to transfer across dialysis membrane immediately. None of it should be detected inside dialysis capsules. There was no PTX in capsules detectable by HPLC after 3 hr, which meant the capsules were empty then. In PBS, the amount of PTX was not able to be identified because larger signal noise in HPLC, until it accumulated to 95% at 24 hr. As shown in Figure 4.7 (b), about 30% of 2',7-triethyl Si PTX remained in dialysis mini capsules after 1 hr, while 10% of PTX, 20% of 2' and 7-triethyl Si PTX were found. Similarly, the mini capsules were completely empty after 3 hr. These results

demonstrated that as molecules, PTX and 2',7-triethyl Si PTX are able to diffuse out of dialysis membrane quickly, possibly shorter than 3 hrs. Their diffusion should not be a limiting factor of drug release if they are encapsulated in nanoparticles and able to release out of nanoparticles.

4.3.3.2 pH 7.4 vs. 6.4

When 2',7-triethyl Si PTX nanoparticles were dialyzed against PBS at pH 6.4 and 7.4, the general release rates showed a similar trend in both cases shown in Figure 4.8, where a burst release pattern was found in short term, and slow release in long term. Overall, nanoparticles released in similar rate in PBS at pH 6.4 and 7.4 both using infinite sink condition and limited sink followed with frequent buffer refresh. The possible reason is that, the hydrolysis of 2',7-triethyl Si PTX is not sensitive to such small difference in pH.

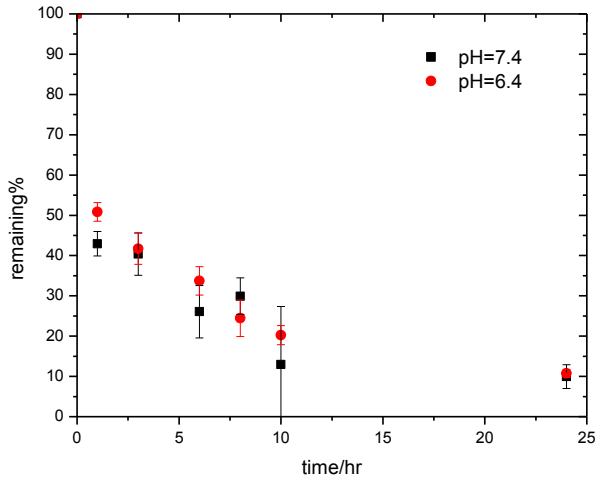

Figure 4.8 Reverse release profiles of 2',7-triethyl Si PTX NPs in PBS at pH 7.4 and 6.4.

4.3.3.3 Silicate Ester Derivatives

In Figure 4.9, *in vitro* release studies in PBS (pH=6.4) were first divided into three groups, in terms of types of silicate ester derivates. Group 1, they were both triethyl Si PTX nanoparticles, but with one silicate derivative at 2'C position (1a) and two silicate derivates at both 2'C and 7C positions (2a). The same applied to Group 2, trioctyl Si PTX (1b & 2b) and Group 3, triisopropyl Si PTX nanoparticles (1c & 2c). Nanoparticles in Group 1 (1a & 2a) had almost complete release in 24 hr, followed by Group 2 (1b & 2b), in 48 hr and Group 3(1c & 2c) in 72 hr because their relative hydrolysis rates of silicate ester derivatives followed in this order a>b>c shown in Table 4.1. These Si PTX prodrugs were hydrophobic enough to be encapsulated in nanoparticles. Once the hydrolysis occurred, their hydrophobcities were reduced by 1-2 orders of magnitude, and 1-5 orders of magnitude indicated by LogP in Table 4.1 if they were converted to be PTX. This resulted in faster diffusion of less hydrophobic Si PTX and PTX itself through membrane and faster release of drug from nanoparticles.

4.3.3.4 One vs. Two Silicate Derivatives

These six Si PTX prodrugs can be also seen as two categories by the number of silicate ester derivatives. Group 1 has only one silicate derivative at 2'C position, 1a, 1b and 1c. Group 2 has two silicate derivates at 2'C and 7C positions, 2a, 2b and 2c. Across all three silicate ester derivatized PTX, nanoparticles loaded with 1a, 1b and 1c have consistently released faster than those loaded with 2a, 2b and 2c, because the cleavage of 2' silicate derivative by hydrolysis was much faster. In comparison, the cleavage of silicate ester at 7C was much hindered. This difference was slightly more obvious for

isopropyl Si PTX nanoparticles but not very distinctive for ethyl Si PTX and octyl Si PTX nanoparticles. This indicated that while the hydrolytic lability played an important role in release rate, the diffusion of Si PTX with one and two silicate derivates was very significant.

(a)

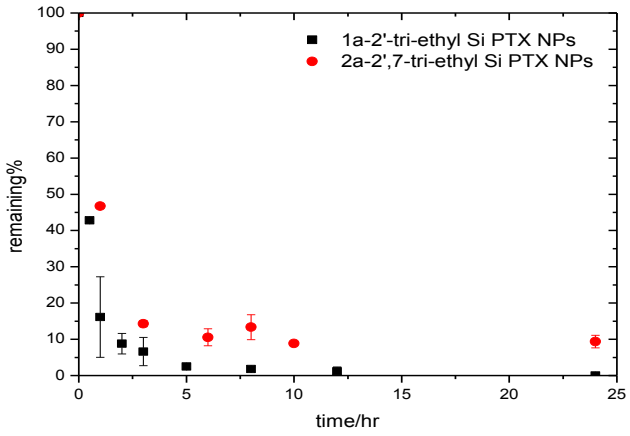

(b)

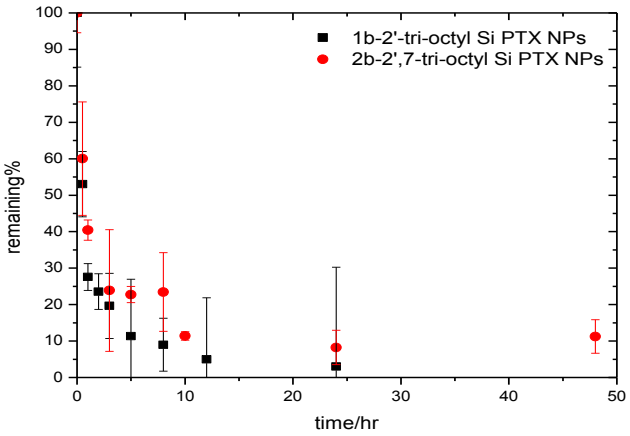

(c)

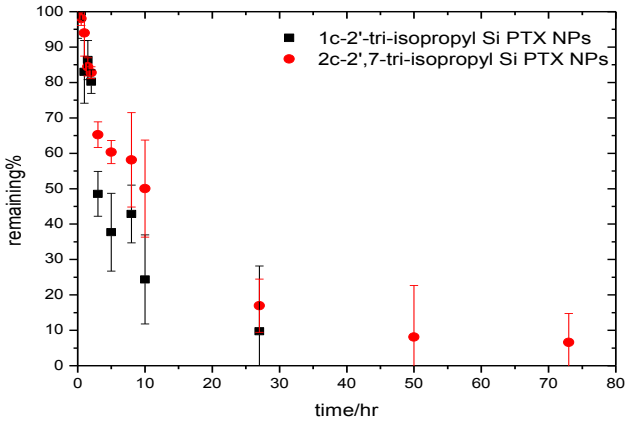

Figure 4.9 Reverse release profiles in PBS at pH 6.4 of a) 1a 2'-triethyl Si PTX and 2a 2',7-triethyl Si PTX NPs, b) 1b 2'-trioctyl Si PTX and 2b 2',7-trioctyl Si PTX NPs and c) 1c 2'-triisopropyl and 2c 2',7-triisopropyl Si PTX NPs.

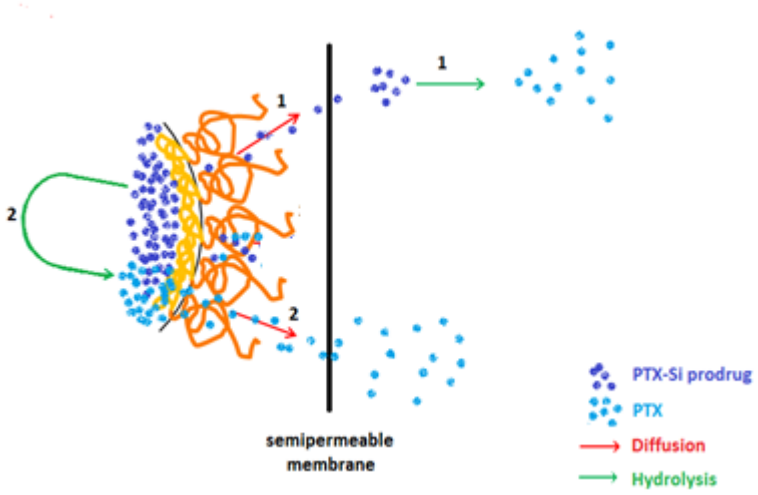

Figure 4.10 Schematic of Si PTX prodrug diffuse and release through dialysis semipermeable membrane, (1) diffusion rate>hydrolysis rate, (2) hydrolysis rate>diffusion rate.

4.4 Conclusions

To sum up, six Si PTX prodrugs synthesized by Wohl et al[59, 60] were used to prepare PEG-*b*-PLGA nanoparticles. The enhanced hydrophobicity of Si PTX allowed nanoparticles to be stable, spherical, size controlled in the range of 50-150 nm. Secondly, *in vitro* drug release protocol was to use dialysis mini capsules, limited sink condition, and to frequently refresh buffer at predetermined time. Reverse release profiles were determined by analyzing the remaining/un-released drug in nanoparticles contained in dialysis capsules. This is meant to overcome detection difficulty of released drug in buffer via HPLC, caused by the extremely low solubility of Si PTX and PTX itself.

With *in vitro* drug release protocol customized, the general release profiles were determined on six batches of nanoparticles loaded with six Si PTX prodrugs, including three types of silicate ester derivatives, each of which was derivatized at one or two

positions. The release rates were attributed to both diffusion of PTX and Si PTX, and tuned hydrolysis rates of Si PTX. The release rates were ranked from slowest to fastest a>b>c, 1a>2a, 1b>2b and 1c>2c, in an increasing order of the relatively hydrolysis rates shown in Table 4.1.

These possible drug release mechanisms are shown in Figure 4.10. (1), prodrugs simply diffuse out of nanoparticles and membrane followed by possible hydrolysis in order to achieve regeneration of PTX. Or, (2) prodrugs with more hydrolytic labile silicate derivatives first hydrolyze back to PTX first, followed by the diffusion of PTX through membrane. Or, (3) prodrugs diffuse and hydrolyze in a similar rate to release PTX. Generally, nanoparticles loaded with these prodrugs presented a burst-and-slow release pattern, which was probably because, the un-encapsulated prodrug/drug and those loosely distributed on the outer region of nanoparticles and diffuse into buffer more quickly, while the prodrug/drug captured in the nanoparticle core slowly diffused out of polymer matrix of nanoparticles.

Based on drug release results shown above, it is still unclear how hydrolysis occurred during the time course of release study. There are questions that need to be answered. For instance, where did hydrolysis take place, in nanoparticles or in PBS? This is very much related to the relation between hydrolysis and diffusion. Specifically put, which occurred first? Is there a difference in hydrolysis rate in nanoparticles and in PBS? Are there any other factors affecting release rates? Many studies have been conducted on polymer degradation[132-136] which can potentially destruct nanoparticle matrix, change morphology and influence drug release, but they often occur after 15-30 days, which

made it impossible for polymer degradation to affect drug release in 24-48 hrs These questions will be discussed in Ch. 5 and Ch.6.

Chapter 5

In Vitro Drug Release Study of Silicate Paclitaxel Diblock Copolymer Protected Nanoparticles (ultracentrifuged)

5.1 Introduction

As shown in previous chapter, we have found all silicate paclitaxel loaded nanoparticles had a common burst-and-release pattern. They did not meet one of the goals of functionalizing paclitaxel with silicate esters, which was to make the paclitaxel prodrugs sufficiently hydrophobic, to let the cleavage of silicate precede the diffusion of the compound, and eventually to help obtain a more extended release pattern. The burst release phenomenon allowed us to wonder whether any improvement can be made during nanoparticle preparation and post-treatment processes, in order to obtain nanoparticles with high purity and more accurate characterization.

It is common in pharmaceutical laboratory using ultracentrifugation[137-139] to separate protein, microparticles and free compounds. As discussed in Chapter 3, we have demonstrated that ultracentrifugation is essential to our nanoparticle preparation as well. Not only did it separate prodrug loaded nanoparticles away from empty polymer nanoparticles and un-encapsulated drug, but also helped to enhance the actual drug loading after separation. Therefore in this chapter, different from Ch. 4, all nanoparticles were freshly made, immediately ultracentrifuged and lyophilized. The loading levels of prodrugs were determined afterwards in the range of 55-75%, which were higher than the

initial formula for particle preparation. More importantly, these particles have shown much more extended release profiles.

The six Si PTX prodrugs studied in this chapter are 2'-triethyl Si PTX (1a), 2'-trioctyl Si PTX (1b), 2'-triisopropyl Si PTX (1c), 2'-ditert butyl/ethyl Si PTX (1d), 2'-trimenthyl Si PTX (1e) and 2',7-bis-triethyl Si PTX (2a)[59]. The first five are paclitaxel with only one silicate ester at 2'C position. The last one is paclitaxel derivatized at both 2'C and 7C positions.

To investigate the effect of silicate esters on particle physical and pharmacokinetic properties in a simpler way, this chapter focuses on mono-Si PTX prodrugs with one silicate ester derivative. Because they only have one cleavage of silicate at the 2'carbon, they simplified the way to identify diffusion and hydrolysis rates, only Si PTX prodrug and PTX were present in buffer and nanoparticles after hydrolysis. In contrast, 2',7-triethyl silicate paclitaxel (2a) was involved with two cleavages of silicate derivatives, four compounds in present via hydrolysis. They were 2'7-triethyl Si PTX, 2'-triethyl Si PTX, 7-triethyl Si PTX and PTX itself. This multiple-compound system clouded the judgment on the completion of the hydrolysis and comparison with diffusion. Moreover, the cytotoxicity of the intermediates from 2',7-triethyl Si PTX, 2' and 7-triethyl Si PTX have not been studied yet.

In vitro drug release studies were not only conducted in PBS at pH 7.4 and 6.4, but also in acetic acid buffer at pH 5.0, in order to compare pH-responsive hydrolysis rates. Beside the quantification of drug/prodrug remaining in particles, the exterior buffer containing released drug/prodrug was also analyzed. A combination of two allowed us to first validate the reverse release protocol as an alternative approach to determine drug

release for extremely hydrophobic drugs, and to discover the relative hydrolysis and diffusion rates of drug/prodrug in different environments, specifically nanoparticles and buffer solution.

The relative hydrolysis rates of these six Si PTX prodrugs were estimated by ^{1}H NMR and hydrophobicity by calculated LogP. Nanoparticles loaded with these prodrugs were formulated using the confined-impingment-jet-dilution (CIJ-D) mixer. Particle size and distribution were characterized by dynamic light scattering (DLS) and morphology by Cryogenic-transmission electron microscopy (Cryo-TEM). Prodrug/drug loading levels and *in vitro* drug release kinetics were determined by high performance liquid chromatography (HPLC).

5.2 Methods and Experiments

5.2.1 Materials

Paclitaxel was obtained from Phytogen Life Sciences. PEG-*b*-PLGA (MW: 5k-10kDa) was synthesized in Dr. Hoye's lab as previously reported [81]. Water (H_2O, HPLC grade), tetrahydrofuran (THF, HPLC grade) and acetonitrile (ACN, HPLC grade) were purchased from Aldrich and used as received. PBS was prepared by dissolving 3.12 g monosodium phosphate and 20.74 g diasodium phosphate in 1 L DI water to achieve pH 7.4, and 10.28 g monosodium phosphate and 6.84 g diasodium phosphate in 1 L DI water for pH 6.4. Monosodium phosphate and diasodium phosphate were purchased from Fisher Scientific. Dialysis mini capsules (MWCO: 10k Da, 0.5-1 mL) were purchased from Thermo Scientific. Silicate prodrugs were synthesized in Dr. Hoye's lab as

previously reported [109, 112]. Their chemical structures are shown in Figure 5.1 and properties in Table 5.1.

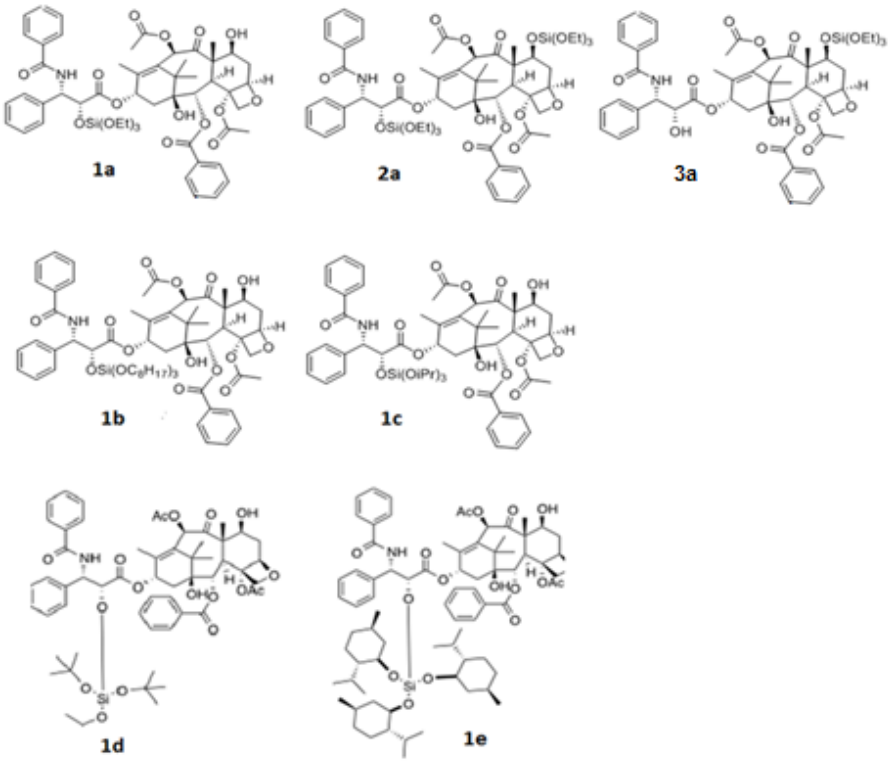

Figure 5.1 Chemical structures of 2'-triethyl Si PTX (1a), 2',7-triethyl Si PTX (2a), 7-triethyl Si PTX (3a), 2'-trioctyl Si PTX (1b), 2'-triisopropyl Si PTX (1c), 2'ditert butyl/ethyl Si PTX (1d) and 2'-trimenthyl Si PTX (1e).

5.2.2 Nanoparticle Preparation

Nanoparticles made with each of Si PTX prodrugs were prepared using CIJ-D mixer via flash nanoprecipitaiton. For one single batch of nanoparticles, 35-40 mg of Si PTX prodrugs (with an equivalent of 25 mg PTX) and 25 mg of PEG-*b*-PLGA were dissolved in 2.5 mL THF, contained in a 3mL syringe. It was impinged rapidly with the other syringe containing 2.5 mL water within 5 seconds. The mixture was drained into 45 mL DI water, in order to further quench nanoparticle growth. The resulting nanoparticle

suspension had total volume of 50 mL with a ratio of 5:95 THF: H_2O and total mass of approximately 60-65 mg nanoparticles. The nanoparticle suspension was further ultracentrifuged (Beckman Coulter, CA) at 50,000 rpm, 4 ^oC, 30 min for three times. The final pellet was removed, lyophilized and stored at 4 ^oC fridge.

Table 5.1 Properties of PTX and Si PTX prodrugs

Substrate	MW/Da	aLogP[a]	ca. K_{rel}[b]	$t_{1/2}$(min)[c]
PTX	854	3.20	N/A	N/A
1a	1016	4.96	18,000	3.7
2a	1178	6.31	15,000 (C2'), 2100 (C7)	4.6 (C2'), 33 (C7)
3a	1016	5.05	2,200	30
1b	1269	7.74	5600	12
1c	1058	5.60	570	120
1d	1072	7.37	1.0	69,000
1e	1347	5.81	5.6	12,000

a: aLogP is calculated by using ALOPS 2.1
b:ca. K_{rel} is calculated relative hydrolysis rate by Wohl's NMR method[59,60].
c: $t_{1/2}$ is half time of hydrolysis by Wohl's NMR method[59,60].

5.2.3 Nanoparticle Characterization

5.2.3.1 Nanoparticle Size and Distribution

As described in Ch.3 and Ch.4, nanoparticles were made via CIJ-D mixer by flash nanoprecipitation. The DLS apparatus (Beckman Coulter, CA) was used to measure nanoparticle sizes. 100 μL suspension with 0.1 wt% nanoparticles was removed by micro

pipette, and diluted with 1 mL DI water in DLS square tube. Three identical samples were sealed with plastic caps. Nanoparticle size was measured and averaged across 150 individual detections. The resulting intensity size d_I was determined by averaging three measurements. Size polydispersities and standard deviations were calculated and recorded automatically. Nanoparticle sizes were also characterized after lyophilization, in order to compare nanoparticle stability and morphology change.

5.2.3.2 Nanoparticle Morphology

My colleague Hanseung Lee conducted nanoparticle morphology characterization by Cryogenic transmission electron microscopy (Cryo-TEM), either with nanoparticle suspension or dried nanopaticle powder. The procedure to prepare samples was described in Ch.3. Cryo-TEM images not only enabled us to see nanoparticle morphology, but also internal core-shell structure when they were observed with objective lens in an under-focused mode (2-4 μm). The under-focused mode was intentionally controlled so that Fresnel fringe (white rings on the boundary of the structure) can appear and that elucidated the core and shell in images. Moreover, hundreds of nanoparticles in Cryo-TEM images were manually counted and Gatan Digital Micrograph 3.11.1 software (Gatan, Pleasanton, CA) was used to analyze sizes of particle core, shell and particle as a whole. The number of counted nanoparticles and the resulting size distribution were discussed in Ch.6.

5.2.3.3 Nanoparticle Drug Loading

Sample preparation methods for HPLC was described in Ch. 3 and Ch.4. When HPLC was used to determine the quantity of (1a) 2'-triethyl Si PTX and (2a) 2',7-triethyl

Si PTX, the mobile phase consisted of a mixture of acetonitrile and water with a volume ratio of 75:25, and was delivered at a flow rate of 1 mL/min. When HPLC was used to determine the quantity of other Si PTX prodrugs (1b, 1c, 1d and 1e), with their increased hydrophobicity, the mobile phase consisted of a mixture of acetonitrile and water in a continuous gradient between a volume ratio of 100:0 to 50:50 of acetonitrile:H_2O, as described in Ch. 4. The Si PTX prodrug loading levels of lyophilized nanoparticles were determined by analyzing the acetonitrile extract using Eq.4.4 in Ch.4.

5.2.4 In Vitro Drug Release

Nanoparticles loaded with each of the Si PTX prodrugs were first lyophilized. 15 mg of nanoparticles in dry powder was weighed and dispersed in 15 mL PBS (pH 7.4 or 6.4) or acetic acid buffer (pH 5.0) using microtip probe sonication for 5 min, the procedure detail of sonication was described in Ch.3. They were put into multiple dialysis mini capsules (500 μL, MWCO: 10 kDa, Thermo Fisher Scientific, IL) and immersed into 10 L PBS. At predetermined time points (0, 1, 2, 4, 6, 8, 12, 24, 48, 72, 96, 120 hr) triplicate capsules were removed and lyophilized and 10 L buffer solution was refreshed afterwards. The lyophilized samples were dissolved in acetonitrile and extracted overnight. The extracts were analyzed by HPLC to determine the amount of drug/prodrug remaining in nanoparticle suspension. Reverse release profiles were plotted displaying the remaining (or unreleased) drug/prodrug as a function of time.

5.2.5 Mass Balance

In order to further validate the reverse release method described above, at each predetermined time, 10 L buffer solution, albeit a huge volume, were lyophilized,

extracted by acetonitrile and quantified by HPLC to determine the amount of released drug. The buffer solution (PBS at pH 7.4 and acetic acid at pH 5.0) of 10 L was transferred into several 60 mL tubes and lyophilized by hundreds of batches. Each batch contained 8-12 tubes of buffer for 24-48 hr lyophilization. After buffer solution collected at one specific time point was completely lyophilized, all the tubes containing dry powder of sodium phosphate and the released drug were rinsed by 1 mL acetonitrile for three times and extracted for 24 hr. Eventually, HPLC was used to determine the amount of released drug obtained from 3 mL acetonitrile extracts. The released drug/prodrug was plotted as a function of time, which generally showed an increasing trend of drug/prodrug% over time. The plot was constructed by adding the quantity of released drug determined at one time point to that obtained from previous time points. It took great caution to transfer buffer from beaker to tubes for lyophilization as well as to collect acetonitrile used extracting the released drug. It was very likely to lose sample during buffer transfer and solvent rinse. Also, when PBS was the buffer solution, a great amount of sodium phosphate was obtained, which was mixed with the released drug after lyophilization. It made more difficult for acetonitrile to extract the released drug from the lyophilized dry powder. After acetonitrile extract was analyzed by HPLC, the error could be huge in some cases, especially when some samples contained a fair amount of the released drug, some didn't have any. The unreleased ones obtained from dialysis mini capsules were also quantified by HPLC. The procedure described above enabled us to check mass balance with the quantity of both remaining/unreleased drug in nanoparticles and the released ones in buffer. This experiment was conducted at pH 7.4 and 5.0.

5.2.6 pH Variation

Another addition of *in vitro* drug release study in this chapter was to investigate the influence of pH on hydrolysis of prodrugs. *In vitro* drug release and mass balance studies were conducted at pH 7.4, 6.4 and 5.0. Following the same protocol above, the unreleased and released drug/prodrug were plotted against time in three buffer solutions. This comparison was meant to discover the pH response of the composition change between PTX and Si PTX prodrugs both in particles and buffer solutions.

5.3 Results and Discussion

5.3.1 Nanoparticle Size and Distribution

Fresh nanoparticles immediately made via CIJ-D mixing were encapsulated with Si PTX prodrugs and well stabilized by PEG-*b*-PLGA, in an averaged intensity size range of 80-150 nm shown in Table 5.2. Noted that, first of all, Si PTX prodrugs were listed in an increasing order of hydrophobicity indicated by aLogP[118] values in Table 5.2, 1a<1c<1e<2a<1d<1b. Nanoparticle sizes appeared to have a decreasing trend with the increasing hydrophobicity of Si PTX prodrugs. It appears to be a linear relation of intensity average size with LogP values with 26% deviation. This trend can be explained by the nucleation and growth mechanism for particle formation. As the Si PTX prodrug was more hydrophobic, its nucleation rate increased but the precipitation rate of hydrophobic block of copolymer should remain constant. As a result, more and smaller nuclei formed until the deposition of PLGA block arrested the particle growth and PEG block stabilized particles. Secondly, 2',7-triethyl Si PTX (2a) NPs had slightly smaller

average particle size than that shown in Table 3.3, but including standard deviation, they both lied in the range of 105-135 nm.

After nanoparticles were ultracentrifuged, lyophilized and dispersed in water, the sizes increased significantly due to nanoparticle aggregation driven by the freezing process of lyophilization[85, 86]. Their intensity average sizes ranged from 200-450 nm with broader size distribution indicated by size polydispersity (PDI). So far, we have not found any influence of aggregation on drug release rates, but for nanoparticles which were designed for a particular size, ultracentrifugation can be problematic.

Table 5.2 Properties of Si PTX loaded nanoparticles

Prodrug	aLogP[a]	Before ultracentrifuge		After ultracentrifuge		
		d_I(nm)[b]	PDI[c]	d_I(nm)	PDI	Drug Loading(%)[d]
1a	4.96	145±9	0.10	423±56	0.25	63.0
1c	5.60	136±1	0.17	201±32	0.34	58.0
1e	5.81	95±2	0.08	197±25	0.31	73.5
2a	6.31	118±13	0.13	312±18	0.65	60.4
1d	7.37	86±2	0.09	245±27	0.36	73.5
1b	7.74	83±6	0.16	214±23	0.23	65.0

a: aLogP is calculated by using ALOPS 2.1.
b: d_I is intensity particle diameter by DLS + standard deviation of averaged particle size within three batches of particles prepared in same condition and formula.
c: PDI is polydispersity index of particle size
d:Drug loading(%) is total of encapsulated prodrug/drug in nanoparticles (after ultracentrifugation) determined by HPLC

5.3.2 Fresh Nanoparticle Morphology and Internal Structure

Freshly made nanoparticles immediately after CIJ-D mixing were imaged via Cryo-TEM images shown in Figure 5.2. Sizes and distribution analysis based on these images are shown in Figure 5.3. They were fairly consistent, within 2-15% compared to d_I by DLS. It indicated that, in the increasing order of hydrophobicity, nanoparticles became smaller in this order 1a>1c>1e>2a>1d>1b. The number of counted nanoparticles is labeled in Figure 5.3. Noted that nanoparticles loaded with 1a and 1c had a significant amount of small particles less than 50 nm, these particles were believed to be empty block copolymer nanoparticles. It can be explained by nucleation and growth mechanism of nanoparticle formation. The Si PTX prodrugs 1a and 1c are less hydrophobic than other prodrugs, their nucleation rates during flash nanoprecipitation are slower than others while the deposition rate of hydrophobic block PLGA are considered constant and similar with other prodrugs. Therefore, the nucleation of 1a and 1c are slower than the deposition of polymer so that they form empty polymer nanoparticles first.

Except size and distribution, the images showed similar internal structure. For example, in Figure 5.2 (1a), they showed a clear core-shell structure. The core displayed a higher contrast probably due to more electron density of Si PTX, and the shell was mostly composed of hydrophobic chains, PLGA while the hydrophilic PEG was likely to be swollen with water and invisible after being vitrified. As nanoparticle size became smaller, for instance, with the most hydrophobic 2'-trioctyl Si PTX (1b), nanoparticles had an average size of approximately 80 nm, where the cores cannot be differentiated, probably because particles were too small to be seen with cores.

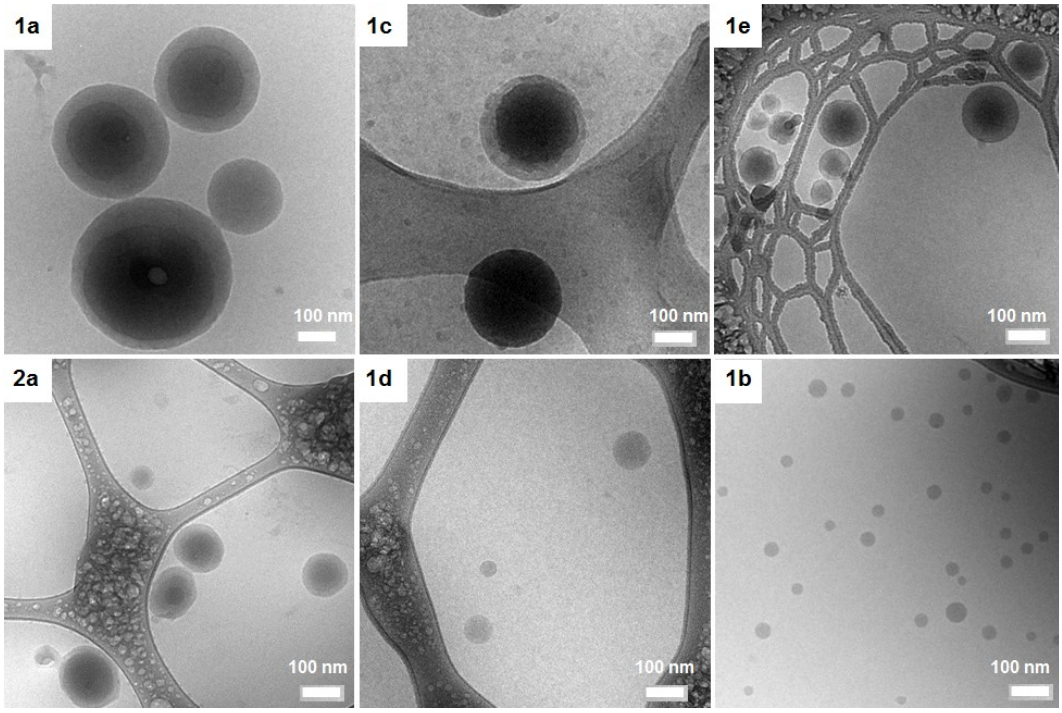

Figure 5.2 Cryo-TEM images of fresh Si PTX loaded PEG-*b*-PLGA protected nanoparticles (before ultracentrifugation).

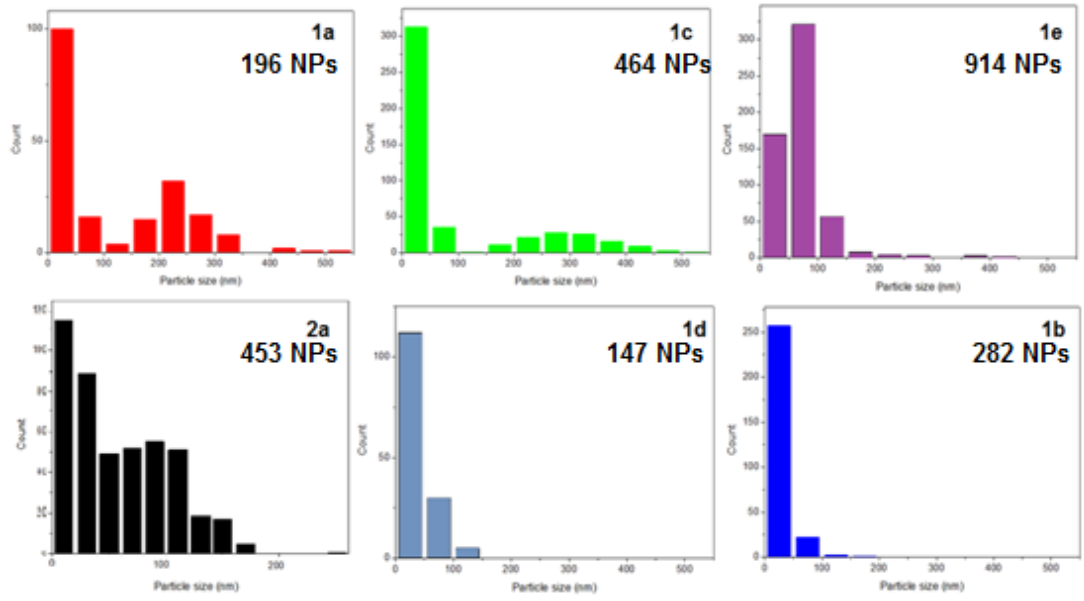

Figure 5.3 Fresh nanoparticle size distribution manually calculated from Cryo-TEM images.

5.3.3 Drug Loading Levels

The drug loadings were determined by dissolving ultracentrifuged and lyophilized nanoparticles in acetonitrile and analyzing acetonitrile extracts by HPLC. The drug loading included the initial Si PTX prodrug, and possibly PTX and intermediates obtained via hydrolysis. The percentage of PTX and intermediates were calculated by converting their concentration back to that of equivalent amount of Si PTX prodrugs. For example, nanoparticles loaded with (2a) 2',7-triethyl Si PTX had a 60.4% of drug loading vs. nanoparticle mass. It included 1.6% of 2',7-triethyl Si PTX hydrolyzed to be PTX, 16.3% to be 2'or 7-triethyl Si PTX and 42.5% of 2',7-triethyl Si PTX as shown in Table 3.3.

Since all nanoparticles in this chapter were ultracentrifuged, the drug loading levels were determined only after the un-encapsulated Si PTX and empty polymer particles were removed from nanosuspension. Although approximately 50% of initial materials used in CIJ-D mixing were removed during ultracentrifugation, the resulting nanoparticles were believed to be only Si PTX loaded ones. The loadings were listed in Table 5.2 showing a range of 58-75% of prodrug in nanoparticles, which has been enhanced greatly from the calculated loading of 55-60% based on the initial formula as nanoparticles were made. This implied that as prepared by FNP, nanoparticles not only had a distribution in size, but also in loading of Si PTX prodrugs as shown in Table 3.3. According to Ch. 3 Eq. 3.7, after ultracentrifugation, nanoparticles loaded with more prodrug had a density of 6.9% higher than solvent mixture. They were more likely to be separated from solvent. Empty polymer micelles, particles and lightly loaded nanoparticles with <4.3% density difference against water, were likely to remain in

supernatant of ultracentrifuged suspension. The empty polymer particles and un-encapsulated prodrugs were discarded by the removal of supernatant. As a result, the final loadings were determined by only heavily loaded nanoparticles.

5.3.4 General Release Rates

In Figure 5.4, the ultracentrifuged nanoparticles loaded with 2',7-triethyl Si PTX (2a) had no obvious burst-release pattern compared to the reverse release profiles of un-ultracentrifuged nanoparticles obtained in Ch.4, but the release of ultracentrifuged nanoparticles was extended from 24 hr to 48 hr. The similar reduction of burst release was also found in other prodrug nanoparticle release studies, the same comparison as Figure 5.4 for 2'-triisopropyl Si PTX (1c) and 2'-trimenthyl Si PTX (1e) nanoparticles were presented in Appendix C. Therefore, the burst release was likely due to the simple diffusion of un-encapsulated prodrugs and those loosely distributed in outer region of nanoparticles.

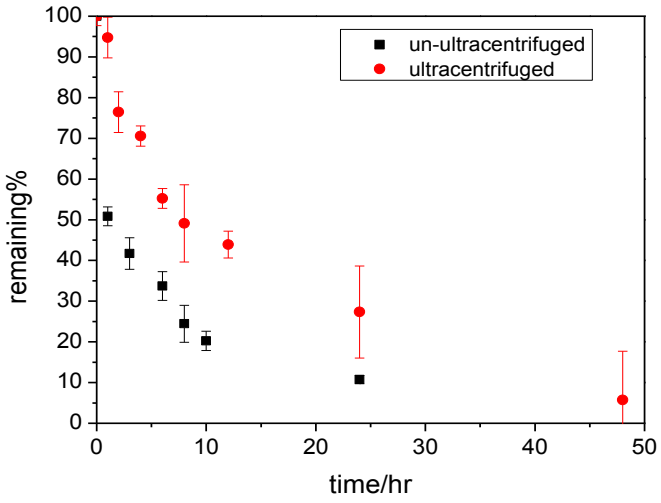

Figure 5.4 Comparison of reverse release profiles for ultracentrifuged 2',7-triethyl Si PTX (2a) and un-ultracentrifuged nanoparticles at pH 7.4.

The reverse release profiles obtained in PBS at pH 7.4 were shown below in Figure 5.5. The general trends were more extended beyond 48 hrs, probably due to the removal of un-encapsulated Si PTX. Among six batches of nanoparticles, 2'7-triethyl Si PTX (2a) nanoparticles were fastest, with completion of 100% release in 48 hrs. 2'-ditert butyl/ethyl Si PTX nanoparticles (1d) were slowest, showing only 55% release in 48 hrs, probably due to its most hydrolytic stability. All nanoparticles of Si PTX derivatized with one silicate ester (1a-1e) started release at different rates shown with the tangent lines in Figure 5.5(a), the rates increased fairly consistent with the increasing hydrolytic lability, but the remaining amount all reached the range of 35-45% at the end of 48 hrs. It implied that the customized hydrolytic lability has tuned the release rates to some extent due to the tuned conversion rates of PTX via hydrolysis along with the varied diffusion rates. The release studies were also conducted in PBS at pH 6.4 but the release rates remained almost the same as pH 7.4. Note that Figure 5.5 only showed the total amount of remaining components in nanoparticles, including both Si PTX prodrugs and PTX, so it is worth investigating in detail the compositions of the two components in each batch of nanoparticles. This will be discussed in the next section.

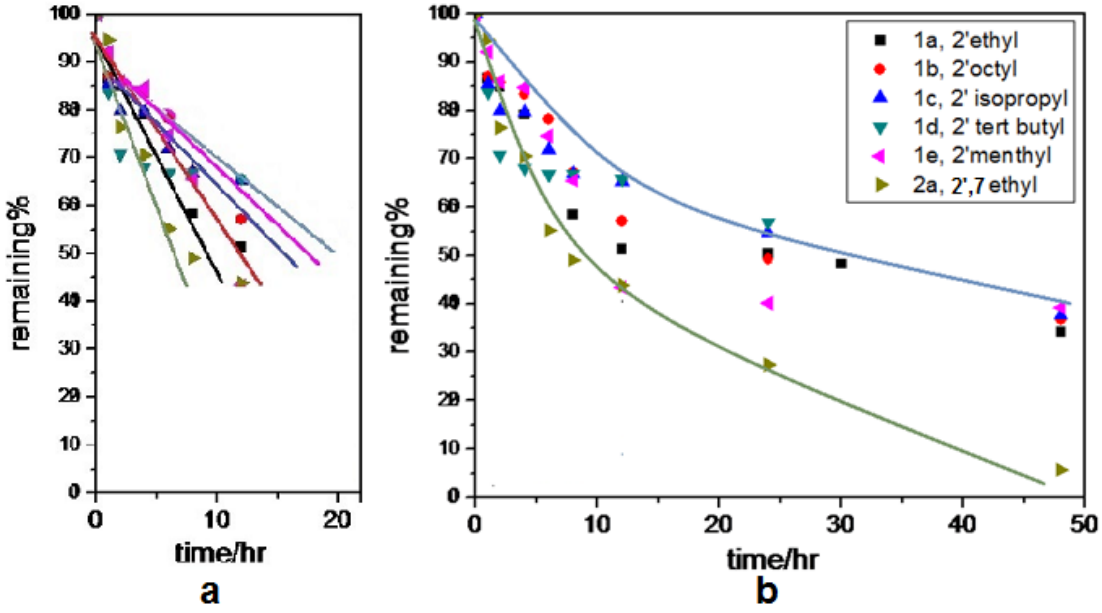

Figure 5.5 General reverse release profiles of nanoparticles in PBS at pH 7.4 in 20 hrs (a) and 48 hrs (b).

5.3.5 Mass Balance

In order to verify the reverse release protocol and check mass balance obtained from nanoparticles and buffer solution during *in vitro* drug release, samples in dialysis mini capsules and buffer solution were both collected and lyophilized at predetermined time. The extracts as the un-released and the released prodrug/drug were both quantified by HPLC.

The mass balance of 2'7-triethyl Si PTX (2a) nanoparticles were studied using PBS at pH 7.4 shown in Figure 5.6. Inside dialysis mini capsule, the components as un-released prodrug/drug were plotted as a function of time for 48 hrs in. The total amount including both Si PTX and PTX showed an almost complete release in 48 hrs. PTX obtained from hydrolysis in nanoparticles reached the peak approximately 9% within 1 hr

and decreased to none later, because PTX were too soluble to be encapsulated in particles so that it diffused into PBS very quickly.

Meanwhile, almost half of the remaining compounds were triethyl Si PTX with one silicate derivative including both 2'-triethyl Si PTX (1a) and 7-triethyl Si PTX (3a), but the majority was 7-triethyl Si PTX (3a). They spiked up to 40% within 1-2 hr, and slowly diffused out. This indicated that the first step of hydrolysis converting 2',7-triethyl Si PTX (2a) to 2'(1a) or 7(3a)-triethyl Si PTX was relatively fast, and comparable to their diffusion rate. Nevertheless, the second cleavage of silicate ester was slower and relatively inactive in nanoparticles, that is why only 10% of PTX at most was found. Unsurprisingly, the amount of 2',7-triethyl Si PTX decreased exponentially over 48 hr as the hydrolysis occurred. The compositions in nanoparticles had almost equal amount of 2',7-triethyl and 2'/7-triethyl Si PTX in 10 hrs, but more 2'/7-triethyl Si PTX appeared later as hydrolysis proceeded. The release mechanism appeared to be a combined contribution of hydrolysis and diffusion of Si PTX prodrugs.

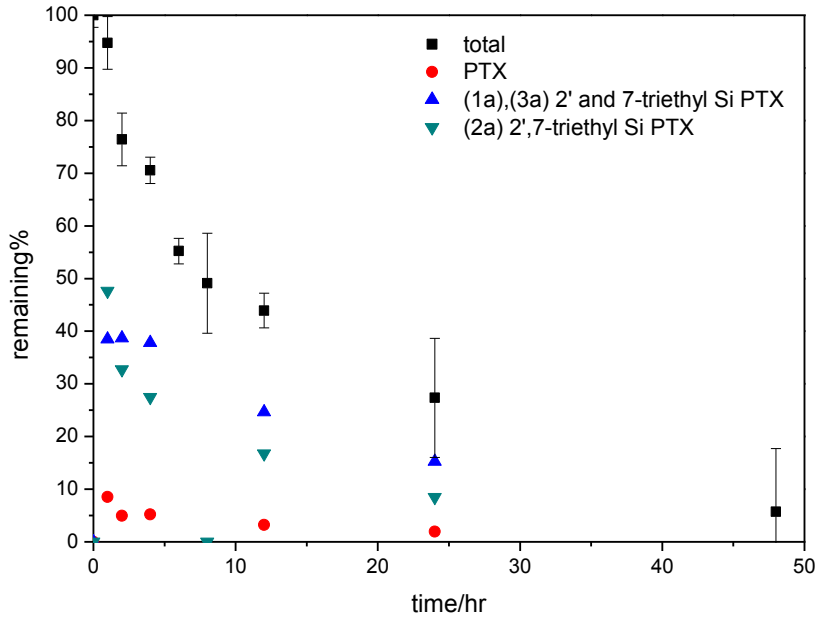

Figure 5.6 Reverse release of (2a) 2'7-triethyl Si PTX nanoparticles in PBS 7.4.

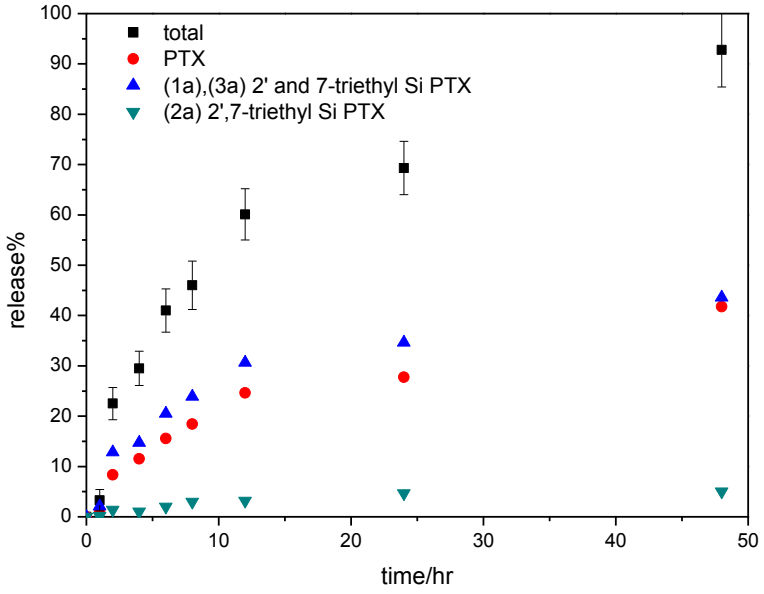

Figure 5.7 Release profile of (2a) 2',7-triethyl Si PTX nanoparticles in PBS 7.4.

In PBS where released drug/prodrug were contained shown in Figure 5.7, the total release was considered complementary to the remaining profile in Figure 5.6. This proved that mass balance was well obtained from two compartments, nanoparticles and PBS. The mass balance was summarized in Table 5.3. Also, it confirmed that the reverse release protocol was a reliable and convenient approach to determine *in vitro* release of highly hydrophobic drug.

Interestingly, the amount of 2',7-triethyl Si PTX in PBS was extremely low. Though it appeared to increase, yet remained under 5% during the entire course of drug release. The majority of the compounds were still 2'or 7-triethyl Si PTX, while PTX was present with slightly smaller but comparable amount. It meant that more cleavage of 2',7-triethyl Si PTX to PTX occurred in PBS than in nanoparticles. At the same time, most of 2',7-triethyl Si PTX has hydrolyzed with first cleavage of silicate. Apparently, as prodrug released into PBS as free molecules, their full contact with buffer led to more hydrolysis. In contrast, molecules captured in nanoparticles were mostly surrounded by hydrophobic blocks PLGA with limited water access. The hydrolysis was limited to certain extent. The huge shift in compositions between nanoparticles and PBS indicated that micro-environment has a very significant role in hydrolysis rate.

Differently, 2'-triethyl Si PTX (1a) nanoparticles had only one possible cleavage in hydrolysis. The compounds in nanoparticles were only 2'-triethyl Si PTX and PTX. There was 35% PTX in particles when the study started shown in Figure 5.8. It indicated that this 2'-triethyl Si PTX was very hydrolytically labile, and a significant amount hydrolysis has already occurred during nanoparticle post-treatments, such as ultracentrifugation, lyophilization and resuspending in PBS. At the end of 48 hr, PTX

decreased to 18%. The amount of 2'-triethyl Si PTX started with 65% and decreased to 18%. The composition ratio of 2'-triethyl Si PTX vs. PTX changed from 65:35 to 50:50 as the hydrolysis occurred in particles.

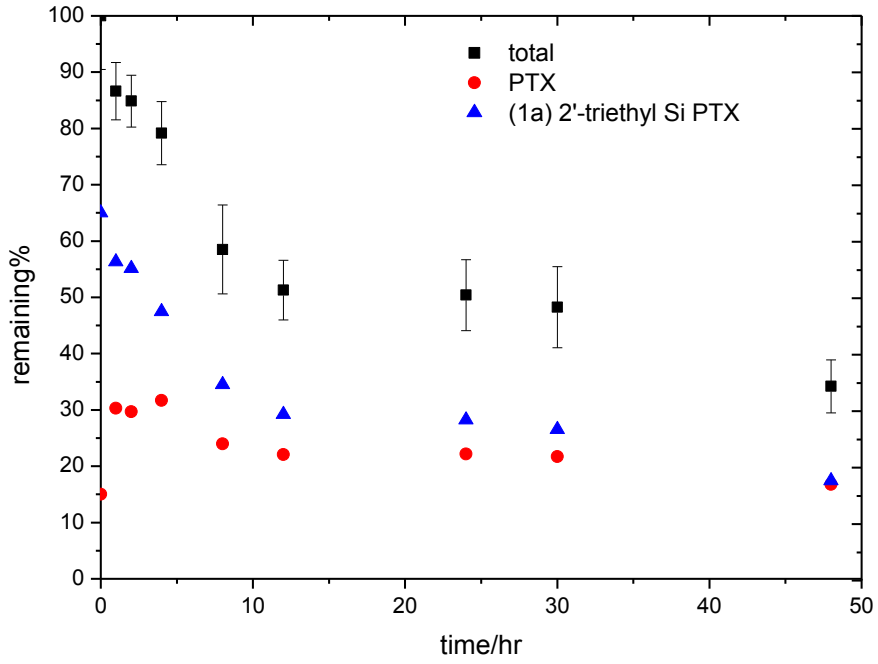

Figure 5.8 Reverse release profile of (1a) 2'-triethyl Si PTX nanoparticles in PBS 7.4.

In PBS, the total release shown in Figure 5.9 was also complementary to the remaining amount obtained from nanoparticles in Figure 5.8. Again, mass balance was well obtained also shown in Table 5.3. There was a significant amount of PTX, due to the diffusion of PTX and hydrolysis of 2'-triethyl Si PTX occurring in PBS. However, 2'-triethyl Si PTX was still the majority of the compositions in buffer solution. The release mechanism for this Si PTX prodrug was also a combination of hydrolysis and diffusion, but hydrolysis appeared to be faster in this case.

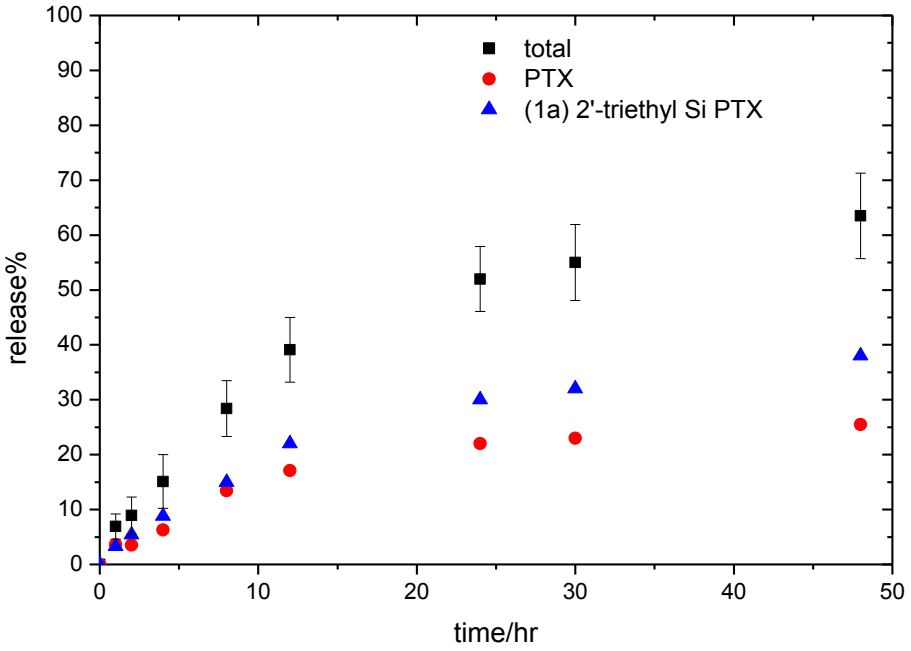

Figure 5.9 Release profile of (1a) 2' -triethyl Si PTX nanoparticles in PBS 7.4.

Another triethyl Si PTX was 7-triethyl Si PTX (3a). It is the first intermediate obtained after the cleavage of 2' silicate ester of 2',7-tri-ethyl Si PTX. This compound was also used to prepare nanoparticles and its reverse release result was shown in Figure 5.10. This experiment was meant to mimic the hydrolysis and diffusion after the first step of hydrolysis of 2',7-triethyl Si PTX. The reverse release rate was similar to 2'-triethyl Si PTX but slightly slower, for it is less labile while the hydrophobicity indiated by LogP was estimated same as 2'-triethyl Si PTX (1a) shown in Table 5.1.

Due to the hydrolytic stability, nanoparticles were mostly loaded with 7-triethyl Si PTX, and only 10% of PTX was found. Suppose 2'7-triethyl Si PTX was resuspended and immersed in PBS. As the hydrolysis occurred, it would first hydrolyze to 7-triethyl Si PTX very quickly. Once it converted to 7-triethyl Si PTX, it was more difficult to convert to PTX. That is why the majority compositions of 2',7-triethyl Si PTX nanoparticles during release were 7-triethyl Si PTX and 2',7-triethyl Si PTX. In contrast, the composition of 2'-triethyl Si PTX after release contained more PTX.

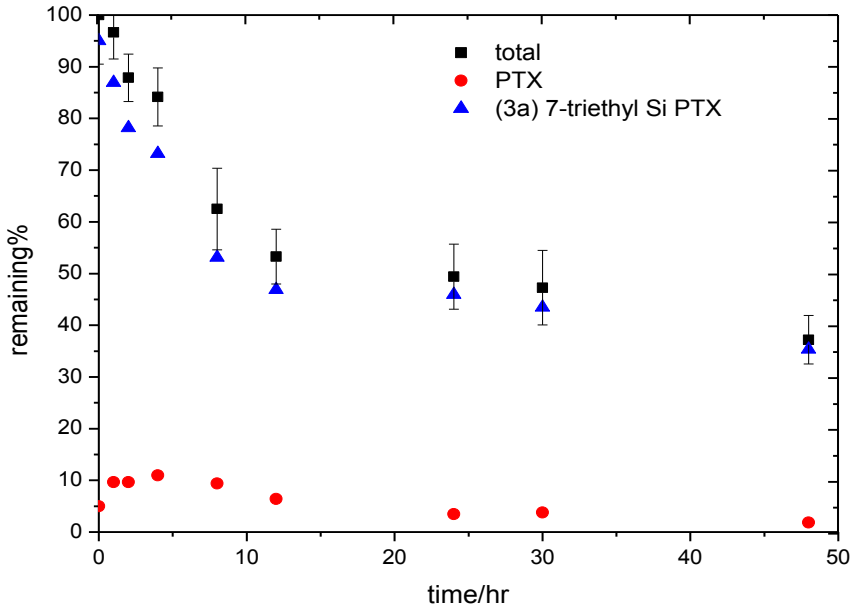

Figure 5.10 Reverse release profile of (3a) 7-triethyl Si PTX nanoparticles in PBS 7.4.

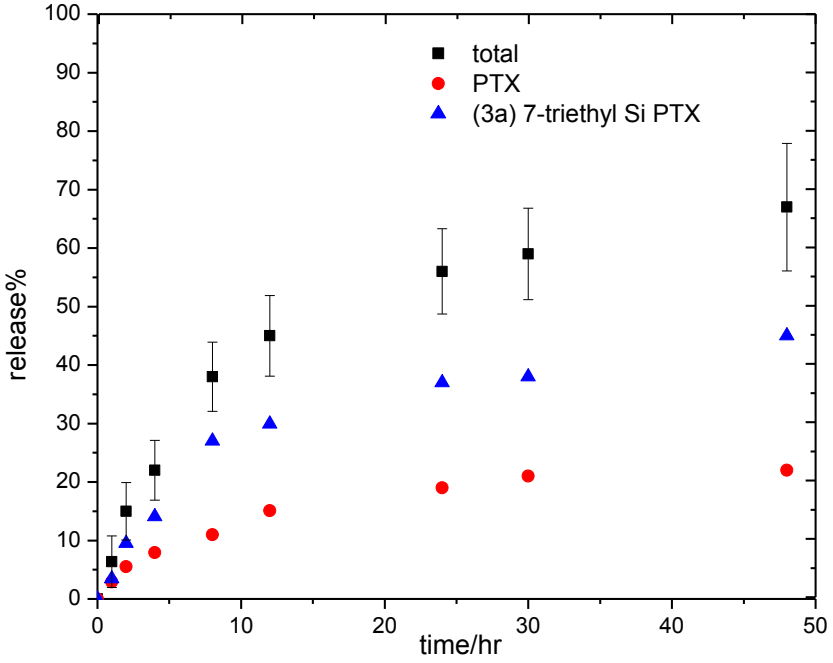

Figure 5.11 Release profile of (3a) 7-triethyl Si PTX nanoparticles in PBS 7.4.

In PBS, PTX obtained via hydrolysis of 7-triethyl Si PTX (Figure 5.11) was more than that from nanoparticles in dialysis mini capsules, which was consistent with cases of 2',7-triethyl Si PTX and 2'-triethyl Si PTX. Nanoparticles cores were surrounded by hydrophobic block PLGA, which created relatively hydrophobic microenvironment. But in PBS, molecules were fully present in water-based solution, which had more chance to hydrolyze.

Figure 5.12 shows that the reverse release of 2'-trioctyl Si PTX (1b) nanoparticles extended beyond 48 hrs. PTX followed a similar trend with that in other Si PTX nanoparticles, which spiked up to 10% and reduced to almost zero later due to diffusion of PTX. However, over 90% of the composition is 2'-trioctyl Si PTX. Different from previous studies, hydrolysis of 2'-trioctyl Si PTX was insignificant in nanoparticles. This

indicated that release mechanism of 2'-trioctyl Si PTX was dominated by its own diffusion.

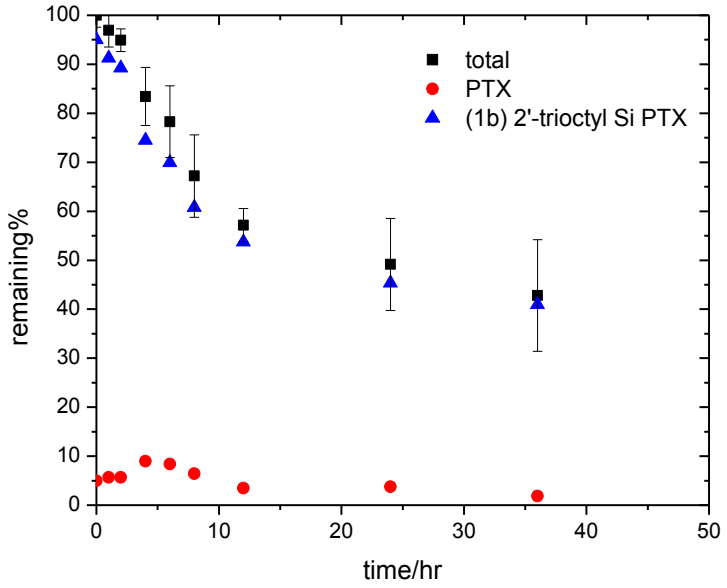

Figure 5.12 Reverse release profile of (1b) 2' trioctyl Si PTX nanoparticles in PBS 7.4.

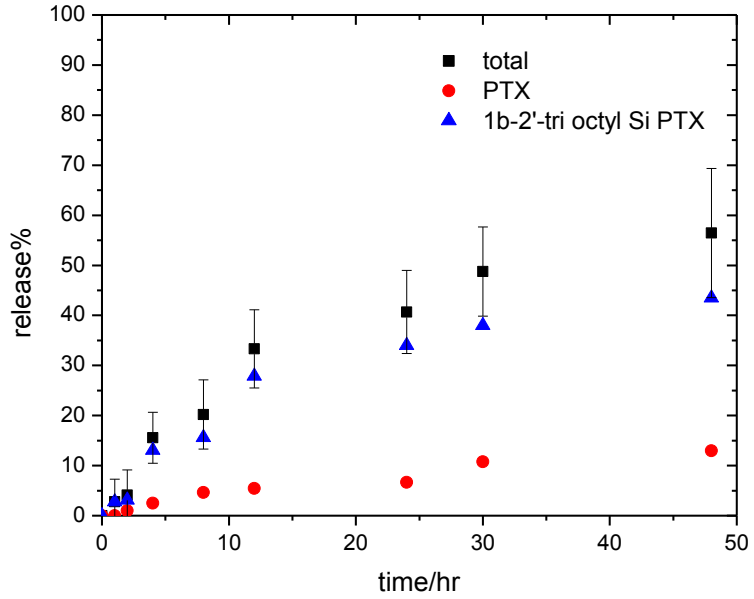

Figure 5.13 Release profile of (1b) 2'-trioctyl Si PTX nanoparticles in PBS 7.4.

In PBS, besides the complementary release trend and mass balance shown in Figure 5.13 and Table 5.3, the majority of the components were 2'-trioctyl Si PTX. Only less than 20% of PTX was obtained at the end of 48 hrs. This has been so far the smallest amount of PTX as released drug, indicating the slowest hydrolysis for 2'-trioctyl Si PTX. This is reasonable with the estimated relative hydrolysis rates shown in Table 5.1. Therefore, the release mechanism for 2'-trioctyl Si PTX was dominant by the diffusion of prodrug. Despite multiple resources of error discussed in 5.2.5, the mass balance experiments presented in this chapter were repeated at least twice with samples collected at selected time points. The uncertainty of the release and remaining drug lied in a range of ±15-20%. The complimentary trend between the remaining and the released drug was consistently observed for all.

Table 5.3 Percentage of Si PTX prodrugs and PTX during release in PBS at pH=7.4

Time/hr	2a, 2',7-triethyl Si PTX		1a, 2'-triethyl Si PTX		3a, 7-triethyl Si PTX		1b, 2'-trioctyl Si PTX	
	Reverse	Release	Reverse	Release	Reverse	Release	Reverse	Release
12	45±4	62±5	52±7	40±6	54±6	45±5	57±6	33±5
24	29±14	68±4	50±6	51±6	50±7	55±10	48±9	40±11
48	7±11	92±2	35±5	63±7	37±5	65±5	--	50±5

Data is shown as total amount of (prodrug&PTX%)±standard deviation.

5.3.6 pH variation

Previous two sections were presented based on *in vitro* release studies in PBS, but there was no significant difference between pH 7.4 and 6.4. Thus, in this section, *in vitro* release studies were conducted in acetic acid buffer prepared at pH 5.0, in the hope

of identifying significant pH-responsive hydrolysis in more acidic buffer. The experimental protocols were same with previous ones except pH.

The first one studied was 2'-triethyl Si PTX (1a) nanoparticles. The total remaining drug/prodrug significantly decreased in an exponential pattern in Figure 5.14. The amount of PTX started to accumulate as hydrolysis occurred and it reached peak value (~20%) with a ratio of 50:50 against 2'-triethyl Si PTX at 4 hrs. At the end of 24 hrs, the amount of prodrug/drug was negligible, meaning the release was completed when both compounds diffused out of particles very quickly. Quite different from release in PBS for 48 hrs, the hydrolysis of 2'-triethyl Si PTX at pH=5.0 occurred faster. It significantly accelerated the entire release process within 24 hrs, due to a combined contribution of hydrolysis and diffusion.

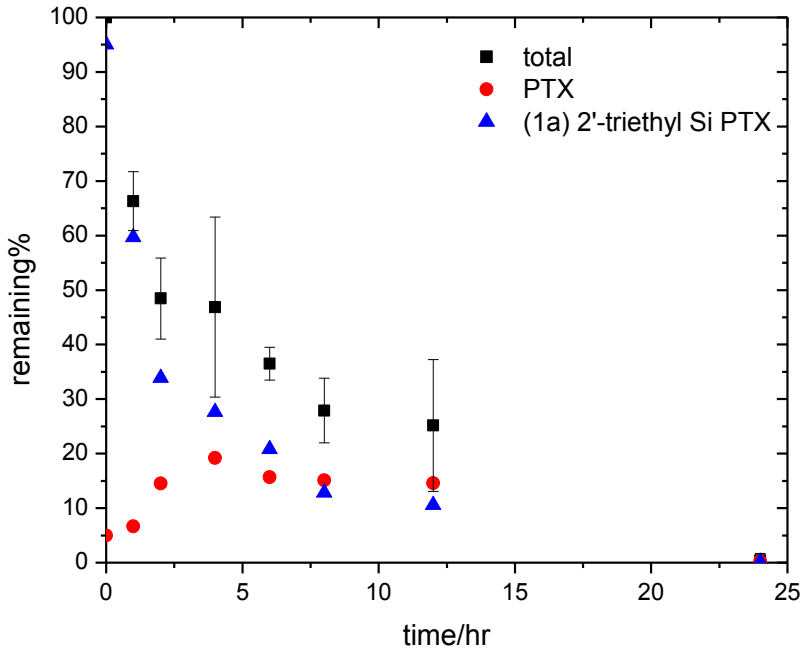

Figure 5.14 Reverse release profile of (1a) 2' -triethyl Si PTX nanoparticles at pH=5.0.

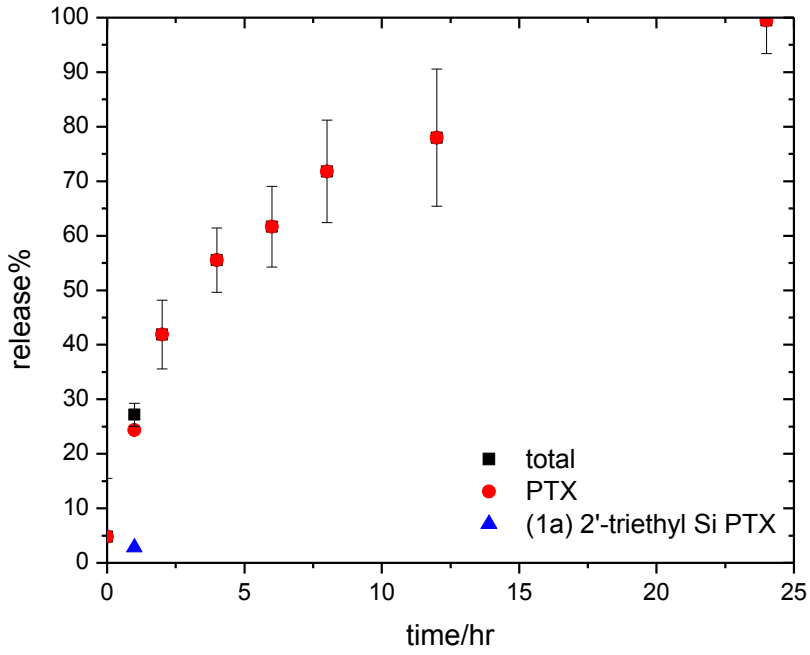

Figure 5.15 Release profile of (1a) 2'-triethyl Si PTX nanoparticles at pH=5.0.

Interestingly in buffer at pH=5.0, only 30% of total loading was detected as 2'-triethyl Si PTX and it quickly diminished, considered being hydrolyzed to PTX. 2'-triethyl Si PTX prodrug was not found after 2 hrs. PTX was the only compound detected for the rest of release time. Obviously, the hydrolysis of 2'-triethyl Si PTX was greatly increased in buffer at pH 5.0. Nanoparticles essentially only released PTX into buffer, but the release rate was too fast. Compared with the release profiles in Figure 5.15, the acidity of buffer solutions had a significant influence on hydrolysis which leads to the possibility of controlled release at varied media conditions.

The second batch of particles was loaded with 2'-trioctyl Si PTX (1b). The release study was carried out for 96 hrs until it was complete. In the reverse release profile in

Figure 5.16, the remaining 2'-trioctyl Si PTX and PTX at 48 hrs was only 30%, which was 15% less than that observed at pH 7.4 in Figure 5.12. PTX obtained via hydrolysis accumulated to a peak of 30% at 8 hr. Obviously, the buffer solution at pH 5.0 induced more hydrolysis in nanoparticles, although 2'-trioctyl Si PTX was less hydrolytically labile than previous 2'-triethyl Si PTX. Over 96 hrs, the loaded drug was mainly composed of 2'-trioctyl Si PTX, except when PTX reached peak at 8 hr. It implied that with both compounds present in nanoparticles, the diffusion of PTX was faster than 2'-trioctyl Si PTX, due to dramatic solubility difference indicated by several orders of magnitude in LogP values.

On the other hand, the released drug/prodrug obtained from buffer almost reached 94% of initial loading in 96 hrs. PTX was the majority of the compositions in the entire time. There was only 15% of 2'-trioctyl Si PTX left in the end. The presence of 2'-trioctyl Si PTX via diffusion and PTX via hydrolysis acted as counter-productive processes, leading to the increased regeneration of PTX. This meant that the release of PTX was dominated by the hydrolysis of 2'-trioctyl Si PTX.

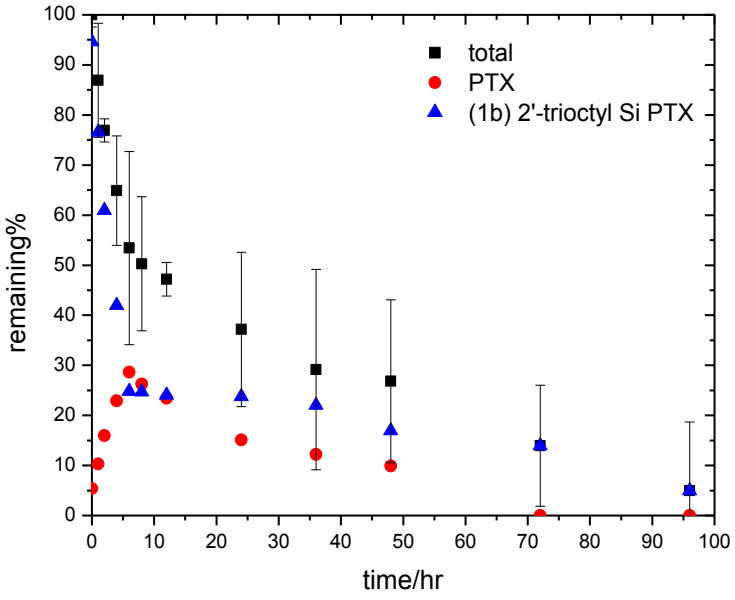

Figure 5.16 Reverse release profile of (1b) 2’ -trioctyl Si PTX nanoparticles at pH=5.0.

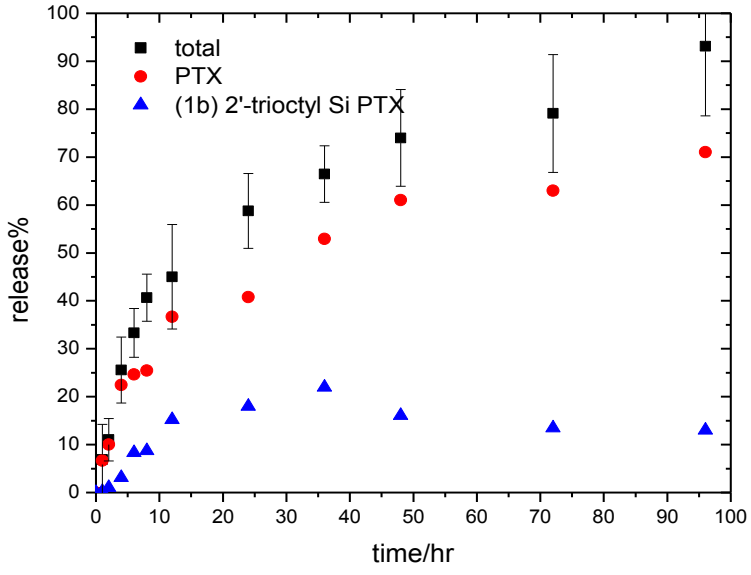

Figure 5.17 Release profile of (1b) 2’-trioctyl Si PTX nanoparticles at pH=5.0.

The release of 2'-trisopropyl Si PTX (1c) nanoparticles was extended to 120 hrs in Figure 5.18. They released in a similar rate of 2'-trioctyl Si PTX, with one more day for completion. PTX reached maximum of 34% at 12 hr, followed with a continuous reduction. 2'-triisopropyl Si PTX was depleted by both diffusion and hydrolysis.

In acetic acid buffer at pH 5.0 shown in Figure 5.19, it started with almost equal amount of 2'-triisopropyl Si PTX and PTX. After 16 hrs, PTX quickly became the majority component, probably because significant amount of PTX diffusion occurred when PTX reached the maximum at 16 hr inside nanoparticles. Different from 2'-trioctyl Si PTX, the amount of 2'-triisopropyl Si PTX increased instead of decreasing in buffer, because it is less hydrophobic, at the same time less hydrolytically labile, so that more isopropyl Si PTX was able to diffuse out of nanoparticles before they could be completely hydrolyzed to PTX. Therefore, more 2'-trisopropyl Si PTX accumulated in buffer solution.

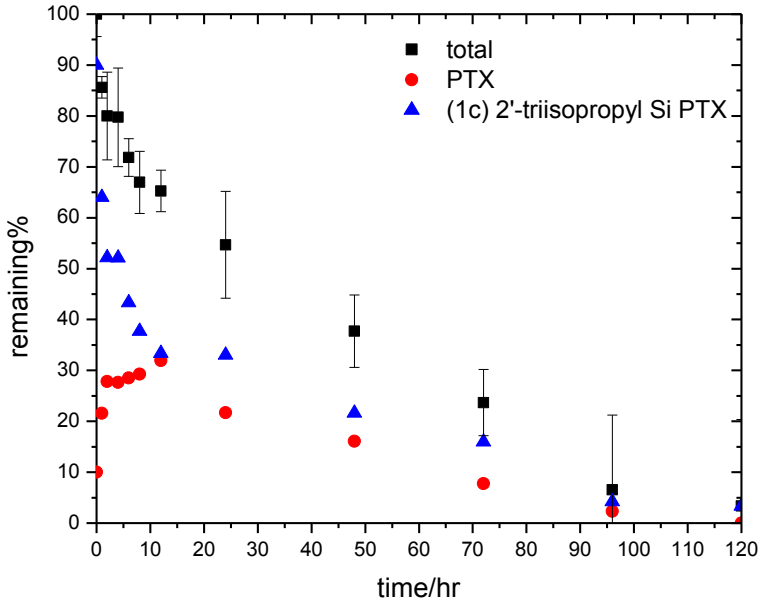

Figure 5.18 Reverse release of (1c) 2'-triisopropyl Si PTX nanoparticles at pH=5.0.

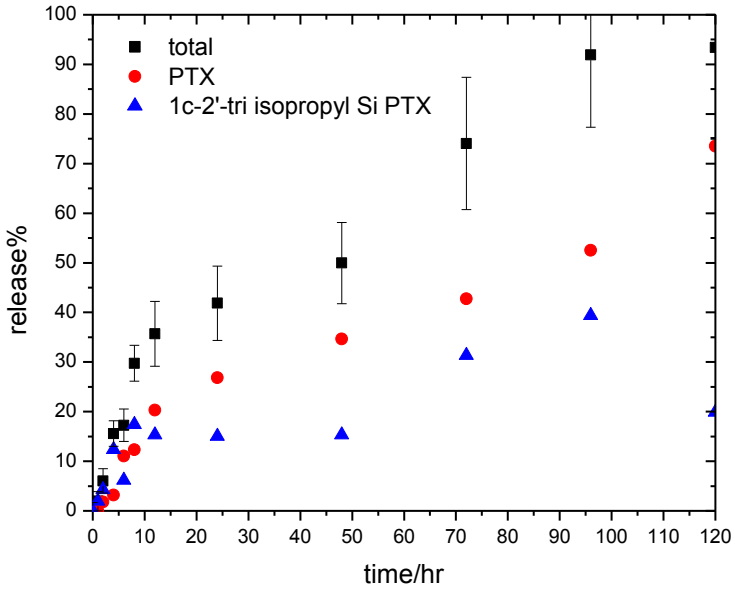

Figure 5.19 Release of (1c) 2'-triisopropyl Si PTX nanoparticles at pH=5.0.

In order to determine the limiting step of release between diffusion and hydrolysis, nanoparticles loaded with 2'-trimenthyl Si PTX (1e) was used in release study at pH=5.0. 2'-trimenthyl Si PTX has similar hydrophobicity with 2'-triisopropyl Si PTX (1c) by LogP (5.81 vs. 5.60) but less hydrolytic labile. Dramatically different from other particles, the reverse release profile of 2'-trimenthyl Si PTX within particles were sustained up to one week shown in Figure 5.20. In 168 hrs, PTX was barely detected. The release process was significantly extended, almost two times slower than 2'-trioctyl Si PTX (1b), despite 1b was more hydrophobic. The increased hydrolytic stability prevented hydrolysis though the buffer was more acidic.

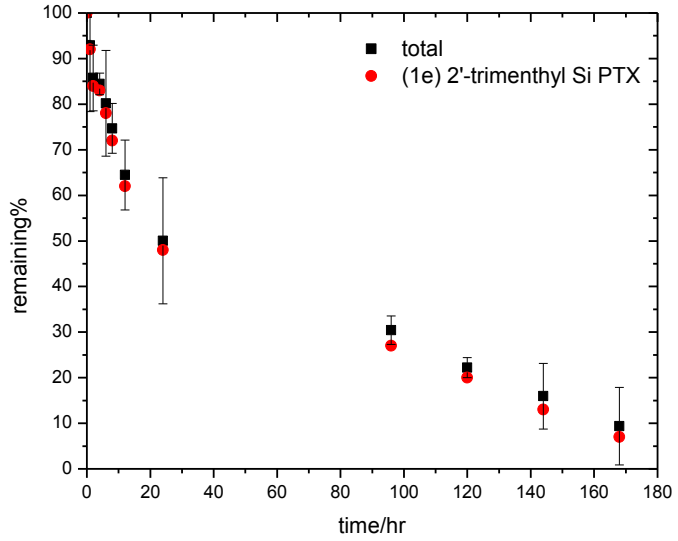

Figure 5.20 Reverse release of (1e) 2'-trimenthyl Si PTX nanoparticles at pH=5.0.

The release profile of 2'-trimenthyl Si PTX shown in Figure 5.21 was quite distinctive from others as well. In the first 12 hrs, there was less than 1% of PTX observed in acetic acid buffer at pH 5.0, meaning that no significant hydrolysis occurred during this time length. PTX started to appear afterward and increased slowly in a linear

pattern till 96 hr. Later, the amount of PTX increased linearly in a faster rate while 2'-trimenthyl Si PTX dropped linearly in a comparative rate. It was obvious that between 96-168 hr, the regeneration of PTX was mainly contributed by the hydrolysis of 2'-trimenthyl Si PTX present in buffer. Also, the percentage of 2'-trimenthyl Si PTX increased greatly from 96 hr to 168 hr, which indicated in this time period, 2'-trimenthyl Si PTX was suddenly able to leave nanoparticles, and it was suspected due to polymer degradation especially the study was conducted in more acidic buffer. 2'-trimenthyl Si PTX has been so far the only prodrug with no evidence of PTX found inside particles, while its hydrolysis was greatly delayed in buffer. Although it is still unknown why hydrolysis was triggered suddenly after 96 hr, but 2'-trimenthyl Si PTX indeed showed the capability of controlling release rates with customized hydrophobicity and hydrolytic lability of silicate esters.

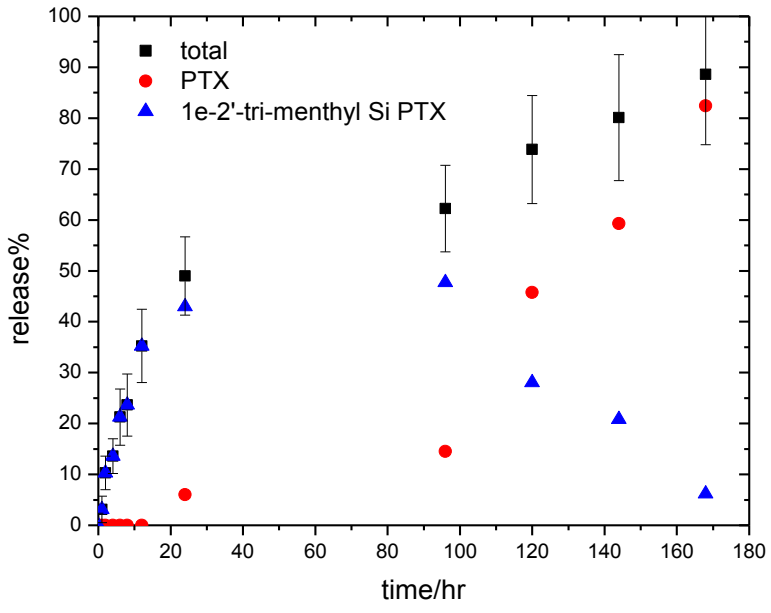

Figure 5.21 Release profile of (1e) 2'-trimenthyl Si PTX nanoparticles at pH=5.0.

The reverse release profile of 2'-ditert butyl/ethyl Si PTX (1d) was presented in Figure 5.22 as the extreme case with highest hydrophobicity and least hydrolytic lability. The release study was conducted for 216 hrs. There was still approximately 46% of 2'-ditert butyl/ethyl Si PTX left in particles. It is expected to take more than two weeks to complete. No trace of PTX was detected at all.

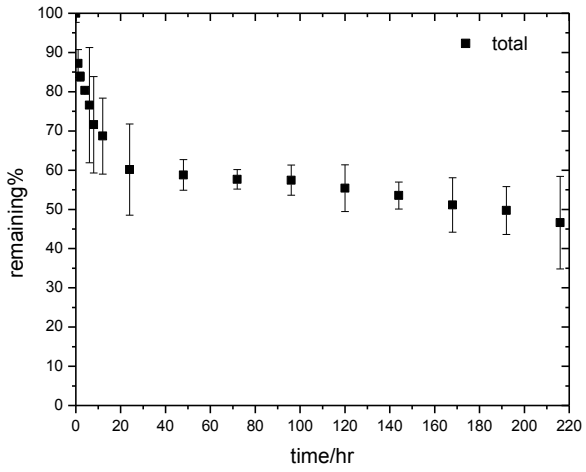

Figure 5.22 Reverse release profile of (1d) 2'-ditert butyl/ethyl Si PTX nanoparticles at pH=5.0.

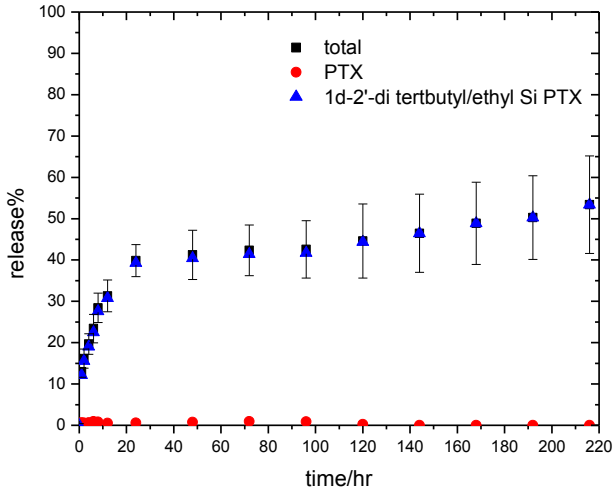

Figure 5.23 Release profile of (1d) 2'-ditert butyl/ethyl Si PTX nanoparticles at pH=5.0.

In acetic acid buffer at pH 5, the total release in Figure 5.23 was consistent with the reverse release profile obtained from nanoparticles in Figure 5.22. 2'-ditert butyl/ethyl Si PTX had the most sustained released but hydrolysis was too slow in this case, which can be problematic to regenerate active form of PTX.

To sum up, the total release profiles at pH 5.0 for all particles were presented in Figure 5.24. The release time was expanded in the range of 24 hr to 216 hrs (1-9 days) with variety of Si PTX prodrugs. The acetic acid buffer at pH=5.0 provided more acidic media condition and induced more evident hydrolysis of the hydrolytic labile prodrugs. However, the hydrophobicity of these prodrugs was also varied in several orders of magnitude indicated by LogP, so the diffusion of these compounds was also a contribution to the total release. Although it is known that the customized hydrophobicity and hydrolytic lability helped to control release rates in different levels, it is very difficult to determine the relative importance of diffusion and hydrolysis because the total release included both Si PTX prodrugs and PTX.

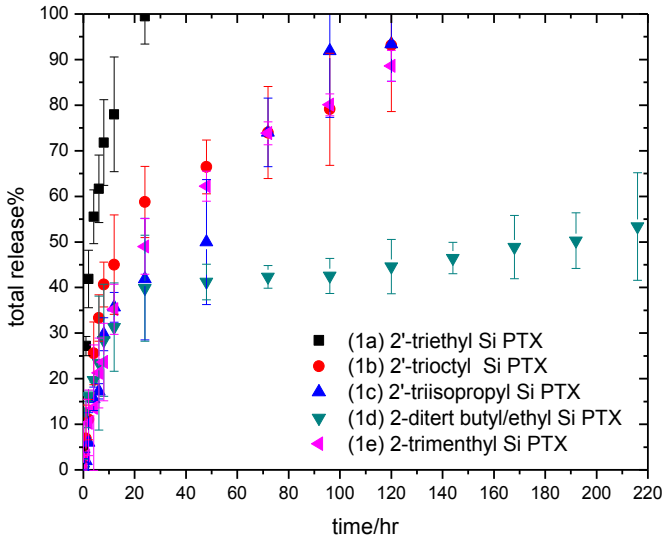

Figure 5.24 Total release profile of Si PTX nanoparticles (1a-1e) in buffer at pH=5.0.

Compared to total release, it is more important to know how these particles regenerated PTX as the active anticancer ingredient. That is why regeneration of PTX during release studies at ph 5.0 and 7.4 were summarized in Figure 5.25. This comparison mainly demonstrated the hydrolysis lability levels of all Si PTX prodrugs when they were encapsulated in polymeric particles and immersed in buffer at different pH. The hydrolysis of prodrugs 1a,1b,1c (pH=5.0) and 2a, 1b (pH=7.4) were relatively fast in short time. As more hydrolytic stable prodrugs, 1d and 1e were extremely slow and sustained in 216 hrs. 1e, as discussed previously only had significant hydrolysis after 96 hrs. 1d, as the most hydrolytic stable one, had no detectable trace of PTX in the entire release time. Despite particles loaded with these prodrugs were able to release PTX-containing compound into buffer, presumably there will be no anticancer efficacy if the active form of PTX cannot be generated. Compared PTX regeneration of 1b, 2'-trioctyl Si PTX in buffer at pH 7.4 and 5.0, the more acidic media induced more hydrolysis. At 96 hr, over 60% of PTX was regenerated at pH=5.0 while only 30% at pH=7.4. This result helped us understand more that the availability of PTX can be controlled by varying the silicate esters.

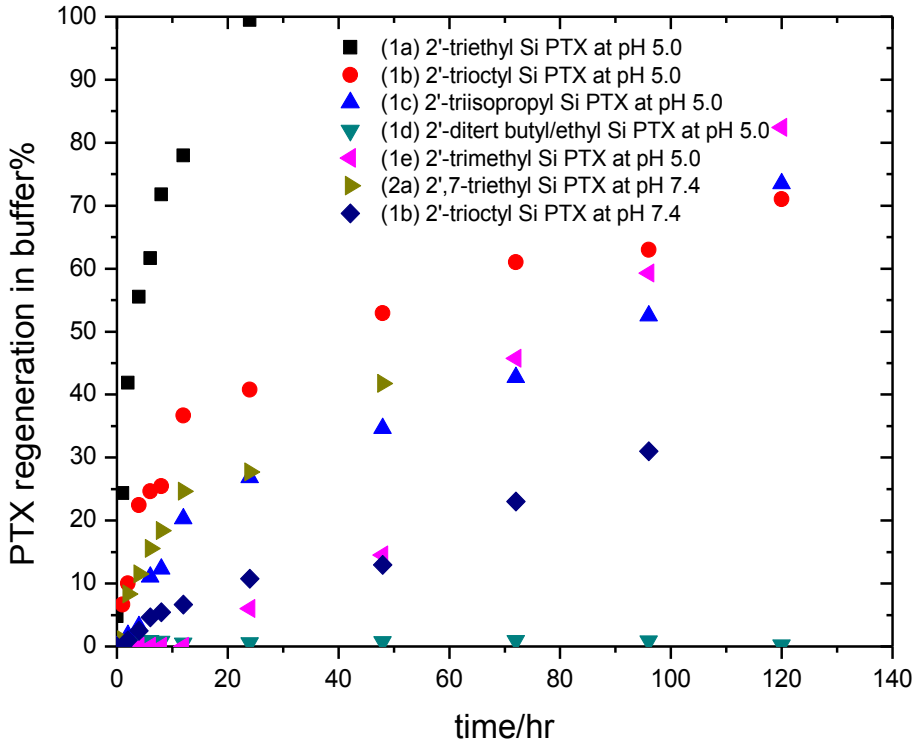

Figure 5.25 PTX regeneration from all Si PTX nanoparticles in buffer at pH=7.4 and 5.0.

Inside nanoparticles, the hydrolysis of prodrugs led to an accumulation of PTX in 10-40% of total drug loading when nanoparticles were immersed in PBS or acetic acid buffer, except 2'-ditert butyl/ethyl Si PTX (1d) and 2'-trimenthyl Si PTX (1e), because these two prodrugs are most hydrolytic stable. So far, there was no obvious relation found between the hydrolytic lability and the amount of PTX accumulated inside nanoparticles. More PTX was found when nanoparticles were immersed in acetic buffer (pH=5.0) than PBS (pH=7.4). For instance, 30% of PTX in maximum inside nanoparticles was found when 2'-trioctyl Si PTX (1b) NPs were immersed in acetic acid buffer, and approximately 10% in PBS.

Table 5.4 Percentage ratio of PTX vs. Si PTX prodrug obtained from buffer (outside NPs)

	Acetic acid buffer pH=5.0					PBS pH=7.4	
Time/hr	1a	1b	1c	1d	1e	2a	1b
12	78/0	37/15	20/15	0.53/31	0/35	25/34	5/28
24	99/0	41/18	26/15	0.57/39	6/43	28/39	17/34
48	n/a	61/16	34/16	0.77/41	15/48	42/48	13/43

1a-1e and 2a are six Si PTX prodrugs encapsulated in nanoparticles and conducted with in vitro drug release study, described in Table 5.1.

As described in Table 5.4, outside nanoparticles, when prodrugs diffused into PBS at pH=7.4, similar amounts of PTX and prodrug were found in the case of 2'-triethyl Si PTX nanoparticles (1a) (25% PTX:38% prodrug) shown in Figure 5.9 and 2',7-triethyl Si PTX nanoparticles (2a) (42% PTX: 48% prodrug) in Figure 5.7. But, for 2'-trioctyl Si PTX NPs (1b), the released prodrug had a ratio of 13% PTX vs. 43% prodrug at 48 hr shown in Table 5.4. When prodrugs diffused into acetic buffer at pH=5.0, the majority of the released drug was PTX in the cases of 2'-triethyl Si PTX (1a), 2'-trioctyl Si PTX (1b) and 2'-triisopropyl Si PTX (1c), while 2'-ditert butyl Si PTX (1d) and 2'-trimenthyl Si PTX (1e) are too stable to regenerate PTX shown in Table 5.4. As the most labile prodrug, 2'-triethyl Si PTX (1a) regenerated PTX completely after 2 hrs they diffused into acetic buffer.

Comparing the relative ratio of prodrug vs. PTX both inside and outside nanoparticles, there was more PTX found outside nanoparticles, probably because the surrounding medium helped to expedite the hydrolysis while the microenvironment

inside nanoparticles were more hydrophobic, rich in hydrophobic block of the block copolymer, and the hydrolysis was limited.

Not only hydrolysis occurred during drug release, hydrolysis of prodrugs and PTX also played an important role in regeneration of PTX. The amount of PTX hydrolyzed from prodrugs usually accumulated to a maximum of 10-40% and then gradually decreased inside nanoparticles, while it continuously increased outside nanoparticles. The diffusion of prodrugs varied depending on the hydrophobicity, particle size and drug loading. So far, we have found all prodrugs present both inside nanoparticles and in buffer, which meant they can diffuse from nanoparticle to buffer although their hydrophobicity have been enhanced with several orders of magnitude indicated by LogP.

Although diffusion and hydrolysis are the two main mechanisms for drug release discussed in this chapter, we cannot rule out other possibilities. As will be discussed in Ch.6, we have found morphology of some nanoparticles changed from spherical to irregular shape and nanoparticles did not have a shell region after 24 hr release study, which indicated block copolymer core-shell structure might be disassembled possibly due to polymer degradation or particle collapse.

5.4 Conclusion

To summarize this chapter, nanoparticles encapsulated with Si PTX prodrugs showed a decreasing trend of average particle size with their increased hydrophobicity. After ultracentrifugation, un-encapsulated prodrugs and empty polymeric particles were removed, leaving heavily loaded particles in suspension. As a result, the prodrug loading levels of the ultracentrifuged nanoparticles have been greatly increased above 70%, with

an average equivalent loading of PTX between 45-60%. This is encouraging, because it proved again that flash nanoprecipitation is a powerful technique to produce nanoparticles with extremely high loading against other nano-scale systems, the sizes and loading of which are controlled by thermodynamic energy. This potentially helps to extend anticancer efficacy of paclitaxel and to reduce dosing cycles of nanoparticle formulations.

In order to characterize pharmacokinetic of these particles, a reverse drug release protocol was developed to mainly determine the remaining compounds left in particles as the un-released drug. When *in vitro* drug release studies were conducted in PBS at pH=7.4 and 6.4, the general release rates of all Si PTX prodrugs were determined in 48 hrs, only showing a limited range of difference. In order to verify the reverse drug release protocol and analyze the composition of drug release, mass balance experiments were conducted comparing the remaining drug and the released one extracted from buffer solution. We observed that more hydrolytic labile prodrugs tended to hydrolyze to PTX first, followed with diffusion of PTX. While prodrugs with medium level of hydrophobicity and hydrolytic lability tended to hydrolyze and diffuse in similar rates. Those less hydrolytic labile prodrugs contributed to the general release mainly via their own diffusion. Therefore, drug release mechanisms can be either dominated by hydrolysis or diffusion or a contribution of the two, depending on the selected Si PTX prodrugs. Other factors may play a role in drug release as well, such as polymer degradation, which will be discussed in Ch. 6.

In the hope of triggering more hydrolysis, *in vitro* drug release and mass balance studies were also conducted in acetic acid buffer at pH=5.0. The total release rates were

significantly accelerated due to faster hydrolysis, and the regeneration of PTX was first characterized showing a broad range from 24 to 216 hrs. Consistently across all the Si PTX prodrugs, PTX regenerated in nanoparticles always piled up to a peak at certain time. For instance, when nanoparticles were immersed in acetic acid buffer at pH=5.0, 2'-triethyl Si PTX (1a) had a relative hydrolysis rate ca. K_{rel}=18,000 shown in Table 5.1 and 20% PTX at 4 hr, 2'-trioctyl Si PTX (1b) had a ca. K_{rel}=5600 and 28% of PTX at 8hr, and 2'-triisopropyl Si PTX (1c) had a ca. K_{rel} =570 and 32% of PTX at 16hr. It was noticed that, as the prodrug was more hydrolytic stable, PTX regeneration reached the peak later. Though the relation between the two was not clearly defined, it implied that the hydrolysis occurring in nanoparticles varied by the choice of silicate ester derivatives. In general, the Si PTX prodrug strategy developed by Wohl and Hoye[59, 60] successfully increased the hydrophobicity of PTX-containing compounds, which allowed us to prepare stable nanoparticles avoiding the Ostwald ripening and recrystallization that has been observed when pure PTX was attempted to be encapsulated in PEG-*b*-PLGA nanoparticles. Secondly, with customized hydrolytic lability, Si PTX prodrugs showed the possibility of controlling *in vitro* drug release and regeneration of PTX by the choice of silicate esters. This is very beneficial to design drug loaded particles with sustained release. Among all prodrugs synthesized by Wohl et al[59, 60], 2'-trioctyl Si PTX (1b) is able to be encapsulated into PEG-*b*-PLGA nanoparticles with an average size of 83 nm. The size distribution measured and observed from Cryo-TEM images are very narrow. As for general drug release, it had an extended time for approximately 96 hrs and we successfully observed the regeneration of PTX via hydrolysis. This prodrug is potentially

a good candidate for PTX-based nanoparticle preparation, considering particle size, morphology, extended release and delivery of PTX.

Chapter 6

Nanoparticle Internal Structure

6.1 Introduction

In pharmaceutical industry, nanoparticles are usually characterized by dynamic light scattering (DLS) technique and reported with an intensity averaged size and distribution[35, 51, 131, 140, 141]. Scanning and transmission electron microscopy are used mainly to observe nanoparticle morphology and confirm particle size distribution with DLS analysis[35, 51, 131, 140, 141]. It is commonly believed that drug loaded polymeric nanoparticles have a core-shell structure[102, 142-144], but nanoparticle internal structure has not been fully investigated to confirm this claim, mostly due to the limitation of techniques on nano-scale measurements and imaging.

Specifically, the problems for these techniques mentioned above are: first of all, many nano-scale systems are large in the range of hundreds of nanometers, and it is not very difficult to observe their morphology. However, our nanoparticles are approximately 100 nm, with an even smaller core. The required techniques must be able to differentiate structure contrast approximately by 10-20 nm. Secondly, DLS usually provides an averaged particle size with a distribution. It cannot tell us structure information of individual particles. That is why microscopy is needed to visualize particles internally and as a whole, both in size and morphology. Scanning electron microscopy is indeed able to image ~100 nm nanoparticles, but particles with coverage of polymer can be easily damaged by electron beam. When polymer provides surface coverage for particles, the contrast is usually very low against the loading materials, which are also organic.

Plus, the resolution is not high enough to differentiate core and shell regions of particles. Therefore, the alternative technique is Cryo-TEM, which freezes particles and assures the integrity of particles during imaging process. Although obtaining contrast can be difficult, beam damage is helpful to differentiate nanoparticle microstructures. For example, the diblock copolymer PEG-*b*-PLGA used in nanoparticle formation is susceptible to the electron beam and they showed a white bubble-like structure. Cryo-TEM provides higher contrast than SEM and core-shell structure can be visualized. That is why results and discussions in this chapter are mainly based on Cryo-TEM images obtained by my colleague, Hanseung Lee.

As nanoparticles are freshly made, they are required to be lyophilized and stored in dry state for long-term use and storage. Lyophilization (or freeze drying)[114, 145] is a process that removes water from a frozen sample by sublimation and desorption under high vacuum condition. Although, lyophilization is very effective to remove water from dispersion, it causes various issues in nanoparticle systems. For instance, after our nanoparticles were lyophilized and re-dispersed at a later time, particle sizes often increased drastically above 200 nm to micron size, because particles were driven into each other during the freezing process, aggregated and even crystallized[86]. To reduce particle size growth, nanosuspension was added with cryoprotectant[146] such as sucrose, glucose etc, before lyophilization as discussed in Ch.3. Particles were not completely recovered to the initial size, but they were at least being reduced to some extent. However, it took 10:1 or higher mass ratio of cryoprotectant vs. nanoparticles to recover particle size. When they were redispersed in buffer and administered via IV injection, the sugar concentration would be far above glucose level in human blood. That will disrupt

the isotonicity and destroy the cells in blood due to concentration gradient between blood and cells. Therefore, nanoparticles with high content of sugar cannot be used for *in vitro* cell culture or *in vivo* animal studies, and certainly cannot be used in clinical practice. Other methods must be explored to recover particle size without cryoprotectant. That is another reason of using microscopy technique to find out whether particles changed in size and morphology and how it occurred during manufacturing and post-treatment.

Drug loading, as a very critical parameter for drug delivery system, is usually determined by the amount of drug loaded with particles. However, it is not always very accurate determining it using freeze dried nanoparticles, due to the possibility that the unloaded drug exists outside particles. Thus, it is necessary to purify the particles via ultracentrifugation to remove the un-encapsulated drug and empty polymer particles. Whether the drug has been completely removed can be confirmed by TEM visualization.

To sum up, the importance of investigating nanoparticle internal structure is presented in several aspects: first, nanoparticle internal structure indicates drug distribution within particles, which is very critical to drug release kinetics. For instance, drug may release faster by simple diffusion and dissolution with less barrier when particles have a loosely packed structure with drug distributed in gradient from core to shell region. This is often seen when the release profile has a burst pattern in the short time. Or release takes longer due to more polymer matrix barrier when drug is mostly captured in the tightly packed core region of particles. In that case, the release not only depends on diffusion, also water diffusion into particles, polymer degradation, prodrug hydrolysis and dissolution, and nanoparticle disassembly.

Secondly, imaging particles allows us understand nanoparticle formation mechanisms, whether particles made via flash nanoprecipitation are formed by nucleation-and-growth where drug and polymer were distinctly phase separated in either core or shell region, or nucleation-and-aggregation where particles are formed as a sum of multiple aggregates. This is a debating question for many researchers and an improved understanding of particle internal structure would help to resolve this puzzle.

Thirdly, nanoparticle stability is strongly related to its structure. For block copolymer particles, it is very important that hydrophilic block (PEG) provides sufficient steric stabilization on particle surface, while hydrophobic block (PLGA) creates sufficiently hydrophobic micro-environment to kinetically trap hydrophobic drug inside. If not, particles might aggregate, or drug diffuses out of particles due to Ostwald ripening, just like our first attempt of making paclitaxel loaded PEG-*b*-PLGA nanoparticles[67].

Last but not least, nanoparticle structure might change over time during any of these processes: manufacturing, lyophilization, storage, and administration. For example, during *in vitro* drug release study, some nanoparticles were not spherical any more after 24-48 hrs. They appeared to shrink and change from spherical to an irregular shape. TEM indicated some of them had crystalline structure. These observations implied several possibilities, polymer degradation, particles disassembly etc. These are worthy studying especially when nanoparticles were designed as drug delivery system. It is very important to determine shelf life and administration method.

As mentioned above, nanoparticle internal structure has been hypothesized[35, 44, 67, 147] and studied via molecular modeling[68]. Pustulka et al,[85, 86] showed core-shell structure

of only 2',7-triethyl Si PTX nanoparticles obtained by Cryo-TEM, but nanoparticles internal structure has not been fully elucidated. Despite the limitation of imaging techniques, nanoparticles loaded with other drug/prodrugs should be studied, in order to find relations among nanoparticle structure, size, and loading, and to further understand nanoparticle formation mechanisms and drug release kinetics. This will benefit researchers on developing nanoparticle technology, controlling nanoparticle size, optimizing drug loading, and designing nanoparticles with desirable drug release kinetics.

6.2 Methods and Experiments

6.2.1 Materials

Paclitaxel was obtained from Phytogen Life Sciences. PEG-*b*-PLGA (MW: 5k-10kDa) was synthesized in Hoye's lab as previously reported[81]. Water (H_2O, HPLC grade) and tetrahydrofuran (THF, HPLC grade) were purchased from Aldrich and used as received. Phosphate buffer saline (PBS) was prepared by dissolving 3.12 g monosodium phosphate and 20.74 g Diasodium phosphate in 1 L DI water to achieve pH 7.4, and 10.28 g monosodium phosphate and 6.84 g diasodium phosphate in 1 L DI water for pH 6.4. Monosodium phosphate and diasodium phosphate were purchased from Fisher Scientific. Si PTX prodrugs were synthesized in Hoye's lab as previously reported[59]. Their chemical structures are shown in Figure 5.1. The physical properties and hydrolytic labilities are shown in Table 5.1.

6.2.2 Nanoparticle Preparation and Post-treatment

Si PTX loaded diblock copolymer PEG-*b*-PLGA protected nanoparticles were prepared using CIJ-D mixer via flash nanoprecipitaiton. The following is a typical procedure for one batch of nanoparticles preparation. 35-40 mg of Si PTX prodrugs (with an equivalent of 25 mg PTX) and 25 mg of PEG-*b*-PLGA were dissolved in 2.5 mL THF, contained in a 3mL syringe. It was impinged rapidly with the other syringe containing 2.5 mL water within 5 seconds. The mixture was immediately drained into 45 mL water, in order to further quench nanoparticle growth. The resulting nanoparticle suspension had total volume of 50 mL with a ratio of 5:95 THF: H_2O and total mass of approximately 60-65 mg nanoparticles.

Block copolymer nanoparticles were prepared impinging 2.5 mL THF containing 25 mg PEG-*b*-PLGA with 2.5 mL water and further diluted into 25 mL water.

PTX loaded PEG-*b*-PLGA protected nanoparticles were not able to be prepared via flash nanoprecipitation due it Ostwald ripening. Instead, PTX powder was imaged using Cryo-TEM.

Ultracentrifugation (Beckman Coulter, CA) was used to purify nanoparticles at 50,000 rpm, 4 ^{o}C, 30 min for three times. The final pellet was removed, lyophilized for 24 hr and stored at 4 ^{o}C refridgerator.

Micro-tip sonication (Misonix Sonicator 3000, NY) was used to redisperse lyophilized nanoparticles by sonicating particle powder in DI water or PBS at concentration of 1 mg/mL using microtip probe (1/8″) in pulse mode, 3-9 volt for 5 min. Sonication in each cycle took 1 minute, and the tube containing nanoparticles were

immersed into ice water for 15-30 seconds, to remove the heat generated by the sonicator. Sonication was repeated with five cycles.

6.2.3 Nanoparticle Size and Distribution

6.2.3.1 Dynamic Light Scattering (REPES vs. Cumulant)

In this work, nanoparticle sizes and distribution were measured by dynamic light scattering (DLS) using two instruments, either ZetaPALS (Brookhaven, CA) or Delsa^{TM} Nano (Beckman Coulter, CA). To summarize the DLS characterization method, they are both described here, as also mentioned in Ch.3.

Using ZetaPALS (Brookhaven, CA), 2 mL nanoparticle suspension were transferred to round glass cuvettes and sealed with double-layered parafilms. Particles were measured using a diode laser BI-DPSS wavelength of 659 nm. The scattering intensity correlation function was collected at 25 ^{o}C and a scattering angle of 90^{o}. The correlation function is a sum of multiple diffusion coefficients, D_i, of each particle, which is converted into particle diameter, d_i, via Stokes-Einstein equation (Eq.6.1),

$$d_i = \frac{\mathrm{k_b}T}{3\pi\eta D_i} \qquad \text{Eq. 6.1}$$

where $\mathrm{k_b}$ is the Boltzmann constant, T is temperature and η is the viscosity of the solvent.

The correlation functions were downloaded from the ZetaPALS instrument and manually fit using the regularized positive exponential sum (REPES) program to determine averaged particles sizes and distribution. REPES yields a series of discrete particle diameters to accumulate the particle size distribution. Differently, most

commercial instruments use cumulant model to determine size and distribution. The software, GENDIST, was used to solve REPES algorithm and yielded an intensity size distribution. The averaged intensity particle size $\overline{d_{\mathrm{I}}}$, is defined in Eq. 6.2,

$$\overline{d_{\mathrm{I}}} = \sum n_i d_i^{\,6} / \sum n_i d_i^{\,5} \qquad \text{Eq. 6.2}$$

where n_i is the number of particles with a diameter of d_i. The averaged mass particle size, $\overline{d_{\mathrm{m}}}$, is defined in Eq. 6.3,

$$\overline{d_{\mathrm{m}}} = \sum n_i m_i d_i / \sum n_i m_i = \sum n_i d_i^{\,4} / \sum n_i d_i^{\,3} \qquad \text{Eq. 6.3}$$

Using Delsa^{TM} Nano (Beckman Coulter, CA), 100 μL suspension with 0.1 wt% nanoparticles was removed by micro pipette, and diluted with 1 mL DI water in DLS square tube. Three identical samples were sealed with a plastic cap. Nanoparticle size was measured and averaged across 150 individual detections. The resulting size d_m was determined by averaging three measurements. Size polydispersities and standard deviations were also calculated and recorded automatically. When lyophilized nanoparitcles were measured by DLS using either of the instruments, particle powder was first weighed and reconstituted in water or PBS with a concentration of 0.1 wt% particles. When nanoparticles used were measured during *in vitro* drug release studies, nanosuspension with an initial concentration of 0.1 wt% of particles was directly transferred from dialysis devices into DLS cuvettes, but over time the concentration may be smaller due to drug release.

6.2.3.2 Nanosight

Nanoparticle sizes were also measured by nanoparticle tracking system (NTA) via Nanosight (Malvern Instrument, UK). Different from dynamic light scattering, sample visualization and individual particle tracking are the unique features for NTA. Particles were tracked through the virtual of scattered light when illuminated by laser light. The light scattered from particles were captured and the Brownian motion of particles were recorded frame by frame. Based on a video recorded for 30-60 seconds, the software tracked the motion of particles on a particle-by-particle basis, which overcame the inherent weakness of DLS as an assemble technique. The hydrodynamic radius of individual particles was calculated based on Stokes-Einstein Relation (Eq.6.1). The concentration of nanoparticles can be calculated as well when individual particles were tracked and counted in camera view with a known volume. Since the video clip is the basis of the analysis, particle size for a particular sample can be characterized many times with proper adjustments in settings, such as camera levels and detection limits. These options enabled us to exclude certain intensity of scattered light such as dust. Also real time events can be accurately characterized if aggregation and dissolution are possible. It has been claimed that NTA by Nanosight can accurately analyze monodisperse and polydisperse samples, and the presence of small amounts of large particles will not compromise the accuracy of the measurements. NTA proved to be suitable to characterize drug loaded nanoparticles, complimenting the measurement of DLS[148].

To prepare sample for Nanosight measurement, 100 μL nanosuspension was removed and diluted with 2 mL DI water, in order to reach the required concentration range: 10^{-7}~10^{-9} particles/mL. The nanosuspension was injected via the inlet port into chamber. As liquid reached the end of the other inlet port, the chamber was completely filled. The chamber was mounted on the stage, with laser plug connected. After the temperature control software was opened, the main software was opened. On main screen, the "capture" window showed nanoparticles under the camera. The Brownian motion was indicated by the movement of scattered light spots. When the instrument was stabilized at room temperature, a 60 second video was recorded. The video was replayed with individual particles being tracked. Based on particle's Brownian motion, the diffusion coefficient was calculated and individual particle size was determined based on Stoke-Einstein relation in Eq.6.1. All particle sizes were calculated and accumulated to create particle size distribution. The intensity distribution of nanoparticles was also

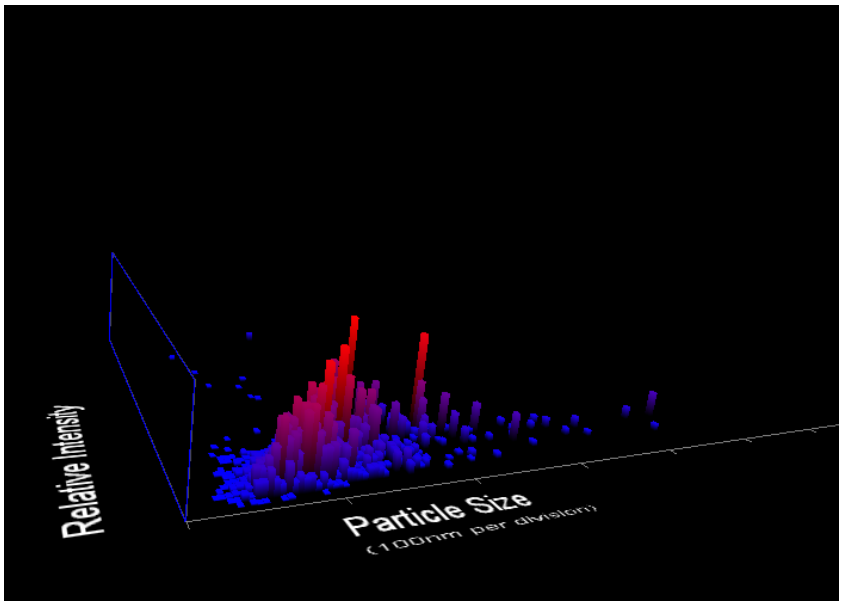

Figure 6.1 An example of particle size/relative intensity/particle population 3D plot from nanosight.

combined to form a 3D figure with particle size, relative intensity, particle population at x,y,z axis shown in Figure 6.1. The mass average sizes were automatically calculated, along with particle concentration.

6.2.4 Nanoparticle Morphology

All Cryo-TEM images shown in this chapter were obtained by my colleague Hanseung Lee. To prepare samples for Cryo-TEM, both fresh nanoparticle suspension and freeze dried nanopaticles were used. A drop of the suspension was dropped onto the grid and frozen under vacuum condition. A lacey carbon Cu grid (01881, 200-mesh, Ted Pella, Ltd., Redding, CA) was glow discharged in a vacuum evaporator at 70 mTorr (DV-502A, Denton Vacuum Moorestown, NJ) for 30 seconds to create a hydrophilic surface on the carbon coated side of the grid. A 2 −3 μL of fresh sample was pipetted onto the carbon side at 22 °C in a Mark III Vitrobot chamber (FEI Company, Hillsboro, OR) with a relative humidity of ~100 %. The excess sample was blotted with 595 filter papers (Ted Pella, Ltd., Redding, CA) 1 − 2 times with a ~1.5 mm offset parameter for 5 seconds to form a thin liquid film. After the blotting, the sample was relaxed for ~3 seconds and immediately plunged into liquid ethane cooled by liquid nitrogen.

The vitrified sample was transferred to a Gatan 626 Cryo-transfer unit (Gatan, Pleasanton, CA) at -194 °C and characterized at -178 °C in the microscope. A 120 kV FEI Tecnai Spirit BioTWIN was used and images were taken digitally with Eagle™ 2k CCD camera (FEI Company, Hillsboro, OR) in a low-dose mode. The images were processed with TEM Imaging and Analysis software package. (Version 4.2 SP1 build 816, FEI Company, Hillsboro, OR). To enhance phase contrast, the images were observed with objective lens in an under-focused mode (2 – 4 μm). The under-focused

model was controlled intentionally so that Fresnel fringe (white rings on the boundary of nanoparticle structure) can appear and that elucidates the core and shell regions in nanoparticles. Bean damage was only used to differentiate the microstructures (e.g, oil, surfactant, water). In this case, the diblock copolymer PEG-*b*-PLGA was susceptible to the electron beam and they showed a white edge, making nanoparticles look like bubbles. Supporting information for this chapter is presented in Appendix D with more images.

6.3 Results and Discussion

6.3.1 Nanoparticle Size and Distribution

Using dynamic light scattering to characterize particle size, we first found it more accurate with calculated average mass size from REPES method than Cumulant model used in most commercial instruments to produce average intensity particle size. However, our nanoparticles were very polydisperse and the intensity average sizes were more skewed to larger particles. In order to understand more about particle size and distribution, we presented intensity average size from DLS, mass average size from Nanosight, and number average size from Cryo-TEM images in Table 6.1. The sizes of all six prodrug nanoparticles decreased as the hydrophobicity of prodrugs increased, this has also been discussed in Ch 5.

Table 6.1 Nanoparticle sizes of silicate PTX prodrug NPs by DLS, NTA & Cryo-TEM.

Prodrug	aLogP	DLS (d_I)/nm	NTA(d_m)/nm	Cryo-TEM (d_n)/nm	
				particle	core
PEG-b-PLGA	n/a	40±10	35±5	20±3	n/a
1a	4.96	145±9	109±7	174±111	119±63
1c	5.60	136±1	98±8	251±76	99±75
1e	5.81	95±2	76±9	71±44	71±26
2a	6.31	118±13	93±12	103±55	92±45
1d	7.37	86±2	69±1	63±40	n/a
1b	7.74	83±6	75±4	56±20	52±34

Note: aLogP is calculated by using ALOPS 2.1, same as in Chapter 5.
Particle sizes are presented as intensity average size ± standard deviation from DLS, mass average size ± standard deviation from NTA (Nanosight) and number average size± standard deviation from Cryo-TEM.

Though Nanosight tracked individual particles by their scattered light, the sum of averaged particle size was closely consistent with DLS across all the Si PTX prodrug nanoparticles with increased hydrophobicity. Because Nanosight presented mass averaged size defined in Eq. 6.3, it is less skewed to larger particles, and overall sizes were smaller than that derived from DLS.

Despite the trend of particle size vs. hydrophobicity, 2'7-triethyl Si PTX (2a) didn't exactly produce nanoparticles smaller with relatively high hydrophobicity compared to Si PTX prodrugs 1a, 1c and 1e. It indicated that nanoparticle size was not only related to the hydrophobicity of loaded prodrug, but also perhaps to the bulkiness and number of silicate ester derivatives. It will be worth studying in future how these aspects affect particle size and distribution.

To analyze particle size based on Cryo-TEM, 200-1000 nanoparticles were manually identified and counted. The number average particle size (*dn*) and core

diameter (*dc*) were measured using all counted nanoparticles and those with visible cores. The number of counted nanoparticles, particle and core size are shown in Table 6.2.

Table 6.2 Nanoparticle and core sizes obtained from Cryo-TEM images.

NPs	# of NPs	d_n(nm)	d_n^c(nm)	%of NPs[c]	d_c(nm)
BCP	n/a	20±5	n/a	n/a	n/a
1a	196	110±110	245±80	20	175±65
2a	453	60±40	100±30	15	70±30
1b	282	35±15	60±40	15	55±35
1c	464	100±125	310±90	15	250±75
1d	147	40±25	85±30	10	60±20
1e	914	55±40	100±45	5	55±40

BCP: diblock copolymer PEG-b-PLGA nanoparticles (without drug loading).
d_n: the number average diameter of all counted nanoparticles from Cryo-TEM images.
d_n^c: the number average diameter of nanoparticles only with visible cores.
d_c: the number average diameter of cores in nanoparticles.

An example of how nanoparticle size and core size were analyzed was given in Figure 6.2. For each batch of nanoparticles, 200-1000 particles in several images were measured to obtain number average size. A line was first drawn across individual particles to identify the diameter, and the averaged size was statistically obtained based on hundreds of particles with high contrast. Notice that there are a few small particles in Figure 6.2, which was expected to be empty polymer particles. They were not counted for particle analysis. As for the core size analysis, in high resolution images, the core of nanoparticles was identified with even higher contrast than the corona region. Core size was a sum of particles with a clear center, which is approximately 15-20% of

nanoparticle population. The calculated standard deviations of particle and core sizes was large, because nanoparticles counted in analysis had a broad size distribution as shown in Figure 6.2. Also, core size was calculated with nanoparticles only with a visible center. For those that didn't have a core or cannot be imaged with a core, they were not counted in analysis either. The selected imaging areas and limited number of counted nanoparticles cannot be a complete representative of the entire population of nanoparticles.

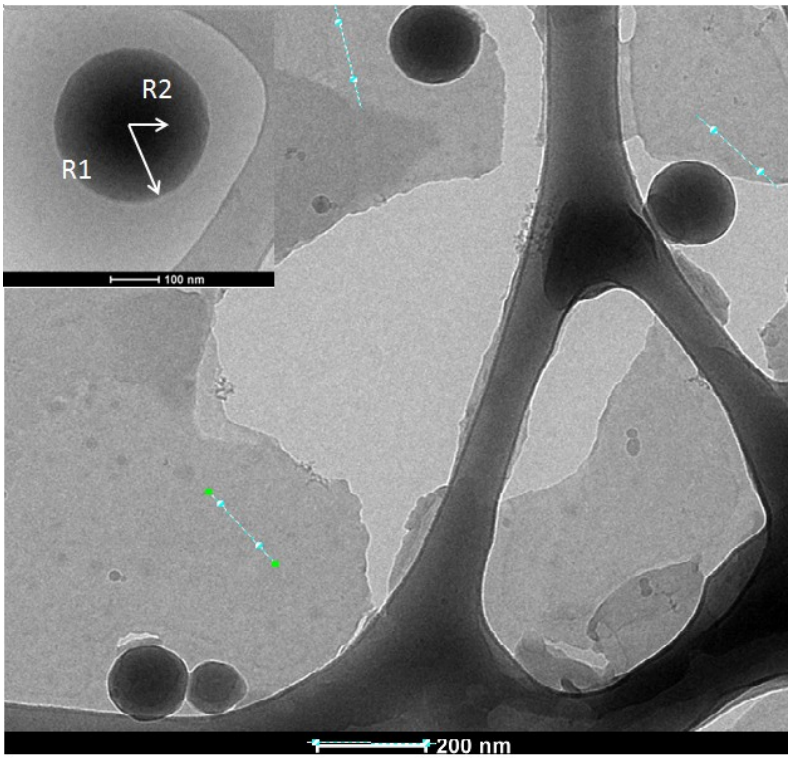

Figure 6.2 An example of particle and core size determination on Cryo-TEM image of 2'-triethyl Si PTX (1a) nanoparticles.

6.3.2 Fresh Nanoparticle Morphology

As shown above and also in Figure 5.2, fresh nanoparticles, right after being made via CIJ-D mixer, were all spherical, but interestingly their sizes and morphology have been changed during the processes of ultracentrifugation, lyophilization, and sonication.

First of all, fresh nanoparticles in each batch of Si PTX were characterized and presented in the following figures. They were only representative of each batch. 2'-triethyl Si PTX (1a) nanoparticles in Figure 6.3 showed particles had a relatively broad distribution. The number average particle size was 196 nm

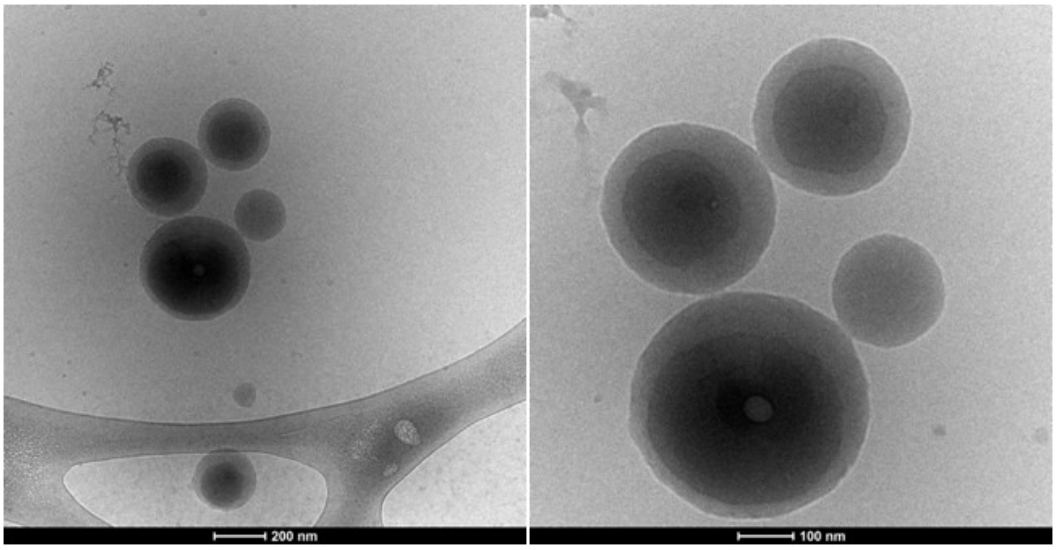

Figure 6.3 Cryo-TEM of fresh 2'-triethyl Si PTX (1a) nanoparticles.

from image analysis and a few ones were up to 300 nm which was extreme and rare cases. Most of particles showed a clear core-shell structure, some did not. We expected that cores with silicate provided more contrast while the shell region with less contrast was mainly composed of polymer. However, it is not possible to distinguish between hydrophilic block PEG and hydrophobic PLGA because of low electron contrast of polymers. The shell region may be only composed of PEG when PLGA was co-

precipitated in the core. Or, the shell region was composed of both PEG and PLGA, since the radius of gyration of PEG was only 2.58 nm[149] and they could be extended though. There were also 150 nm nanoparticles without a core in contrast, it might be loaded without any Si PTX, lightly loaded but failed to show contrast or the electron beam destroyed the shell during TEM imaging. Some extremely small particles were approximately 20 nm, and it was mostly likely to be empty polymer nanoparticles.

Most of 2',7-triethyl Si PTX (2a) nanoparticles were spherical with an average intensity size of 118 nm. It has two silicate ester derivatives compared to 1a, and the hydrophobicity has been increased significantly indicated by aLogP in Table 6.1, that is presumably why particle size were smaller than that of 1a. However, the core size distribution was much broader, when some of the particles have a 9:1 of core vs. particle ratio and some appeared to have very small cores shown in Figure 6.4.

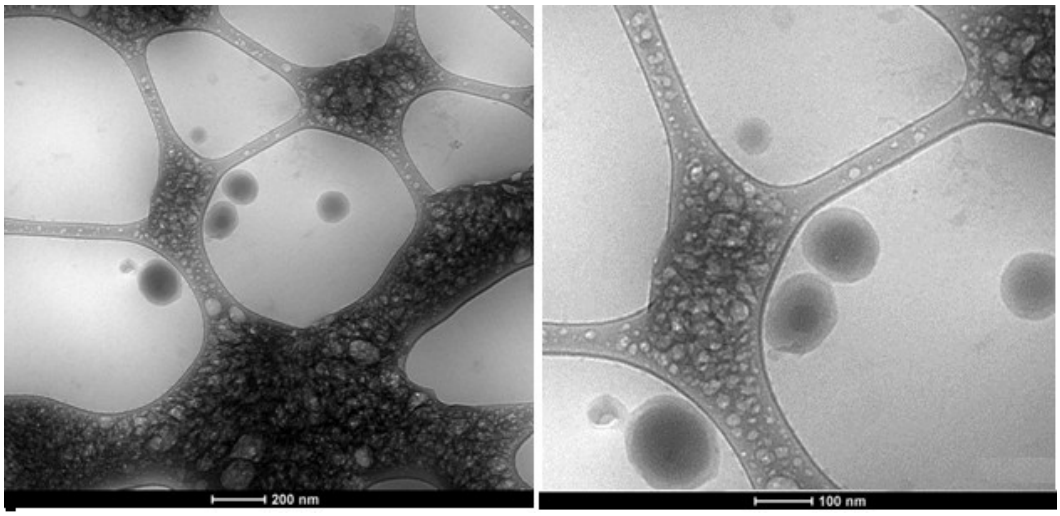

Figure 6.4 Cryo-TEM of fresh 2'7-triethyl Si PTX (2a) nanoparticles.

2'-trioctyl Si PTX (1b) is the most hydrophobic drug in this synthesized Si PTX prodrug family. Unsurprisingly, the nanoparticles had the smallest particles size confirmed by DLS, NTA and Cryo-TEM. It was probably because the high

hydrophobicity drove 1b to precipitate and nucleate faster than other prodrugs during FNP. More and smaller nuclei formed until the block copolymer arrested the nucleate without further growth. It may also result in stronger cooperative adsorption between prodrug and hydrophobic block of the polymer due to similar hydrophobicity,

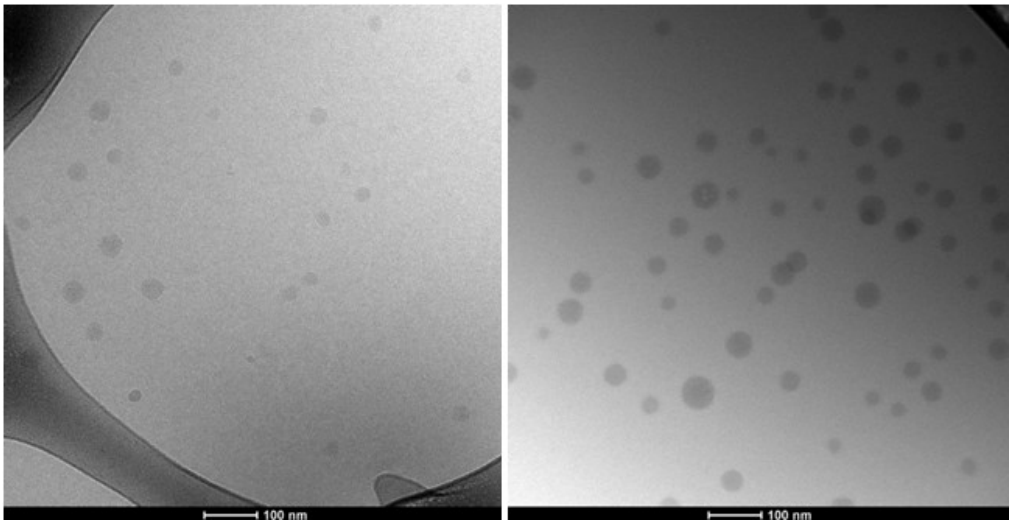

Figure 6.5 Cryo-TEM of fresh 2'-tri-octyl Si PTX (1b) nanoparticles.

which made the particle tightly packed. Thus, these particles had smaller average size and narrower distribution. The contrast was relatively high for the whole particle and it was very challenging to define the cores in Figure 6.5.

2'-triisopropyl PTX Si (1c) nanoparticles had second largest average size measured by DLS. From Cryo-TEM images in Figure 6.6, it appeared to have a broad size distribution similar to 2'-triethyl PTX Si particles, because of the similar hydrophobicity. But, the large particles showed a very distinctive core-shell structure. The particles were mostly composed of dark core with approximately 10-20 nm of shell region, but shell region can barely be seen for some particles. It has also been observed that low contrast spot inside particles shown in Figure 6.6, appearing to be polymer particles, of which no solid explanation was found yet.

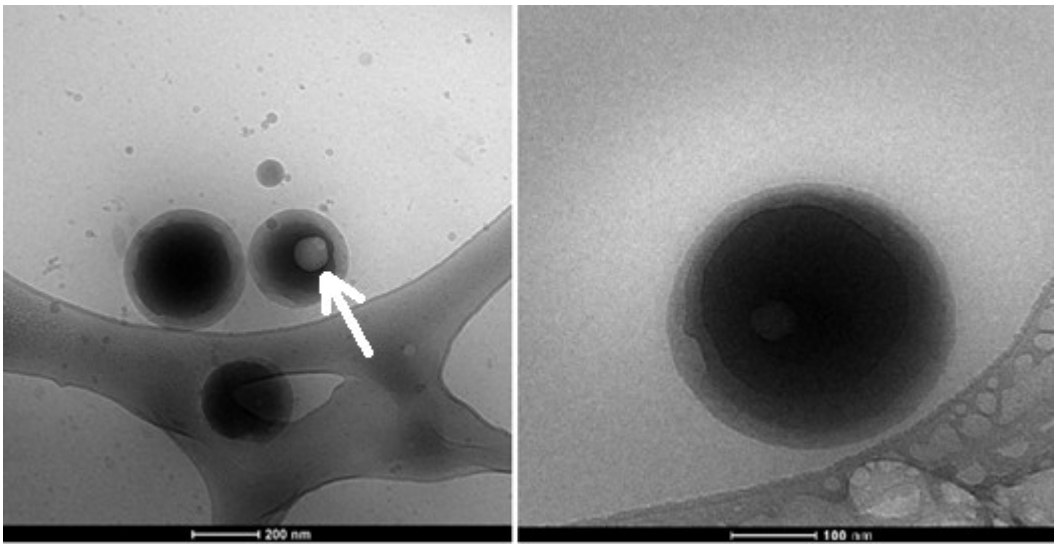

Figure 6.6 Cryo-TEM of fresh 2'-triisopropyl Si PTX (1c) nanoparticles.

2'-ditert butyl/ethyl PTX Si (1d) particles are the second smallest among all the Si PTX nanoparticles. Figure 6.7 showed particles were less than 100 nm, which was relatively consistent with an average size of 86 nm by DLS. The particles did show a dark core but from multiple images obtained, there were insufficient particles with cores to be statistically analyzed. However, it is firmly believed that this particular Si PTX was successfully encapsulated into nanoparticles, because their sizes were much larger than empty polymer nanoparticles and there was no crystalline structure of the prodrug been observed in Cryo-TEM.

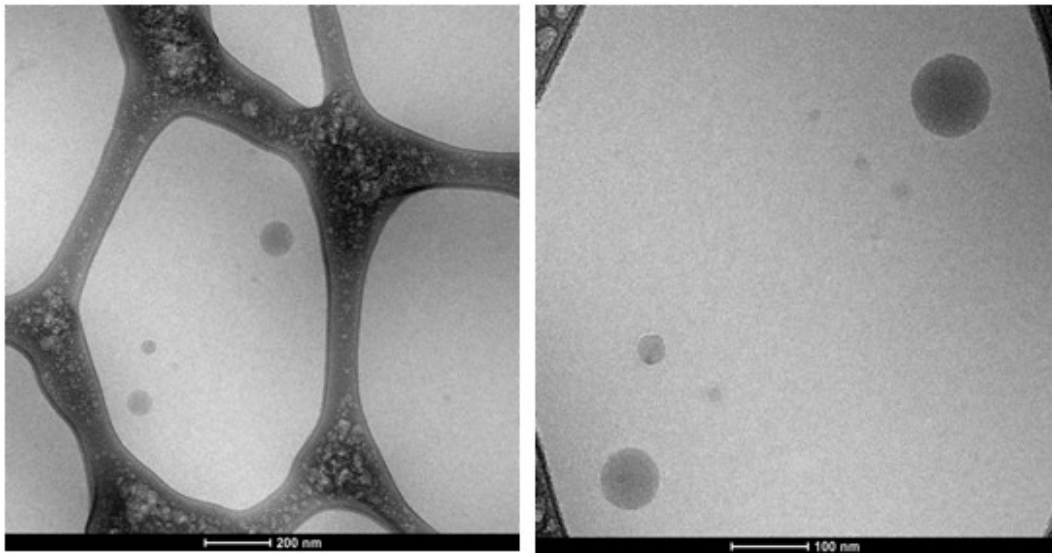

Figure 6.7 Cryo-TEM of fresh 2'-ditert butyl/ethyl Si PTX (1d) nanoparticles.

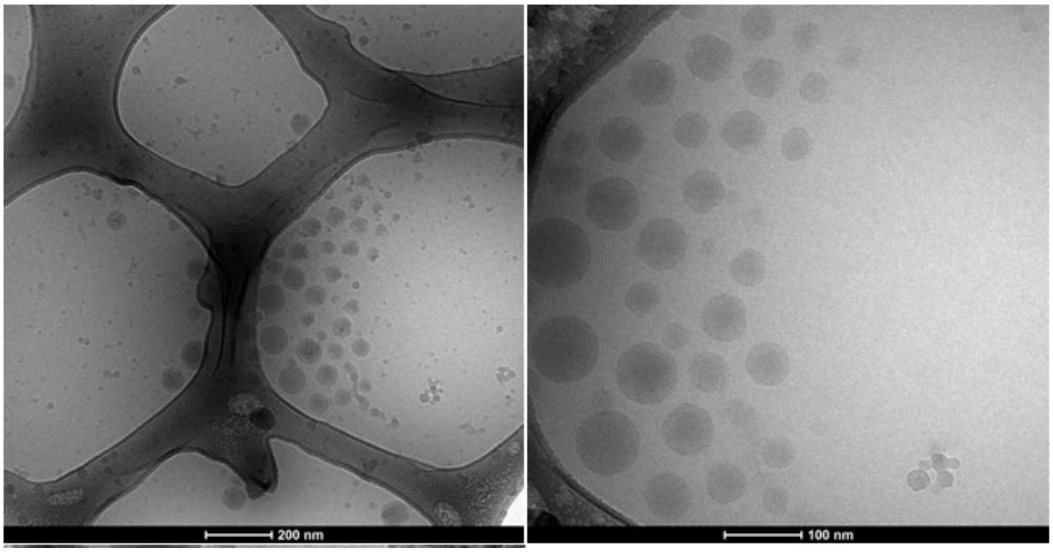

Figure 6.8 Cryo-TEM of fresh 2'-trimenthyl Si PTX (1e) nanoparticles.

2'-trimenthyl Si PTX (1e) nanoparticle also had relatively small particle size with an average of 95 nm, despite the bulkiness of trimenthyl silicate derivative. Core structure was observed in Figure 6.8, but oddly the contrast between core and shell regions was not as high as other small particles (less than 100 nm), such as 2'-trioctyl Si

PTX (1b). The size distribution shown below was broader than those two, since 2'-tri-menthyl Si PTX (1e) was much less hydrophobic and more likely causing more particle growth during FNP.

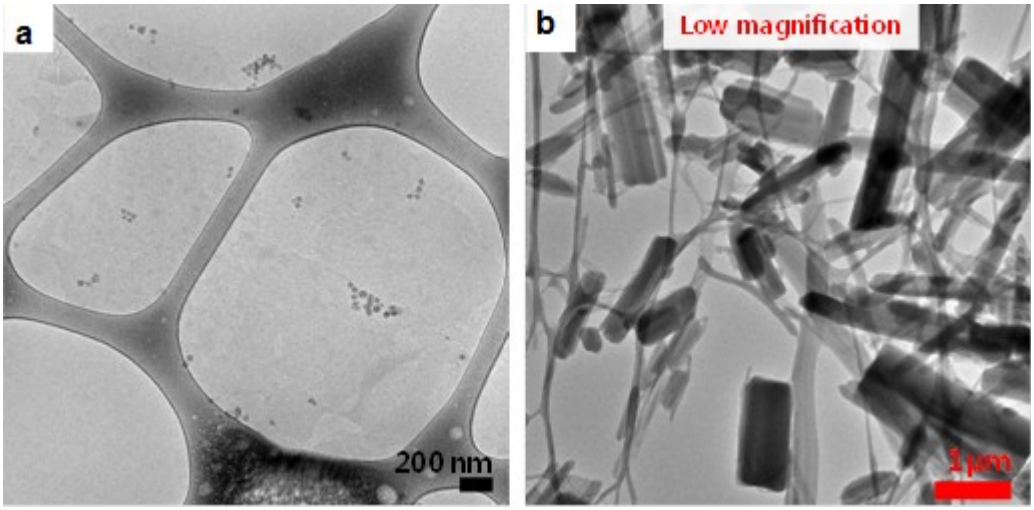

Figure 6.9 Cryo-TEM of PEG-*b*-PLGA nanoparticles (a) and TEM of PTX powder (b).

From all the images with silicate paclitaxel prodrugs loaded nanoparticles shown above, there were also approximately 20 nm nanoparticles present, which we expected to be empty polymer nanoparticles. In order to confirm this assumption, two control groups of Cryo-TEM images were obtained, one of which was from freshly made empty PEG-*b*-PLGA nanoparticles without any drug in formulation and the other was from paclitaxel itself shown in Figure 6.9

In Figure 6.9 (a), nanoparticles formed by PEG-*b*-PLGA itself had an average size of 20 nm and they were identical with what we have observed in images of prodrug loaded nanoparticles. This demonstrated that those unidentified small particles in images of prodrug loaded nanoparticles were empty polymer particles. It is reasonable not take these particles into consideration for size analysis of particle cores. In Figure 6.9 (b),

paclitaxel itself forms micron-size crystalline structure which has never been found in those prodrug loaded nanoparticles, it indicated that there was no crystallization of paclitaxel and prodrugs which were less water soluble. Prodrugs were most likely to be amorphous in nanoparticles. This is very encouraging in pursuit of enhancing bioavailability and dissolution for drug delivery system.

6.3.3 Lyophilized Nanoparticle Morphology

The first time we attempted to lyophilize nanoparticles, fresh nanoparticles via FNP were directly sent to be lyophilized without any washing step. As dry powder of particles was obtained, they were re-dispersed in DI water, and the redispersion was used to prepare TEM samples. Four examples of lyophilized nanoparticles were given below in Figure 6.10. Nanoparticles loaded with four different silicate paclitaxel prodrugs did not have any clear trend of particle size with hydrophobicity. Though we were able to identify individual particles in 100-200 nm with their core-shell structure, they mostly aggregated together, which made it impossible to measure particle size accurately by DLS or NTA, because the measured sizes were mainly from aggregates as a whole and they were up to micron size. The aggregation was widely believed to occur during freezing process and Pustulka et al. has proven that by comparing sizes of freeze-and-dried particles and freeze-and-thawed particles[86].

As water freezes and turns into ice during freezing process, nanoparticles in suspension are expelled to the area of higher concentration. As a result, particles are driven into each other and aggregate together. Also, the crystallization of ice applies a mechanical stress on particles leading to their destabilization. Another possible cause of particle aggregation was sonication. The micro-tip sonication generates intense energy

and heat. When the heat is not dissipated completely in short time and suspension tube is immersed in ice/water bath, particles become softer and irreversibly fuse into each other. Noted that with our first attempt of lyophilization, ultracentrifugation was not used to wash particles, therefore there were also many empty polymer particles and un-encapsulated prodrug molecules present in suspension, significantly observed in Figure 6.10.

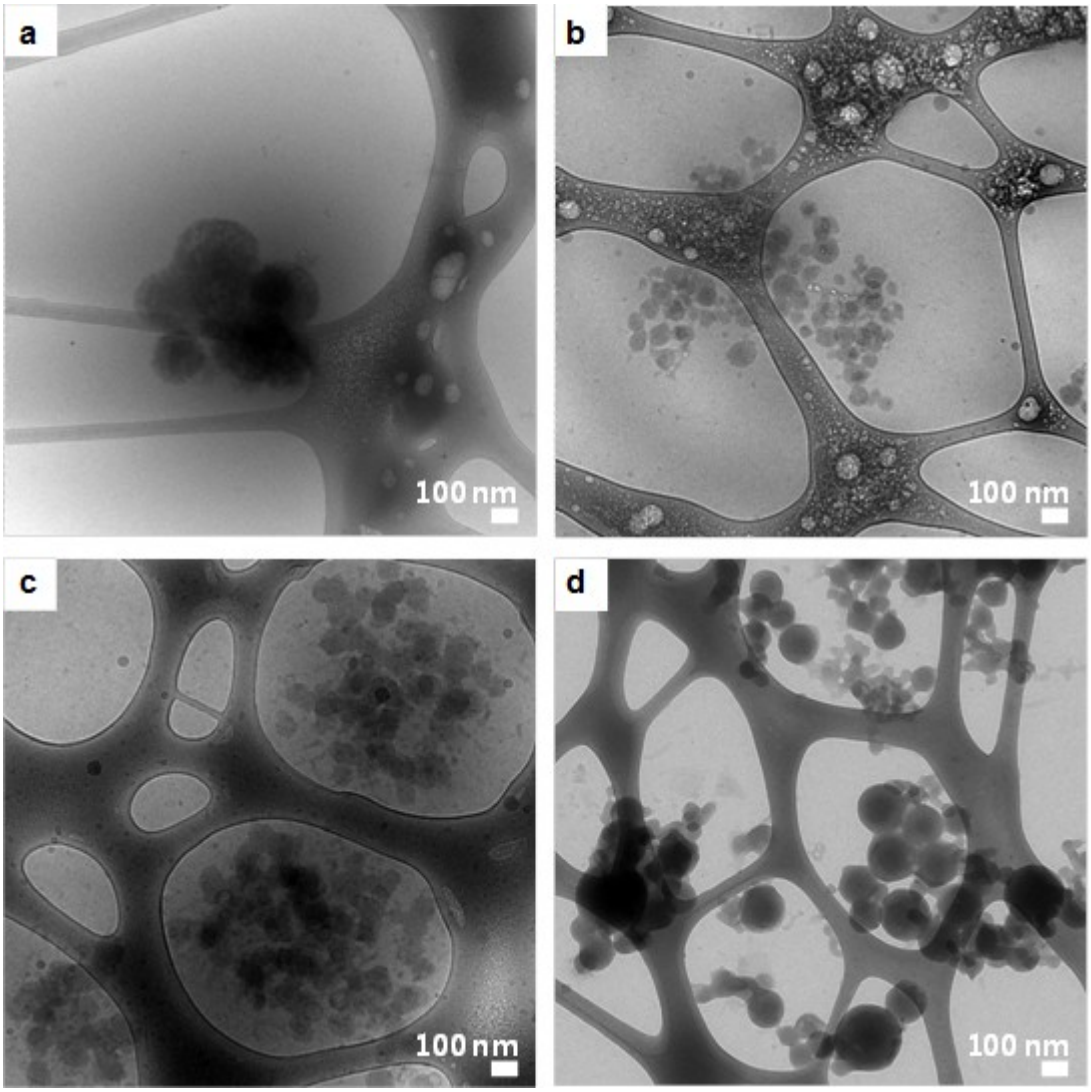

Figure 6.10 Cryo-TEM images of freeze dried and water suspended nanoparticles without ultracentrifugation loaded with (a) 2'-triethyl PTX Si, (b) 2'7-triehtyl PTX Si, (c) 2'-trioctyl PTX Si, and (d) 2'-trimenthyl PTX Si, respectively.

In order to purify nanoparticles, we ultracentrifuged fresh nanosuspension first and then freeze dried them in lyophilizer for 24 hrs. The dry powder was redispersed in PBS and prepared for *in vitro* drug release study. Cryo-TEM samples were prepared both at 0 hr and 24 hr during the release study. Since samples at 0 hr were prepared right after redispersing dry particles, it is a good comparison with Figure 6.10, of which the only difference was ultracentrifugation. As shown below in Figure 6.11, the population of nanoparticles was dominant by large particle with high contrast in cores. Small polymer particles were still present but much more reduced. The calculated density of our prodrug loaded nanoparticles were within 5% difference with solution, it is very challenging and time-consuming to separate them completely from solvent using ultracentrifugation, and polymer nanoparticles were more difficult to remove. However, ultracentrifugation indeed removed a significant amount of empty polymer nanoparticles and un-encapsulated prodrugs. The aggregation still occurred during freeze drying, which would continue to be a challenge we strive to overcome.

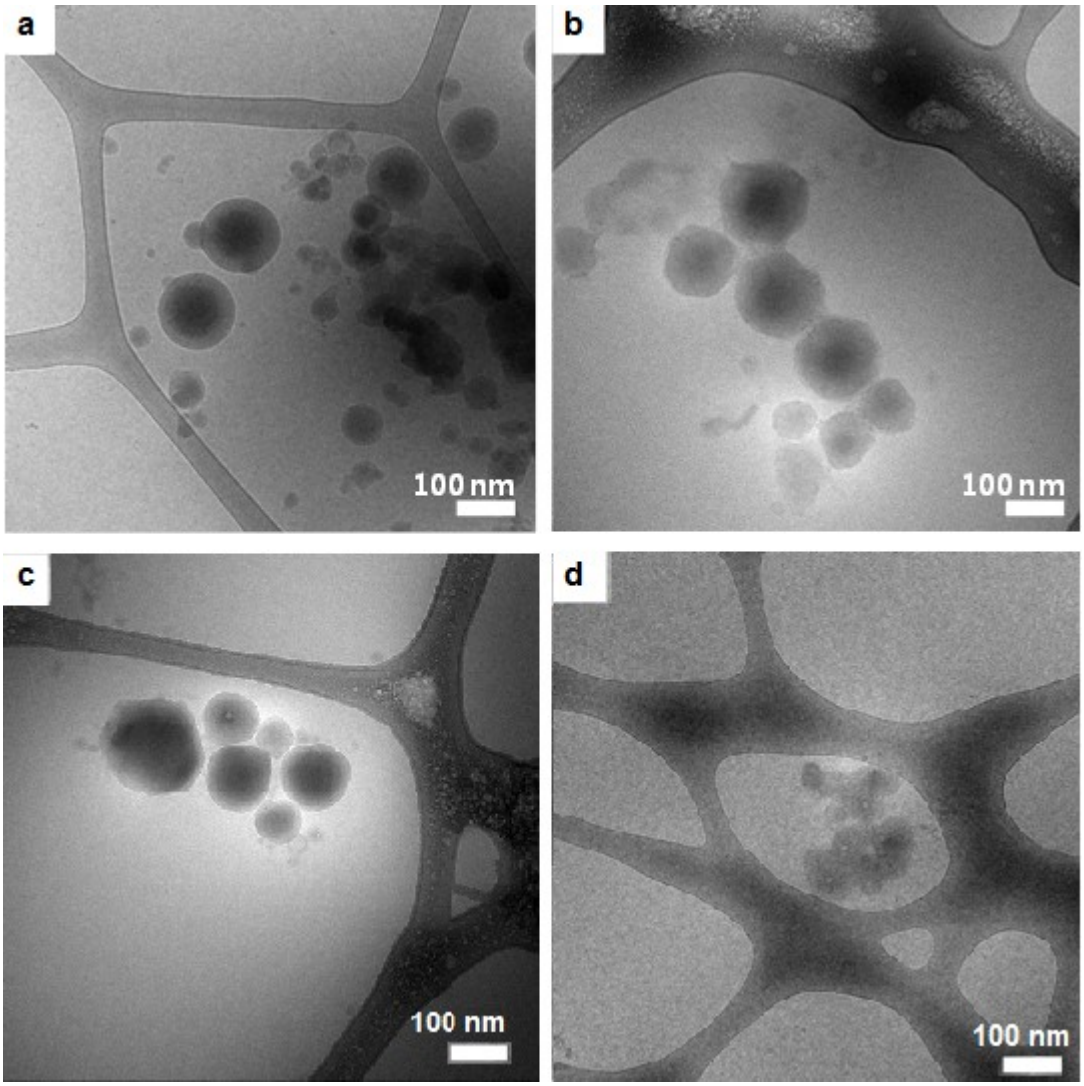

Figure 6.11 Cryo-TEM images of 0 hr release of nanoparticles loaded with (a) 2'-triethyl PTX Si, (b) 2'7-triethyl PTX Si, (c) 2'-ditert butyl/ethyl PTX Si, and (d) 2'-trimenthyl PTX Si, respectively.

After 24 hrs of *in vitro* drug release study, nanoparticle suspension was removed from dialysis capsules. The attempt of using DLS to measure particle size failed because the nanosuspension was too dilute, so DLS cannot collect statistically sufficient amount of scattering to calculate particle size. The suspension was further used to prepare TEM samples, shown in Figure 6.12.

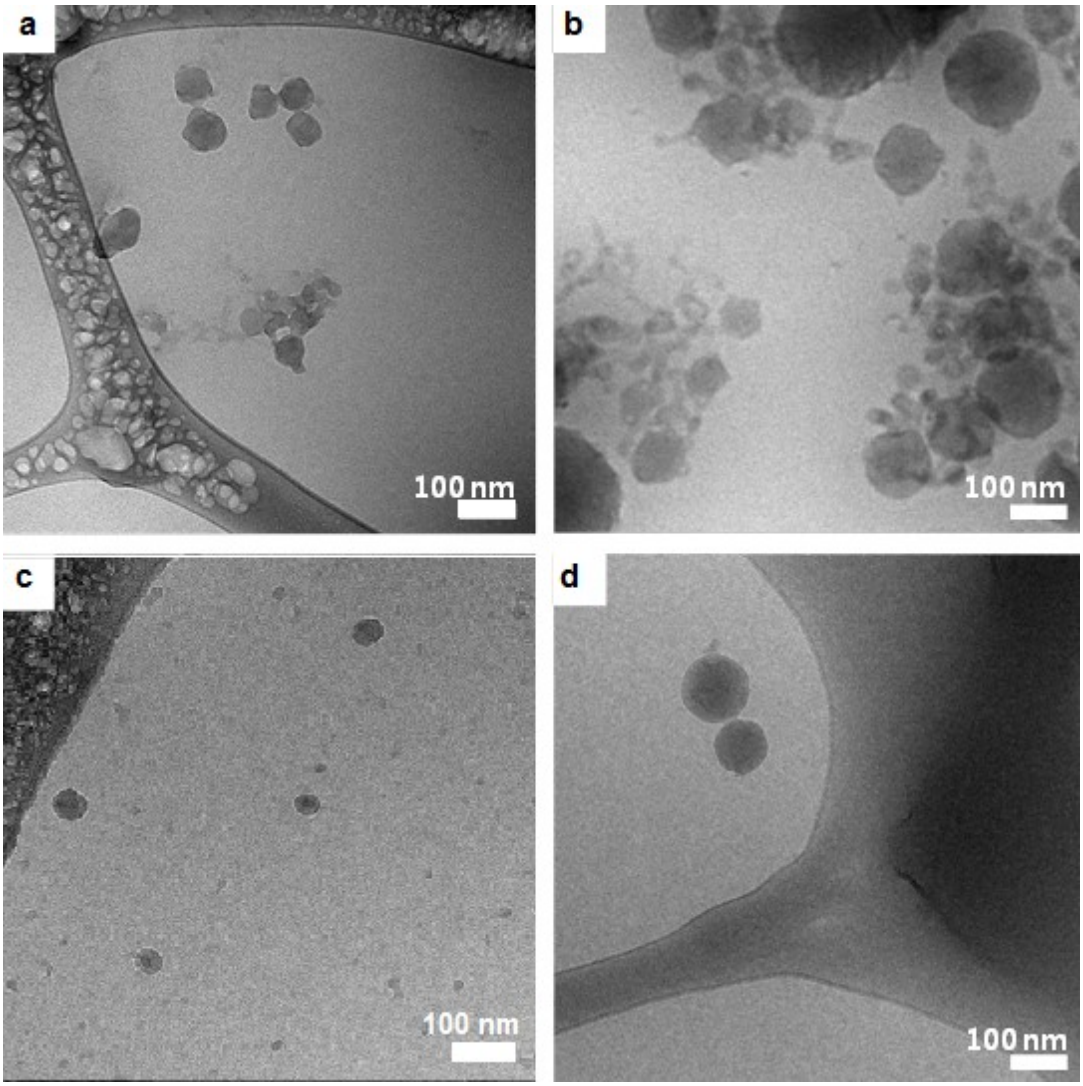

Figure 6.12 Cryo-TEM images of 24 hrs release of nanoparticles loaded with (a) 2'-triethyl PTX Si, (b) 2'7-triethyl PTX Si, (c) 2'-ditert butyl/ethyl PTX Si, and (d) 2'-trimenthyl PTX Si, respectively

Interestingly, Figure 6.12(a) shows nanoparticles loaded with 2'triethyl Si PTX (1a) prodrug 24 hr after immersed in PBS. Compared to Figure 6.11(a) at 0 hr of the same suspension, nanoparticle sizes were significantly reduced, and they changed from spherical to irregular shape. Particles appeared to shrink without polymer shell protection, and it has been hypothesized to be polymer degradation. However, our preliminary results showed that polymer degradation occurred evidently only after 16

days, which is out of the timeframe of drug release study. Until now, we have not identified the reason, albeit it will be part of our future work investigating the influence of polymer degradation on particle structure and possible particle collapse over time. Another interesting observation is, Figure 6.12(c) and (d) showed nanoparticles loaded with 2'-ditert butyl/ethyl Si PTX (1d) and 2'-tri-menthyl Si PTX (1e) at 24 hr, respectively. There was no noticeable morphology change like (a). Since these two Si PTX prodrugs were most hydrophobic and hydrolytic stable, their release and hydrolysis rates were a lot slower than 2'-triethyl Si PTX (1a). It leads to another hypothesis that drug release that left particle core more loose or empty might cause particle structure to rearrange as well.

6.4 Conclusion

In this chapter, six Si PTX prodrugs synthesized by Wohl et al[59, 60] were successfully encapsulated into PEG-*b*-PLGA nanoparticles. As nanopartiles were freshly prepared via CIJ-D mixer, they were characterized by DLS, NTA, and Cryo-TEM. All fresh nanoparticles were spherical and mostly loaded with Si PTX prodrugs. The intensity average size d_I measured by DLS displayed a trend that nanoparticles became smaller with increased hydrophobicity of loaded prodrugs. Their size distribution went narrower as well. Size analysis from NTA and Cryo-TEM, also done right after CIJ-D mixing and before ultracentrifugation, showed mass average size d_m and number average size d_n of particles correspondingly, which were smaller because d_m and d_n, were less skewed by the larger particles. These two measurements also confirmed the trend of smaller particles with higher hydrophobicity of the loaded prodrugs.

Cryo-TEM technique has clearly demonstrated that nanoparticles have the core-shell structure with high contrast in the center, which was most likely encapsulating silicate prodrugs. Usually, large particles had large cores, but in small ones, it was very difficult to visualize cores. Particles were either too small to differentiate the contrast or possibly small particles did not have drug loaded in their cores. As control groups, empty polymer particles and PTX itself were also imaged by TEM. Polymer particles had a relatively uniform size in 10-20 nm. PTX crystallized into micro size. In Cryo-TEM images of prodrug nanoparticles, we found a portion of small particles in 20 nm which was believed to be polymer particles, and there was no recrystallization found, which meant no unencapsualted prodrugs recrystallize outside particles.

The core-shell structure allowed us to propose a three-layer model[85] for nanoparticle internal structure. With the aid of high resolution in Cryo-TEM, no aggregates or primary nucleates were observed in cores of nanoparticles, it also implied that the mechanism of nanoparticle formation is more favored towards nucleation and growth. During CIJ-D mixing via flash nanoprecipitation, water miscible organic solvent (e.g., THF) and water were impinged rapidly creating supersaturation condition for drug and polymer, the hydrophobic drug precipitated out of solution and nucleated as particles. Once the hydrophobic block of block copolymer co-precipitated and was adsorbed to drug particles, it arrested the growth of drug particles. Meanwhile, the hydrophilic block stayed in solution, covered particle surface and provided steric stabilization for particles. The drug mainly formed the core of particles, while block copolymer formed the shell region. In Cryo-TEM images, the hydrophilic block PEG was likely swollen with vitrified water with low electron density, so it was probably invisible. Despite that, Cryo-

TEM has been the most supportive evidence for three-layer core shell structures. Pustulka et al[86] have also used other techniques to identify internal structures such as DSC and NMR, they all consistently indicated this three-layer core shell model of block copolymer drug loaded nanoparticle internal structure.

As nanoparticles were lyophilized, particles tended to aggregate because of the mechanical stress caused by crystallization of ice during freezing. We have attempted to use cryoprotectant like sucrose to eliminate aggregation, however, with addition of sucrose (10:1 mass ratio of sucrose vs. NPs), particle sizes were slightly recovered with less aggregation, but still problematic. In order to use these particle formulations for *in vitro* and *in vivo* studies, nanoparticles cannot be redispersed with such high concentration of sucrose, because it was much higher than blood sugar level. Nanoparticles with sucrose would disrupt the isotonic solution balance in cell culture and body fluid. Currently, we are still in search of alternatives without cryoprotectant to recover particle size after lyophilization, such as sonication.

Ultracentifugation was used to remove empty polymer particles and un-encapsulated drug in suspension. Cryo-TEM images confirmed that nanoparticles were purified with less polymer particles. During *in vitro* drug release study, some of the nanoparticles have been through a significant morphology change. They appeared to shrink from spherical to irregular shape, of which the reason has not been determined yet. We highly hypothesized that polymer might degrade to certain extent, leaving particles without shell coverage, or particle shell perhaps collapses.

Chapter 7 Summary and Outlook

Ch.2 described a simpler design of confined impingement jets-dilution (CIJ-D) mixer, utilizing flash nanoprecipitation to prepare nanoparticles made of hydrophobic materials. The design was modified based on Prud'homme's confined impingement jets (CIJ) mixer. The interior dimensions and specifications on manufacturing CIJ-D mixer were listed in details. Our design introduced an addition of dilution stage in order to achieve high supersaturation condition above a ratio of 1:1 of anti-solvent/solvent. To understand the effect of dilution, β-carotene, as a model drug, was used to prepare nanoparticles with varied ratio of anti-solvent/solvent mixing. To test the performance of CIJ-D mixer, β-carotene nanoparticles were also formulated by both multi-inlet vortex mixer (MIVM) and CIJ-D mixer at varied flow conditions. Particle size and stability were consistent between two mixing processes. Smaller particles were produced in more turbulent mixing indicated by high Reynolds number. This demonstrated that, it is very important, not only to achieve high supersaturation, but sufficiently turbulent mixing in order to create small particles made with hydrophobic materials.

In Ch.3, paclitaxel (PTX), an anti-cancer drug, was introduced to formulate nanoparticles via CIJ-D mixer. Diblock copolymer PEG-*b*-PLGA was used as a particle stabilizer. We first encountered difficulty producing stable PTX loaded nanoparticles because PTX recrystallized out of dispersion in 90 min due to Ostwald ripening. A chemical modification strategy was introduced here to make PTX more hydrophobic in an effort to prevent Ostwald ripening. A series of silicate ester derivatized PTX was synthesized in Hoye's lab with enhanced hydrophobicity and tuned hydrolytic lability.

These compounds were presumably inactive and considered as prodrug of PTX. Their hydrolysis was expected to convert prodrug back to active form of PTX. A series of Si PTX prodrugs were used to prepare nanoparticles and they were successfully stabilized by PEG-*b*-PLGA without any significant recrystallization and aggregation. They were characterized by DLS, NTA, SEM, Cryo-TEM and HPLC in size, distribution and drug loading. Additionally, several purification techniques, such as membrane filter, hollow fiber filtration, and ultracentrifugation. And ultracentrifugation was found to be the best approach to remove un-encapsulated prodrug and empty polymer particles. Another particle post-treatment, lyophilization was investigated as well. It was found that nanoparticles tended to aggregate together during freezing process and after lyophilized dry powder of particles was redispersed in solution, particles size increased significantly due to severe aggregation. To better recover particle size, cryoprotectants like sucrose and sonication were used. Although cryoprotectants were able to reduce particle size closer to initial size of fresh particles, it is impossible to administer nanoparticles with sucrose *in vitro* and *in vivo* because the high concentration of sucrose in particle dispersion will cause cell shrink as hypertonic effect. While we are still working hard to find other cryoprotectants with less concentration to recover particle size, a standard procedure of nanoparticle preparation was described as: nanoparticles are first formulated via CIJ-D mixer in 95:5 ratio of H_2O:THF. They are ultracentrifuged and lyophilized without cryoprotectants. They are stored as dry powder and redispersed for administration *in vitro* and *in vivo*.

In Ch.4, *in vitro* drug release studies were first introduced with a series of Si PTX prodrug nanoparticles. To customize a drug release protocol for these nanoparticles

loaded with highly hydrophobic materials, several experimental conditions were explored, such as infinite sink, limited buffer and frequently refreshed buffer. Due to the extremely low solubility of these prodrugs in aqueous solution, a dialysis-based reverse release protocol was established to determine the remaining prodrug loaded in nanoparticles, instead of the released ones in buffer. Mini dialysis capsules were chosen to carry out *in vitro* drug release study for quantity accuracy and handling convenience. The preliminary release results shown in this chapter were based on Si PTX prodrug loaded nanoparticles without ultracentrifugation, a significant burst release pattern was observed in short time due to the un-encapsulated prodrug in dispersion. However, in the following chapter, nanoparticles were all ultracentrifuged and lyophilized before *in vitro* and *in vivo* studies.

Ch.5 studied *in vitro* drug release on nanoparticles loaded with six Si PTX prodrugs, respectively, five of which were mono silicate ester derivatized only at 2'carbon of PTX and one was bis-triethyl Si PTX derivatized at 2' and 7 carbon of PTX. With addition of ultracentrifugation, release profiles of all nanoparticles were more extended in a range of 24-96 hrs without obvious burst release. Their release rates appeared to increase following an order of increasing hydrolytic lability. To verify the reliability of reverse release protocol, mass balance studies were conducted to determine the released drugs in buffer and the remaining ones in nanoparticles. Not only did we obtain a complementary release and reverse profiles, we were also able to see composition change inside nanoparticles and in buffer solution, indicating the hydrolysis rates of these prodrugs in different conditions, either encapsulated in nanoparticles or surrounded in water. In the hope of observing more hydrolysis of prodrugs, *in vitro* drug

release studies were conducted in PBS first at pH=6.4 and 7.4 to mimic tumor and normal tissue conditions, and then at pH=5.0. The general release profiles were significantly altered because of pH-responsive hydrolysis.

In Ch.6, we focused on nanoparticle size and morphology characterization mainly by DLS, NTA and Cryo-TEM, which was greatly contributed by my colleague, Hanseung Lee. Particle sizes were not only directly measured by DLS and NTA, and also hundreds of Cryo-TEM images. The particle size results were consistent among DLS, NTA and Cryo-TEM. Besides, morphology of nanoparticles were visualized in Cryo-TEM, showing a core-shell internal structure, which was the first direct evidence confirming nanoparticles were kinetically formed based on nucleation and growth mechanism. During *in vitro* drug release studies, we also found particles became smaller and irregular in shape, and seemed to lose shell region. These evidences have inspired us to initiate current work on diblock copolymer degradation from nanoparticles.

Overall the work in this dissertation:

1) Modified confined impingement jets mixer with a dilution stage and demonstrated that CIJ-D mixer can produce nanoparticles composed of hydrophobic materials as well as multi-inlet vortex mixer. The dilution step overcame the limitation of Prud'homme's CIJ mixer with equal volume of solvent/anti-solvent mixing and provided high supersaturation condition to create small nanoparticles based on nucleation and growth. The threshold of flow rates was also identified to create sufficiently turbulent mixing condition.

2) Successfully formulated paclitaxel-based PEG-*b*-PLGA stabilized nanoparticles with a chemical modification strategy. Wohl and Hoye modified paclitaxel

with a series of silicate ester derivatives with enhanced hydrophobicity and tuned hydrolytic lability.

3) Established standard nanoparticle formation process with post-treatments, including ultracentrifugation, lyophilization and sonication.

4) Developed a reverse *in vitro* drug release protocol to determine the remaining drug in nanoparticles and confirmed the reliability of this protocol by conducting mass balance studies.

5) Characterized a series of Si PTX loaded nanoparticles by DLS, NTA, HPLC, SEM, Cryo-TEM in terms of particle size, distribution, drug loading and morphology.

6) Characterized *in vitro* drug release of a series of Si PTX nanoparticles and quantified their composition change of prodrug and drug via hydrolysis over time. The general release rates increased with more hydrolytic labile prodrugs. With tuned hydrophobicity and hydryolytic lability, the choice of prodrug significantly affected the release rate of prodrug and regeneration of PTX. Hydrolytic lability appeared to play a more important role in regeneration of PTX and general release rate.

7) The core-shell structure of all Si PTX nanoparticles were visualized by Cryo-TEM and their morphology change and disappearance of shell during drug release study was also observed, which indicated the possibility of *in vitro* polymer degradation and particle collapse.

Besides the progress achieved in this work, there are also a few lessons I learned from our mistakes and omissions.

1) We started making PTX-based PEG-*b*-PLGA nanoparticles using (2a) 2',7-triethyl Si PTX. This Si PTX prodrug has two intermediates via hydrolysis, which made

it more complicated to determine the drug release mechanism. Also, the synthesis was very difficult, compared to other Si PTX prodrugs with only one silicate ester derivatives.

2) At the earlier stage of developing *in vitro* drug release study, nanoparticles were not ultracentrifuged which resulted in a large amount of unencapsulated drug/prodrug mixed with nanoparticles in dry powder. As shown in drug release results, a burst-release pattern was constantly observed until we realized that the unencapsulated drug/prodrug must be removed from nanoparticles in order to characterize drug release kinetics more accurate.

3) As *in vitro* drug release studies proceeded, polymer degradation was not considered as a factor to affect drug release rates until we observed significant nanoparticle morphology change on Cryo-TEM images, which indicated nanoparticles disassembled or was destructed.

To anticipate the future development, there are still challenges and research interests that have not been explored.

1) Nanoparticle we have formulated so far only contained one pharmaceutical ingredient. To design multi-functional nanoparticles, it will be very interesting to co-load two or more ingredients in particles. Those ingredients can be two compounds with different release characteristics or varied functions, such as imaging agent, fluorescent labels. Appendix E presented a experimental trial of coloading two Si PTX prodrugs within nanoparticles at varied mass ratio. Although it was not successful, more systematic studies should be planned and more drugs and functional agents should be explored.

2) Following with Zhu's work, diblock copolymer PEG-*b*-PLGA (MW: 5k-10kDa) was identified as the best particle stabilizer. However, other diblock copolymers

and their effect of MW should also be studied. Moreover, triblock copolymer should be investigated as well, because they are expected to form either more intense hydrophilic region or loops when two hydrophobic blocks embedded in particles. Thus, different block copolymers with adjusted MWs are hypothesized to create different internal structures. With the powerful tool of Cryo-TEM imaging, these differences might be identified. These variables will further play an important role in particle size, distribution, drug loading and release profiles.

3) Since this thesis has established *in vitro* drug release protocol for Si PTX nanoparticles, *in vivo* or *in vitro* release study in other medium such as serum should be further developed, in order to mimic biological condition better and to correlate drug release rates with other *in vitro* and *in vivo* studies, such as cytotoxicity, biodistribution and tumor growth inhibition.

4) We have made a great deal of efforts to visualize nanoparticles, especially their internal structure and morphology change during drug release study, we speculate block copolymer might degrade in the same course of time. *In vitro* polymer degradation studies should be conducted along with drug release studies, in order to see the effect of polymer degradation on drug release.

References

1. World Health Organization, Cancer. http://www.who.int/mediacentre/factsheets/fs297/en/.
2. Wang, X.; Yang, L.; Chen, Z. G.; Shin, D. M., Application of nanotechnology in cancer therapy and imaging. *CA Cancer J Clin* 2008, 58, 97-110.
3. Matsumura, Y.; Maeda, H., A new concept for macromolecular therapeutics in cancer chemotherapy: mechanism of tumoritropic accumulation of proteins and the antitumor agent smancs. *Cancer research* 1986, 46, 6387-92.
4. Maeda, H., Macromolecular therapeutics in cancer treatment: the EPR effect and beyond. *J Control Release* 2012, 164, 138-44.
5. Maeda, H., The enhanced permeability and retention (EPR) effect in tumor vasculature: the key role of tumor-selective macromolecular drug targeting. *Adv Enzyme Regul* 2001, 41, 189-207.
6. Greish, K., Enhanced permeability and retention (EPR) effect for anticancer nanomedicine drug targeting. *Methods Mol Biol* 2010, 624, 25-37.
7. Bisht, S.; Maitra, A., Dextran-doxorubicin/chitosan nanoparticles for solid tumor therapy. *Wiley Interdiscip Rev Nanomed Nanobiotechnol* 2009, 1, 415-25.
8. Akbulut, M.; D'Addio, S. M.; Gindy, M. E.; Prud'homme, R. K., Novel methods of targeted drug delivery: the potential of multifunctional nanoparticles. *Expert Review of Clinical Pharmacology* 2009, 2, 265-282.
9. Venugopal, J.; Prabhakaran, M. P.; Low, S.; Choon, A. T.; Zhang, Y. Z.; Deepika, G.; Ramakrishna, S., Nanotechnology for nanomedicine and delivery of drugs. *Curr Pharm Des* 2008, 14, 2184-200.
10. Bai, S.; Thomas, C.; Rawat, A.; Ahsan, F., Recent progress in dendrimer-based nanocarriers. *Crit Rev Ther Drug Carrier Syst* 2006, 23, 437-95.
11. Rabinow, B. E., Nanosuspensions in drug delivery. *Nat Rev Drug Discov* 2004, 3, 785-96.
12. Hobbs, S. K.; Yuan, F.; Cima, L. G.; Jain, R. K., Tumor microvascular pore cutoff size:implications for macromolecules and particle drug delivery. *International Journal of Macrocirculation: Clinical & Experimental* 1996, 218.
13. Lipinski, C. A., Poor aqueous solubility-An industry wide problem in drug discovery. *Am. Pharm. Rev.* 2002, 5, 82-85.
14. Tamilvanan, S., Oil-in-water lipid emulsions: implications for parenteral and ocular delivering systems. *Progress in Lipid Research* 2004, 43, 489-533.
15. Discher, D. E.; Eisenberg, A., Polymer vesicles. *Science* 2002, 297, 967-73.
16. Jun, Y. J.; Toti, U. S.; Kim, H. Y.; Yu, J. Y.; Jeong, B.; Jun, M. J.; Sohn, Y. S., Thermoresponsive Micelles from Oligopeptide-Grafted Cyclotriphosphazenes. *Angewandte Chemie International Edition* 2006, 45, 6173-6176.
17. Kakizawa, Y.; Kataoka, K., Block copolymer micelles for delivery of gene and related compounds. *Advanced Drug Delivery Reviews* 2002, 54, 203-222.
18. Kataoka, K.; Harada, A.; Nagasaki, Y., Block copolymer micelles for drug delivery: design, characterization and biological significance. *Advanced Drug Delivery Reviews* 2001, 47, 113-131.

19. Savić, R.; Luo, L.; Eisenberg, A.; Maysinger, D., Micellar Nanocontainers Distribute to Defined Cytoplasmic Organelles. *Science* 2003, 300, 615-618.
20. Toti, U. S.; Moon, S. H.; Kim, H. Y.; Jun, Y. J.; Kim, B. M.; Park, Y. M.; Jeong, B.; Sohn, Y. S., Thermosensitive and biocompatible cyclotriphosphazene micelles. *Journal of Controlled Release* 2007, 119, 34-40.
21. Lian, T.; Ho, R. J. Y., Trends and developments in liposome drug delivery systems. *Journal of Pharmaceutical Sciences* 2001, 90, 667-680.
22. Ghoroghchian, P. P.; Frail, P. R.; Susumu, K.; Blessington, D.; Brannan, A. K.; Bates, F. S.; Chance, B.; Hammer, D. A.; Therien, M. J., Near-infrared-emissive polymersomes: Self-assembled soft matter for in vivo optical imaging. *Proceedings of the National Academy of Sciences of the United States of America* 2005, 102, 2922-2927.
23. Ahmed, F.; Pakunlu, R. I.; Brannan, A.; Bates, F.; Minko, T.; Discher, D. E., Biodegradable polymersomes loaded with both paclitaxel and doxorubicin permeate and shrink tumors, inducing apoptosis in proportion to accumulated drug. *Journal of Controlled Release* 2006, 116, 150-158.
24. Ghoroghchian, P. P.; Lin, J. J.; Brannan, A. K.; Frail, P. R.; Bates, F. S.; Therien, M. J.; Hammer, D. A., Quantitative membrane loading of polymer vesicles. *Soft Matter* 2006, 2, 973-980.
25. Kataoka, K.; Matsumoto, T.; Yokoyama, M.; Okano, T.; Sakurai, Y.; Fukushima, S.; Okamoto, K.; Kwon, G. S., Doxorubicin-loaded poly(ethylene glycol)–poly(β-benzyl-l-aspartate) copolymer micelles: their pharmaceutical characteristics and biological significance. *Journal of Controlled Release* 2000, 64, 143-153.
26. Kumar, V.; Prud'homme, R. K., Thermodynamic limits on drug loading in nanoparticle cores. *Journal of Pharmaceutical Sciences* 2008, 97, 4904-4914.
27. Bai, Z.; Lodge, T. P., Thermodynamics and Mechanism of the Block Copolymer Micelle Shuttle between Water and an Ionic Liquid. *The Journal of Physical Chemistry B* 2009, 113, 14151-14157.
28. Lee, J. C. M.; Santore, M.; Bates, F. S.; Discher, D. E., From Membranes to Melts, Rouse to Reptation: Diffusion in Polymersome versus Lipid Bilayers. *Macromolecules* 2001, 35, 323-326.
29. Li, Z.; Kesselman, E.; Talmon, Y.; Hillmyer, M. A.; Lodge, T. P., Multicompartment Micelles from ABC Miktoarm Stars in Water. *Science* 2004, 306, 98-101.
30. Liu, C.; Hillmyer, M. A.; Lodge, T. P., Evolution of Multicompartment Micelles to Mixed Corona Micelles Using Solvent Mixtures. *Langmuir* 2008, 24, 12001-12009.
31. Liu, C.; Hillmyer, M. A.; Lodge, T. P., Multicompartment Micelles from pH-Responsive Miktoarm Star Block Terpolymers†. *Langmuir* 2009, 25, 13718-13725.
32. Zhu, Z.; Anacker, J. L.; Ji, S.; Hoye, T. R.; Macosko, C. W.; Prud'homme, R. K., Formation of Block Copolymer-Protected Nanoparticles via Reactive Impingement Mixing. *Langmuir* 2007, 23, 10499-10504.
33. Zhu, Z.; Margulis-Goshen, K.; Magdassi, S.; Talmon, Y.; Macosko, C. W., Polyelectrolyte stabilized drug nanoparticles via flash nanoprecipitation: a model study with beta-carotene. *J Pharm Sci* 2010, 99, 4295-306.
34. Johnson, B. K.; Prud'homme, R. K., Chemical processing and micromixing in confined impinging jets. *AIChE Journal* 2003, 49, 2264-2282.

35. Johnson, B. K.; Prud; homme, R. K., Flash NanoPrecipitation of Organic Actives and Block Copolymers using a Confined Impinging Jets Mixer. *Australian Journal of Chemistry* 2003, 56, 1021-1024.
36. Johnson, B. K.; Prud'homme, R. K., Mechanism for Rapid Self-Assembly of Block Copolymer Nanoparticles. *Physical Review Letters* 2003, 91, 118302.
37. Johnson, B. K., Prud'homme,R.K. Process and apparatuses for preparing nanoparticles compositions with amphiphilic copolymers and their use. 2004.
38. Liu, Y.; Fox, R. O., CFD predictions for chemical processing in a confined impinging-jets reactor. *AIChE Journal* 2006, 52, 731-744.
39. Liu, Y.; Cheng, C.; Prud'homme, R. K.; Fox, R. O., Mixing in a multi-inlet vortex mixer (MIVM) for flash nano-precipitation. *Chemical Engineering Science* 2008, 63, 2829-2842.
40. Han, J.; Zhu, Z.; Qian, H.; Wohl, A. R.; Beaman, C. J.; Hoye, T. R.; Macosko, C. W., A simple confined impingement jets mixer for flash nanoprecipitation. *J Pharm Sci* 2012, 101, 4018-23.
41. Kumar, V.; Hong, S. Y.; Maciag, A. E.; Saavedra, J. E.; Adamson, D. H.; Prud'homme, R. K.; Keefer, L. K.; Chakrapani, H., Stabilization of the Nitric Oxide (NO) Prodrugs and Anticancer Leads, PABA/NO and Double JS-K, through Incorporation into PEG-Protected Nanoparticles. *Molecular Pharmaceutics* 2009, 7, 291-298.
42. Budijono, S. J.; Shan, J.; Yao, N.; Miura, Y.; Hoye, T.; Austin, R. H.; Ju, Y.; Prud'homme, R. K., Synthesis of Stable Block-Copolymer-Protected NaYF4:Yb3+, Er3+ Up-Converting Phosphor Nanoparticles. *Chemistry of Materials* 2009, 22, 311-318.
43. Ungun, B.; Prud'homme, R. K.; Budijon, S. J.; Shan, J.; Lim, S. F.; Ju, Y.; Austin, R., Nanofabricated upconversion nanoparticles for photodynamic therapy. *Optics Express* 2009, 17, 80-86.
44. Gindy, M. E.; Panagiotopoulos, A. Z.; Prud'homme, R. K., Composite block copolymer stabilized nanoparticles: simultaneous encapsulation of organic actives and inorganic nanostructures. *Langmuir* 2008, 24, 83-90.
45. Shi, L.; Shan, J.; Ju, Y.; Aikens, P.; Prud'homme, R. K., Nanoparticles as delivery vehicles for sunscreen agents. *Colloids and Surfaces A: Physicochemical and Engineering Aspects* 2012, 396, 122-129.
46. Wani, M. C.; Taylor, H. L.; Wall, M. E.; Coggon, P.; McPhail, A. T., Plant antitumor agents. VI. Isolation and structure of taxol, a novel antileukemic and antitumor agent from Taxus brevifolia. *Journal of the American Chemical Society* 1971, 93, 2325-2327.
47. Zhang, J. A.; Anyarambhatla, G.; Ma, L.; Ugwu, S.; Xuan, T.; Sardone, T.; Ahmad, I., Development and characterization of a novel Cremophor® EL free liposome-based paclitaxel (LEP-ETU) formulation. *European Journal of Pharmaceutics and Biopharmaceutics* 2005, 59, 177-187.
48. Singla, A. K.; Garg, A.; Aggarwal, D., Paclitaxel and its formulations. *International Journal of Pharmaceutics* 2002, 235, 179-192.
49. Swindell, C. S.; Krauss, N. E.; Horwitz, S. B.; Ringel, I., Biologically active taxol analogs with deleted A-ring side chain substituents and variable C-2' configurations. *Journal of Medicinal Chemistry* 1991, 34, 1176-1184.

50. Tarr, B. D.; Yalkowsky, S. H., A new parenteral vehicle for the administration of some poorly water soluble anti-cancer drugs. *J Parenter Sci Technol* 1987, 41, 31-3.
51. Danhier, F.; Lecouturier, N.; Vroman, B.; Jérôme, C.; Marchand-Brynaert, J.; Feron, O.; Préat, V., Paclitaxel-loaded PEGylated PLGA-based nanoparticles: in vitro and in vivo evaluation. *J Control Release* 2009, 133, 11-7.
52. Weiss, R. B.; Donehower, R. C.; Wiernik, P. H.; Ohnuma, T.; Gralla, R. J.; Trump, D. L.; Baker, J. R., Jr.; Van Echo, D. A.; Von Hoff, D. D.; Leyland-Jones, B., Hypersensitivity reactions from taxol. *Journal of clinical oncology : official journal of the American Society of Clinical Oncology* 1990, 8, 1263-8.
53. BioScience, A. Abraxane (paclitaxel protein-bound particles for injectable suspension.
54. Administration, U. S. F. a. D., ABRAXANE^{TM} for Injectable Suspension (paclitaxel protein-bound particles for injectable suspension) (albumin-bound). 2005.
55. Gradishar, W. J.; Tjulandin, S.; Davidson, N.; Shaw, H.; Desai, N.; Bhar, P.; Hawkins, M.; O'Shaughnessy, J., Phase III trial of nanoparticle albumin-bound paclitaxel compared with polyethylated castor oil-based paclitaxel in women with breast cancer. *Journal of clinical oncology : official journal of the American Society of Clinical Oncology* 2005, 23, 7794-803.
56. Smith, J., Overview of breast cancer drug therapy. *US PHARMACIST* 2005, 30, 9.
57. Kim, H. J.; Kim, K. H.; Yun, J.; Kim, S. H.; Lee, S. C.; Bae, S. B.; Kim, C. K.; Lee, N. S.; Lee, K. T.; Kim, D. J.; Park, S. K.; Won, J. H.; Hong, D. S.; Park, H. S., Phase II Clinical Trial of Genexol® (Paclitaxel) and Carboplatin for Patients with Advanced Non-small Cell Lung Cancer. *Cancer Res Treat* 2011, 43, 19-23.
58. Squibb, B.-M., Taxol (Paclitaxel) Injection. 2007.
59. Wohl, A. R.; Michel, A. R.; Kalscheuer, S.; Macosko, C. W.; Panyam, J.; Hoye, T. R., Silicate Esters of Paclitaxel and Docetaxel: Synthesis, Hydrophobicity, Hydrolytic Stability, Cytotoxicity, and Prodrug Potential. *Journal of Medicinal Chemistry* 2014, 57, 2368-2379.
60. Wohl, A. R. Synthesis and Characterization of Silicate Esters Prodrugs and Poly(ethylene glycol)-b-poly(lactic-co-glycolic acid) Block Copolymers for Formulation into Prodrug-Loaded Nanoparticles. University of Minnesota-Twin Cities, 2012.
61. Lee, H. Structure and Dynamics in Self-Assembled Soft Materials. University of Minnesota-Twin Cities, 2014.
62. Ferrari, M., Cancer nanotechnology: opportunities and challenges. *Nat Rev Cancer* 2005, 5, 161-71.
63. Feng, S.-S.; Chien, S., Chemotherapeutic engineering: Application and further development of chemical engineering principles for chemotherapy of cancer and other diseases. *Chemical Engineering Science* 2003, 58, 4087-4114.
64. Faraji, A. H.; Wipf, P., Nanoparticles in cellular drug delivery. *Bioorg Med Chem* 2009, 17, 2950-62.
65. Horn, D.; Rieger, J., Organic Nanoparticles in the Aqueous Phase-Theory, Experiment, and Use. *Angew Chem Int Ed Engl* 2001, 40, 4330-4361.
66. Johnson, B. K., Prud'homme, R.K., Flash nanoprecipitation of organic actives and block copolymers using Confined Impinging Jets Mixer. *Aust J Chem* 2003, 56, 1021-1024.

67. Zhu, Z. Polymer stabilized nanosuspensions via flash nanoprecipitation: nanoparticle formation, formulation and stability. University of Minnesota, 2010.
68. Cheng, J. C.; Vigil, R. D.; Fox, R. O., A competitive aggregation model for flash nanoprecipitation. *J Colloid Interface Sci* 2010, 351, 330-42.
69. Gavi, E.; Marchisio, D. L.; Barresi, A. A., CFD modelling and scale-up of Confined Impinging Jet Reactors. *Chemical Engineering Science* 2007, 62, 2228-2241.
70. Akbulut, M.; Ginart, P.; Gindy, M. E.; Theriault, C.; Chin, K. H.; Soboyejo, W.; Prud'homme, R. K., Generic Method of Preparing Multifunctional Fluorescent Nanoparticles Using Flash NanoPrecipitation. *Advanced Functional Materials* 2009, 19, 718-725.
71. Lince, F.; Marchisio, D. L.; Barresi, A. A., Smart mixers and reactors for the production of pharmaceutical nanoparticles: Proof of concept. *Chemical Engineering Research and Design* 2009, 87, 543-549.
72. Daniele, L. M.; Liliana, R.; Antonello, A. B., Design and scale-up of chemical reactors for nanoparticle precipitation. *AIChE Journal* 2006, 52, 1877-1887.
73. Hunter, T. G.; Nash, A. W., Liquid-Liquid Extraction Systems. *Industrial & Engineering Chemistry* 1935, 27, 836-845.
74. R.E., T., Liquid extraction. 2nd ed.; McGraw-Hill: New York, 1963.
75. Lee, L. J., J. M. Ottino, W. E. Ranz, C. W. Macosko, Impingement Mixing in Reaction Injection Molding. *Polymer Engineering & Science* 1980, 20.
76. Macosko, C. W., RIM, fundamentals of reaction injection molding. *Hanser, New York* 1989.
77. Nguyen, L. T., N. P. Suh, Processing of Polyurethane/Polyester Interpenetrating Polymer Networks by Reaction Injection Molding: Part 2. Mixing at High Reynolds Numbers and Impingement Pressures. *Polymer Engineering & Science* 1986, 26, 799.
78. Gindy, M. E., Pnagiotopoulos, A. Z., Prud'homme, R. K., Composite Block Copolymer Stabilized Nanoparticle: Simultnaneous Encapsulation of Organic Actives and Inorganic Nanostructure. *Langmuir* 2008, 24, 83-90.
79. Liu, Y., Cheng, C., Liu, Y., Prud'homme, Y.K., Fox, R.O., Mixing in a multi-inlet vortex mixer (MIVM) for flash nano-precipitation. *Chemical Engineering Science* 2008, 63, 2829-2842.
80. D'addio, S. M. Flash Nanoprecipitation Video. http://www.princeton.edu/research/news/princetoninvention/video/index.xml.
81. Qian, H.; Wohl, A. R.; Crow, J. T.; Macosko, C. W.; Hoye, T. R., A Strategy for Control of "Random" Copolymerization of Lactide and Glycolide: Application to Synthesis of PEG-b-PLGA Block Polymers Having Narrow Dispersity. *Macromolecules* 2011, 44, 7132-7140.
82. Harvard Apparatus. http://www.harvardapparatus.com/.
83. Jakeš, J., Testing of the constrained regularization method of inverting Laplace transform on simulated very wide quasielastic light scattering autocorrelation functions. *Czech J Phys* 1988, 38, 1305-1316.
84. Jakes, J., Regularized positive exponential sum (REPES) program - A way ofinverting laplace transform data obtained by dynamic light scattering. *Collect. Czech. Chem. Commun* 1995, 60, 1781-1797.

85. Pustulka, K. M.; Wohl, A. R.; Lee, H. S.; Michel, A. R.; Han, J.; Hoye, T. R.; McCormick, A. V.; Panyam, J.; Macosko, C. W., Flash Nanoprecipitation: Particle Structure and Stability. *Molecular Pharmaceutics* 2013, 10, 4367-4377.
86. Pustulka, K. Polymer stabilized nanosuspension via flash nanoprecipitation: particle formulation, structure and freeze drying. University of Minnesota, 2012.
87. Mordi, R. C.; Walton, J. C.; Burton, G. W.; Hughes, L.; Keith, I. U.; David, L. A.; Douglas, M. J., Oxidative degradation of β-carotene and β-apo-8′-carotenal. *Tetrahedron* 1993, 49, 911-928.
88. Chow S., S. C., Macosko C.W., Chow A., Comparative assessment of the performance between confined impingement jets and multi-inlet vortex mixers for controlled production of curcumin nanoparticles. In *American Association of Pharmaceutical Scientists*, McCormick Place, Chicago, Illinois, 2011.
89. Cheng, K.; Yeung, C.; Ho, S.; Chow, S.; Chow, A. L.; Baum, L., Highly Stabilized Curcumin Nanoparticles Tested in an In Vitro Blood–Brain Barrier Model and in Alzheimer's Disease Tg2576 Mice. *The AAPS Journal* 2013, 15, 324-336.
90. Chow, A. H. L.; Chow, S. F.; Zhang, X. R.; Wan, K. Y.; Cheng, K. K.; Baum, L. W., Engineering of polymer-stabilized nanoparticles for drugs with log p values below 6 by controlled antisolvent precipitation. Google Patents: 2013.
91. Chow, S. F.; Sun, C. C.; Chow, A. H. L., Assessment of the relative performance of a confined impinging jets mixer and a multi-inlet vortex mixer for curcumin nanoparticle production. *European Journal of Pharmaceutics and Biopharmaceutics*.
92. Zhu, Z., Flash Nanoprecipitation: Prediction and Enhancement of Particle Stability via Drug Structure. *Molecular Pharmaceutics* 2014, 11, 776-786.
93. Wani, M. C.; Taylor, H. L.; Wall, M. E.; Coggon, P.; McPhail, A. T., Plant antitumor agents. VI. The isolation and structure of taxol, a novel antileukemic and antitumor agent from Taxus brevifolia. *J Am Chem Soc* 1971, 93, 2325-7.
94. Pinkel, D., The use of body surface area as a criterion of drug dosage in cancer chemotherapy. *Cancer research* 1958, 18, 853-6.
95. Co., S. G. Genexol. http://www.trademarkia.com/genexol-75071685.html.
96. Kim, S. C.; Kim, D. W.; Shim, Y. H.; Bang, J. S.; Oh, H. S.; Wan Kim, S.; Seo, M. H., In vivo evaluation of polymeric micellar paclitaxel formulation: toxicity and efficacy. *J Control Release* 2001, 72, 191-202.
97. Oerlemans, C.; Bult, W.; Bos, M.; Storm, G.; Nijsen, J. F.; Hennink, W. E., Polymeric micelles in anticancer therapy: targeting, imaging and triggered release. *Pharmaceutical research* 2010, 27, 2569-89.
98. Desai, N., *Nab Technology: a drug delivery platform utilising endothelial gp60 receptor-based transport and tumour derived SPARC for targeting*. 16th ed.; Drug Delivery Report: 2007/2008.
99. Chaubal, M., Polylactides/glycolides-excipients for injectable drug delivery & beyond. Drug Delivery Technology: 2002; Vol. 2, pp 34-36.
100. Sheftel, V. O., *Indirect Food Additives and Polymers: Migration and Toxicology*. 2000.
101. Joshi, B. K. P. a. M. S., The effect of supersaturation on the induction period of potassium dihydrogen phosphate crystals grown from aqueous solution. *Journal of Physics D: Applied Physics* 1976, 9, 1253.

102. Riley, T.; Heald, C. R.; Stolnik, S.; Garnett, M. C.; Illum, L.; Davis, S. S.; King, S. M.; Heenan, R. K.; Purkiss, S. C.; Barlow, R. J.; Gellert, P. R.; Washington, C., Core−Shell Structure of PLA−PEG Nanoparticles Used for Drug Delivery. *Langmuir* 2003, 19, 8428-8435.
103. Haag, R.; Kratz, F., Polymer therapeutics: concepts and applications. *Angew Chem Int Ed Engl* 2006, 45, 1198-215.
104. Kong, G.; Braun, R. D.; Dewhirst, M. W., Hyperthermia enables tumor-specific nanoparticle delivery: effect of particle size. *Cancer research* 2000, 60, 4440-5.
105. Gabizon, A.; Goren, D.; Horowitz, A. T.; Tzemach, D.; Lossos, A.; Siegal, T., Long-circulating liposomes for drug delivery in cancer therapy: a review of biodistribution studies in tumor-bearing animals. *Advanced Drug Delivery Reviews* 1997, 24, 337-344.
106. Goldberg, M.; Langer, R.; Jia, X., Nanostructured materials for applications in drug delivery and tissue engineering. *Journal of biomaterials science. Polymer edition* 2007, 18, 241-68.
107. Staples, M.; Daniel, K.; Cima, M. J.; Langer, R., Application of micro- and nano-electromechanical devices to drug delivery. *Pharmaceutical research* 2006, 23, 847-63.
108. Ratke, L.; Voorhees, P. W., *Growth and Coarsening: Otswald Ripening in Materials Processing*. New York, 2002.
109. Hoye, T. R.; WOHL, A.; Macosko, C. W.; Panyam, J., Silicate prodrugs and nanoparticles. Google Patents: 2012.
110. Wu, K.-M., A new classification of prodrugs: regulatory perspectives. *Pharmaceuticals* 2009, 2, 5.
111. Macosko, C. W.; Hoye, T. R.; Panyam, J., Beyond Taxol®: Nanoparticle Delivery of a Paclitaxel Silicate Prodrug. Minnesota Future Grant: 2009.
112. Wohl, A. R.; Michel, A. R.; Kalscheuer, S.; Macosko, C. W.; Panyam, J.; Hoye, T. R., Silicate esters of paclitaxel and docetaxel: synthesis, hydrophobicity, hydrolytic stability, cytotoxicity, and prodrug potential. *Journal of Medicinal Chemistry*.
113. De Jaeghere, F.; Allémann, E.; Feijen, J.; Kissel, T.; Doelker, E.; Gurny, R., Freeze-Drying and Lyopreservation of Diblock and Triblock Poly(Lactic Acid)–Poly(Ethylene Oxide) (PLA–PEO) Copolymer Nanoparticles. *Pharmaceutical Development and Technology* 2000, 5, 473-483.
114. Franks, F., Freeze-drying of bioproducts: putting principles into practice. *Eur J Pharm Biopharm* 1998, 45, 221-9.
115. Chacon, M.; Molpeceres, J.; Berges, L.; Guzman, M.; Aberturas, M. R., Stability and freeze-drying of cyclosporine loaded poly(D,L lactide-glycolide) carriers. *Eur J Pharm Sci* 1999, 8, 99-107.
116. Abdelwahed, W.; Degobert, G.; Fessi, H., Investigation of nanocapsules stabilization by amorphous excipients during freeze-drying and storage. *Eur J Pharm Biopharm* 2006, 63, 87-94.
117. Layre, A. M.; Couvreur, P.; Richard, J.; Requier, D.; Eddine Ghermani, N.; Gref, R., Freeze-drying of composite core-shell nanoparticles. *Drug Dev Ind Pharm* 2006, 32, 839-46.
118. vcclab ALOPS 2.1.

119. Turner, C. W.; Franklin, K. J., Studies of the hydrolysis and condensation of tetraethylorthosilicate by multinuclear (1h, 17o, 29si) nmr spectroscopy. *Journal of Non-Crystalline Solids* 1987, 91, 402-415.
120. Spectrum Labs. http://www.spectrumlabs.com/filtration/.
121. Di Carlo, D.; Edd, J. F.; Humphry, K. J.; Stone, H. A.; Toner, M., Particle segregation and dynamics in confined flows. *Phys Rev Lett* 2009, 102, 094503.
122. D'Addio, S. M.; Kafka, C.; Akbulut, M.; Beattie, P.; Saad, W.; Herrera, M.; Kennedy, M. T.; Prud'homme, R. K., Novel method for concentrating and drying polymeric nanoparticles: hydrogen bonding coacervate precipitation. *Mol Pharm* 2010, 7, 557-64.
123. Floyd, A. G., Top ten considerations in the development of parenteral emulsions. *Pharmaceutical Science & Technology Today* 1999, 2, 134-143.
124. Oh, K. S.; Song, J. Y.; Cho, S. H.; Lee, B. S.; Kim, S. Y.; Kim, K.; Jeon, H.; Kwon, I. C.; Yuk, S. H., Paclitaxel-loaded Pluronic nanoparticles formed by a temperature-induced phase transition for cancer therapy. *Journal of Controlled Release* 2010, 148, 344-350.
125. D'Souza, S. S.; DeLuca, P. P., Methods to assess in vitro drug release from injectable polymeric particulate systems. *Pharm Res* 2006, 23, 460-74.
126. Abdel-Mottaleb, M. M.; Lamprecht, A., Standardized in vitro drug release test for colloidal drug carriers using modified USP dissolution apparatus I. *Drug development and industrial pharmacy* 2011, 37, 178-84.
127. Washington, C., Drug release from microdisperse systems: a critical review. *International Journal of Pharmaceutics* 1990, 58, 1-12.
128. Mu, L.; Feng, S. S., Fabrication, characterization and in vitro release of paclitaxel (Taxol®) loaded poly (lactic-co-glycolic acid) microspheres prepared by spray drying technique with lipid/cholesterol emulsifiers. *Journal of Controlled Release* 2001, 76, 239-254.
129. Kolishetti, N.; Dhar, S.; Valencia, P. M.; Lin, L. Q.; Karnik, R.; Lippard, S. J.; Langer, R.; Farokhzad, O. C., Engineering of self-assembled nanoparticle platform for precisely controlled combination drug therapy. *Proc Natl Acad Sci U S A* 2010, 107, 17939-44.
130. Gu, F.; Zhang, L.; Teply, B. A.; Mann, N.; Wang, A.; Radovic-Moreno, A. F.; Langer, R.; Farokhzad, O. C., Precise engineering of targeted nanoparticles by using self-assembled biointegrated block copolymers. *Proc Natl Acad Sci U S A* 2008, 105, 2586-91.
131. Zhang, J. A.; Anyarambhatla, G.; Ma, L.; Ugwu, S.; Xuan, T.; Sardone, T.; Ahmad, I., Development and characterization of a novel Cremophor EL free liposome-based paclitaxel (LEP-ETU) formulation. *European journal of pharmaceutics and biopharmaceutics : official journal of Arbeitsgemeinschaft fur Pharmazeutische Verfahrenstechnik e.V* 2005, 59, 177-87.
132. Avgoustakis, K.; Beletsi, A.; Panagi, Z.; Klepetsanis, P.; Karydas, A. G.; Ithakissios, D. S., PLGA-mPEG nanoparticles of cisplatin: in vitro nanoparticle degradation, in vitro drug release and in vivo drug residence in blood properties. *J Control Release* 2002, 79, 123-35.
133. Zolnik, B. S.; Burgess, D. J., Effect of acidic pH on PLGA microsphere degradation and release. *J Control Release* 2007, 122, 338-44.

134. Houchin, M. L.; Topp, E. M., Physical properties of PLGA films during polymer degradation. *Journal of Applied Polymer Science* 2009, 114, 2848-2854.
135. Mohammad, A. K.; Reineke, J. J., Quantitative Detection of PLGA Nanoparticle Degradation in Tissues following Intravenous Administration. *Molecular Pharmaceutics* 2013, 10, 2183-2189.
136. Garcia, J. T.; Farina, J. B.; Munguia, O.; Llabres, M., Comparative degradation study of biodegradable microspheres of poly(DL-lactide-co-glycolide) with poly(ethyleneglycol) derivates. *J Microencapsul* 1999, 16, 83-94.
137. Iwamoto, S.-i.; Kawasaki, T.; Kambayashi, J.-i.; Ariyoshi, H.; Monden, M., Platelet Microparticles: A Carrier of Platelet-Activating Factor? *Biochemical and Biophysical Research Communications* 1996, 218, 940-944.
138. Hamel, E.; Lin, C. M., Separation of active tubulin and microtubule-associated proteins by ultracentrifugation and isolation of a component causing the formation of microtubule bundles. *Biochemistry* 1984, 23, 4173-4184.
139. Emilienne Soma, C.; Dubernet, C.; Bentolila, D.; Benita, S.; Couvreur, P., Reversion of multidrug resistance by co-encapsulation of doxorubicin and cyclosporin A in polyalkylcyanoacrylate nanoparticles. *Biomaterials* 2000, 21, 1-7.
140. Avgoustakis, K., Pegylated poly(lactide) and poly(lactide-co-glycolide) nanoparticles: preparation, properties and possible applications in drug delivery. *Curr Drug Deliv* 2004, 1, 321-33.
141. Prabha, S.; Zhou, W. Z.; Panyam, J.; Labhasetwar, V., Size-dependency of nanoparticle-mediated gene transfection: studies with fractionated nanoparticles. *Int J Pharm* 2002, 244, 105-15.
142. Chan, J. M.; Zhang, L.; Yuet, K. P.; Liao, G.; Rhee, J.-W.; Langer, R.; Farokhzad, O. C., PLGA–lecithin–PEG core–shell nanoparticles for controlled drug delivery. *Biomaterials* 2009, 30, 1627-1634.
143. Hu, Y.; Xie, J.; Tong, Y. W.; Wang, C. H., Effect of PEG conformation and particle size on the cellular uptake efficiency of nanoparticles with the HepG2 cells. *J Control Release* 2007, 118, 7-17.
144. Gaumet, M.; Gurny, R.; Delie, F., Fluorescent biodegradable PLGA particles with narrow size distributions: preparation by means of selective centrifugation. *Int J Pharm* 2007, 342, 222-30.
145. De Jaeghere, F.; Allémann, E.; Feijen, J.; Kissel, T.; Doelker, E.; Gurny, R., Freeze-drying and lyopreservation of diblock and triblock poly(lactic acid)-poly(ethylene oxide) (PLA-PEO) copolymer nanoparticles. *Pharm Dev Technol* 2000, 5, 473-83.
146. Abdelwahed, W.; Degobert, G.; Stainmesse, S.; Fessi, H., Freeze-drying of nanoparticles: formulation, process and storage considerations. *Adv Drug Deliv Rev* 2006, 58, 1688-713.
147. Liu, Y.; Tong, Z.; Prud'homme, R. K., Stabilized polymeric nanoparticles for controlled and efficient release of bifenthrin. *Pest Manag Sci* 2008, 64, 808-12.
148. Filipe, V.; Hawe, A.; Jiskoot, W., Critical evaluation of Nanoparticle Tracking Analysis (NTA) by NanoSight for the measurement of nanoparticles and protein aggregates. *Pharm Res* 2010, 27, 796-810.
149. Hienmenz, P. C.; Lodge, T. P., *Polymer Chemistry*. 2nd ed.; Taylor & Francis Group: CRC Press, 2007.

Appendix A: β-carotene loaded PEG-*b*-PLA Nanoparticles Preparation via Vortex and CIJ-D Mixer

First, empty PEG-*b*-PLA nanoparticles, without β-carotene were prepared with both CIJ-D and vortex mixer. As MW of PLA increased from 2k to 15 kDa, there was barely any difference in size (30~35 nm) via the CIJ mixing (Figure A.1(a)). It seems that the CIJ mixer is more efficient to make small nanoparticles, when MW of PEG-*b*-PLA is larger. The vortex mixer functions equally well in terms of producing small polymer nanoparticles, but exhibiting a linear relation of nanoparticle size vs. MW of PLA. In contrast, the sizes of nanoparticles prepared via CIJ-D mixing were affected only by the mixing process.

Second, when PEG-*b*-PLA nanoparticles were loaded with β-carotene, nanoparticle sizes were generally larger than those without β-carotene (Figure A.1(b)). By vortex mixing, β-carotene loaded nanoparticles were unexpectedly smallest when the MW of PEG-*b*-PLA was 5k-10kDa. Below MW of PLA=10kDa, nanoparticle sizes decreased with longer PLA, probably because β-carotene and hydrophobic PLA interacted more strongly. They constructed tighter and smaller nanoparticle cores within where PLA chains were more entrapped. Above 10kDa, nanoparticle sizes climbed presumably because it's now dominant for long PLA chain to stretch, rather than being entrapped in the cores. However, it's uncertain if this increase indicated by only one point is reliable.

Third, nanoparticles in saline solution were slightly larger than those in non-saline solution, via both vortex and CIJ mixing. This is because that the addition of 1 wt% of NaCl destroyed electrostatic stabilization of nanoparticles, but nanoparticles were still

protected by steric stabilization from BCPs. Nanoparticle sizes were reproducible within the three batches.

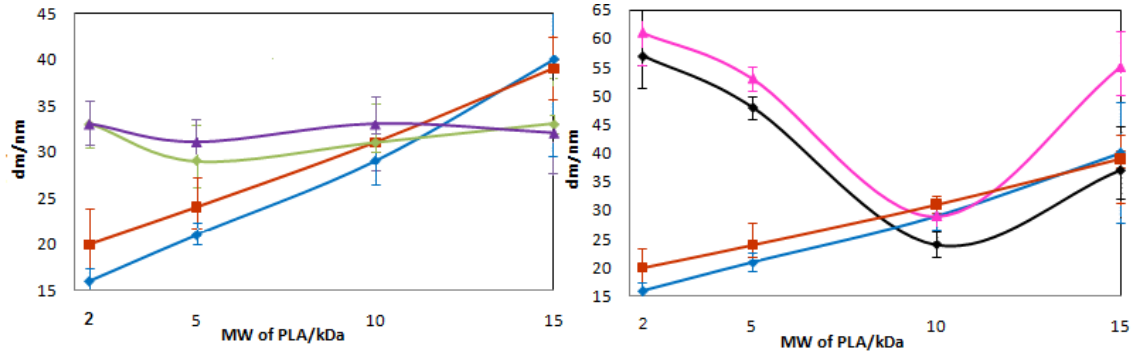

Figure A.1 (a) PEG-*b*-PLA (polymer-only) NPs.
—in nonsaline solution via vortex mixer
—in saline solution via vortex mixer
—in nonsaline solution via CIJ mixer
—in saline solution via CIJ mixer

(b) PEG-*b*-PLA NPs made via vortex mix.
—without *β*-carotene in nonsaline solution
—without *β*-carotene in saline solution
—with *β*-carotene in nonsaline solution
—with β-carotene in saline solution

The summary of nanoparticle sizes for Figure A.1 is listed in Table A.1. Figure A.2-5 show the mass and intensity average sizes of empty PEG-b-PLA (with varied MW) nanoparticle analyzed by DLS (Brookhaven Instrument, CA) and REPES method

Table A.1 PEG-*b*-PLA protected *β-carotene* nanoparticle size by the CIJ-D and vortex mixer.

PLA-*b*-PEG	β-carotene	NaCl 1wt%							
		w/o				w/			
		Vortex Mixer		CIJ mixer		Vortex Mixer		CIJ mixer	
		d/nm	*σ/nm*	*d/nm*	*σ/nm*	*d/nm*	*σ/nm*	*d/nm*	*σ/nm*
2k-*b*-5k	w/o	16/16/0.02	±2	33/42/0.20	±3	20/65/1.12	±5	33/48/0.35	±4
	w/	57/194/3.51	±8	-	-	61/191/3.67	±6	-	-
5k-*b*-5k	w/o	21/23/0.77	±2	29/86/0.56	±3	24/38/0.46	±3	31/58/1.31	±5
	w/	48/112/2.37	±2	-	-	53/288/4.24	±2	-	-
10k-*b*-5k	w/o	29/88/1.19	±4	31/100/1.13	±4	31/102/1.16	±2	33/91/0.69	±8
	w/	24/42/0.62	±3	27/106/1.24	±2	29/53/0.88	±3	49/209/1.37	±6
15k-*b*-5k	w/o	40/109/1.09	±10	33/51/0.17	±7	39/253/4.05	±4	32/82/0.22	±6
	w/	37/62/0.62	±6	-	-	55/63/0.27	±7	-	-

Note: Data d is shown as mass average size/intensity average size/span.
σ is the standard deviation of the mean mass average size.

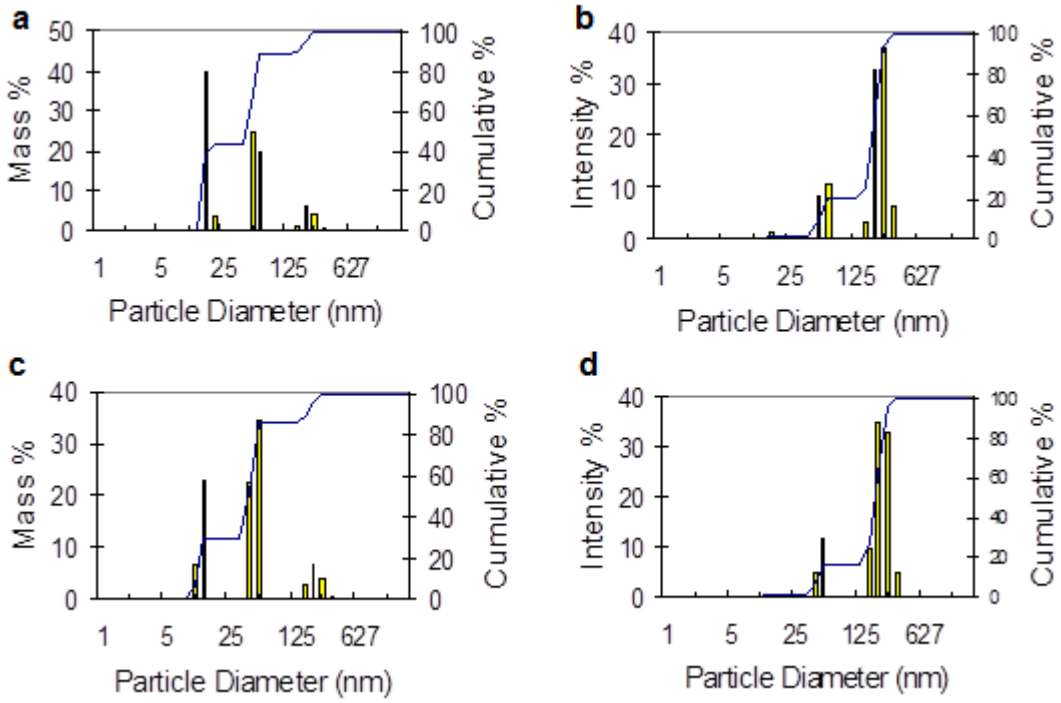

Figure A.2 Mass average size and intensity average size of PEG-*b*-PLA (MW: 5k-2kDa) only nanoparticles without saline (a) & (b) and with saline solution (c) and (d).

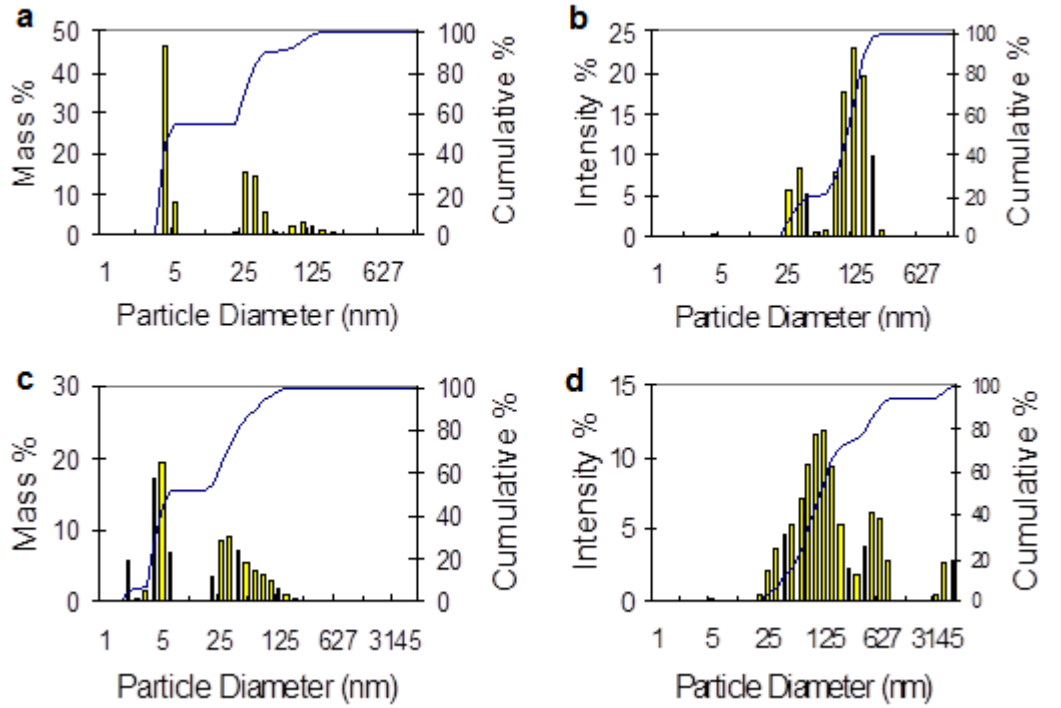

Figure A.3 Mass average size and intensity average size of PEG-*b*-PLA (MW: 5k-5kDa) only nanoparticles without saline (a) & (b) and with saline solution (c) and (d).

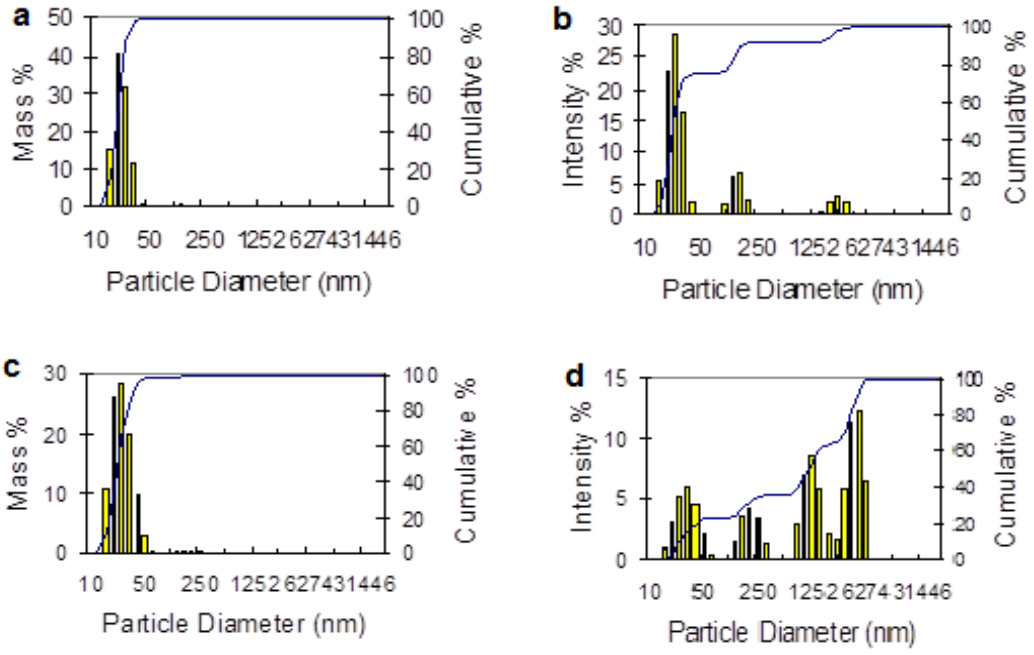

Figure A.4 Mass average size and intensity average size of PEG-*b*-PLA (MW: 5k-10kDa) only nanoparticles without saline (a) & (b) and with saline solution (c) and (d).

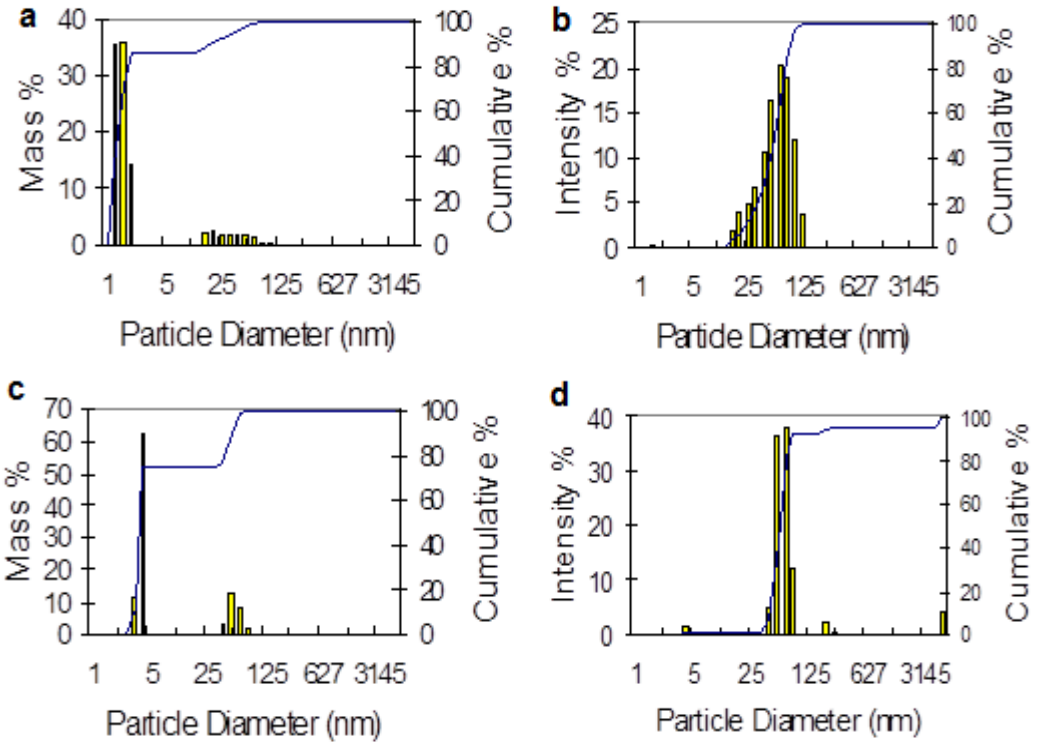

Figure A.5 Mass average size and intensity average size of PEG-*b*-PLA (MW: 5k-15kDa) only nanoparticles without saline (a) & (b) and with saline solution (c) and (d).

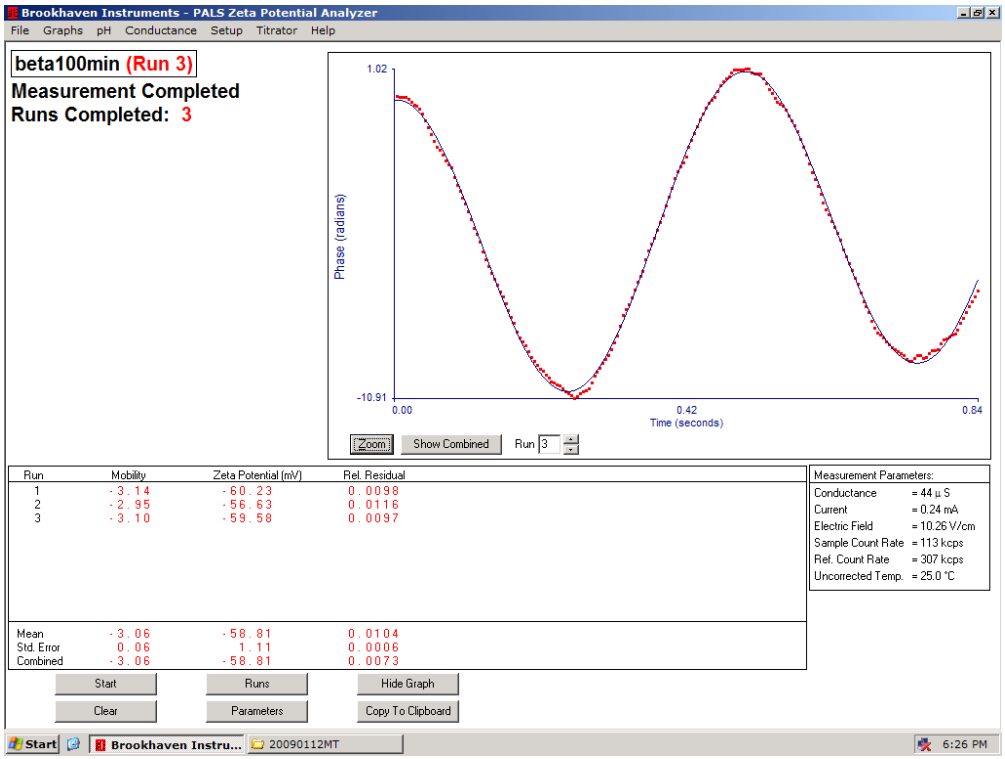

Figure A.6 An example of zeta pontential measurement of β-carotene only nanoparticles

Table A.2 Pure β-carotene nanoparticle size at varied time and saline/non-saline solution.

	d_m/nm	d_I/nm
Pure β-carotene (10min after mixing)	47	182
Pure β-carotene (60min after mixing)	40	172
β-carotene+chitosan (without salt)	43	202
β-carotene+chitosan (with salt)	47	330

Since we have found bimodal distribution of block copolymer protected drug loaded nanoparticles, we suspected the small portion of nanoparticles with very small size was block copolymer nanoparticles or micelles. To determine whether it is kinetically formed nanoparticles or micelles at thermodynamic equilibrium state, PEG-*b*-

PLGA micelles were prepared by dissolving 6 mg of PEG-*b*-PLGA (MW: 5k-10kDa) with 1ml acetone, adding 9ml H_2O in constant flow rate during 20 hours while stirring the solution in the whole process. The sizes were measured by DLS (Brookhaven, CA).

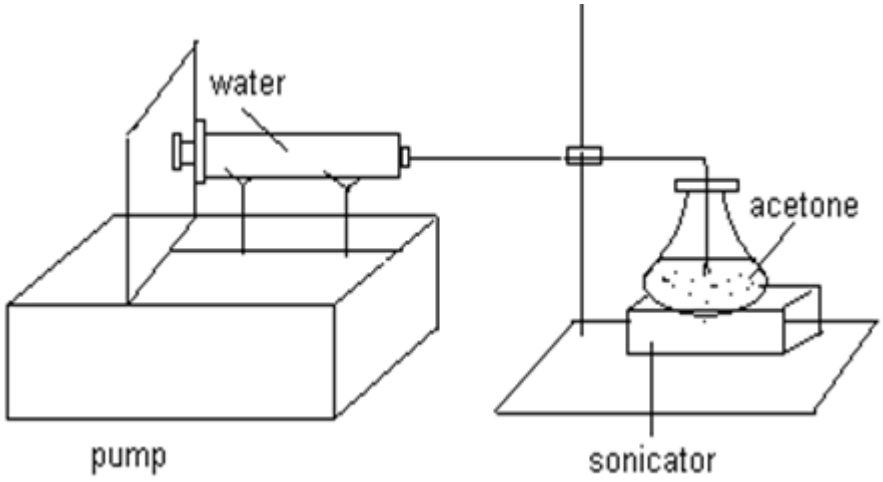

Figure A.7 Schematic of diblock copolymer micelle formation experiment.

Table A.3 Sizes of diblock copolymer micelles at varied time.

time	sample	d_m/nm	d_I/nm
1st day	PEG5K-PLGA10K	16/8.3	443/543.0/1.2
2nd day	PEG5K-PLGA10K	21/8.0	648/598.8/1.2
After 1 week	PEG5K-PLGA10K	26/7.1	647/607.3/1.2
	PEG5K-PLGA10K	27	385
	PEG5K-PLA10K	22	94

Mass average size d_m is shown as Mass size/Mass PDI;
Intensity average size d_I is shown as Size from Repes method/Size from DLS machine/Size PDI from Repes.
Shaded area is Zhengxi &Haitao's data.

To test nanoparticle stability, PEG-b-PLA nanoparticles in both saline and aqueous solution were measured by DLS over time up to one week. They were very stable in both cases, without significant particle increase or aggregation.

Table A.4 Sizes of PEG-*b*-PLA nanoparticles at varied time.

	time	w/o NaCl		w NaCl 1wt%	
		d_m/nm	d_I/nm	d_m/nm	d_I/nm
PEG5K PLA5K	0.5hr	23/1.8	138/150.2/2.4	28/2.2	191/113.4/2.5
	1hr	25/2.1	180/201.3/5.3	29/2.1	159/135.4/1.7
	48hr	25/1.9	148/118.6/1.6	27/1.9	297/146.6/7.3
	1 week	28/1.7	98/58.3/1.5	33/1.5	78/62.9/1.4

Mass average size d_m is shown as Mass size/Mass PDI;
Intensity average size d_I is shown as Size from Repes method/Size from DLS machine/Size PDI from Repes.

Appendix B: Reynolds Number Calculation

Reynolds number is defined as below:

$$\mathrm{Re} = \frac{\text{inertial force}(=\rho V^2)}{\text{viscous force}\ (=\frac{\mu V}{L})} = \frac{\rho V L}{\mu}$$

In our case, $L = D$

$$S = \pi(\frac{D}{2})^2 \quad \text{or} \quad S = W \cdot H$$

$$Re = \sum_{i=1}^{n} Re_i = \frac{\rho D}{S} \sum_{i=1}^{n} \frac{Q_i}{\eta_i}$$

$$Re = \sum_{i=1}^{n} Re_i = \frac{4\rho}{\pi D} \sum_{i=1}^{n} \frac{Q_i}{\eta_i}$$

D is stream inlet diameter, W is the width of cross-sectional area, H is the height of cross-sectional area, or S is the cross-sectional area of inlet pathway. Calculation is separated for round and rectangular cross-section. ρ is the density of mixture, Q_i is the flow rate of *ith* stream, η_i is the viscosity of *ith* stream. Reynolds number is calculated as the summation of different stream components.

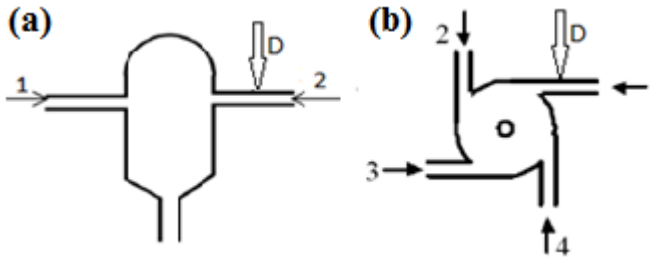

Figure B.1 Interior structures of (a) the CIJ mixer and (b) the vortex mixer.

Calculation examples are shown below:

1. In CIJ mixing

Via equation (S5), n=2, Q_1=Q_2=solution volume/mixing time=$2.5\times10^{-6}$$m^3$/mixing time, ρ_1=1.0×10^3 kg·m^{-3}(H_2O), ρ_2=8.89×10^2 kg·m^{-3}(THF), η_1= 1.0×10^{-3} Pa·s, η_2=4.8×10^{-4} Pa·s, D=5×10^{-4}m.

At mixing time= 4.23 s, Q_1=Q_2=2.5×10^{-6} m^3/4.23s=5.91×10^{-7} m^3/s

$Re= (4/\pi D) \times\Sigma(\rho Q/ \eta)_{n=2}$ = [4/($\pi\times5\times10^{-4}$ m)] ×[(1.0×10^3 kg·m-$^3\times5.91\times10^{-7}$ m^3/s)/ 1.0×10^{-3} Pa·s +(8.89×10^2 kg·$m^{-3}\times5.91\times10^{-7}$ m^3/s)/ 4.8×10^{-4} Pa·s]

Re= 4292

2. In vortex mixing

Via equation (S5), n=4, Q_1=Q_2=solution volume/mixing time=2.5×10^{-6} m^3/mixing time, Q_3=Q_4= solvent volume/mixing time=22.5×10^{-6} m^3/mixing time, ρmixture=1.0×10^3 kg·m^{-3}(≈ρ_{water}), η= 1.0×10^{-3} Pa·s, D=1.45×10^{-3} m.

At mixing time= 25.05s, Q_1=Q_2=2.5×10^{-6} m^3/25.05s=9.98×10^{-8} m^3/s, Q_3=Q_4=22.5×10^{-6} m^3/25.05s=8.98×10^{-7} m^3/s

$Re= (4\rho/\pi D\eta) \times\Sigma(Q)_{n=4}$ = [$4\times1.0\times10^3$ kg·m^{-3}/($\pi\times1.45\times10^{-3}$ m× 1.0×10^{-3} Pa·s)] ×($2\times9.98\times10^{-8}$ m^3/s +$2\times8.98\times10^{-7}$ m^3/s)

Re= 1753

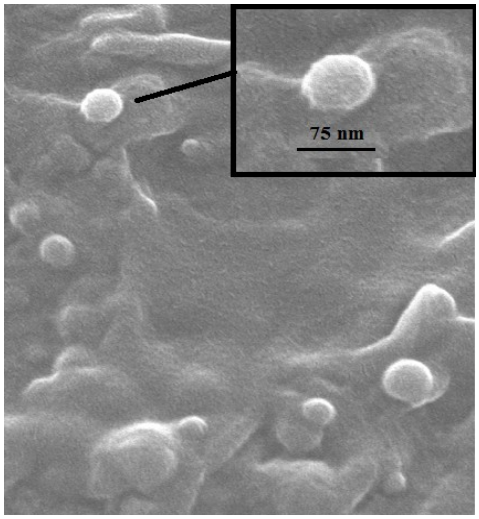

Figure B.2 SEM image of *β*-carotene NPs made by the vortex mixer at *Re*=1753.

Table B.1 Reynolds number (*Re*) vs. Mass average size (d_m) via the vortex mixer

t_{mix}/s	Q_{THF}/ m^3/s	Q_{water}/ m^3/s	Re	$d_m \pm \sigma$ /nm
25.05	9.98×10^{-8}	8.98×10^{-7}	1753	67±5
45.19	5.53×10^{-8}	4.98×10^{-7}	972	72±7
60.00	4.17×10^{-8}	3.75×10^{-7}	744	90±5
143.08	1.75×10^{-8}	1.57×10^{-7}	307	98±12
287.10	8.71×10^{-9}	7.84×10^{-8}	153	103±8
570.48	4.38×10^{-9}	3.94×10^{-8}	77	126±10
1156.00	2.16×10^{-9}	1.95×10^{-8}	38	257±23

Table B.2 Reynolds number (Re) vs. Mass average size (dm) via the CIJ-D mixer

t_{mix}/s	Q/ m^3/s	Re	dm±σ /nm	tmix/s	Q/ m^3/s	Re	dm±σ /nm
7.62	3.28×10^{-7}	2393	48±4	28.76	8.69×10^{-8}	643	84±17
7.92	3.15×10^{-7}	2302	57±9	39.58	6.32×10^{-8}	461	74±5
10.50	2.38×10^{-7}	1737	56±9	56.71	4.41×10^{-8}	321	102±7
12.50	2.00×10^{-7}	1459	49±10	125.00	2.00×10^{-8}	145	97±8
20.48	1.22×10^{-7}	890	58±15	180.00	1.39×10^{-8}	101	128±7
22.91	1.09×10^{-7}	796	55±8	258.86	9.66×10^{-9}	70	137±3

Appendix C: Nanoparticle Post-treatment: Ultracentrifugation, Sonication and Lyophilization

In order to purify nanoparticles, two types of nanoparticles were filtered by 450 nm filters, and the particle sizes were measured before and after filtration. There was no clear size difference between these two conditions shown in Table C.1, which indicated that simple filter filtration is not able to filter nanoparticles by size.

Table C.1 Nanoparticle sizes before and after 450 nm membrane filtration.

NPs	dl/nm(before filtration)	dl/nm (after filtration)
2'-triethyl Si PTX (1a)	115 nm	120 nm
2'-tri isopropyl Si PTX (1c)	136 nm	138 nm

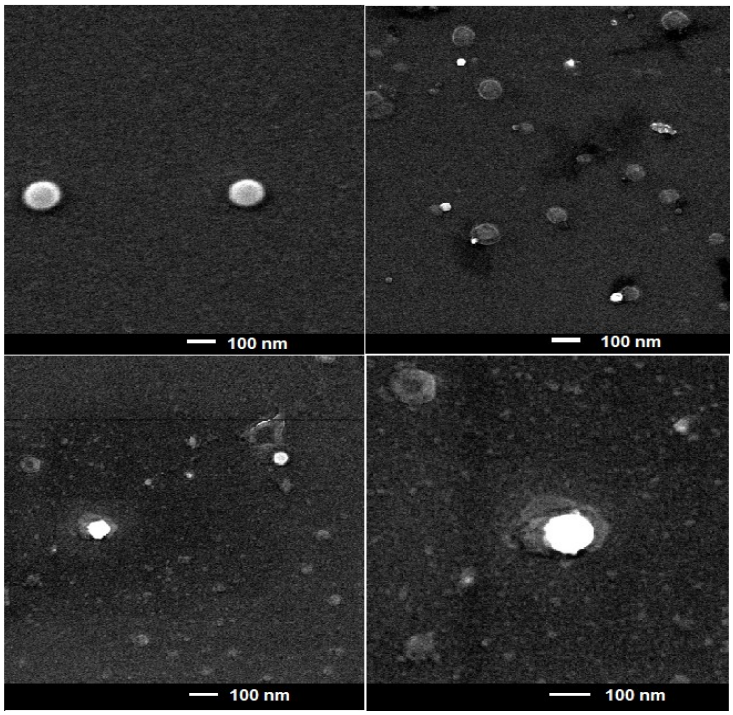

Figure C.1 SEM images of 2',7-tri-ethyl Si PTX (2a) NPs after lyophilization and membrane filtration.

After the filtered nanoparticles were lyophilized, they were redispersed and imaged by SEM. Figure C.1 showed that there were many small nanoparticles in the range of 20-50 nm and bigger ones ≥100 nm despite the filtration. It also indicated that filter filtration failed to differentiate particles by size.

When nanoparticles were ultrancentrifuged, nanoparticle sizes were measured from supernatants and pellets collected in the end, and the loading of each samples were determined by HPLC.

Table C.2 Physical properties of 2'-triethyl Si PTX(1a) NPs during ultracentrifugation.

	d_I(nm)	PDI	NP:drug mass(mg)	Loading%
Fresh	109	0.100	36.7/20.0	54.5
Supernatant 1	44	0.260	9.7/5.1	52.6
Supernatant 2	48	0.340	2.42/1.0	41.3
Supernatant 3	40	0.440	1.08/0	0
Pellet	195	0.260	15.7/9.9	63.0

d_I: intensity average size of nanoparticles measured by DLS.
PDI: polydispersity of size.

Table C.3 Physical properties of 2'-trioctyl Si PTX(1b) NPs during ultracentrifugation.

	d_I(nm)	PDI	NP:drug mass(mg)	Loading%
Fresh	75	0.165	24.5/13.5	55.3
Supernatant 1	73	0.195	10.8/4.3	39.8
Supernatant 2	80	0.271	5.6/2.1	37.5
Supernatant 3	66	0.102	3.2/1.1	34.4
Pellet	83	0.084	3.9/2.5	65.0

d_I: intensity average size of nanoparticles measured by DLS.
PDI: polydispersity of size.

Table C.4 Physical properties of 2'-triisopropyl Si PTX(1c) NPs during ultracentrifugation.

	d_I(nm)	PDI	NP:drug mass(mg)	Loading%
Fresh	136	0.084	60.0/30.0	50.0
Supernatant 1	80	0.229	16.2/6.9	43.0
Supernatant 2	138	0.221	14.6/3.5	24.1
Supernatant 3	272	0.136	1.1/0	0
Pellet	113	0.129	26.4/11.9	58.0

d_I: intensity average size of nanoparticles measured by DLS.
PDI: polydispersity of size.

Table C.5 Physical properties of 2'-ditert butyl/ethyl Si PTX(1d) NPs during ultracentrifugation.

	d_I(nm)	PDI	NP:drug mass(mg)	Loading%
Fresh	83	0.071	35.5/19.7	55.5
Supernatant 1	80	0.159	10.7/2.6	24.1
Supernatant 2	110	0.130	8.6/2.6	30.0
Supernatant 3	150	0.173	0/0	n/a
Pellet	220	0.202	16.3/11.9	73.5

d_I: intensity average size of nanoparticles measured by DLS.
PDI: polydispersity of size.

Table C.6 Physical properties of 2'-trimenthyl Si PTX(1e) NPs during ultracentrifugation.

	d_I(nm)	PDI	NP:drug mass(mg)	Loading%
Fresh	90	0.080	62.9/38.3	60.9
Supernatant 1	54	0.221	13.2/7.0	53.8
Supernatant 2	58	0.281	7.8/4.0	51.2
Supernatant 3	59	0.270	5.63/2.9	52.3
Pellet	130	0.172	28.8/21.2	73.5

d_I: intensity average size of nanoparticles measured by DLS.
PDI: polydispersity of size.

Not only does ultracentrifugation has a significant influence on nanoparticle size and loading, but also in vitro drug release profiles. The ultracentrifuged nanoparticles release slower than those have not been ultracentrifuged ones in short term. For example, 2'-triisopropyl Si PTX (1c) and 2'-trimenthyl Si PTX nanoparticles release in PBS at pH=7.4 in Figure C.2 and C.3.

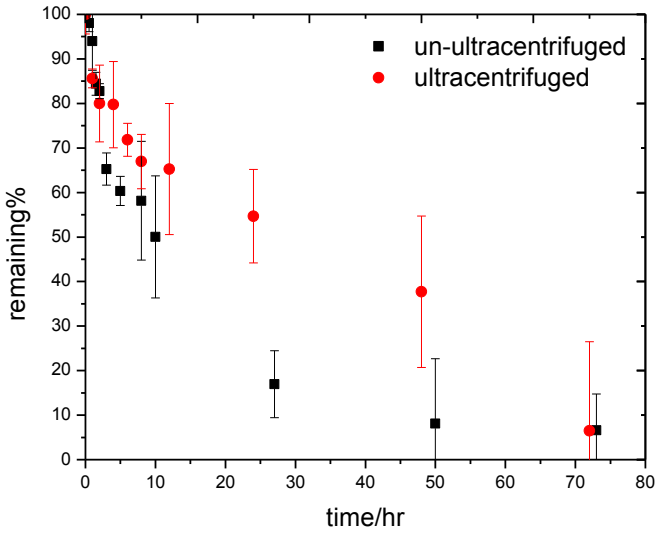

Figure C.2 Comparison of reverse release profiles for ultracentrifuged 2'-triisopropyl Si PTX (1c) nanoparticles and un-ultracentrifuged ones at pH=7.4

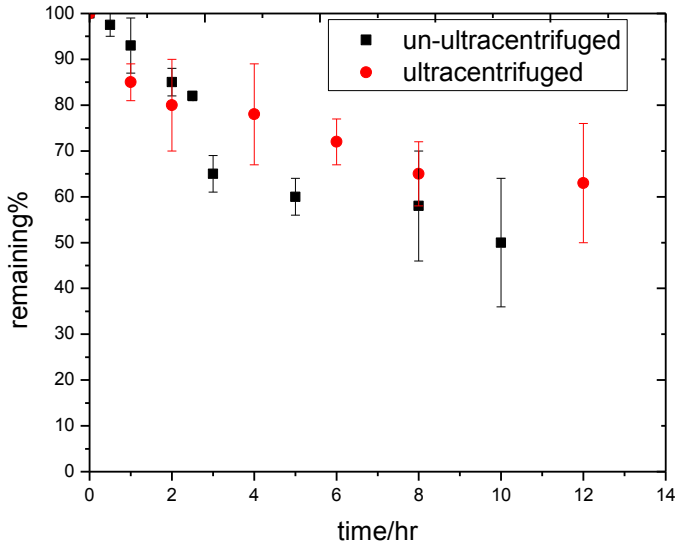

Figure C.3 Comparison of reverse release profiles for ultracentrifuged 2'-trimenthyl Si PTX (1e) nanoparticles and un-ultracentrifuged ones at pH=7.4

In order to reduce particle aggregation during freezing of lyophilization, sucrose, as cryoprotectant was added in nanosuspension before lyophilization. Combining sonication with varied length of time, we studied the effect of cryoprotect and sonication time on particle size recovery. 2',7-triethyl Si PTX nanoparticles were prepared using CIJ-D mixer. The nanoparticle suspension was split in half. Sucrose, as cryoprotectant, was added in one vial of nanosuspension with a mass ratio of 10:1 sucrose: NPs. The other was without sucrose. They were both lyophilized. The nanoparticles in dry state were redispersed in PBS at pH=7.4. These two vials of nanoparticles were measured by DLS (Beckman Coulter, CA) after 2 and 5 min sonication. They were let sit at room temperature for 72 hrs. DLS measurements continued to be taken in 24 hr and 72 hr. Particle size are summarized in Table C.7 and size distributions are shown in Figure C.4.

Table C.7 2',7-triethyl Si PTX (2a) NP sizes comparison with and without sucrose.

particles	dI (nm) w/o sugar	dI (nm) w/ sugar
2 min sonication	308	155
5 min sonication	110	96
24hr	124	102
72hr	157	104

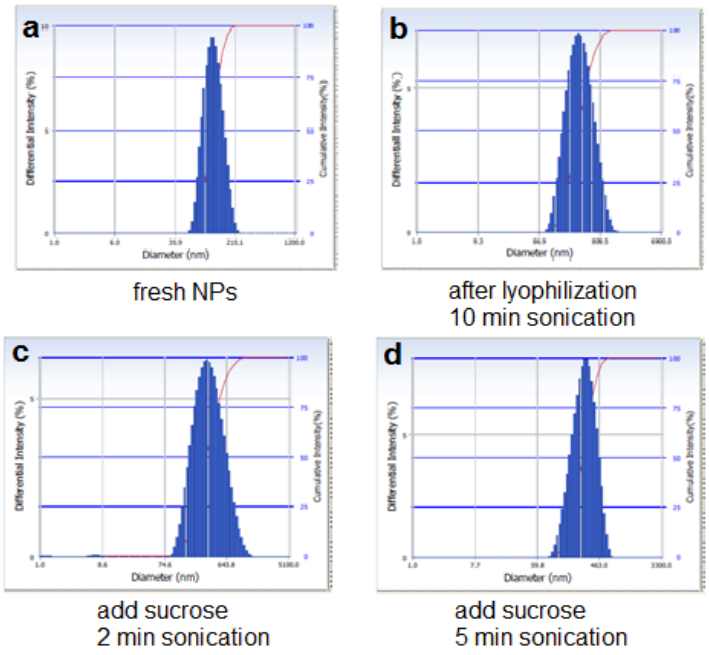

Figure C.4 Nanoparticle size distribution of 2',7-triethyl Si PTX NPs (2a) with sucrose during sonication.

Appendix D: Cryo-TEM images of Si PTX Nanoparticles

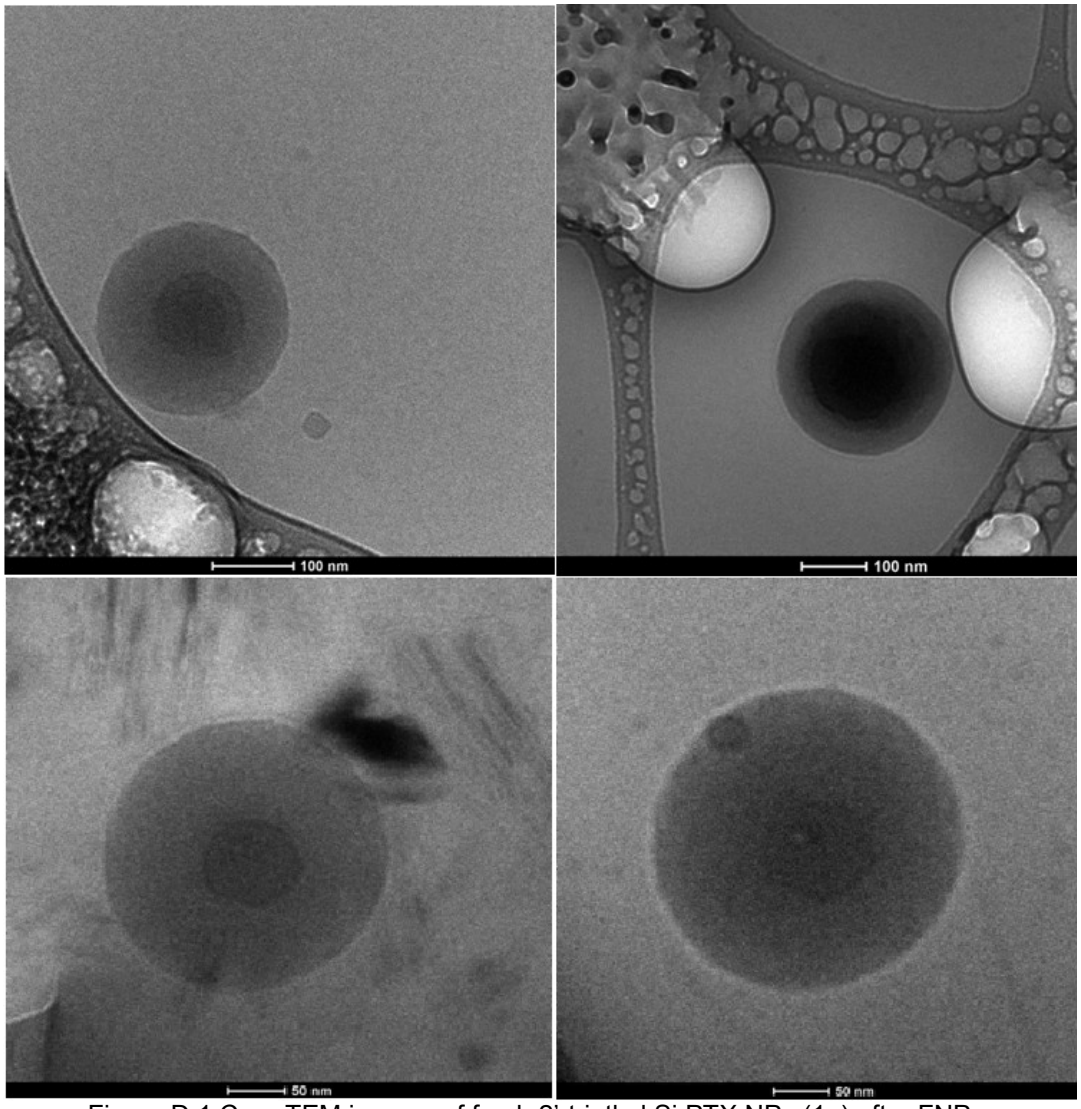

Figure D.1 Cryo-TEM images of fresh 2'-triethyl Si PTX NPs (1a) after FNP.

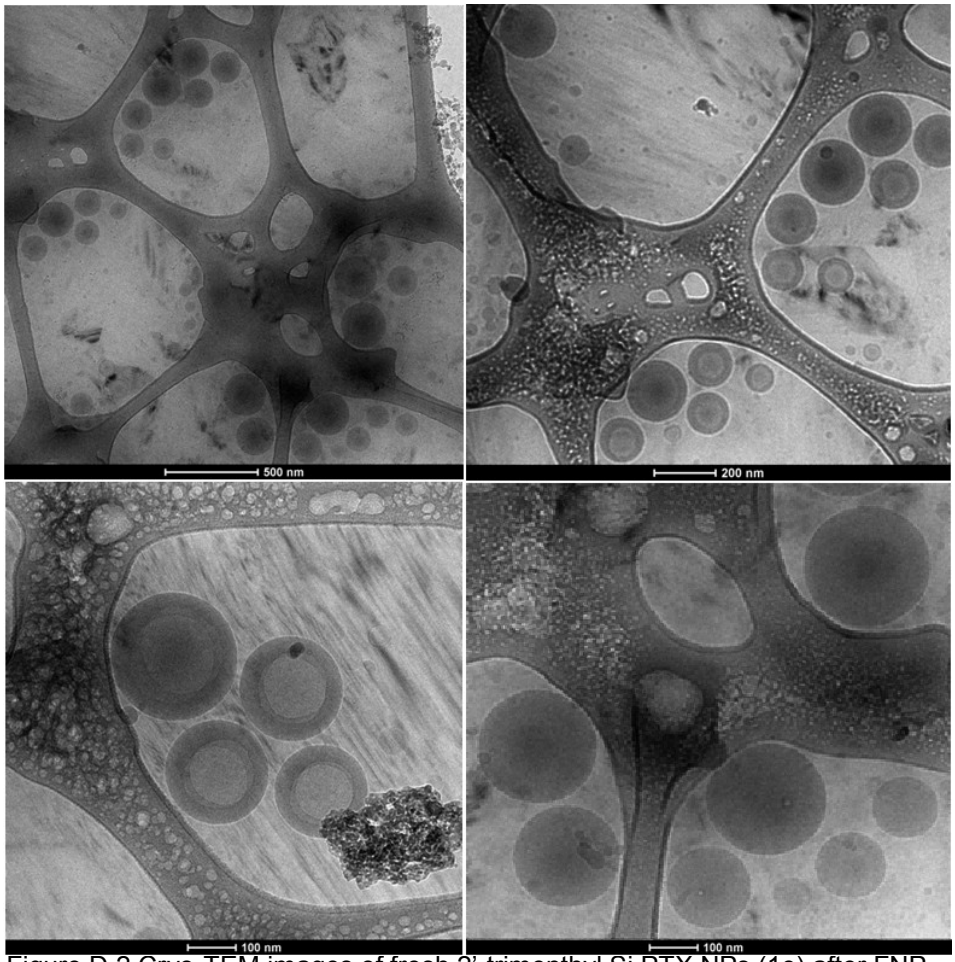

Figure D.2 Cryo-TEM images of fresh 2'-trimenthyl Si PTX NPs (1e) after FNP.

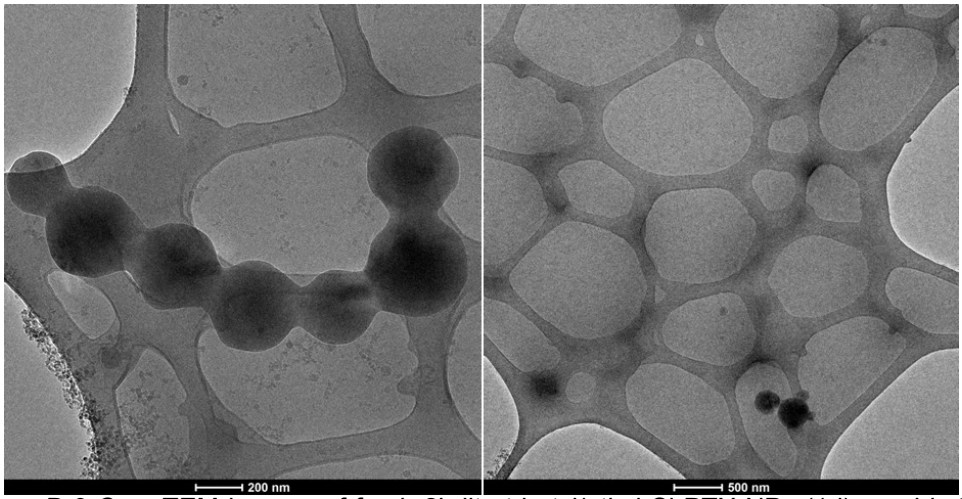

Figure D.3 Cryo-TEM images of fresh 2'-ditert butyl/ethyl Si PTX NPs (1d) aged in 7 days in 95:5 volume ratio of THF/H_2O solution.

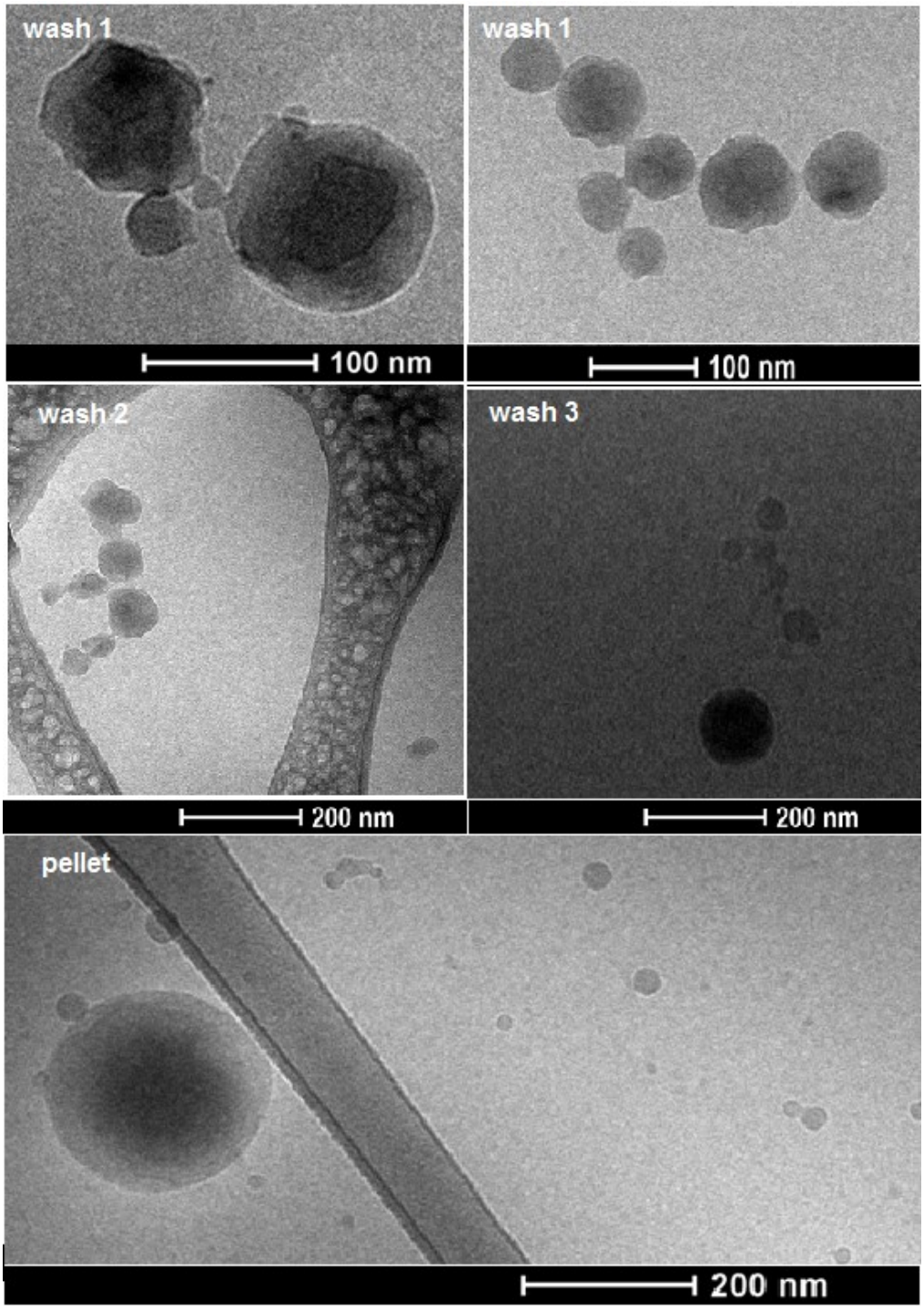

Figure D.4 Cryo-TEM images of 2'-triisopropyl Si PTX NPs (1c) during ultracentrifugation.

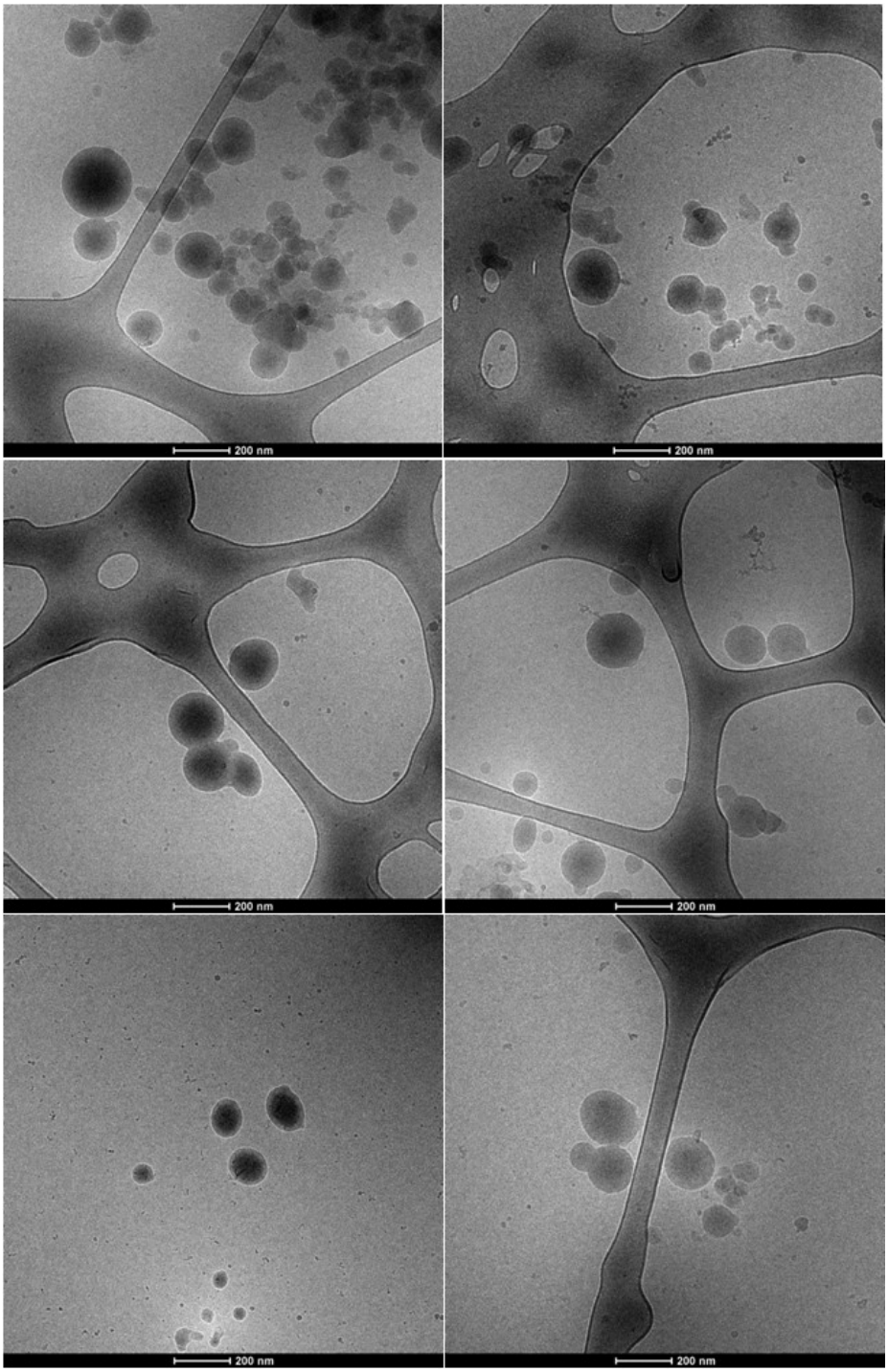

Figure D.5 Cryo-TEM images of 0 hr release of 2'-tri-ethyl Si PTX (1a) NPs.

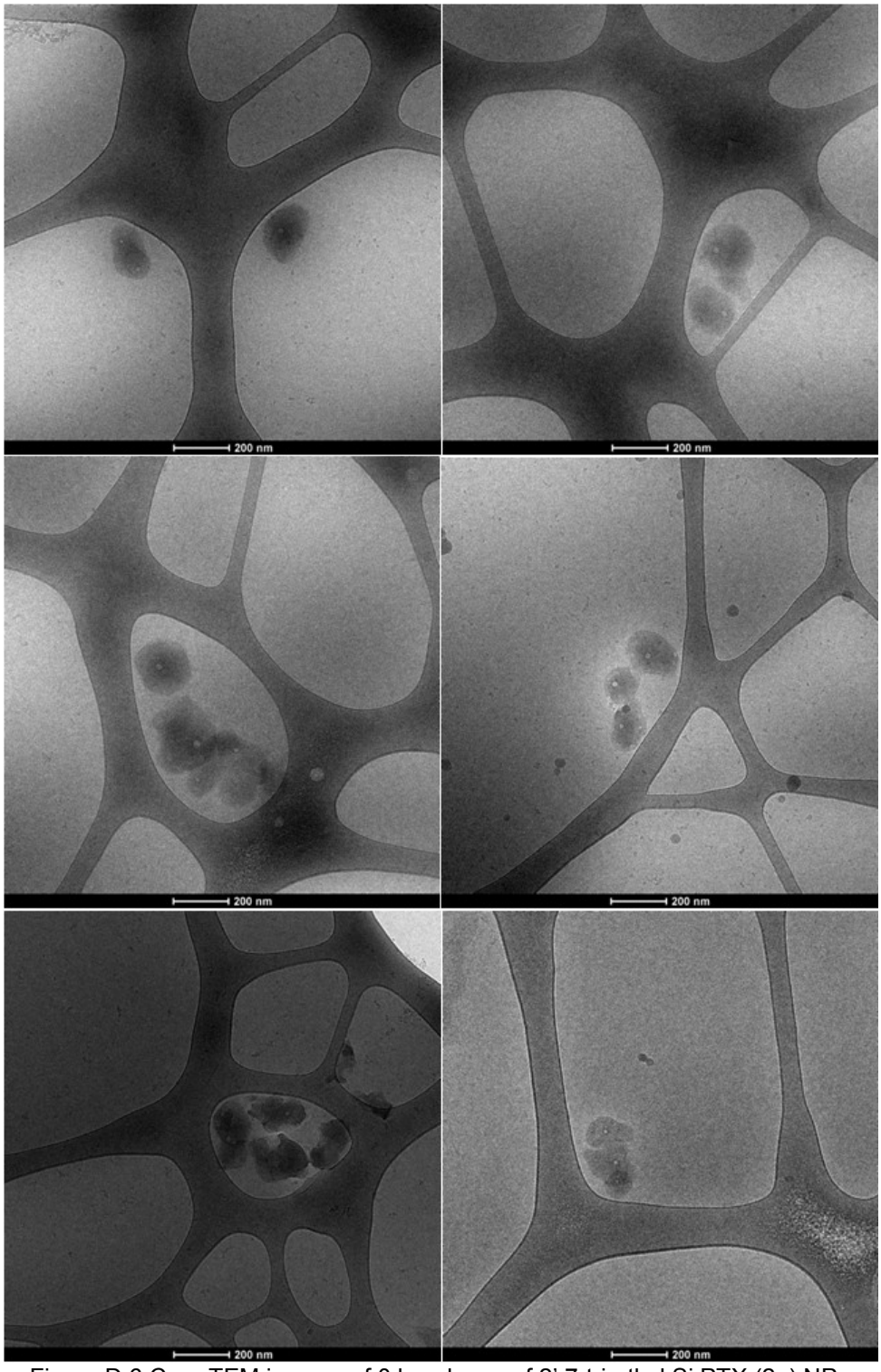

Figure D.6 Cryo-TEM images of 0 hr release of 2',7-tri-ethyl Si PTX (2a) NPs.

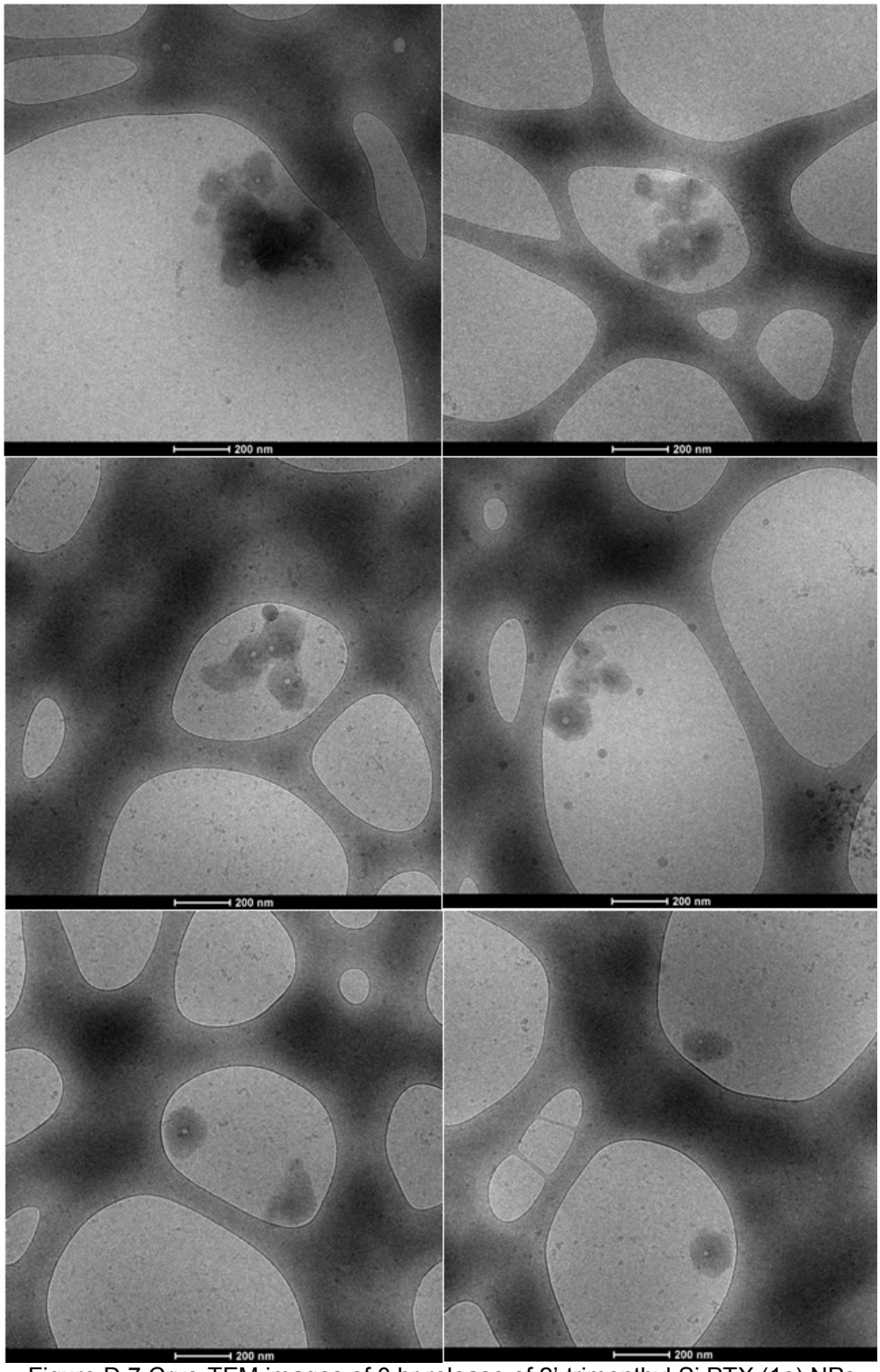

Figure D.7 Cryo-TEM images of 0 hr release of 2'-trimenthyl Si PTX (1e) NPs.

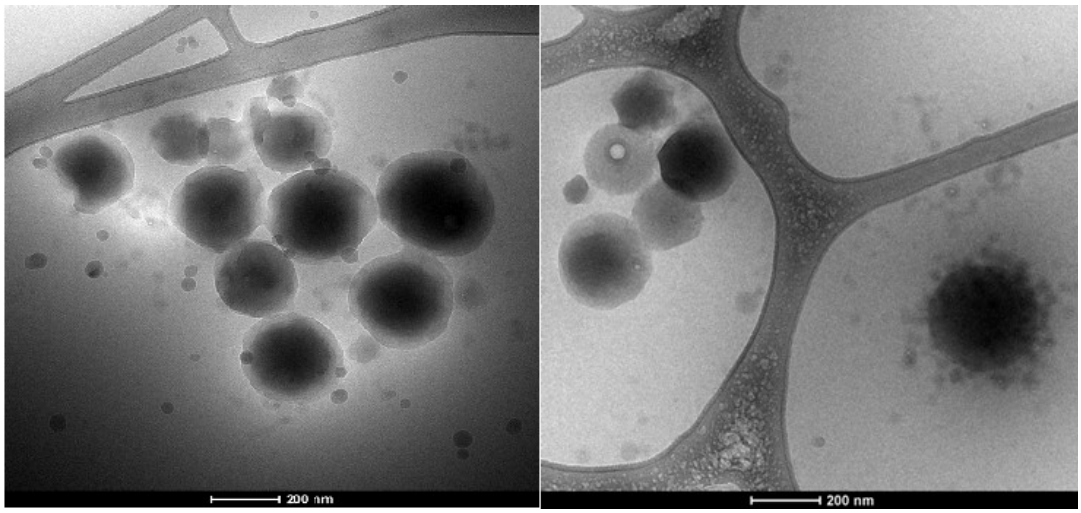

Figure D.8 Cryo-TEM images of 0 hr release of 2'-ditert butyl/ethyl Si PTX (1d) NPs.

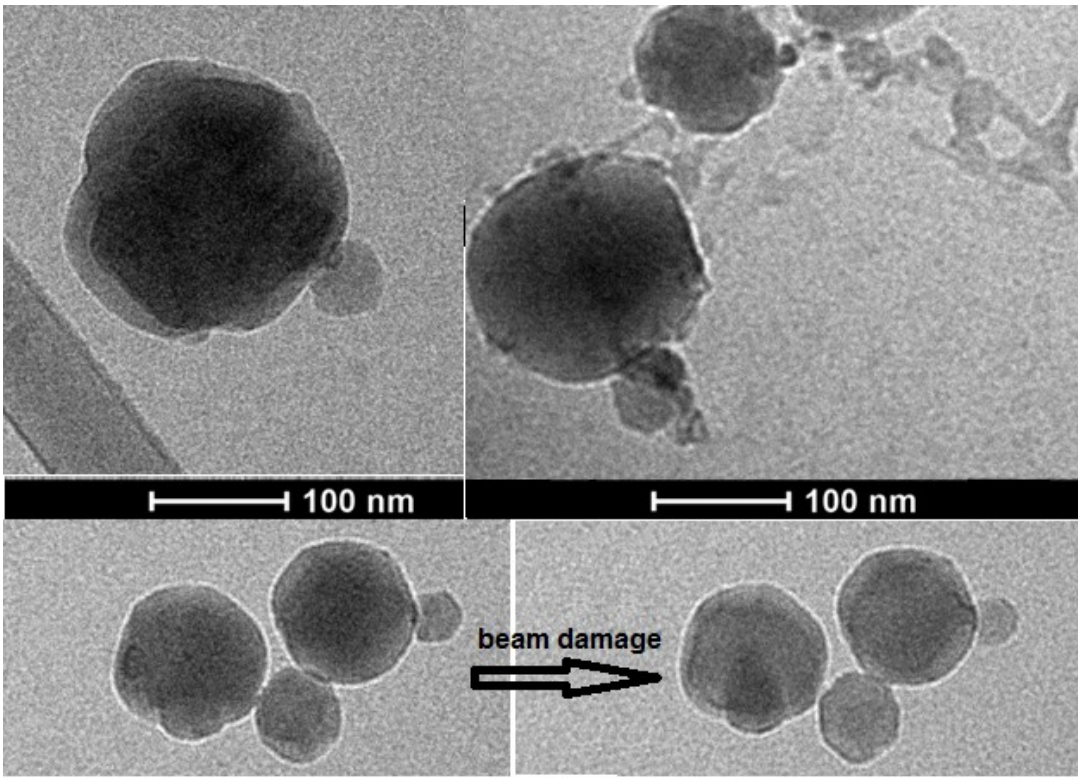

Figure D.9 Cryo-TEM images of 24 hr release of 2'-tri-ethyl Si PTX (1a) NPs.

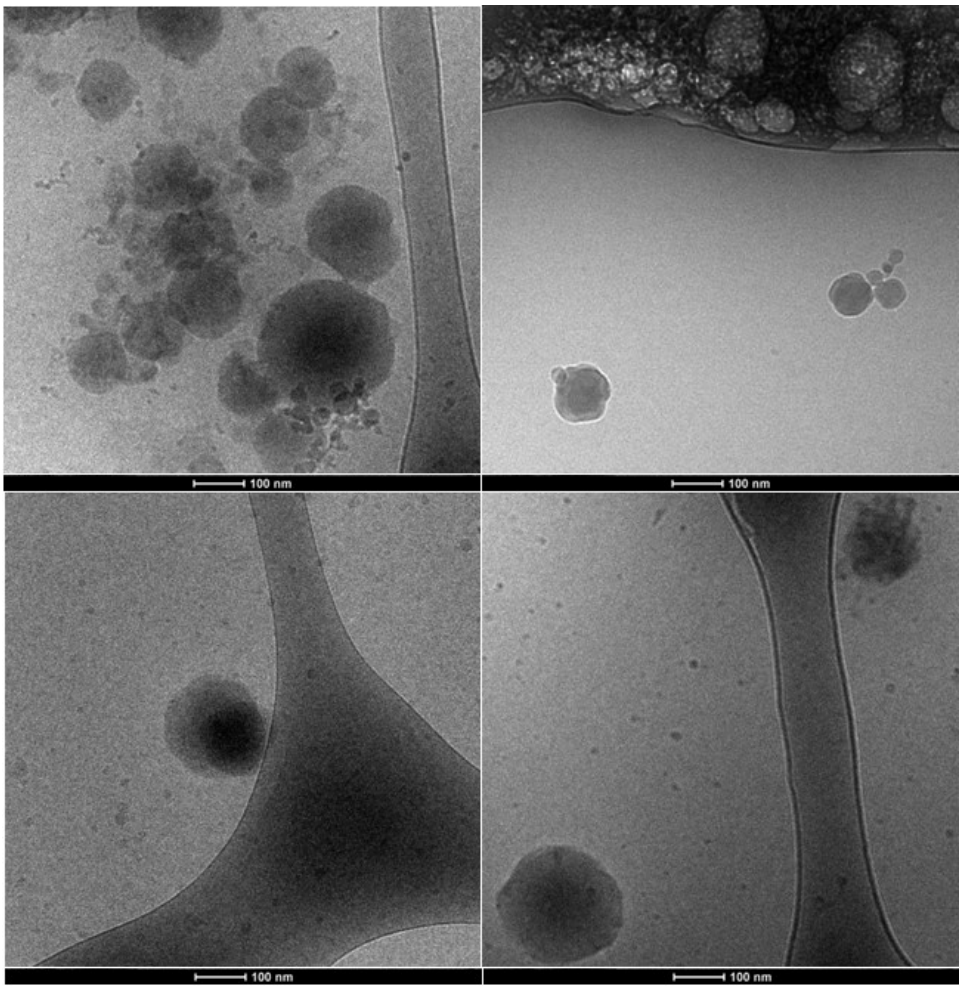

Figure D.10 Cryo-TEM images of 24 hr release of 2',7-triethyl Si PTX (2a) NPs.

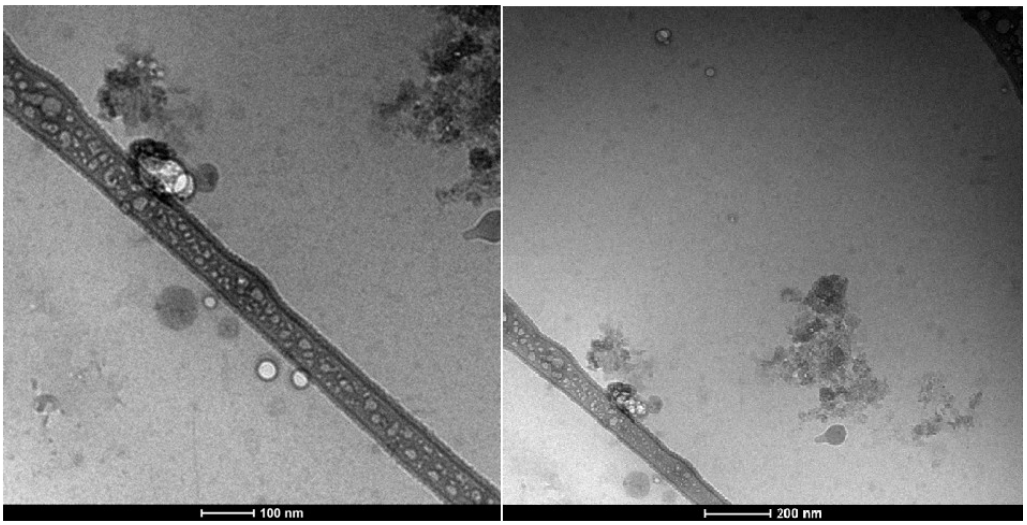

Figure D.11 Cryo-TEM images of 24 hr release of 2'-triisopropyl Si PTX (1c) NPs.

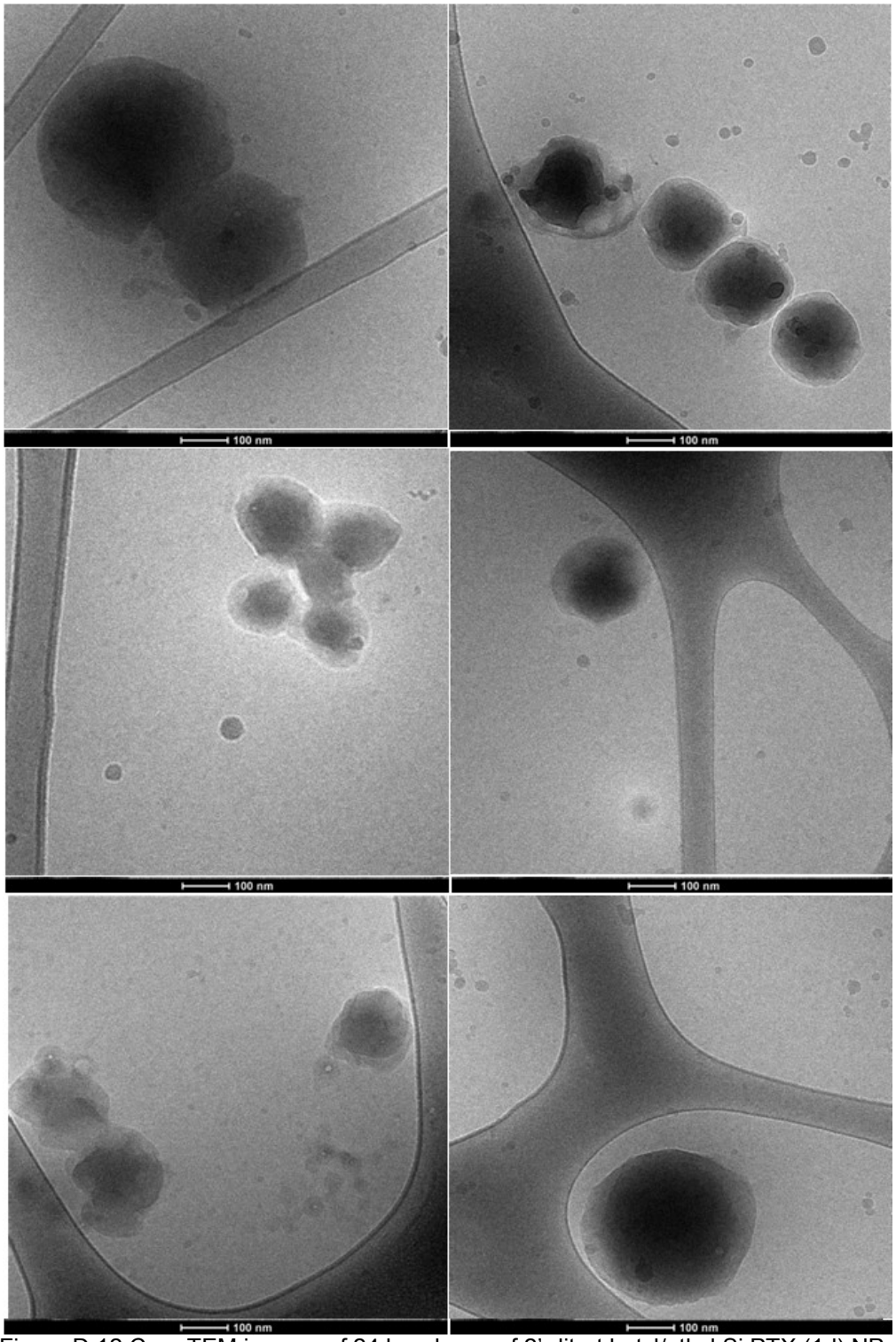

Figure D.12 Cryo-TEM images of 24 hr release of 2'-ditert butyl/ethyl Si PTX (1d) NPs.

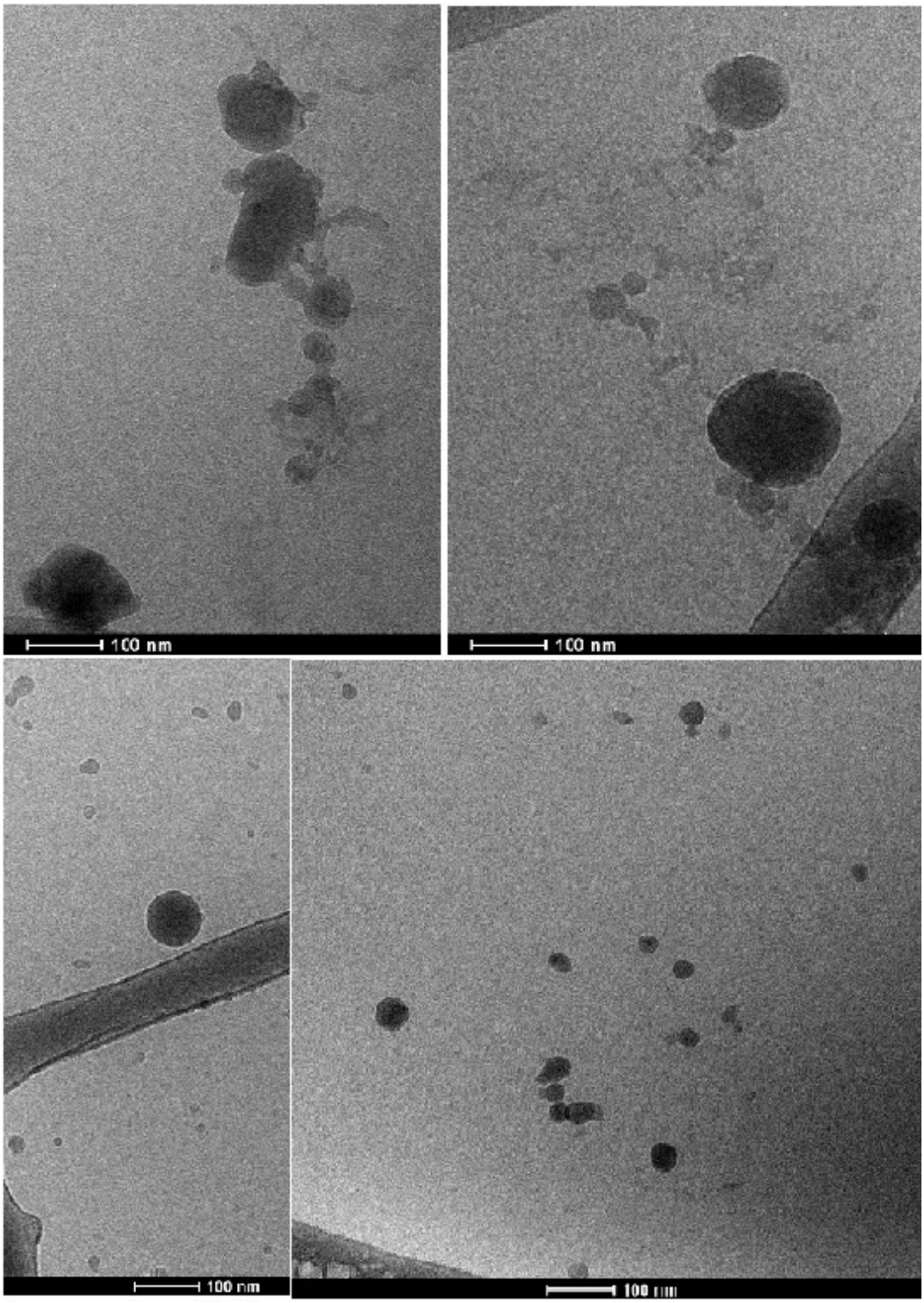

Figure D.13 Cryo-TEM images of 24 hr release of 2'-trimenthyl Si PTX (1e) NPs.

Appendix E: Nanoparticles Coloaded with Two Si PTX Prodrugs

We attempted to prepare nanoparticles coloaded with two Si PTX prodrugs, with one of which is more hydrolytical labile and the other one is stable. The goal is to develop a nanoparticle formulation which is able to release drug both in short time and long time due to two distinctive hydrolysis rate of prodrugs. The nanoparticles were prepared by mixing 14.8 mg of 2'-triethyl Si PTX(1a) (with equivalent of 12.5 mg PTX) and 15.6 mg 2'-ditert butyl/ethyl Si PTX (1d) and 25 mg PEG-*b*-PLGA (MW: 5k-10kDa) together. All materials were dissolved in 2.5 mL THF, impinged with 2.5 mL DI water and diluted by 45 mL DI water by CIJ-D mixer. The resulting nanosuspension were first measured by DLS, then ultracentrifuged and lyophilized for 24 hr. The dry powder was stored in 4˚C fridge. The example of colading nanoparticles has an ideal loading of 25%:25% when equal mass of two prodrugs were mixed, and the rest of 50% will be polymer mass. Shown in Table E.1, A series of mass ratios of prodrugs were used shown as 1d:1a, in attempt to achieve nanoparticles with varied loading of coloaded prodrugs. Nanoparticle sizes were measured by DLS (Beckman Coulter, CA). The ideal loading of PTX% in nanoparticle mass was obtained from the initial materials used for flash nanoprecipitation. The actual loading was determined by HPLC using ultracentrifuged and lyophilized nanoparticles.

As seen below, nanoparticle sizes decreased as more 2'-ditert butyl/ethyl Si PTX (1d) prodrug was added during flash nanopercipitation. As we know, nanoparticles only loaded with 1d were smaller than those with 2'-triethyl Si PTX (1a) shown in Ch.5 and Ch.6. Therefore, it is highly likely that nanoparticles were not successfully coloaded with

two prodrugs. Instead, one portion of nanoparticles was only loaded with 1d, and the other only with 1a.

In terms of PTX loading, nanoparticles tended to encapsulate more 2'-ditert butyl/ethyl Si PTX (1d) than 2'-triethyl Si PTX (1a), which resulted in higher relative loading of 1d:1a comparing actual loading with ideal loading. I speculated that 2'-ditert butyl/ethyl Si PTX is more hydrophobic, so it nucleates faster during flash nanoprecipitation. It is possible that nanoparticles were encapsulated with most of the nucluei with 1d and less 1a, or the majority of nanoparticles were only loaded with 1d, but not 1a.

Moreover, the coloading nanoparticles were not successful in terms of combining the drug release characteristics of both 1a and 1d nanoparticles. Figure E.1 showed that, the coloading nanoparticles release in a similar rate with that of only loaded with 1d, it again demonstrated that the coloading nanoparticles are probably composed of nanoparticles only loaded with 1d.

Therefore, in order to achieve coloading two Si PTX prodrugs with very different hydrophobicity, new strategies should be developed in terms of mixing condition, formulation development etc.

Table E.1 Physical properties of the colaoding nanoparticles.

1d:1a	Size/nm	Ideal loading%	Actual loading%
0:100	145	0:47.5	0:47.5
10:90	145	4.5:33	4.9:40
30:70	132	15:21	15:32
50:50	85	21.5:2.5	23:9.5
100:0	84	53:0	53:0

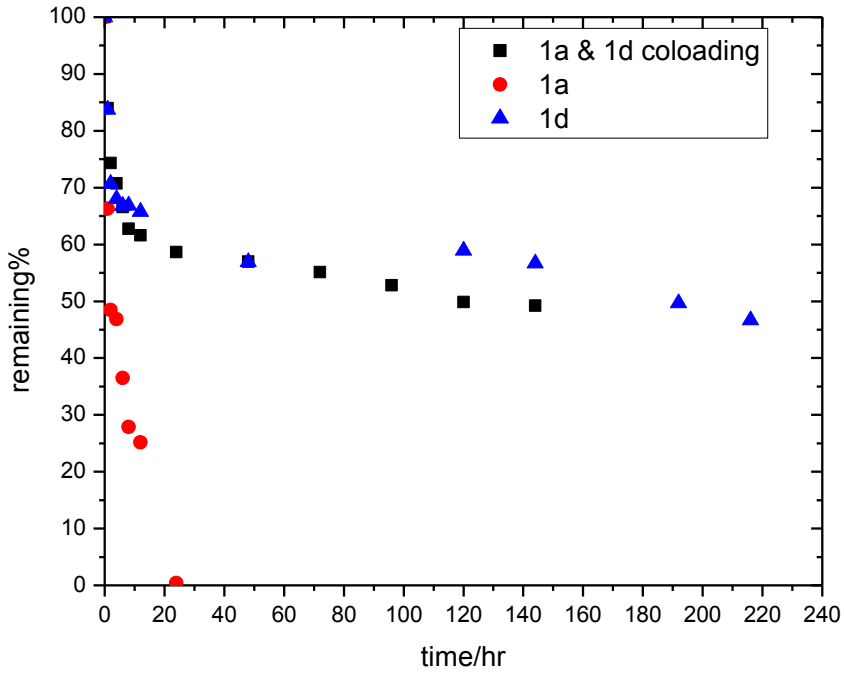

Figure E.1 Reverse release profiles of (1) 1a & 1d coloading NPs, (2) 1a, 2'-triethyl Si PTX NPs and (3) 1d, 2'-ditert butyl/ethyl Si PTX NPs.